01 Jun 1987

Design of automotive structural components using high strength sheet steels structural behavior of members consisting of flat and curved elements

M. Brad Parks

Wei-Wen Yu
Missouri University of Science and Technology, wwy4@mst.edu

Civil Engineering Study 87-2
Structural Series

Ninth Progress Report

DESIGN OF AUTOMOTIVE STRUCTURAL COMPONENTS USING HIGH STRENGTH SHEET STEELS

STRUCTURAL BEHAVIOR OF MEMBERS CONSISTING OF FLAT AND CURVED ELEMENTS

by

M. Brad Parks
Research Assistant

Wei-Wen Yu
Project Director

A Research Project Sponsored by American Iron and Steel Institute

June 1987

Department of Civil Engineering

University of Missouri-Rolla

Rolla, Missouri

PREFACE

This report is based on a dissertation presented to the Faculty of the Graduate School of the University of Missouri-Rolla (UMR) in partial fulfillment of the requirements for the degree of Doctor of Philosophy in Civil Engineering.

The financial assistance granted by the American Iron and Steel Institute (AISI) and the technical guidance provided by members of the AISI Task Force on Structural Design and Research of the Transportation Department and the AISI staff are gratefully acknowledged. These members are: Messrs. S. J. Errera, D. M. Bench, A. E. Cornford, Jim Davidson, Charles Haddad, Emil Hanburg, Al Houchens, L. J. Howell, A. L. Johnson, R. G. Lang, B. S. Levy, Kuang-Huei Lin, Hickmat Mahmood, Don Malen, D. J. Meuleman, M. S. Rashid, Joe Rice, W. J. Riffe, Robin Stevenson, Brian Taylor, R. J. Traficanti, T. L. Treece, M. T. Vecchio, and David Whittaker.

All materials used in the experimental study were donated by Bethlehem Steel Corporation, Inland Steel Company, and National Steel Corporation.

Appreciation is expressed to Messrs. K. Haas, R. Haselhorst, J. Tucker, and A. Johnston, staff of the Department of Civil Engineering, for their support. The valuable assistance provided by Dr. C. Santaputra throughout the curved element study is greatly appreciated.

ABSTRACT

Local buckling of stiffened and unstiffened curved elements has been investigated both experimentally and analytically. Stiffened curved elements are supported along both longitudinal edges while unstiffened curved elements are supported along one longitudinal edge with the other longitudinal edge free.

A series of stub column, beam, and shear tests have been performed for sections containing curved elements. The tested specimens were formed from sheet steels with yield strengths ranging from 27 to 88 ksi. The radius-to-thickness, R/t, values of the curved elements varied from 12 to 438 whereas the arc length-to-thickness, b/t, ratios ranged from 23 to 218.

As a result of these tests and existing curved element theory, semi-empirical expressions have been developed for the prediction of local buckling, caused by uniform axial compression, for both types of curved elements. Approximate methods have been established for prediction of curved element local buckling caused by bending. Also, an approximate technique has been derived to predict the interaction between the local buckling of flat and curved elements.

A nonlinear finite element program has been successfully employed to predict local buckling of both stiffened and unstiffened curved elements when subjected to uniform axial compression.

TABLE OF CONTENTS

TABLE OF CONTENTS (Cont.)

TABLE OF CONTENTS (Cont.)

TABLE OF CONTENTS (Cont.)

TABLE OF CONTENTS (Cont.)

TABLE OF CONTENTS (Cont.)

TABLE OF CONTENTS (Cont.)

LIST OF ILLUSTRATIONS

LIST OF ILLUSTRATIONS (Cont.)

LIST OF ILLUSTRATIONS (Cont.)

LIST OF ILLUSTRATIONS (Cont.)

LIST OF ILLUSTRATIONS (Cont.)

LIST OF ILLUSTRATIONS (Cont.)

LIST OF TABLES

LIST OF TABLES (Cont.)

LIST OF TABLES (Cont.)

LIST OF TABLES (Cont.)

I. INTRODUCTION

A. GENERAL

Many structural components are composed either partially or totally of curved elements. Curved elements are often found in automotive structural components (Figure 1.1) and corrugated sheets. Because curved elements are widely used, and because existing knowledge of their structural behavior is lacking, the present investigation was initiated to develop improved analysis and design procedures.

The accurate analytical prediction of the compressive strength of curved elements is extremely difficult. This difficulty arises primarily because: 1) large deflection theory, which is much more complex than linear theory, must be used to analyze curved element buckling caused by axial stresses, 2) curved elements with appreciable curvature are quite sensitive to imperfections, 3) curved elements with small curvatures are particularly sensitive to edge restraints at their boundaries, and 4) the effects of residual stresses and cold work are difficult to predict. Because of the complexities involved in predicting the critical buckling stress of curved elements, it is essential that design expressions for the compression of such elements be empirical or at least semi-empirical in nature.

In this study, local buckling of both stiffened and unstiffened curved elements, has been examined. As shown in Figure 1.2, stiffened curved elements are supported on both longitudinal edges whereas

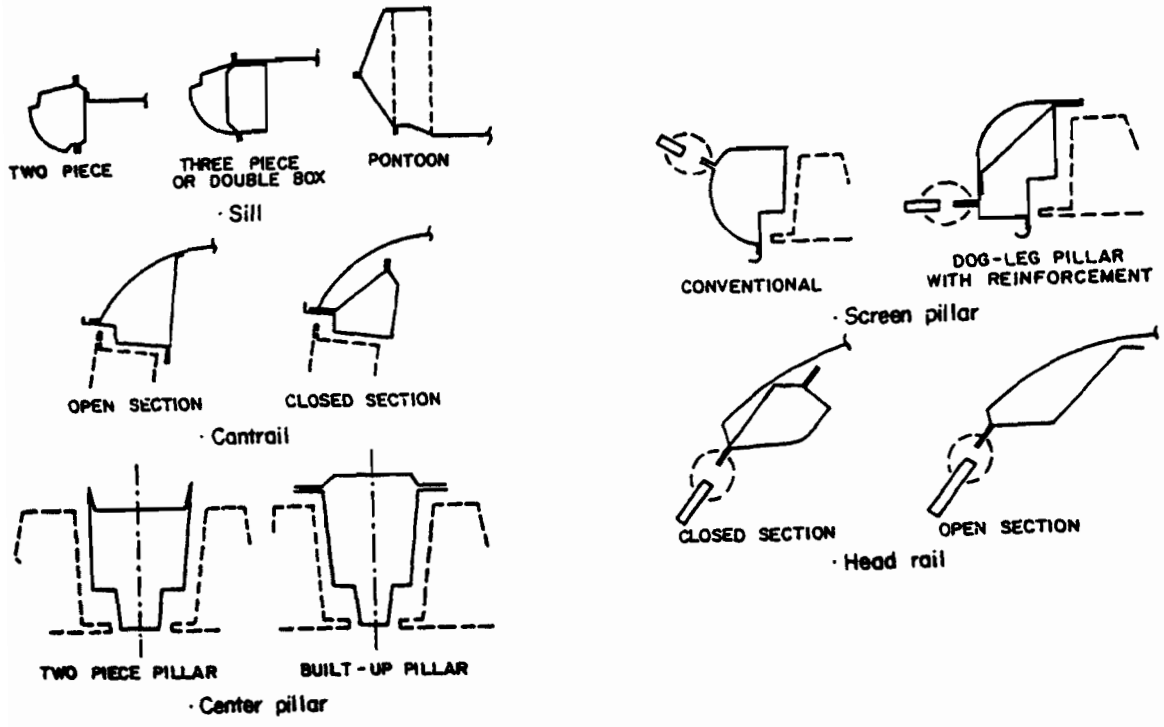

Fig. 1.1 Typical Automotive Structural Members[1]

unstiffened curved elements are supported on one longitudinal edge with the other longitudinal edge free. It should be noted that there are three important parameters that govern the elastic local buckling of curved elements. The parameters are the radius, R, the arc length, b, and the thickness, t.

A series of stub column tests has been performed in order to investigate local buckling of both stiffened and unstiffened curved elements subject to uniform axial compression. The interaction between the local buckling of curved and flat elements also has been examined through the use of stub column tests.

Beam tests also have been performed for both types of curved elements. The purpose of the beam tests is to study the stress gradient effect on local buckling, which is caused by bending, over the depth of the curved element. A series of shear specimens have been tested for beam sections with curved webs.

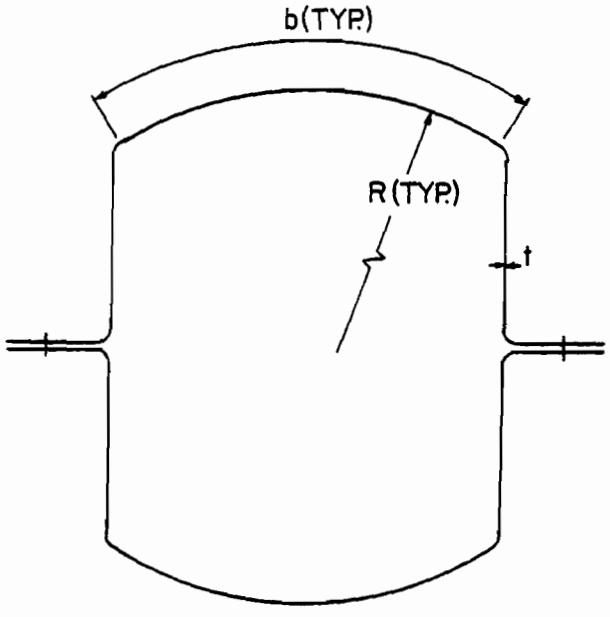

(a) Stiffened Curved Flanges

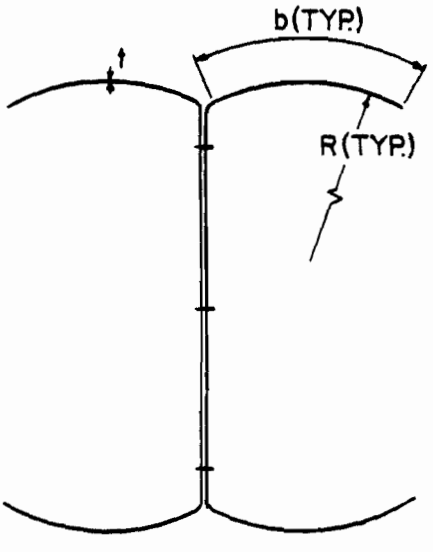

(b) Unstiffened Curved Flanges

Figure 1.2 Two Types of Curved Elements

In addition to the experimental study, a nonlinear finite element program called "ADINA" has been employed for the prediction of local buckling of curved elements caused by uniform axial compression.

The research work discussed herein was a part of a research project entitled "Structural Behavior of Automotive Structural Components Using High Strength Sheet Steels". The project, which began in 1982, was conducted at the University of Missouri-Rolla under the sponsorship of the American Iron and Steel Institute.

B. PURPOSE OF INVESTIGATION

The primary purpose of the present investigation is to study the structural behavior of cold-formed steel members composed of flat and curved elements. Based on the analytical and experimental work discussed herein, prediction methods have been developed for each of the following conditions:

1) local buckling of both stiffened and unstiffened curved elements subject to uniform axial compression,
2) interaction between local buckling of flat and curved elements subject to uniform axial compression,
3) local buckling of both stiffened and unstiffened curved elements subject to bending stresses; and
4) buckling of curved webs subject primarily to shearing stresses.

Also, the post-buckling behavior of both stiffened and unstiffened curved elements has been investigated.

C. SCOPE OF INVESTIGATION

The present study is composed of both an analytical and experimental investigation of cold-formed steel members consisting of curved elements.

In the first phase of the investigation, all available literature that is related to local buckling of curved elements was reviewed. Section II contains a summary of the literature survey.

The main portion of the curved element study is described in Section III. After a brief introduction in Section III.A, each of the curved element tests are described in detail in Section III.B.

Based on the results of the curved element tests and existing theory of curved element behavior, methods for the prediction of local buckling of curved elements have been developed. These methods are summarized in Section III.C. Section III.D provides a comparison of the predicted failure loads to the test values.

In Section III.E, a nonlinear finite element program, which is used to predict local buckling of curved elements subject to uniform axial compression, is described. The predicted failure loads from the program are compared to the test results.

A summary of all the newly developed curved element analysis procedures is provided in Section IV. Section V illustrates the substantial increase in ultimate load capacity of curved elements over flat elements with similar dimensions and boundary conditions. Finally, Section VI presents a general review of the curved element research findings.

II. REVIEW OF LITERATURE

A. GENERAL

In the early portion of the study, many publications and research reports concerning curved element behavior were reviewed. Section II.B contains a summary of the existing methods for the prediction of local buckling of curved elements.

The available literature for prediction of the collapse load of cross sections containing flat and curved elements is described in Section II.C. Section II.D first summarizes the effective width approach for flat elements and then provides a review of effective width equations for curved elements. Finally, the available procedures for the analysis of shear buckling of curved elements are given in Section II.E.

Because of the difficulty involved in deriving a practical, theoretical expression for local buckling of unstiffened curved elements, and because they have not been commonly used in the past, there is virtually no available literature on the local buckling of unstiffened curved elements. Thus, the emphasis of the following literature review is on the stiffened curved element.

It should be noted that in the literature the terms curved element, curved plate, and curved panel are used interchangeably.

B. LOCAL BUCKLING OF STIFFENED CURVED ELEMENTS

The accurate prediction of the local buckling stress of curved elements is extremely complex. It seems that classical stability equations based on linear theory are insufficient because they consistently overestimate the critical buckling stress, f_{cr}, of curved elements. The major cause of this overestimation is the fact that buckling of curved elements is accompanied by compressive transverse membrane stresses, which result in a deflected geometry that is unstable. For this reason, large deflection theory is essential for reasonably accurate prediction of f_{cr}. It has been observed that when compressive membrane stresses are produced transverse to the direction of buckling, such as for the compressive buckling of curved elements or cylinders, large deflection theory is required. However, when tensile membrane stresses are produced perpendicular to the direction of buckling, such as for buckling caused by lateral pressure on a relatively short, closed cylinder, torsion on a cylinder, or compression on flat plates, linear theory is sufficient to predict f_{cr}.[2]

There have been attempts to describe the buckling of a stiffened curved plate based on a geometric parameter, Z_b, and a buckling coefficient, k_c, as follows:[2]

$$Z_b = (b^2/Rt)\sqrt{(1-\mu^2)} \tag{2.1}$$

and

$$k_c = \frac{12(1-\mu^2)}{\pi^2 E} f_{cr} (b/t)^2 \tag{2.2}$$

in which:

E = modulus of elasticity

t = curved plate thickness

R = radius of curved plate

b = circumference of curved plate

μ = elastic Poisson's ratio

Figure 2.1 shows the relationship between k_c and Z_b for a series of compression tests made by Jackson and Hall[3] on curved panels made of an aluminum alloy.[2] Other similar test results are provided in References 4 through 9.

At values of $Z_b < 10$, the behavior of curved plates is approximately the same as that of flat plates with similar boundary conditions, and thus the buckling coefficient, k_c, approaches that of a flat plate. The boundary conditions applied by Jackson and Hall[3] were between simple support and clamped conditions. Therefore, an average of the buckling coefficients for flat plates of these two limiting cases, $k_c = 5.7$, was used to plot the portion of the k_c - Z_b curve for $Z_b < 10$.[2]

For Z_b values > 1000, long cylinder behavior dominates, and the effects of boundary conditions are negligible. By observing the relationship between Z_b and k_c shown in Figure 2.1, it can be seen that for large values of Z_b, the buckling coefficient appears to be linearly related to Z_b. Thus, the resulting equation takes on the form of the classical buckling equation for cylinders:

$$f_{cr} = CEt/R \qquad (2.3)$$

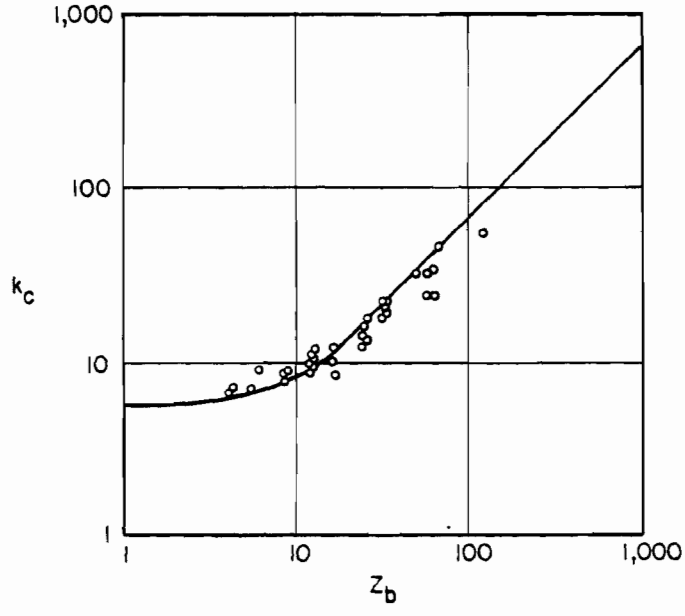

Figure 2.1 Comparison of Test Data With Theory for Axially Compressed Curved Plates[3]

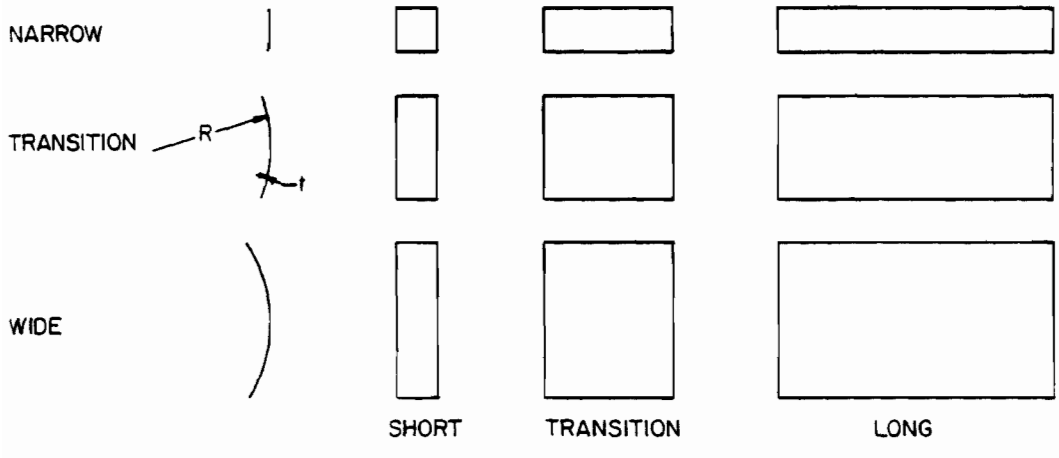

Figure 2.2 Ranges of Possible Curved Plate Geometries[2]

in which C represents the slope of the relationship between f_{cr} and $E(t/R)$.

In the intermediate range of $10 < Z_b < 1000$, where boundary conditions still exert considerable influence on f_{cr},[10] extreme difficulty is experienced in prediction of the critical buckling stress. It seems obvious that some sort of transition curve must exist between the two limiting cases described above. A few of the more successful attempts to develop such a curve are described in Section II.B.1.

The range of the various possible geometries of curved plates is illustrated in Figure 2.2.[2] Of the possibilities shown in Figure 2.2, only the extreme combinations of a long curved plate with large curvature (e.g., a closed cylinder) and a short curved plate with small curvature (e.g., a flat plate) are well researched and defined. All other combinations fall into the previously described transistion range.

In the following sections, the elastic and inelastic buckling and post-buckling behaviors of curved plates are discussed, and a brief summary of some of the methods proposed for the prediction of the buckling stress is included.

1. Elastic Buckling.

a. Transition Equations. Many attempts have been made over the years to develop a transition equation that would accurately predict the critical stress of curved plates when the geometric parameters of the plates lie somewhere between those of flat plates and complete cylinders. One of the first such attempts was performed by Redshaw[11,12]

who developed the following relationship based on the classical energy approach:[2]

$$f_{cr} = \frac{E}{6(1-\mu^2)}\left[\sqrt{12(1-\mu^2)\,\frac{t^2}{R^2} + \frac{\pi^4 t^4}{b^4}} + \frac{\pi^2 t^2}{b^2}\right] \qquad (2.4)$$

in which

f_{cr} = elastic buckling stress of a curved element supported on all sides (i.e., "stiffened curved element"), ksi

E = modulus of elasticity, ksi

μ = elastic Poisson's ratio

t = curved element thickness, in.

R = curved element radius, in.

b = curved element arc length, in.

It can be seen that this equation reduces to the theoretical buckling stress for cylinders when $(b/t)^2$ is large compared to R/t. Also, if the radius of a plate is very large, (i.e., R approaches infinity) the critical buckling stress approaches that of a flat plate.

Sechler and Dunn[13] later showed that Eq. (2.4) could be expressed in terms of the flat plate and cylindrical shell buckling stresses as shown below:

$$(f_{cr}/E)_{sc} = \sqrt{(f_{cr}/E)_c^2 + 1/4\,(f_{cr}/E)_f^2} + 1/2\,(f_{cr}/E)_f \qquad (2.5)$$

in which

$(f_{cr}/E)_{sc}$ = buckling stress ratio of a simply supported curved element subject to uniform compression

$(f_{cr}/E)_{c}$ = buckling stress ratio of a full cylinder with the same R/t ratio as the curved element

$(f_{cr}/E)_{f}$ = buckling stress ratio of a simply supported flat plate with the same b/t ratio as the curved element

Several other investigations into the development of transition equations for curved plates have been performed. Among the more noteworthy are the semi-empirical investigations conducted by Stowell,[14] Wenzek,[15] and Lindquist.[8] Levy[16] on the basis of large deflection theory developed the equations required to predict f_{cr}.

b. Post-Buckling Behavior. The post-buckling behavior for the elastic buckling of curved plates depends on the geometry of the plates and the magnitude of the initial imperfections. It should come as no surprise that just as for initial elastic buckling, the post-buckling behavior of curved plates also varies between the extremes of a flat plate and cylinder.

For $Z_b < 10$, a curved plate acts much the same as a flat plate with similar dimensions. Thus, as shown in Figure 2.3, the effects of initial imperfections are insignificant, and the compressive load increases well past f_{cr}. The ultimate load is reached when the effects of plasticity become predominant.

At values of $Z_b > 1000$, the post-buckling behavior of a curved plate should be similar to that of a cylinder. From Figure 2.3[10], it can be seen that for cylinders, the load-carrying capacity drops off

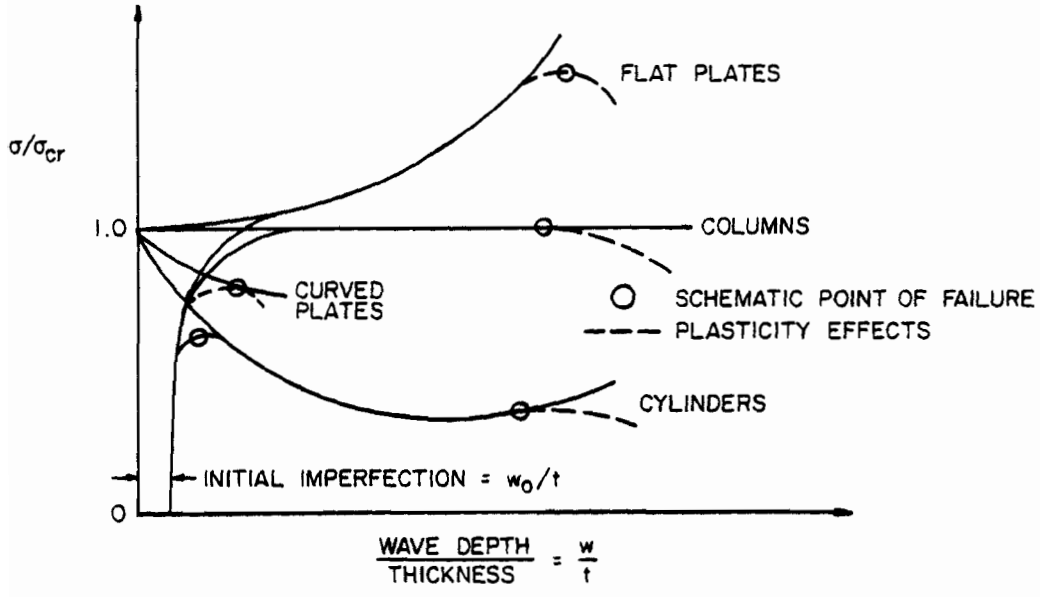

(a) Elastic Buckling

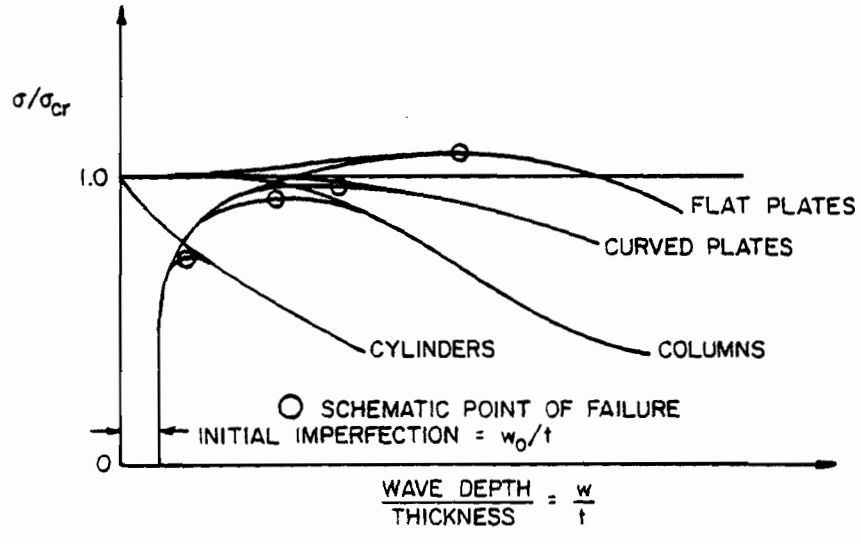

(b) Plastic Buckling

Figure 2.3 Schematic Postbuckling Behavior of Various Axially Loaded Structural Elements[10]

sharply after initial buckling and never regains the original buckling stress in the post-buckling range. Thus, the initial buckling stress, f_{cr}, and failure are coincident.[2]

In the intermediate range of $10 < Z_b < 1000$, there is obviously a transistion between the post-buckling effects of flat plates and cylinders. However, there are no known studies of the exact post-buckling behavior of curved plates in this range.

2. Inelastic Buckling. If the various parameters described in Section II.B are such that the critical buckling stress is greater than the proportional limit of a given material, the buckling is said to be inelastic, and an adjustment in the elastic buckling equations must be made. (It is important to note that this type of buckling only occurs for materials with gradual yielding stress-strain curves. An example of a typical gradual yielding stress-strain curve is shown in Figure 2.4(b). For sharp yielding materials with stress-strain curves similar to Figure 2.4 (a), elastic buckling prevails until f_{cr} reaches the yield point of the material.) This adjustment is necessary because the elastic buckling equations were developed under the assumption that the stress and strain were linearly related. However, for stresses above the proportional limit, the relationship between stress and strain is, by definition, nonlinear. In order to account for the nonlinear stress-strain relationship, the value of the modulus of elasticity, E, is replaced in the elastic buckling equation by a reduced modulus. Several different approaches for the calculation of such a reduced modulus are reviewed in the following sections.

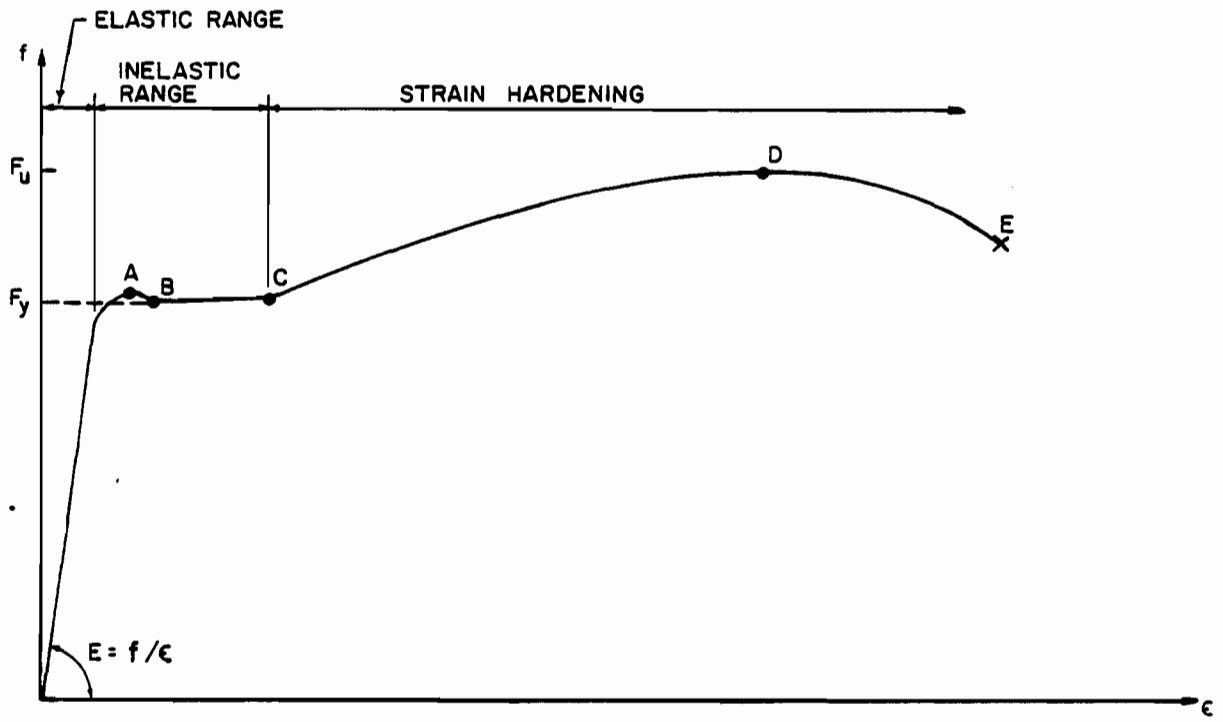

(a) Sharp-Yielding Steel

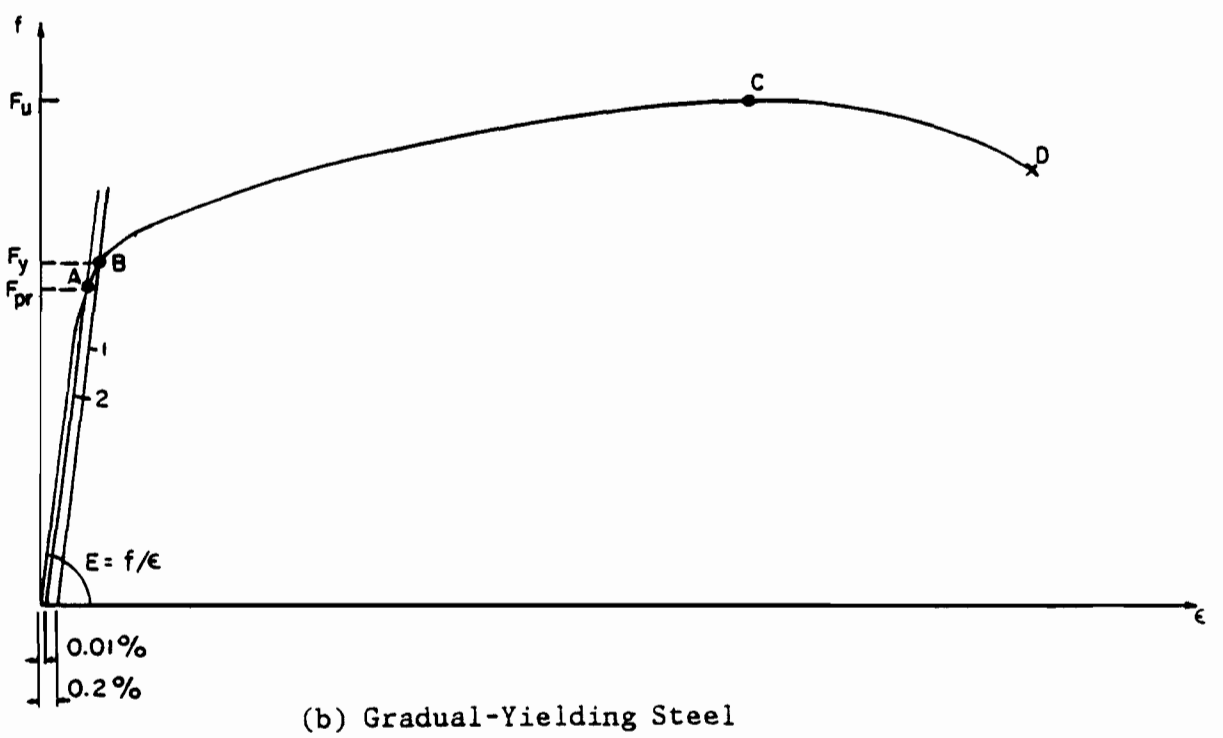

(b) Gradual-Yielding Steel

Figure 2.4 Stress-Strain Curves of Carbon Steel Sheets[28]

a. Initial Buckling.

i. Tangent Modulus Method. In 1895, Engesser[17] proposed that the modulus of elasticty, which is the slope of the stress-strain curve in the elastic range, should be replaced by the instantaneous slope of the stress-strain diagram in the inelastic range. The instantaneous slope is defined as the tangent modulus, E_t, as shown in Figure 2.5. Thus, in the elastic range, $E_t = E$. In the inelastic range, the value of E_t may be substantially less than E.

Bleich[18] proposed the following approximation for the tangent modulus that can be employed for any material if the proportional limit, F_{pr}, and the yield point, F_y, are known.

$$E_t/E = \frac{(f_{cr}/F_y)(1-(f_{cr}/F_y))}{(F_{pr}/F_y)(1-(F_{pr}/F_y))} \qquad (2.6)$$

ii. Secant Modulus Method. This method is quite similar to the tangent modulus method. The only difference is in the definition of the secant modulus, E_s. The secant modulus is defined as the slope of a line from the origin of the stress-strain diagram to the critical stress. The value of E_s is illustrated in Figure 2.5.

In the mid 1940's, Schuette,[7] who used this method for curved plates constructed of magnesium alloy materials, reported fair agreement between the predicted and test results.

iii. Reduced Modulus Method. This method was originally proposed by Engesser[17] and later revised by von Karman.[19] The reduced modulus, E_r, (also known as the double modulus) is a function of the original

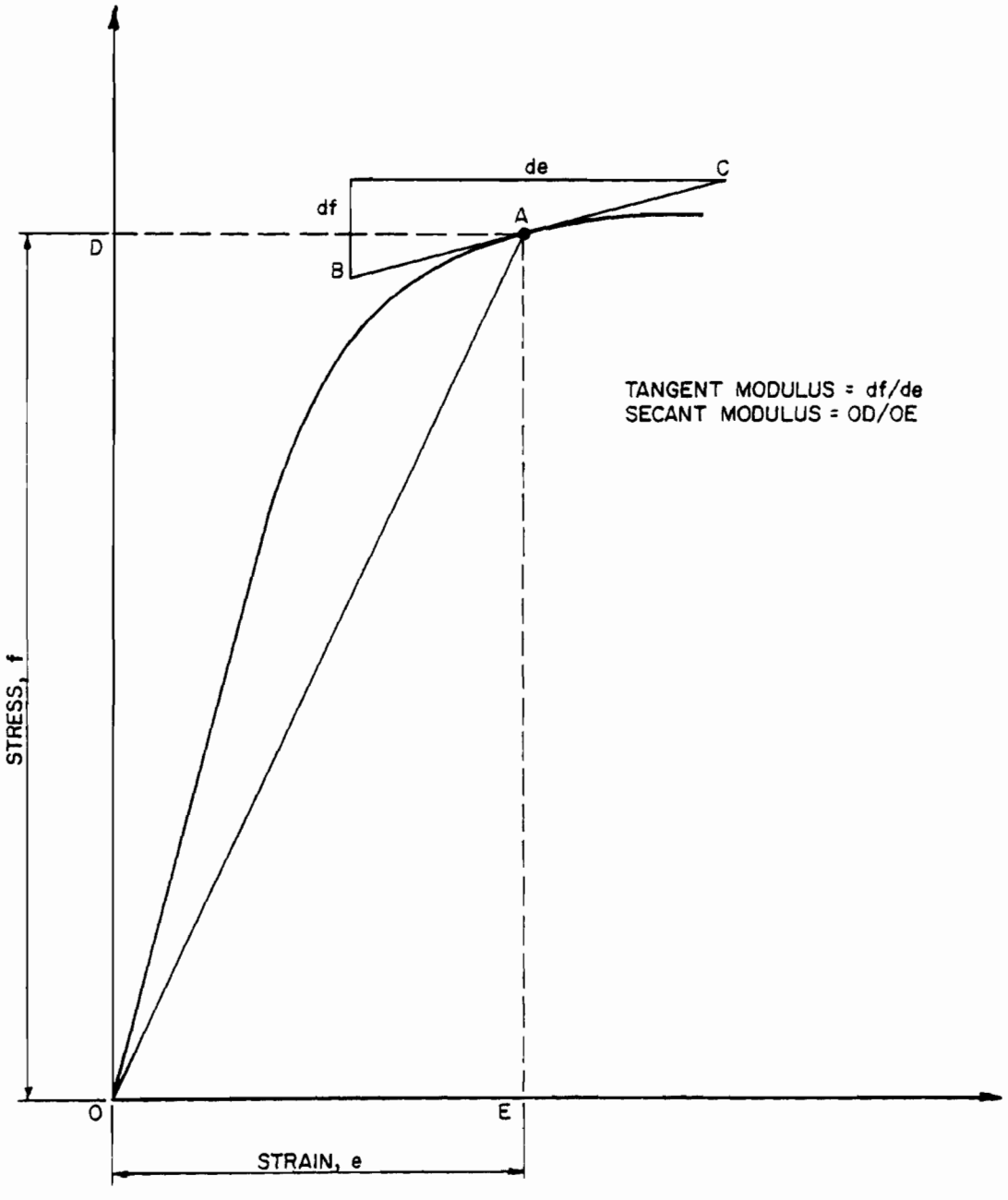

Fig. 2.5 Graphical Representation of the Tangent and Secant Moduli.

modulus, E, the tangent modulus, E_t, and the shape of the cross section. This modulus is derived from the equilibrium equations in the cross section at the onset of buckling and, thus, is technically more correct than the tangent modulus method.[20] The reduced modulus is defined as

$$E_r = \frac{EI_1}{I} + \frac{E_t I_2}{I} \tag{2.7}$$

in which I_1 and I_2 are the moments of inertia with respect to the neutral axis of the tensile and compressive stresses caused by column instability. For a more detailed description of the reduced modulus, the reader is referred to the work of Bleich.[18]

According to Fischel,[20] the reduced modulus for compression members with rectangular cross sections, such as flat plates, may be expressed as

$$E_r = \frac{4EE_t}{(\sqrt{E} + \sqrt{E_t})^2} . \tag{2.8}$$

Fischel reports good correlation between the test results of curved plates made of aluminum alloy and the predicted values of f_{cr} when Equation (2.8) is used for the calculation of E_r.

iv. Gerard's Method. Another method for reducing the modulus of elasticity is given by Gerard[2] as,

$$n = \frac{E_s}{E}\sqrt{\frac{(1-\mu^2)}{(1-\nu^2)}\frac{E_t}{E_s}}, \qquad (2.9)$$

in which $\nu = \mu_p - (\mu_p - \mu)(E_s/E)$ and μ_p = plastic Poisson's ratio. The remaining terms have been previously defined. The inelastic buckling stress is computed as the elastic buckling stress times n.

In checking the test data published by Schuette[7] on curved plates made of magnesium alloy, good agreement was obtained between the test results and those predicted by using the above value of n. It is interesting to note that in using this method, the accuracy of the predicted results was better than the accuracy obtained when the secant modulus method was used with the same data.[2]

b. Post-Buckling Behavior. The approximate buckling and post-buckling behavior of flat plates and columns that buckle inelastically is shown in Figure 2.3(b). Again, depending on the value of Z_b, the behavior of curved plates would be expected to be somewhere between that of a flat plate and a cylinder.

C. COMPRESSION MEMBERS CONSISTING OF FLAT AND CURVED ELEMENTS

Structural engineers are often faced with the problem of predicting the collapse load of compression members composed of both flat and curved elements. This problem is particularly evident for relatively "short" columns for which the critical buckling load is normally governed by local buckling or yielding of the individual elements of the cross section. If test results are not readily

available, the engineer usually determines the strength of the given cross section based on the summation of the local buckling strengths of the individual flat and curved plate elements.[13,21-23] This procedure is desirable because the buckling stress of each of the curved and flat elements may be predicted by using existing equations. The boundary conditions of the elements are assumed to be either simply supported, if they are bounded by other elements, or free. Figure 2.6 illustrates the assumed boundary conditions for some typical cross sections.

Two methods found in the literature for predicting the critical stress of cross sections composed of flat and curved elements are reviewed in the following discussion.

1. Air Force Method. The Air Force method assumes that curved elements, unlike flat elements, possess no post-buckling strength and thus, failure of the cross section is assumed when the critical stress is reached in a curved element. This method was originally published by Newell and Sechler[22] and can best be described by the following example:

If, in the cross section shown in Fig. 2.6(b), $f_{cr3}<f_{cr1}$ and $f_{cr3}<f_{cr2}$, then the critical stress will be

$$f_{cr} = \frac{f_{cr3}(2A_1 + 2A_2 + A_3)}{2A_1 + 2A_2 + A_3} = f_{cr3}. \qquad (2.10)$$

If $f_{cr1}<f_{cr3}$ and $f_{cr2}>f_{cr3}$, the critical stress will be

$$f_{cr} = \frac{f_{cr1}(2A_1) + f_{cr3}(2A_2 + A_3)}{2A_1 + 2A_2 + A_3}. \qquad (2.11)$$

If $f_{cr1}<f_{cr3}$ and $f_{cr2}<f_{cr3}$, the critical stress will be

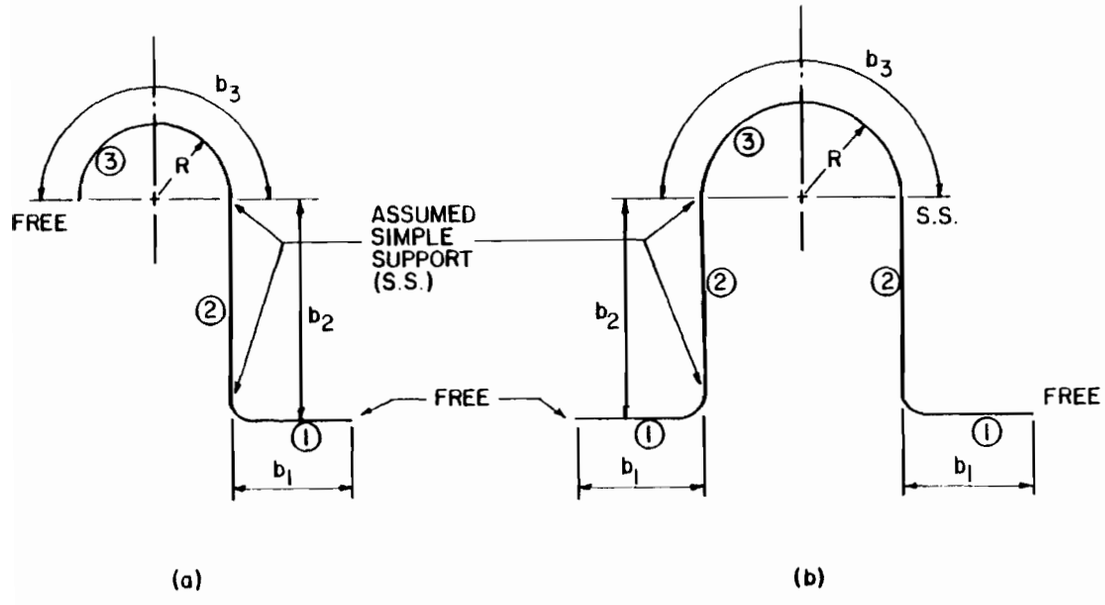

Fig. 2.6 Typical Cross-Sections Consisting of Flat and Curved Elements.

$$f_{cr} = \frac{f_{cr1}(2A_1) + f_{cr2}(2A_2) + f_{cr3}(A_3)}{2A_1 + 2A_2 + A_3} \quad . \tag{2.12}$$

In Equations (2.10) through (2.12), f_{cr1}, f_{cr2}, and f_{cr3} are the local buckling stresses of elements 1, 2, and 3 as shown in Figure 2.6(b). A_1, A_2, and A_3 are the respective areas of each element. The average stress over the entire cross section at which failure is predicted is f_{cr}.

As previously stated, the curved elements are assumed to have no post-buckling strength; thus, when the first curved element reaches its buckling stress, the total capacity of the section is obtained. Should a flat element buckle before the curved element, the flat element is assumed to carry its buckling load (without additional gain in post-buckling strength) until the critical stress is reached in a curved element. Of course, the maximum value of any of the above stresses is limited to the yield strength of the material.

2. Crockett's Method. A slightly different approach for predicting the critical stress of this type of cross section has been introduced by Crockett.[23] Crockett's method is based on a series of tests on aluminum sheet stiffeners when used alone or in combination with aluminum sheets. The tests results obtained with this method for the most part are within 15 percent of those predicted. The basic equation used to predict the critical stress is as follows:

$$F_{cc} = K \frac{\Sigma b_n t_n f_{cn}}{\Sigma b_n t_n} = KF_{ccl} \qquad (2.13)$$

in which:

F_{cc} = final predicted crippling stress, psi for $L/r < 20$

F_{ccl} = uncorrected predicted stress = $\Sigma b_n t_n f_{cn} / \Sigma b_n t_n$

K = the stability shape factor given in Table 1 of Ref. 23 and in Table 2.1 of Ref. 60

$b_n t_n$ = area of individual element, in^2.

f_{cn} = average ultimate stress of the individual element, given empirically by Figures 2 and 3 of Ref. 23 for flat and curved elements, respectively, psi

r = the radius of gyration of the stiffener about an axis parallel to the sheet in a stiffener-sheet combination, in.

L = length of stiffener or panel, in.

3. Comparison of the Air Force and Crockett's Method. There are two basic differences between Crockett's method and the Air Force method. The first is the introduction of the stability shape factor, K, by Crockett, which accounts for the differences in cross sectional shapes. The other is that Crockett's method does not limit the critical stress to that of the curved elements.

Because there is only a limited amount of published test data on the compression of cross sections with flat and curved elements, it is difficult to make any broad conclusions about the accuracy of either method. It does seem that the stability shape factor suggested by

Crockett would be desirable because it is obvious that cross sections with sloped elements would be less stable than those composed of straight elements. However, the fact that Crockett does not limit the critical stress of the cross section to that of the curved elements appears undesirable because curved elements are noted for their small post-buckling strengths.

In any event, the authors of both methods suggest that these procedures be used only for preliminary design. The adequacy of the final designs should be proven by tests.

4. Additional Literature. Other procedures, which may be useful for computing the compressive strength of members composed of flat and curved elements, consist of 1) an equation for the prediction of the compressive buckling stress of a curved flange by Buchert,[24] 2) a method developed by Needham[25] for compression members composed entirely of flat elements in which he divided the cross section into a series of angles in order to account for the cold work effect in the cold-formed corners, 3) an empirical approach used by Gerard[10] who presented the critical stress in terms of the number of corners in the cross section, and 4) the design criteria given by the Aluminum Association in the "Specification for Aluminum Structures"[26] for aluminum curved plates and elements.

D. EFFECTIVE WIDTH OF COMPRESSION ELEMENTS

The concept of an "effective width" was originally introduced by von Karman et. al.[27] to simplify the calculations needed to predict the ultimate strength of flat plates. Since that time, there has been a considerable amount of research performed in this area for flat plates;

however, the research data for curved plates are quite limited. Therefore, in the following sections, the effective width concept for flat plates is discussed to provide background information for possible future studies on the effective width of curved plates. Also, the available studies on the effective width of curved plates are briefly reviewed.

1. Flat Plates. For stiffened flat plates, which are supported along both longitudinal edges, such as the upper flange of a hat section, the stress distribution after buckling becomes nonuniform with the maximum stress occurring along the supported edges. With the application of more load, the maximum edge stress increases until the yield strength of the material is reached. At this point, the maximum post-buckling strength of the plate is normally assumed to be reached.[28] Figure 2.7 illustrates the different stress distributions in the plate as the load is progressively increased.

The effective width is defined as an imaginary width of plate, b_e, (as shown in Figure 2.8)[28], which, when loaded with the maximum edge stress, f_{max}, resists the same ultimate load as the full width plate described above. In other words,

$$\int_0^w f\,dx = b_e f_{max}. \qquad (2.14)$$

Because the actual stress distribution, f, across the full width of the buckled plate is not easily determined, approximate methods are employed to determine the effective width.

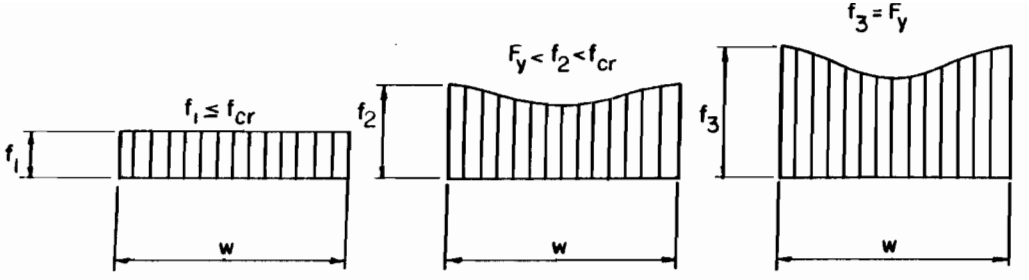

Figure 2.7 Consecutive Stages of Stress Distribution in Stiffened Flat Compression Elements[28]

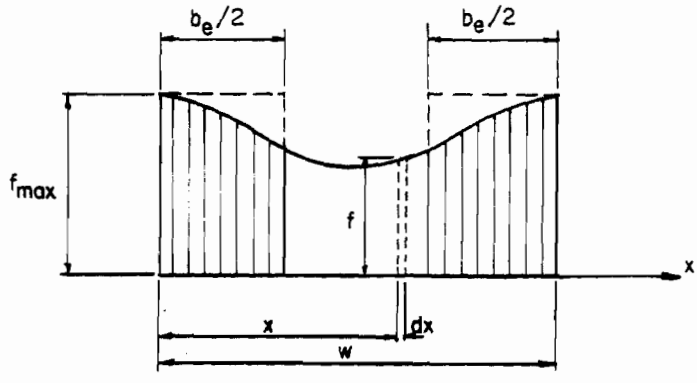

Figure 2.8 Effective Width of a Stiffened Flat Compression Element[28]

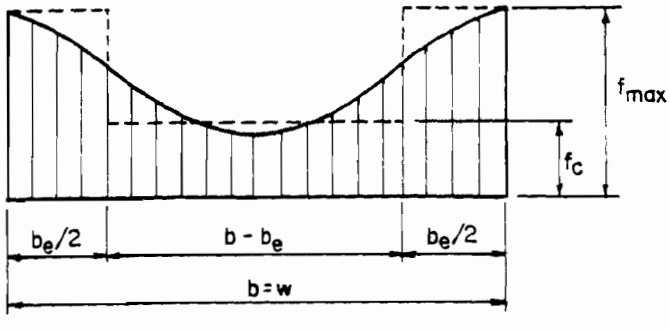

Figure 2.9 Effective Width of a Stiffened Curved Compression Element[36]

In 1932, von Karman[27] suggested that the effective width, b_e, can be approximated as the width of plate, which buckles just when the compressive stress reaches the yield point of the material. Therefore, based on this assumption, the effective width may be derived from the theoretical equation for the buckling of flat plates by setting $f_{cr} = F_y$, i.e.,

$$f_{cr} = F_y = \frac{\pi^2 E}{3(1-\mu^2)(b_e/t)^2} \quad . \tag{2.15}$$

Thus,

$$b_e = Ct\sqrt{\frac{E}{F_y}} = 1.9t\sqrt{\frac{E}{F_y}} \tag{2.16}$$

in which

$$C = \frac{\pi}{\sqrt{3(1-\mu^2)}} = 1.9$$

$\mu = 0.3$ = elastic Poisson's ratio

t = flat plate thickness

Based on an experimental investigation conducted by Winter[29] and much experience in the design of flat plates, [28,30] the constant, C, given in Equation (2.16) has been modified such that the revised effective width equation is as follows:

$$b_e = 1.9t\sqrt{\frac{E}{f_{max}}}\left[1-0.415(t/w)\sqrt{\frac{E}{f_{max}}}\right] \tag{2.17}$$

An equation similar to Equation (2.17) was developed by Winter[29] for the effective width of unstiffened flat compression elements. Unstiffened flat elements are supported along only one of the unloaded edges while the other unloaded edge is free. This equation is

$$b_e = 0.8t\sqrt{\frac{E}{f_{max}}}\left[1-0.202(t/w)\sqrt{\frac{E}{f_{max}}}\right]. \qquad (2.18)$$

Additional research conducted at Cornell University[32-34] has shown good agreement with Equation (2.18).

Equations (2.17) and (2.18) are replaced in the 1986 AISI Specification[31] for buildings by a single equation which can be used for both stiffened and unstiffened flat elements by specifying the value of the buckling coefficient, k, of the respective flat element. The effective width approach, as given in the 1986 Specification, is shown below.

$$b_e = w \quad \text{when } \lambda \leq 0.673 \qquad (2.19)$$

$$b_e = \rho w \quad \text{when } \lambda > 0.673 \qquad (2.20)$$

in which:

b_e = effective width, in. (Fig. 2.8)

w = full width of compression element, in.

t = thickness, in.

$\rho = (1-.22/\lambda)/\lambda$

λ is a slenderness factor determined as follows:

$$\lambda = \frac{1.052}{\sqrt{k}} \frac{w}{t} \sqrt{\frac{f}{E}}$$

f = actual stress at the edge of compression element, ksi.

k = 4.00 = buckling coefficient for stiffened flat elements; or

k = 0.43 = buckling coefficient for unstiffened flat elements depending on the application.

2. Curved Plates. As stated earlier, the available research data on the effective width of curved plates are limited. For values of $Z_b < 10$, Levy[16] showed that on the basis of a theoretical analysis, the effective width of curved plates is not appreciably different than for flat plates. This is not surprising because for buckling considerations, it has been shown in Section II.A that for $Z_b < 10$ the behavior of flat and curved plates is practically identical.

Based on test data collected by Ramberg et al.[35] for aluminum alloy curved plates, the effective width is approximately given by

$$\frac{b_e}{b} = \sqrt{K_c} \frac{t}{b} \sqrt{\frac{E}{f_e}} \qquad (2.21)$$

in which

b_e = effective width of curved plate

b = circumference of curved plate

t = thickness of curved plate

f_e = edge stress

$$K_c = \frac{\pi^2 k_c}{12(1-\mu^2)} \; ; \; k_c \text{ as determined in Ref. 2}$$

It should be noted that the above equation is good for Z_b ranges of 0 to 10 and 24 to 32 and for effective width ratios, b_e/b, in the range of 0.45 to 1.0.[35]

For effective width ratios less than approximately 0.45, the test data obtained by Jackson and Hall[3] for aluminum alloy curved plates seem to exhibit the following relationship for effective width:

$$\frac{b_e}{b} = K_p^{0.43} \left[\frac{t}{b} \sqrt{\frac{E}{f_e}} \right]^{0.85} \tag{2.22}$$

in which

K_p = buckling coefficient for flat plates, for a long plate with clamped edges $K_p = 6.3$

The data that form the basis for Equation (2.22) are obtained for $0 < Z_b < 125$.

Gerard[10] warned that Equations (2.21) and (2.22) should be used with caution for $Z_b > 30$ because of the limited range of Z_b in the tested specimens.

Another method for using the effective width concept to predict the ultimate strength of curved panels is given by Sechler and Dunn[13] and is applied in similar form by Barton.[36] For this method, the effective

width is defined in exactly the same manner as previously described for flat plates with the same developed width. However, unlike flat plates, curved panels are assumed to carry the critical buckling stress of a complete cylinder (with the same thickness and radius as the panel) over the width of panel between the assumed boundaries of the effective width. The assumed post-buckled stress distribution is shown in Figure 2.9.[36] Thus the ultimate load carrying capacity, P_{total}, is given by

$$P_{total} = b_e t f_{max} + (b - b_e) t f_c \tag{2.23}$$

in which

b_e = effective width of curved plate determined in the same manner as a flat plate with similar dimensions

f_{max} = maximum edge stress along the supported edge

f_c = the critical buckling stress of a complete cylinder with same thickness and radius as a curved panel

t = curved panel thickness

In Table 8.2 provided by Sechler,[13] the results of tests performed on aluminum curved panels at the Massachusetts Institute of Technology are compared to the values predicted by Equation (2.23) with f_{max} set equal to the yield stress of the material. The range of P_{total}/P_{test} was found to vary from 0.77 to 1.37; however, in most cases, the values of P_{total} and P_{test} did not differ by more than 10 percent.

By using the data presented in this Table[13], the range of Z_b was calculated to be 8.4 to 687. For values of Z_b appreciably greater than

this range (i.e., $Z_b > 1000$), there seems to be little use for the effective width concept because initial buckling and failure are coincident. According to Levy,[16] other studies of the post-buckling strength of curved plates are given by von Karman and Tsien,[37,38] Cox and Clemshaw,[39] Newell,[40] Ebner,[41] and Wenzek.[15]

E. CURVED PLATES SUBJECT TO SHEAR LOADING

1. Unreinforced Curved Plates. The buckling stress for an unreinforced curved plate loaded primarily in shear, such as the curved web of a beam, is considerably greater than the buckling stress for a flat plate of the same dimensions.[42] Just as for the axial compression of curved plates, the theoretical buckling stresses are usually greater than those observed experimentally. The following theoretical buckling stress equation was derived by Batdorf et al.[43] for the theoretical shear buckling stress, τ_{cr}, for curved plates:

$$\tau_{cr} = K_s E(t/b)^2 \tag{2.24}$$

in which K_s is a function of the length, circumference, radius, and thickness of the curved plate.

An empirical equation has been proposed in ANC-5[44] as:

$$\tau_{cr} = \frac{\pi^2}{12(1-\mu^2)} E(t/b)^2 K + K_1 E(t/R) \tag{2.25}$$

in which the first term represents the shear buckling stress for a flat

plate, and the last term the additional shear stress that the curved plate can resist because of its curvature. A value of $K_1 = 0.10$ is recommended.[44] The value of K is defined below.

Another approach for estimating the buckling stress of a curved panel subject to shear loading is given by Gerard in Reference 4. According to Gerard, if $Z_b < 30$, the curved panel may be conservatively assumed to buckle at the shear buckling stress of a flat element with similar dimensions. In other words,

If $Z_b \leq 30$,

$$\tau_{cr} = (\tau_{cr})_f. \tag{2.26}$$

If $Z_b > 30$,

$$\tau_{cr} = 0.37(\sqrt{Z_b})(\tau_{cr})_f \tag{2.27}$$

in which

τ_{cr} = critical shear buckling stress of a curved panel

$(\tau_{cr})_f$ = critical shear buckling stress of a flat panel

$$= \frac{\pi^2}{12(1-\mu^2)} E(t/b)^2 K$$

If $a/b > 1$, $K = 5.34 + 4(b/a)^2$

If $a/b < 1$, $K = 4.00 + 5.34(b/a)^2$

a = axial length of curved panel

b = circumferential width of curved panel

$Z_b = (b^2/Rt)\sqrt{(1-\mu^2)}$

It should be noted that the above equations were developed for curved panels subject to pure shear loading such as would be obtained in torsion. Also, each of the equations was developed for elastic buckling. Obviously, some modification must be made for inelastic buckling.

2. Longitudinally Stiffened Curved Plates. There has been some study of curved plates with longitudinal stiffeners in which the "tension field"[42] concept is employed. In the pure tension field concept, as proposed by Wagner and Ballerstedt,[45] the curved plate is assumed to be completely flexible. Thus, its compressive strength is considered negligible, and the curved plate is assumed to buckle freely at an angle of 45° to the shear stress (i.e., the direction of maximum compressive stress caused by pure shear). Because even very thin, curved webs have appreciable in-plane stiffness, this assumption is generally considered invalid. Thus a "semi-tension field" analysis is normally employed in which the compressive stiffness of curved webs is taken into consideration. Semi-empirical methods of analysis and design for longitudinally stiffened curved webs are given by Kuhn and Griffin.[46]

III. STRUCTURAL BEHAVIOR OF MEMBERS CONSISTING OF CURVED ELEMENTS

A. GENERAL

Because of the extreme difficulty in the accurate analytical prediction of the local buckling stress of curved elements, it seems that any reasonable prediction equation must be empirical or at least semi-empirical in nature. Thus, a series of tests have been performed for sections containing either stiffened or unstiffened curved elements. The stiffened curved elements were subjected to three different loading conditions. They were: (1) uniform axial compression, (2) bending, and (3) shear. Only the conditions of uniform axial compression and bending were tested for the unstiffened curved elements. A complete discussion of each of these tests is included in Section III.B.

Based on the results of these tests, semi-empirical methods have been developed for the prediction of the local buckling stress of curved elements. These methods are described in Section III.C.

B. EXPERIMENTAL INVESTIGATION OF CURVED ELEMENTS

1. Summary of All Curved Element Test Specimens. All of the curved element specimens were formed by Wania Ornamental Wire and Iron Co. in St. Louis, Missouri. A press brake operation, which employed a series of circular "pipe" dies, was used to form the curved elements. The mechanical properties of the six materials used in these specimens

are listed in Table 3.1. Figure B.1 provides a comparison of the stress-strain curves of each material as determined from longitudinal compression coupon tests. Table 3.2 lists the nominal cross-sectional dimensions for each type of specimen. The number of tests that have been performed are given in Table 3.3. As shown in Table 3.3, a total of 127 specimens have been tested for the local buckling of curved elements. Typical cross-sections for each type of specimen are shown in Figures 3.1 through 3.4.

The specimen designation is best explained by the following example. For the 80DKAS3-1 specimen, the first four characters represent the AISI material designation.[47] The next two characters, "AS", in this case, show that the specimen is fabricated from the "A" profile (Figure 3.1) and that it is used as a stub column specimen. If an "I" follows these two characters, that signifies that the specimen is used to determine the interaction between the local buckling of the flat and curved elements in that particular specimen. The following digit represents the flange curvature (for instance, "3" signifies R = 2 in. for the AS3 profile, see Table 3.2). Finally, the last digit designates the specimen number for each type of section. Note that, for the two 50XF materials, the nominal thickness (in thousandths of an inch) is also included in the specimen designation (in parenthesis) to distinguish between the two materials.

The radii of the curved flanges were measured by two different methods, depending on the curvature. For the relatively flat curvatures (R > 4 in.), the curvature was measured by first tracing the outline of the curve and then graphically determining the radius. For the sharper

Table 3.1 Material Properties and Thicknesses of Six Sheet Steels Used for Curved Element Tests

Material Designation	$(F_{pr})_c$ (ksi)	$(F_y)_c$ (ksi)	$(F_y)_t$ (ksi)	$(F_u)_t$ (ksi)	Elongation (%)	t (in.)
80XF	77.1	89.4	88.3	98.7	22.8	0.082
50XF(78)	49.1	63.6	57.2	66.5	27.3	0.078
80SK	53.0	75.4	82.2	88.8	12.7	0.061
80DK	45.9	54.1	58.2	87.6	25.7	0.048
50XF(39)	41.4	58.9	54.2	63.1	33.3	0.039
30SK	16.4	26.8	26.5	44.7	45.7	0.030

Notes:

1) $(F_{pr})_c$ and $(F_y)_c$ are based on longitudinal compression coupon tests.

2) $(F_y)_t$, $(F_u)_t$, and Elongation are determined from longitudinal tension coupon tests.

3) Elongation was measured over a 2-in. gage length.

Table 3.2 Nominal Dimensions of Test Specimens Consisting of Curved Elements

Specimen No.	R (in.)	b (in.)	Length (in.)	Load Type
AS1	15	4.01	13	Compression
AS2	3.5	4.26	13	Compression
AS3	2	6.29	13	Compression
ASI1	15	4.01	13	Compression
ASI2	3.5	4.26	13	Compression
ASI3	2	6.29	13	Compression
AB1	15	4.01	60	Bending
AB2	3.5	4.26	60	Bending
AB3	2	6.29	60	Bending
BS1	15	4.01	13	Compression
BS2	3.5	4.26	13	Compression
BS3	2	6.29	13	Compression
BV1	15	4.01	30	Shear
BV2	3.5	4.26	30	Shear
BV3	2	6.29	30	Shear
CS1	4	2.02	12	Compression
CS2	1.25	2.32	12	Compression
CS3	1	3.14	12	Compression
CSI1	4	2.02	12	Compression
CSI2	1.25	2.32	12	Compression
CSI3	1	3.14	12	Compression
CB1	4	2.02	60	Bending
CB2	1.25	2.32	60	Bending
CB3	1	3.14	60	Bending
DB1	2	3.14	60	Bending
DB2	2	4.19	60	Bending

Table 3.3 Number of Tests for Each Material

Specimen No.	Material Designation						
	30SK	50XF(39)	50XF(78)	80SK	80DK	80XF	Total
AS1	2	2	2	-	2	-	8
AS2	1	1	1	-	1	-	4
AS3	1	1	1	-	1	-	4
ASI1	0	1	1	-	1	-	3
ASI2	1	1	1	-	1	-	4
ASI3	1	1	1	-	1	-	4
AB1	1	1	1	1	1	1	6
AB2	1	1	1	1	1	1	6
AB3	1	1	1	1	1	1	6
BS1	-	-	-	1	-	1	2
BS2	-	-	-	1	-	1	2
BS3	-	-	-	1	-	1	2
BV1	1	1	1	-	1	-	4
BV2	1	1	1	-	1	-	4
BV3	1	1	1	-	1	-	4
CS1	1	1	2	2	1	2	9
CS2	1	1	1	1	1	1	6
CS3	1	1	1	1	1	1	6
CSI1	1	1	0	0	1	0	3
CSI2	1	1	1	1	1	1	6
CSI3	1	1	1	1	1	1	6
CB1	1	1	1	1	1	1	6
CB1	1	1	1	1	1	1	6
CB3	1	1	1	1	1	1	6
DB1	1	1	1	-	1	1	5
DB2	1	1	1	-	1	1	5
TOTAL	23	24	24	15	24	17	127

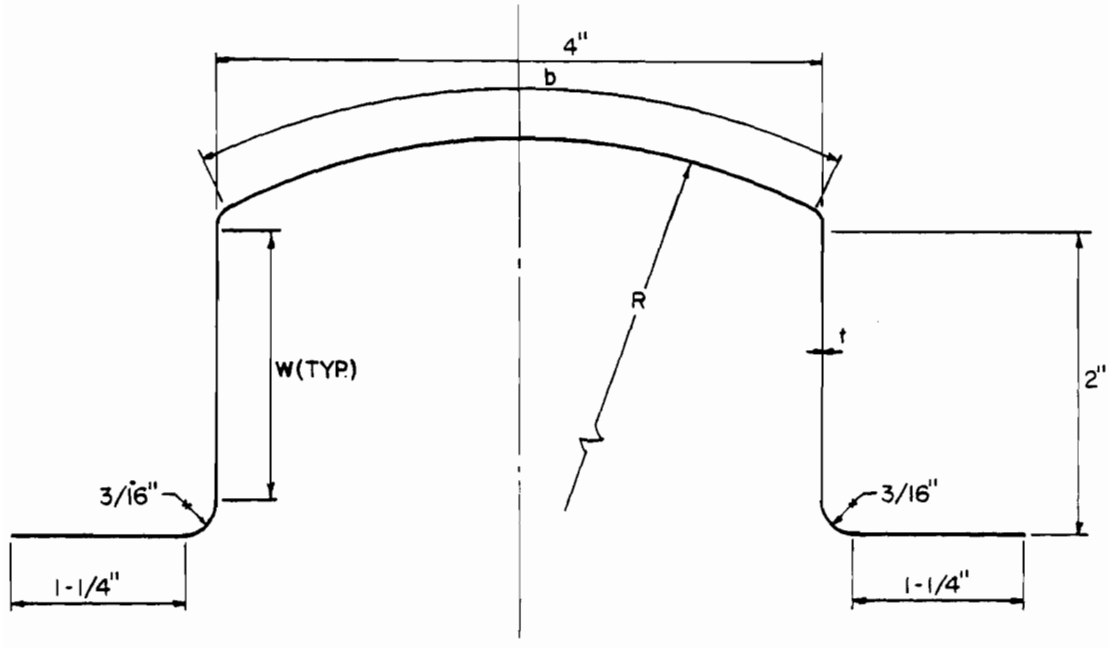

Figure 3.1 Nominal Dimensions of AS, ASI, and AB Profiles

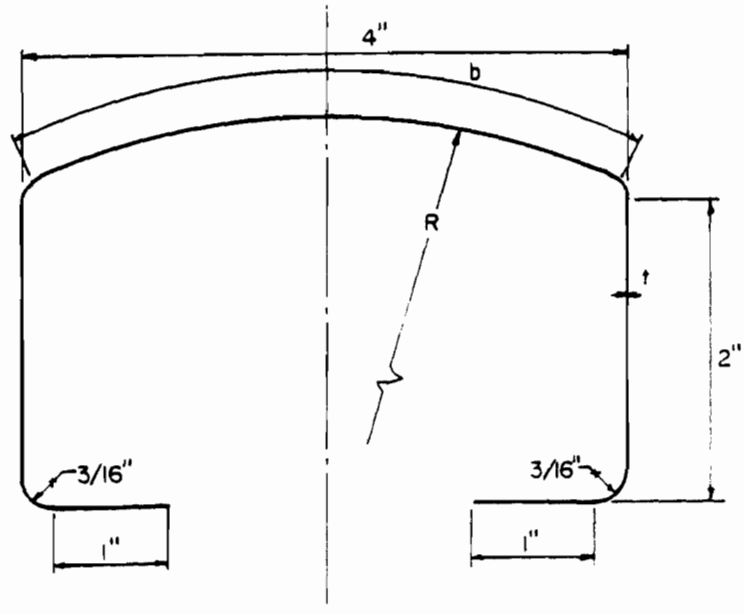

Figure 3.2 Nominal Dimensions of BS and BV Profiles

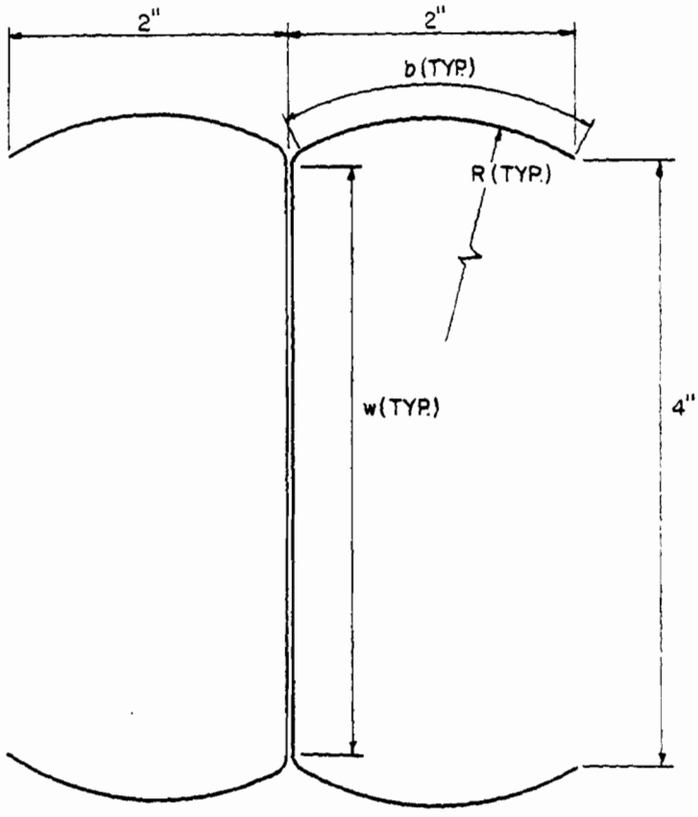

Figure 3.3 Nominal Dimensions of CS, CSI, and CB Profiles

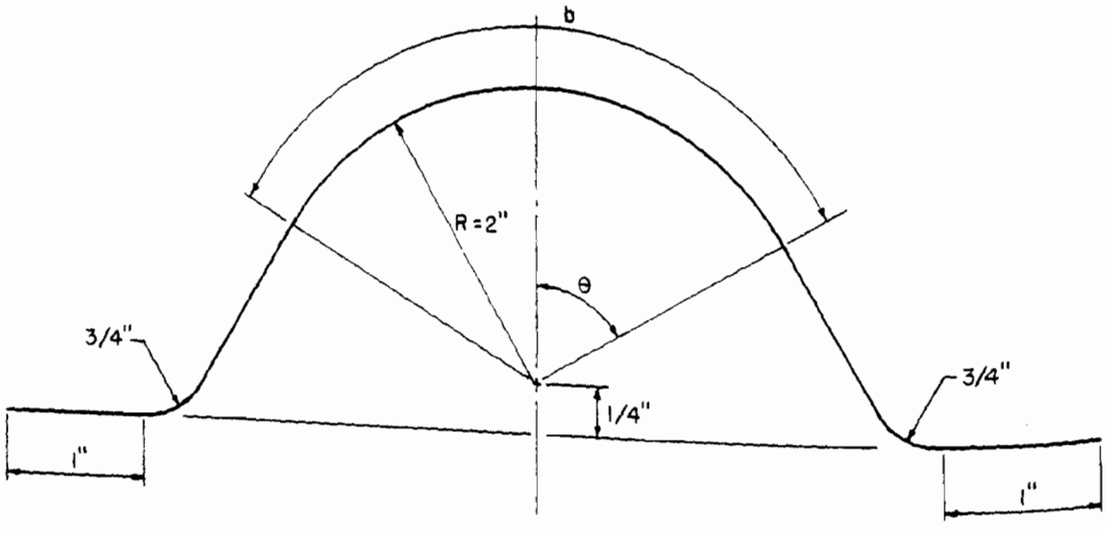

Figure 3.4 Nominal Dimensions of DB Profiles

curvatures, the radii could be more accurately determined by measuring the arc and chord lengths of the flanges and then computing the radii based on these values.

2. Stiffened Curved Elements.

a. Description of Stub Column Tests for Initial Stiffened Curved Element Failure - AS Specimens.

i. Specimens. Because of a limited supply of specimens, both the AS and BS profiles were used for the stiffened curved element stub column tests. As shown in Figures 3.1 and 3.2, the AS and BS profiles are identical except for the lower flange stiffeners. Table 3.3 lists the type of profile used for each material. As shown in Table 3.3, a minimum of one test has been performed for each material and curvature. Table 3.2 lists the three different curvatures of the curved flanges (R = 2, 3.5, or 15 in.). The three curvatures of the AS specimens may be compared in Figure 3.5. Table A.1 provides the measured cross sectional dimensions of the AS specimens. A total of 22 specimens were tested for the initial buckling of stiffened curved elements. Because the AS and BS profiles are identical, as far as the curved elements are concerned, all of the stub column specimens for initial buckling of stiffened curved elements will, henceforth, be referred to as "AS" specimens. The AS stub columns were approximately 13 in. long.

As shown in Figure 3.6, the AS specimens were fabricated by connecting the unstiffened flat flanges of two identical "hat" sections. Vertical bracing (3/4 X 3/4 X 1/8 in.) was attached to the flat webs in order to prevent premature web buckling. Each brace was connected to the respective web by three 1/4-in. diameter bolts. The

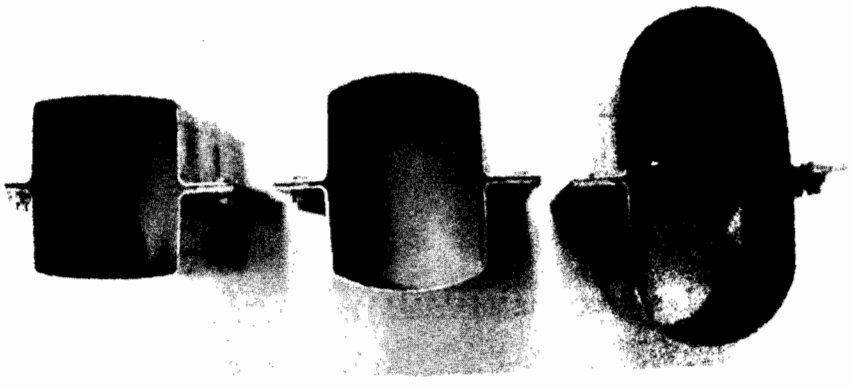

AS1
ASI1

AS2
ASI2

AS3
ASI3

Figure 3.5 Comparison of Three Curvatures of Stiffened Curved Elements

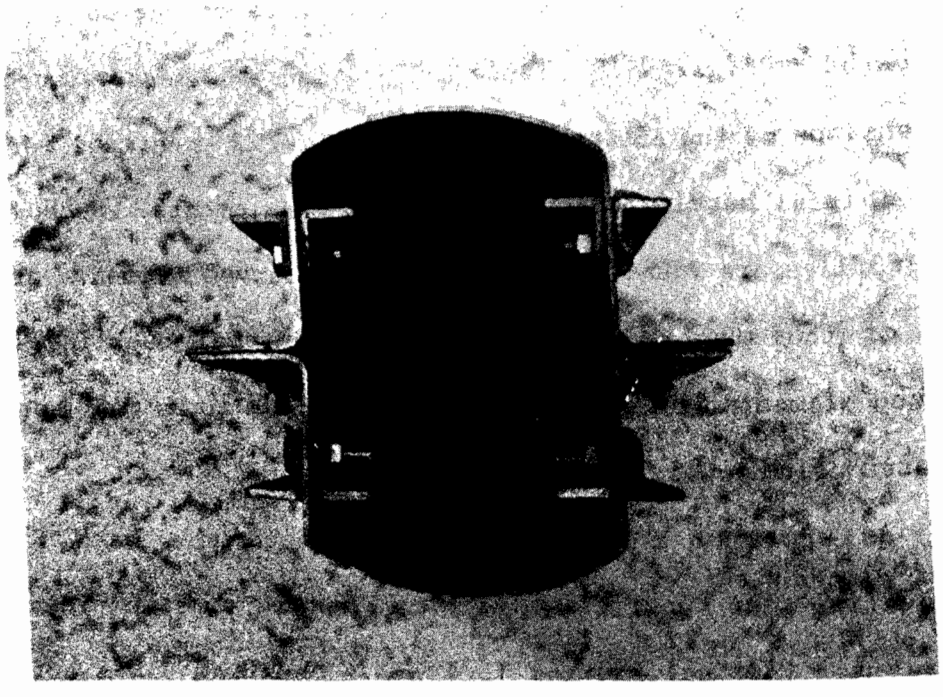

Figure 3.6 Typical Cross Section for the AS Stub Column Specimens

upper and lower bolt holes were elongated so that no load could be transferred from the web to the bracing. Also, a thin layer of aluminum foil, coated with WD-40, was placed between each brace and the web. Using this procedure, it was impossible for the bracing to carry any appreciable load.

The ends of the AS stub column specimens were milled flat and parallel, with their longitudinal axis perpendicular to the milled ends. Flatness of the ends was checked by placing the stub columns on a flat, level surface and observing any rocking or light that might be visible between the specimen and the flat surface. If the ends were not found to be flat, the milling procedure was repeated until the ends were made as flat as possible.

ii. Strain Measurements. A total of twelve strain gages were used to measure strains at midheight of the stub column specimens. The gage locations are shown in Figure 3.7. The critical buckling stress for the curved elements was determined by using the modified strain reversal method (described in Ref. 48) for the strain output of the paired gages located in the middle of each flange. According to the strain reversal method, buckling is obtained when the magnitude of the strain recorded from one of the paired gages begins to decrease.

Additional strain gages were placed at the edge of the curved elements so that the average strains associated with buckling could be measured. All of the strain gages were used in the procedure for aligning the specimens.

iii. Waving and Deformation Measurements. Out-of-plane waving of the curved flanges was recorded at twelve points along the middle of

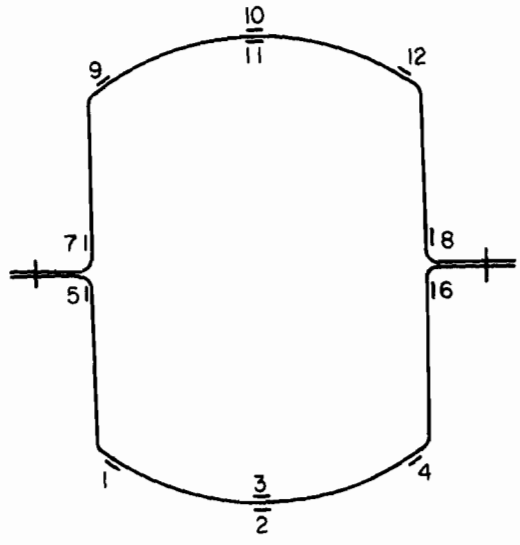

Figure 3.7 Location of Strain Gages for AS Stub Column Specimens

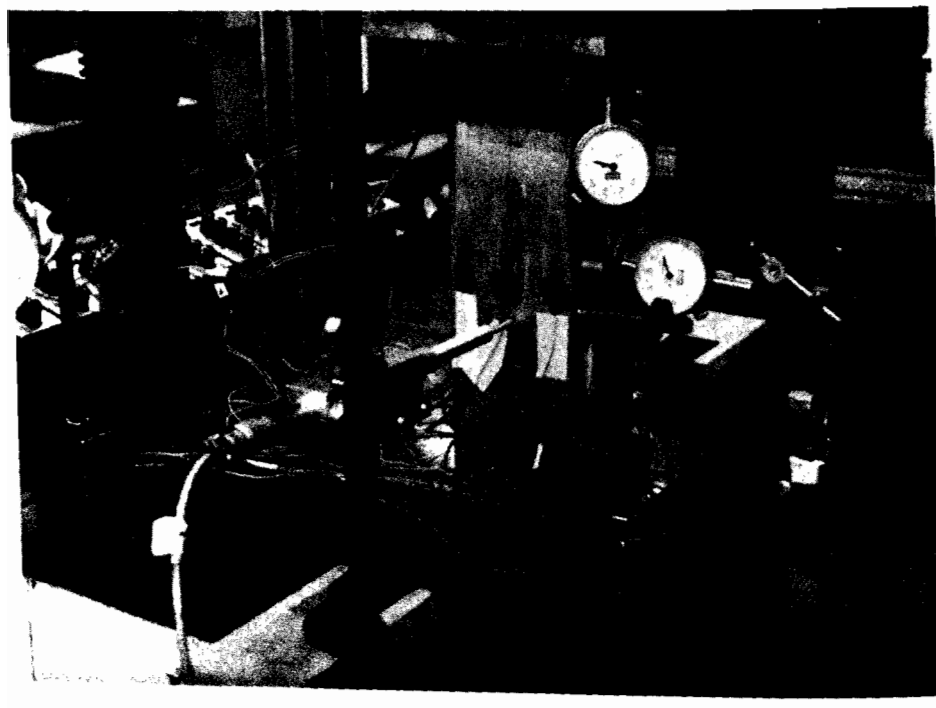

Figure 3.8 Test Setup for AS and ASI Stub Column Specimens

each flange. At each point, the wave deformation was measured by a horizontally mounted linear variable differential transformer (LVDT) that was attached to a moveable vertical stand. The heigth of the LVDT was adjusted by sliding along the vertical stand. Figure 3.8 shows the completed test setup for the measurement of waving. In order to measure waving of both curved flanges, the base of the stand was placed in a slotted block adjacent to each flange. The widths of the slots were such that the vertical stand base fit snuggly in the slot and thus no torsional rotation of the stand could occur. The purpose of the slotted blocks was to maintain a fixed reference point from which waving could be measured.

Before testing, the LVDT (with vertical stand base in the slotted block) was oriented such that its axis was perpendicular to the desired flange; the slotted block was then clamped to the base of the testing machine. After clamping, the vertical stand could be moved to the other flange and the same procedure repeated there. Using the above procedure, both the wave depth and shape could be determined for any load level. Wave readings, taken at a small preload, were particularly useful as a measure of initial imperfection of the curved elements.

Wave readings were recorded at four typical levels for each of the stub column tests: (1) at the beginning of each test (under a slight preload), (2) at approximately half the predicted failure load, (3) shortly after initial buckling of the first curved flange, and (4) at overall failure of the specimen. In many cases, (3) and (4) occurred simultaneously such that only one set of readings was possible at failure.

Also, lateral deflection at midheight of one of the curved flanges and cross head movement were recorded at load level. These measurements were used to monitor the overall performance of the specimen and to check the appropriate instrumentation.

iv. Equipment and Testing Procedure. All but five of the AS stub column specimens were tested in the 120,000 pound capacity Tinius Olsen testing machine located in the Engineering Research Laboratory at UMR. Figure 3.9 shows the testing machine along with the remaining equipment used in the stub column tests. The five remaining specimens, because of their relatively high expected failure load, were tested in a 200,000 pound capacity Tinius Olsen testing machine located in the Materials Laboratory of the Civil Engineering Building at UMR. The accompanying equipment was exactly the same as shown in Figure 3.9.

An Electronics/Ltd., 40 channel data acquisition system (Figure 3.10) was used to measure the strain gage output. An additional acquisition system (Figure 3.11) measured the load output from the Tinius Olsen machine and the waving from the LVDT. An IBM Personal Computer (Figure 3.12) was used to coordinate the electronic equipment and store the load, strain, and wave output at each load level.

Before fabrication, each of the paired A profiles were measured individually as described in Section III.B.1. Once measured, the hat sections were connected as previously described, and their ends milled flat. After attaching the strain gages, the stub column was placed in the Tinius Olsen machine. Flat, hardened steel base plates provided the bearing surface for the ends of the specimens. The strains were made uniform over the stub column cross section by the following procedure.

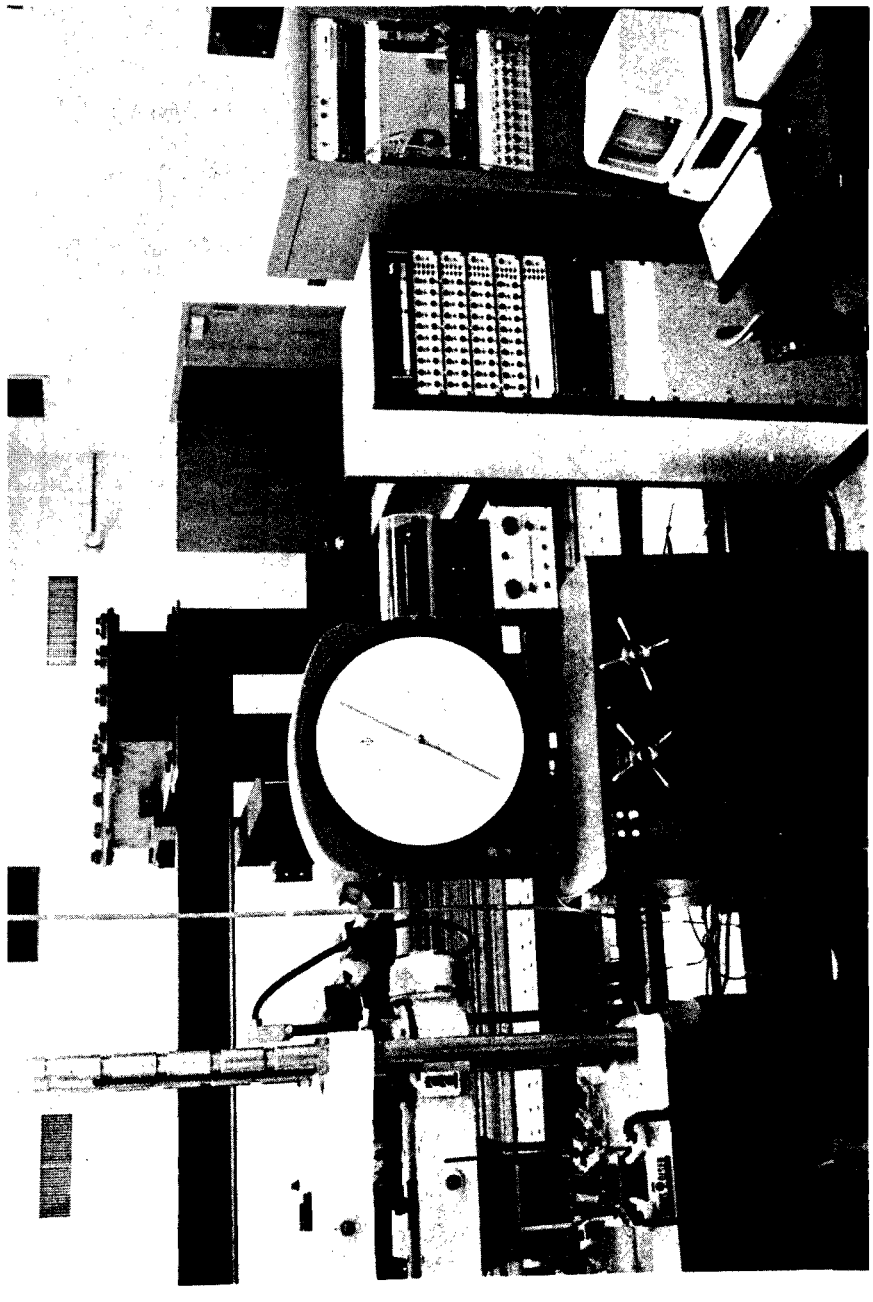

Figure 3.9 Equipment Used in Curved Element Tests

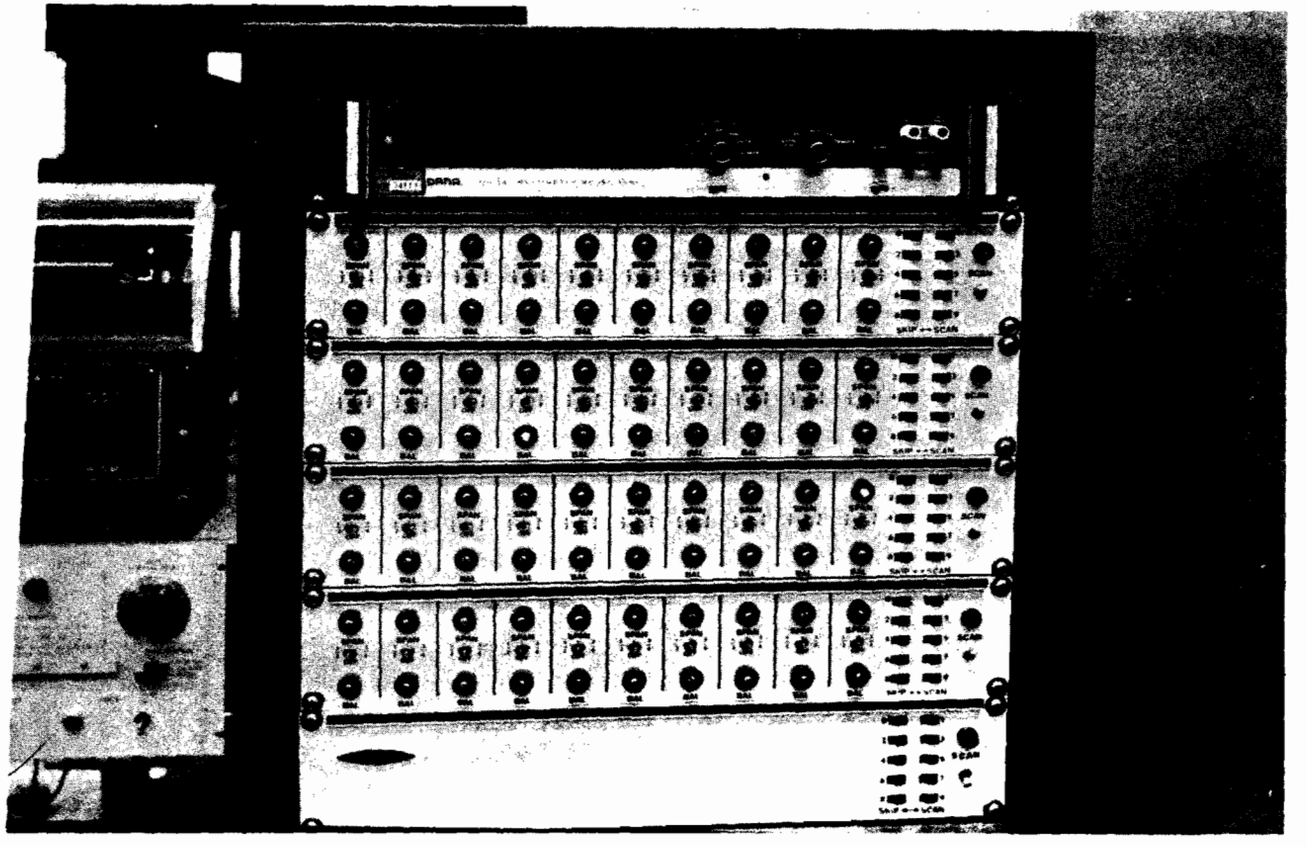

Figure 3.10 40 Channel, Electronics/Ltd. Data Acquisition System

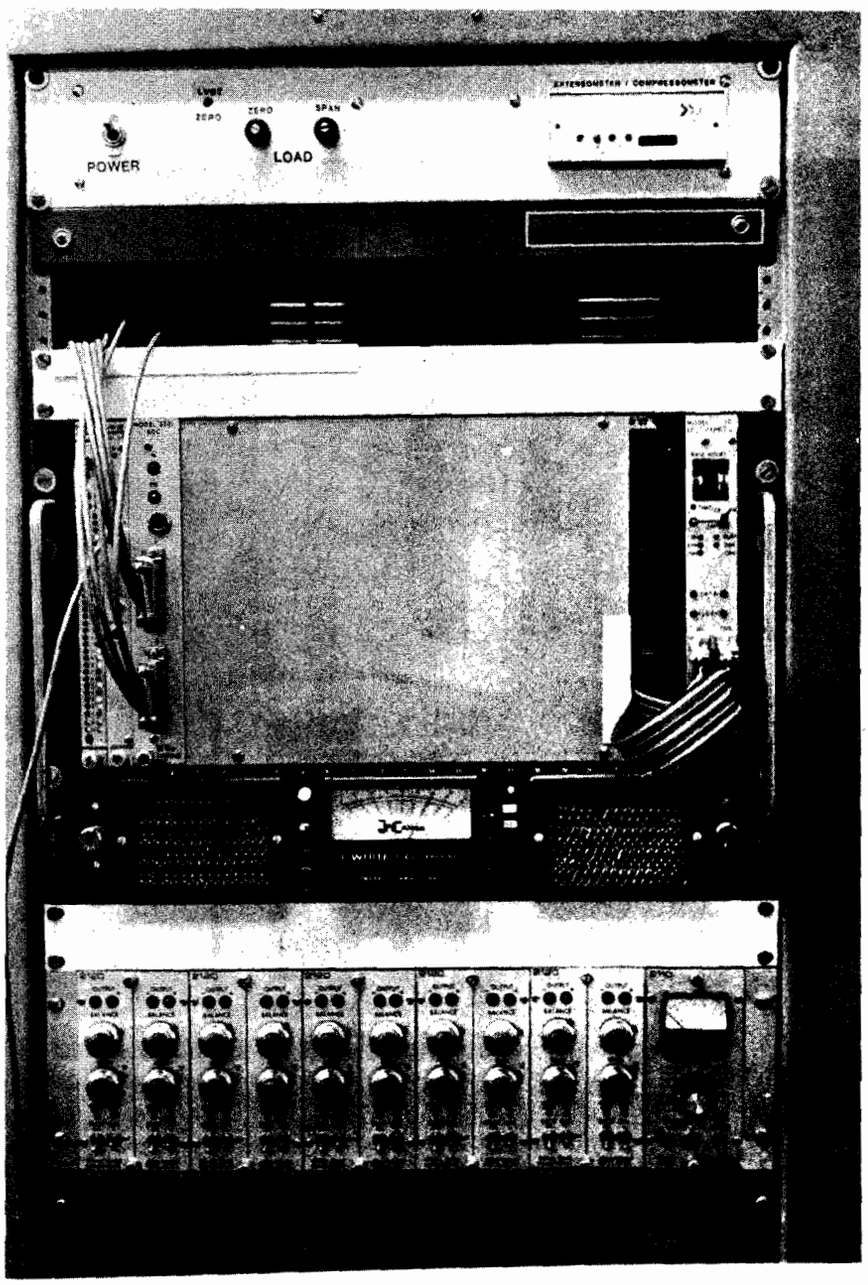

Figure 3.11 Data Acquisition System
Used for Load and Waving

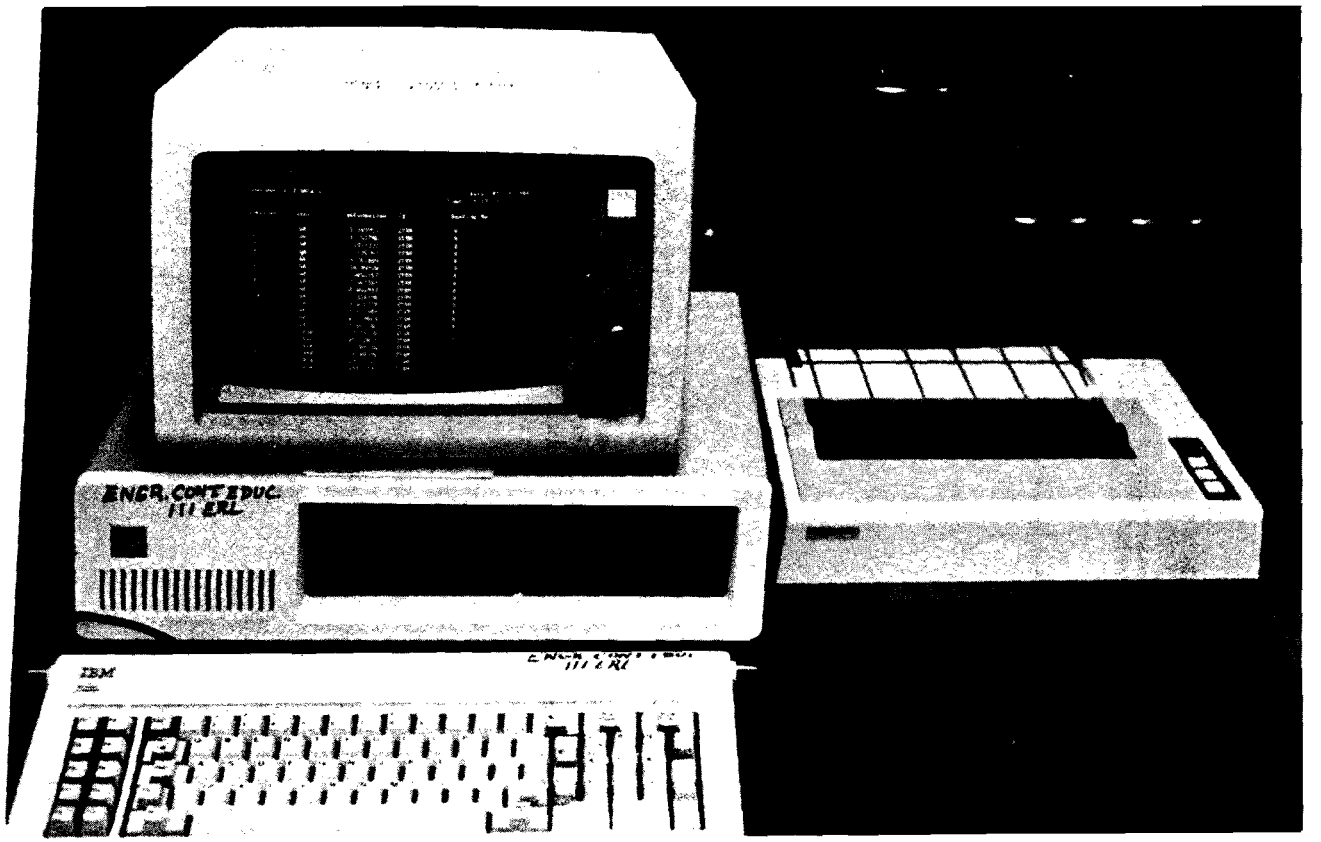

Figure 3.12 IBM Personal Computer

First, a small preload was applied and the resulting strains recorded for all strain gages. If necessary, thin layers of aluminum foil were added to the ends of the stub columns in the regions of low strain. This procedure was repeated until the strain distribution was essentially uniform over the cross section.

Next, the slotted blocks, which were used in the measurement of waving, were positioned and then clamped to the lower plate of the Tinius Olsen machine. The test setup is shown in Figure 3.8. At this point the test was ready to begin.

As mentioned earlier, the load was applied by either a 120,000 or 200,000 pound capacity Tinius Olsen testing machine. The load increments were such that a minumum of ten load levels were measured before failure of the specimen. Between load levels, the load was increased very slowly so that any strain rate effect on the mechanical properties was negligible. Once the desired load level was reached, the load was held constant for a period of time to allow the specimen to stabilize.

At each load level, load and the corresponding strains were recorded and stored by the computer. Wave readings were measured by the LVDT as described in Section III.B.2.a.ii at the beginning of the test, at approximately one-half of the failure load, and at or close to failure of the specimen. Between wave readings, a stationary dial gage, placed near midheight of one of the curved flanges, was used to monitor the movement of the flange. Also measured at each load level was the cross head movement. The ultimate load was taken directly from the Tinius Olsen machine as the maximum load that the specimen could withstand.

v. Typical Failure Modes. Two types of failure modes occurred for the stiffened curved elements. For the flatter curvatures of the stiffened curved elements, local buckling normally occurred in the elastic range (or just slighty into the inelastic range). The resulting failure mode was in the form of a diamond. This type of failure seems reasonable since the diamond buckle pattern is commonly observed for cylinders with relatively large R/t ratios. The failure was very sudden with a sharp drop in the load withstood by the specimen. A loud "pop" accompanied the elastic buckling failure. Figure 3.13 shows a typical failure of this type.

A wrinkling type of failure was observed for the highly curved elements that failed well into the inelastic range. As might be expected, the failure was much more gradual than the diamond buckling mode. Figure 3.14 shows a typical wrinkling failiure. Again, this type of failure is not unexpected since the wrinkling (or "ring") mode of failure occurs for cylinders with relatively small R/t values.[49] Table 3.4 provides a summary of the failure modes in the curved elements of each AS specimen.

Very little, if any, waving of the stiffened curved elements occurred before initial buckling. A possible physical explanation of the relatively small waving of curved elements, as compared to flat elements of similar dimensions, is the increased stiffness transverse to the length of the element provided by the curvature. A typical plot of waving along the longitudinal axis of a stiffened curved element is given in Figure B.2.

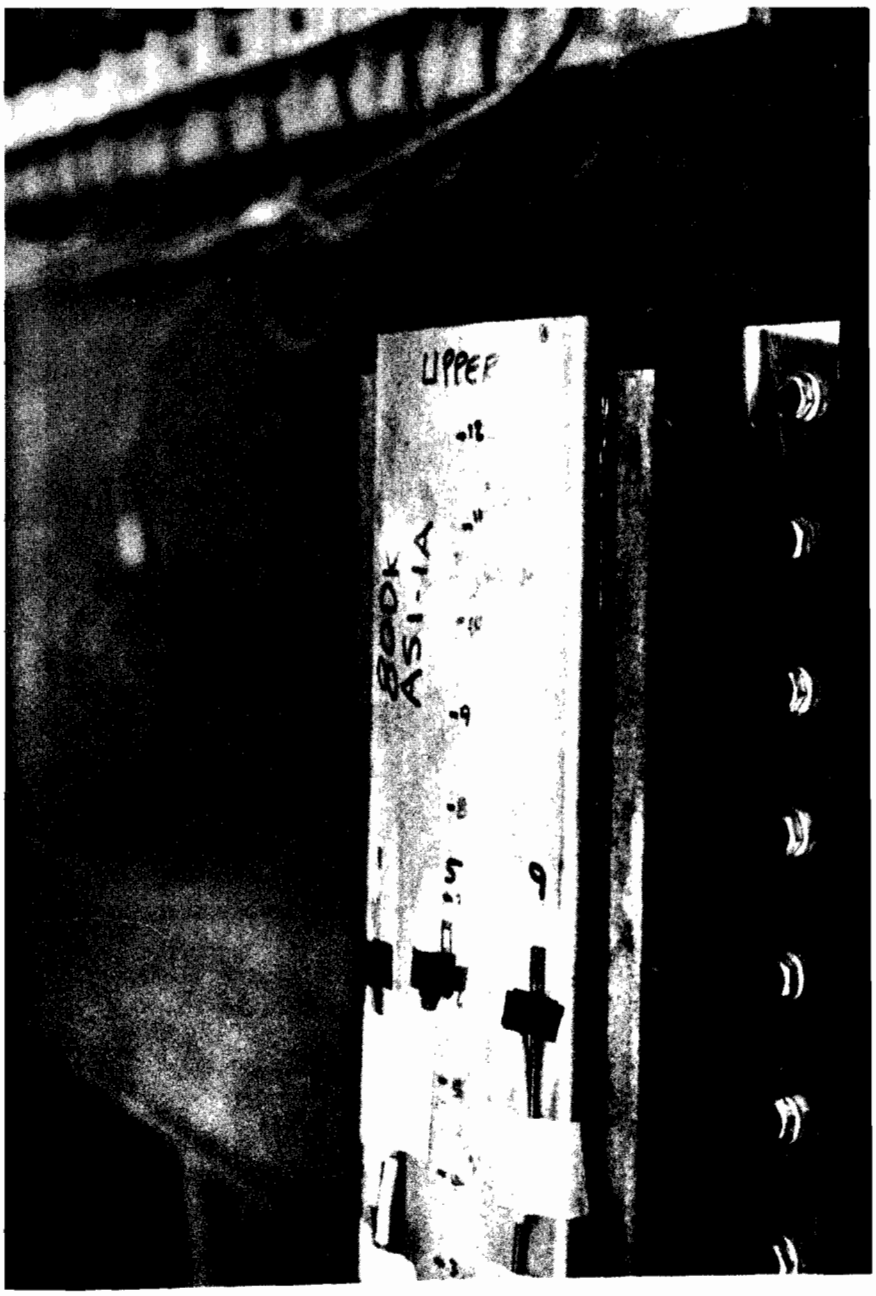

Figure 3.13 Typical Diamond Buckle Pattern

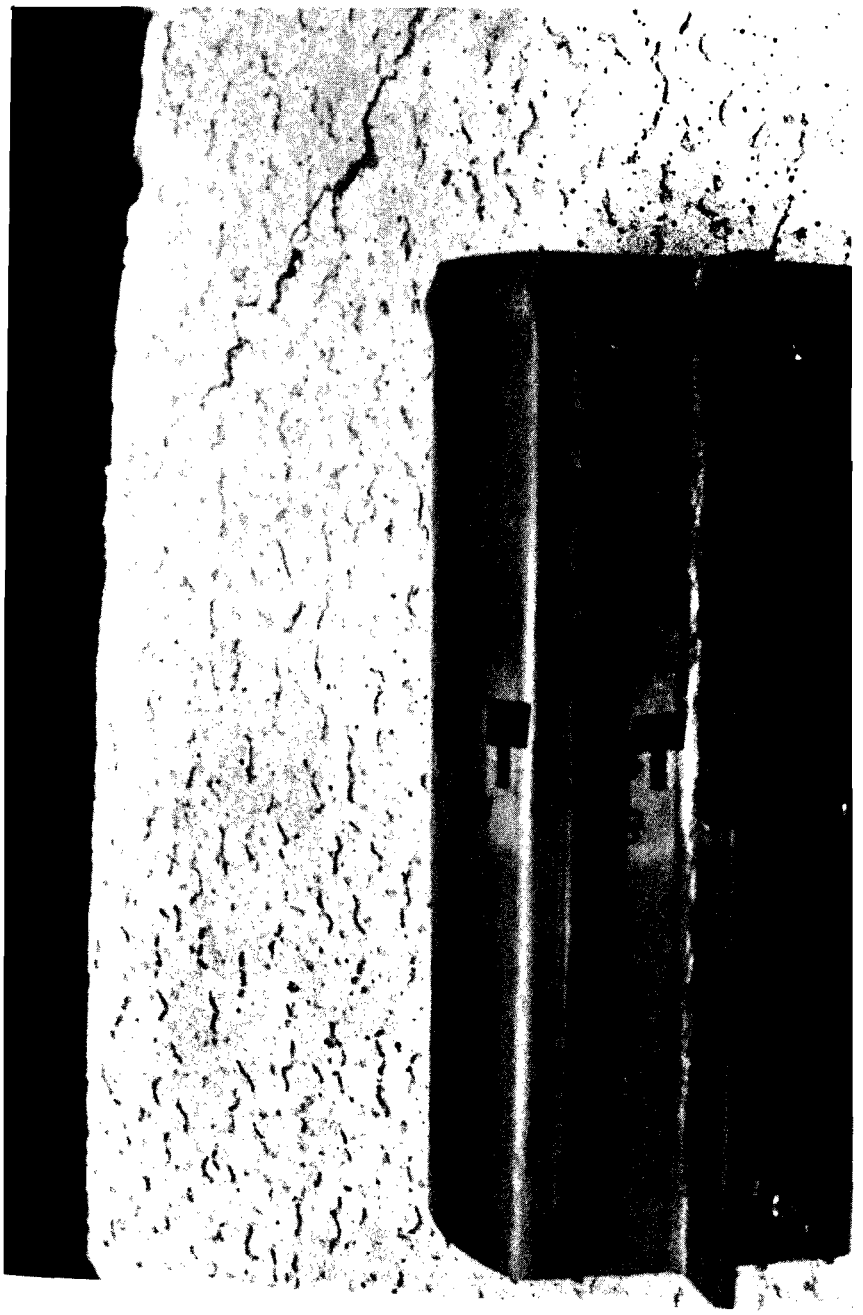

Figure 3.14 Typical Wrinkling Failure

Table 3.4 Failure Modes Observed in the AS Specimens

Specimen	Failure Mode	Type of Failure
80XFBS3-1	Wrinkle	Inelastic
50XF(78)AS3-1	Wrinkle	Inelastic
80SKBS3-1	Wrinkle	Inelastic
80DKAS3-1	Wrinkle	Inelastic
50XF(39)AS3-2	Wrinkle	Inelastic
30SKAS3-1	Wrinkle	Inelastic
80XFBS2-1	Wrinkle	Inelastic
50XF(78)AS2-1	Wrinkle	Inelastic
80SKBS2-1	Wrinkle	Inelastic
80DKAS2-1	Diamond	Inelastic
50XF(39)AS2-1	Wrinkle	Inelastic
30SKAS2-1	Wrinkle	Inelastic
80XFBS1-1	Diamond	Inelastic
50XF(78)AS1-1	Diamond	Inelastic
50XF(78)AS1-2	Diamond	Inelastic
80SKBS1-1	Diamond	Inelastic
80DKAS1-1	Diamond	Inelastic
80DKAS1-2	Diamond	Elastic
50XF(39)AS1-1	Diamond	Elastic
50XF(39)AS1-2	Diamond	Elastic
30SKAS1-1	Diamond	Elastic
30SKAS1-2	Diamond	Elastic

Note:

Inelastic failure indicates that the average stress upon local buckling exceeded the proportional limit of that particular material. Elastic failure, on the other hand, indicates that the average stress at local buckling was less than the proportional limit of that particular material.

As mentioned earlier, the cross head movement of the Tinius Olsen calculations, the cross head movement was monitored in order to detect the onset of any nonlinear behavior in the specimen. As expected, buckling of the curved flanges occurred soon after the beginning of nonlinear cross head movement. Figure B.3 shows a typical plot of load versus cross head movement.

b. Description of Stub Column Tests for the Interaction Between Stiffened Flat and Curved Elements - ASI Specimens.

i. Specimens. The ASI stub column test specimens for the interaction between stiffened curved and flat elements are identical to the AS specimens. The only exception is the omission of the vertical bracing that was attached to the flat webs to prohibit their buckling. Therefore, in some cases, the flat webs of the ASI specimens actually buckled before the curved elements. The interaction between the local buckling of stiffened flat and curved elements could be observed as a result of these tests. The number of tests performed for each material and curvature is shown in Table 3.3. As shown, a total of 11 ASI stub column tests were performed. Table 3.2 lists the three basic radii of the curved flanges (R = 2, 3.5, or 15 in.). The three curvatures of the ASI specimens may be compared in Figure 3.5. Table A.2 provides the measured cross sectional dimensions for the ASI specimens.

Just as for the AS stub columns, the ends of the ASI stub column specimens were milled flat and parallel, with their longitudinal axis perpendicular to the milled ends. Flatness of the ends was checked by placing the stub columns on a flat, level surface and observing any rocking or light that might be visible between the specimen and the flat

surface. If the ends were not found to be flat, the milling procedure was repeated until the ends were made as flat as possible.

ii. Strain Measurements. A total of sixteen strain gages were used to measure strains at midheight of the stub column specimens. The gage locations are shown in Figure 3.15. Note the addition of paired strain gages to either side of the flat element as well as on the curved element. Using these gages, the critical buckling stress of any of the elements could be determined by using the modified strain reversal method (described in Ref. 48).

Additional strain gages were placed at the edge of the curved elements so that the average strains associated with buckling could be measured. All of the strain gages were used in the procedure for aligning the specimens.

iii. Waving and Deformation Measurements. Out-of-plane waving of the curved flanges was recorded at twelve points along the middle of each flange. At each point, the wave deformation was measured by a horizontally mounted linear variable differential transformer (LVDT) using the same procedure as previously described for the AS stub column specimens. The cross head movement was also recorded at each load level.

iv. Equipment and Testing Procedure. Exactly the same equipment and testing procedure was used for the ASI stub column tests as was previously described for the AS stub columns. The test setup for the ASI stub column tests is shown in Figure 3.8.

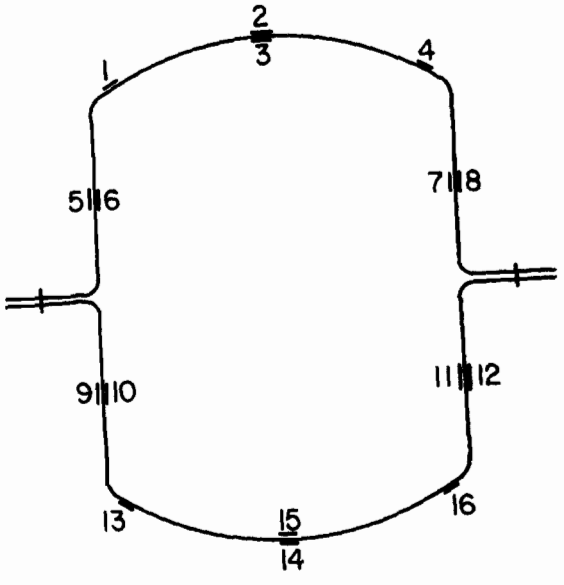

Figure 3.15 Location of Strain Gages on ASI Stub Column Specimens

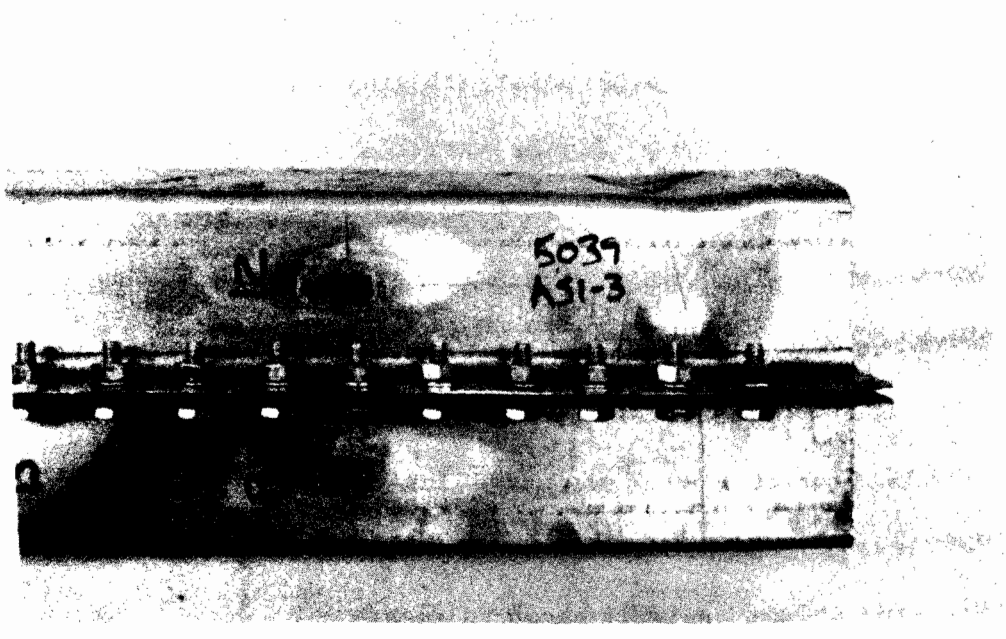

Figure 3.16 Typical Diamond Buckle in an ASI1 Stub Column Specimen

v. Typical Failure Modes. Before buckling of the curved element, distinct waves could be felt in the flat webs along the length of the specimen. Also, buckling of the flat element could be seen in the output of the paired strain gages. Even though the flat webs were buckled, the total load resisted by the cross section continued to increase until the critical buckling stress of a curved element was obtained. At that point (or very soon after), total collapse of the cross section occurred and the section could not withstand any further increase in load.

The failure modes for the curved elements was practically identical to those observed in the previously tested AS stub columns. In other words, a diamond buckling pattern was observed for those curved elements that failed in the elastic range (or just slightly into the inelastic range). A typical failure that was initiated by diamond buckling is shown in Fig. 3.16. The curved elements that failed at stresses well into the inelastic range exhibited a "wrinkling" mode of failure at their ends. Figure 3.17 shows a typical failure that was initiated by a wrinkling failure in the curved elements. The failure mode that occurred for each ASI specimen is given in Table 3.5.

Upon collapse of the ASI3 stub columns, the buckled wave of the flat element spread into the curved element until an angle of approximately thirty degrees was obtained between the flat web and a tangent to the curved element. Because an angle greater than thirty degrees already existed between the flat and curved elements of the ASI1 and ASI2 specimens, no such movement of the flat element into the curved element occurred. The failure modes of the ASI1, ASI2, and ASI3 specimens may be compared in Fig. 3.18.

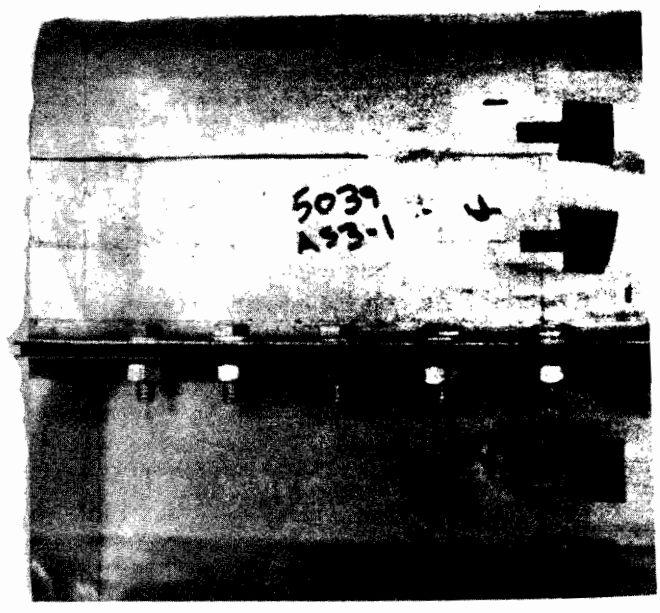

Figure 3.17 Typical Wrinkling Failure in an ASI3 Stub Column Specimen

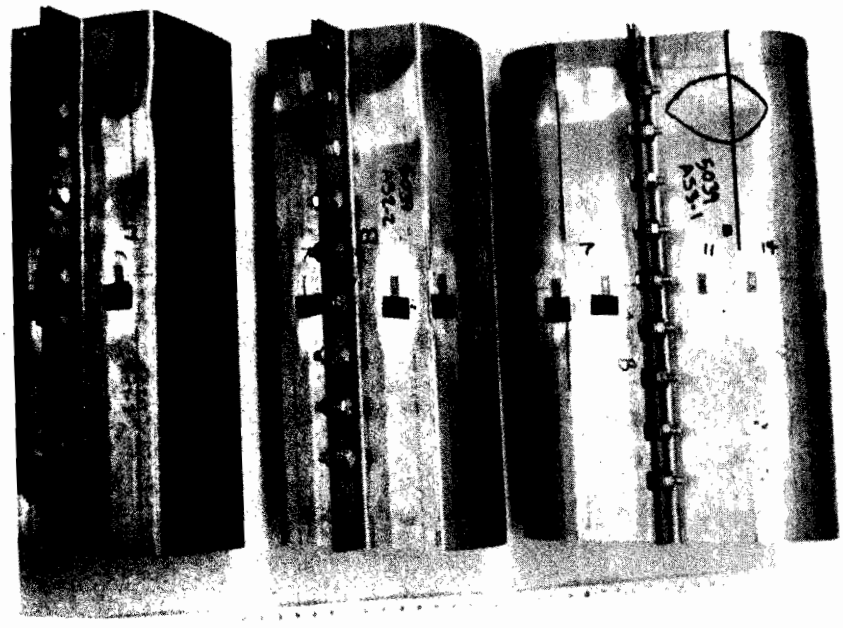

Figure 3.18 Comparison of Failure Modes in the ASI Specimens

Table 3.5 Failure Modes Observed in the ASI Specimens

Specimen	Failure Mode	Type of Failure
50XF(78)AS3-2	Wrinkle	Inelastic
80DKAS3-2	Wrinkle	Inelastic
50XF(39)AS3-1	Wrinkle	Inelastic
30SKAS3-2	Wrinkle	Inelastic
50XF(78)AS2-2	Wrinkle	Inelastic
80DKAS2-2	Diamond	Inelastic
50XF(39)AS2-2	Wrinkle	Inelastic
30SKAS2-2	Wrinkle	Inelastic
50XF(78)AS1-3	Diamond	Elastic
80DKAS1-3	Diamond	Elastic
50XF(39)AS1-3	Diamond	Elastic

Note:

Inelastic failure indicates that the average stress upon local buckling exceeded the proportional limit of that particular material. Elastic failure, on the other hand, indicates that the average stress at local buckling was less than the proportional limit of that particular material.

c. Description of Beam Tests for Stiffened Curved Elements - AB Specimens.

i. Specimens. As shown in Figure 3.1, the AB profile is the same basic section as used for the AS stub column, except that only half of the stub column cross section is tested as a beam. Table 3.2 lists the three basic radii of the curved flanges (R=2, 3.5, or 15 in.). The three curvatures of the AB beam specimens may be compared in Figure 3.19. The measured dimensions of the AB beam specimens are provided in Table A.3. As shown in Table 3.3, one test has been performed for each material and curvature. A total of 18 AB beam tests were performed. The length of the beam specimens is 60 in.

ii. Strain Measurements. A minimum of six foil strain gages were used to measure strains at midspan of the AB beam specimens. The gage locations are shown in Figure 3.20. Additional paired strain gages were attached along the centerline of the AB1 curved flanges at points halfway between midspan and the inner load points of the beams. These gages were added to detect any early signs of buckling away from midspan. Again, the critical buckling stress was determined by using the modified strain reversal method for the strain output of the paired gages located along the centerline of the compression flanges. Because of the relatively short wavelength of the AB2 and AB3 specimens, it was virtually impossible to detect buckling from the strain gage output and thus, no additional paired gages were attached to these specimens. The gages on the tension flanges of all the AB specimens were used to check the location of the neutral axis and also to detect any tilting of the cross-section.

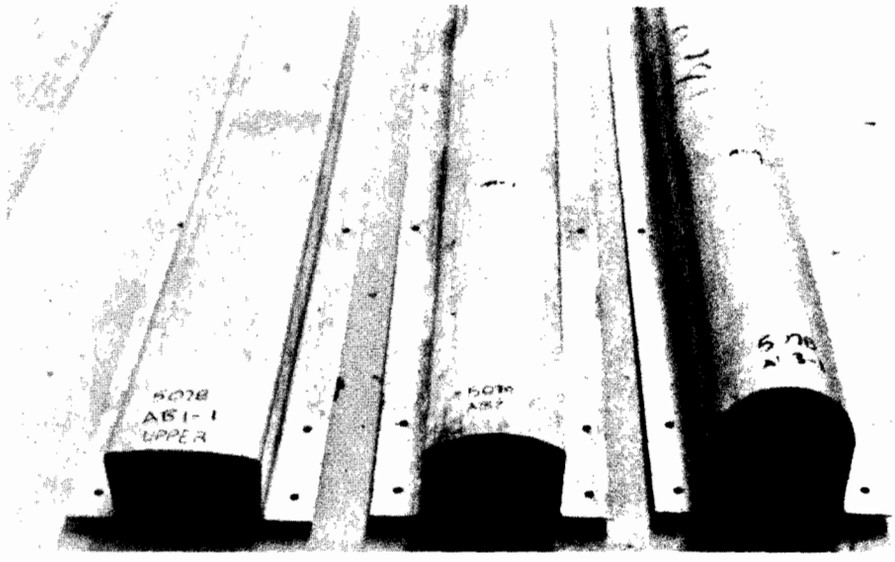

AB1 AB2 AB3

Figure 3.19 Comparison of Three Curvatures of AB Beam Specimens

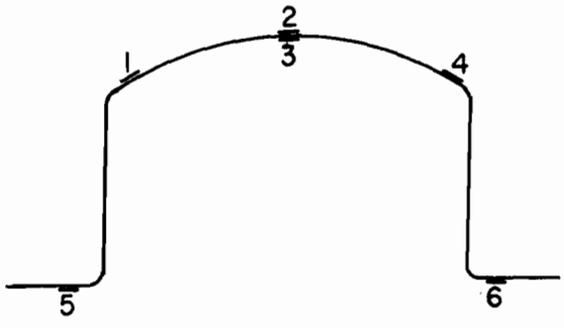

Figure 3.20 Location of Strain Gages on AB Beam Specimens

iii. Waving and Deformation Measurements. Because of the beam deflection, no practical method could be obtained for measuring the waving of the curved flanges. The beam deflection under both tension flanges was measured at midspan by dial gages.

iv. Equipment and Testing Procedure. The same data acquisition system and Tinius Olsen testing machine were used as previously described for the AS stub column tests. As shown in Figure 3.21, the load was applied to the webs of the beam specimens at their quarter points. T-sections were used to transmit the load to the web. Six 1/4-in. dia., high strength bolts connected each T-section to the beam webs. A closeup of the T-sections is shown in Figure 3.22.

As mentioned earlier, the load was applied by a Tinius Olsen testing machine. The load increments were such that a minimum of ten load levels were measured before failure of the specimens. Between load levels, the load was increased very slowly such that any strain rate effect on the mechanical properties was negligible. Once the desired load level was reached, the load was held constant for a period of time to allow the specimen to stabilize. At each load level, the load and corresponding strains were measured and stored by the computer. Also, the beam deflection was measured at each load level. The ultimate load was taken directly from the Tinius Olsen machine as the maximum load that the specimen could withstand.

v. Typical Failure Modes. Failure of the stiffened curved elements subject to bending was quite similar to the failure observed in the previously tested AS stub columns. In other words, a diamond buckling pattern was again observed for those curved elements that

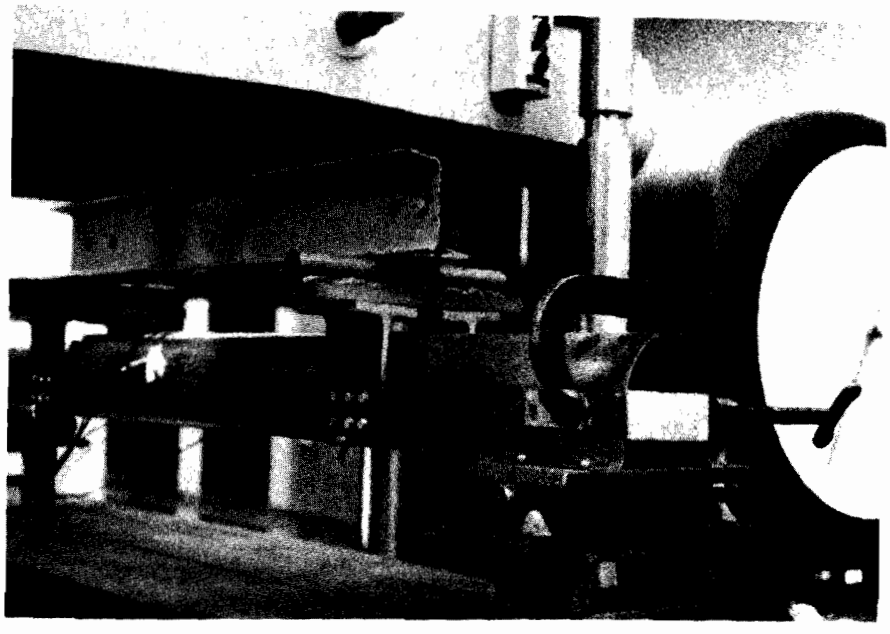

Figure 3.21 Test Setup for AB Beam Specimens

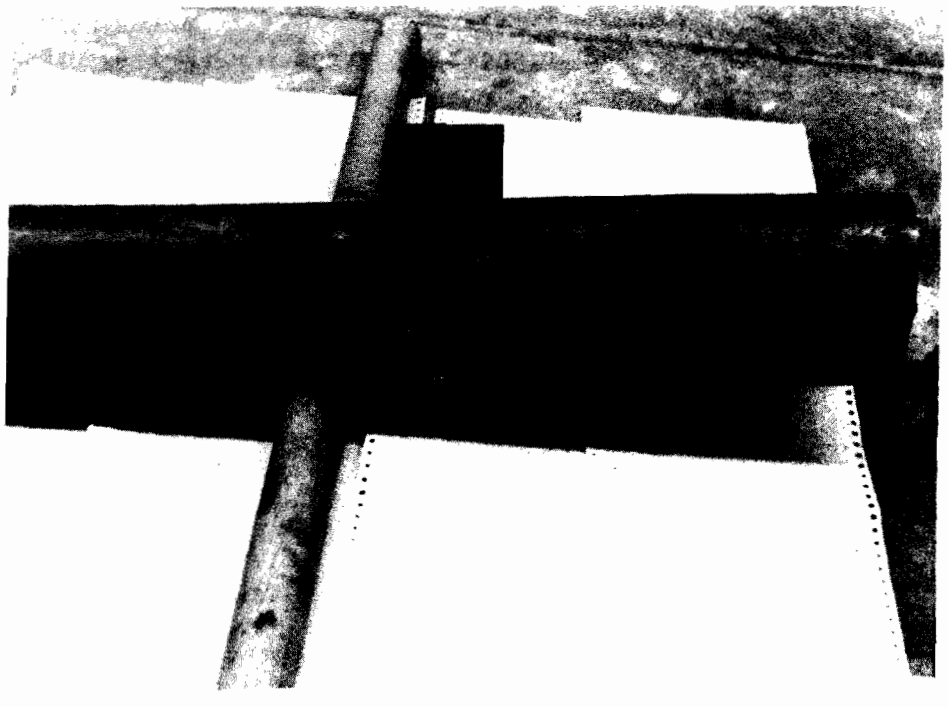

Figure 3.22 Closeup of T-Sections Used to Apply Load to AB Beam Specimens

failed in the elastic range or just into the inelastic range. However, the diamond buckling mode seemed to occur at slightly higher stress levels than in the stub columns. The reason for this is believed to be the more favorable stress distribution caused by bending. A typical diamond buckling failure is shown in Figure 3.23. As expected, the curved elements that failed well into the inelastic range failed by the previously discussed "wrinkling" mode. Figure 3.24 shows a typical wrinkling mode of faliure. The failure modes of the AB1, AB2, and AB3 specimens may be compared in Figure 3.25. Table 3.6 provides a summary of the curved element failure mode for each of the AB specimens.

As earlier mentioned, deflection of the beam was measured at midspan for each load level. Beam deflection was monitored in order to ensure that the load was applied uniformly across the specimen and to detect the onset of any nonlinear behavior in the beam. As expected, buckling of the curved flanges occurred soon after the begining of nonlinear load-deflection behavior. A typical plot of load versus deflection is shown in Figure B.4.

d. Description of Beam Tests for Stiffened Curved Elements - DB Specimens.

i. Specimens. The DB beam profile is shown in Figure 3.4. The purpose of these specimens is to determine the effect of sloped webs when used in conjunction with a stiffened curved compression flange. As shown in Table 3.2, only one radius is used for the DB specimens, with the difference in the two types of specimens being the arc length of the curved elment ($\theta = 45^{o}$ or 60^{o}). Again, the length of the beam specimens is 60 in. The number of tests for each material and curvature are shown

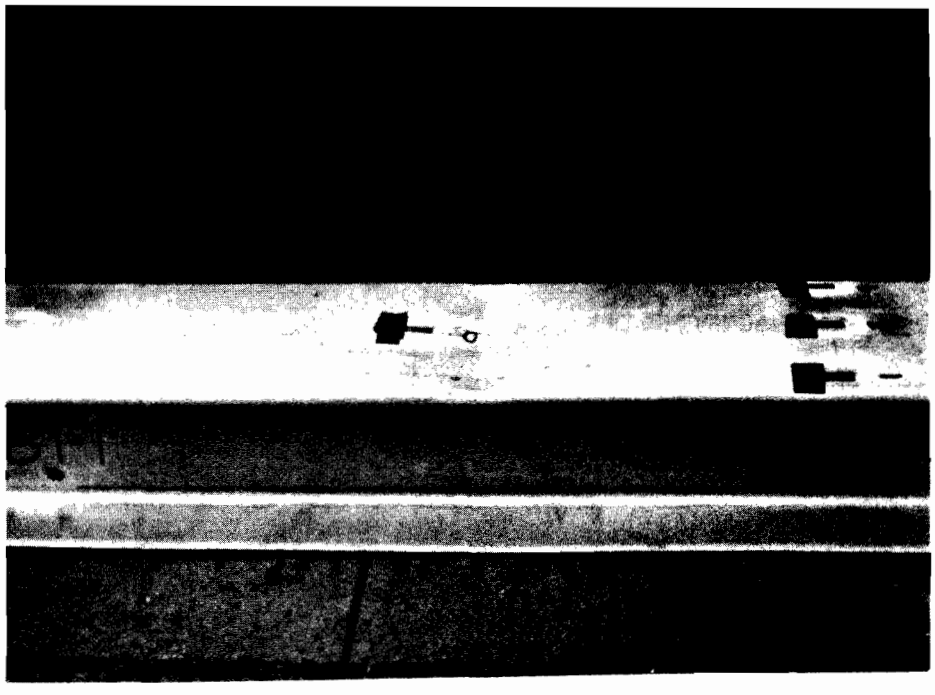

Figure 3.23 Typical Diamond Buckle in an AB Beam Specimen

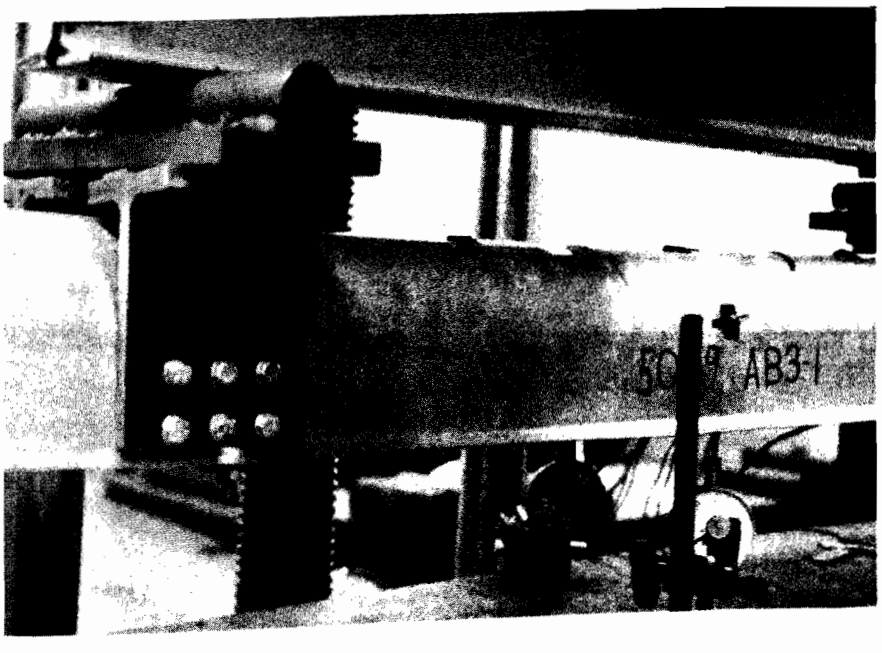

Figure 3.24 Typical Wrinkling Failure in an AB Beam Specimen

Table 3.6 Failure Modes Observed in the AB Specimens

Specimen	Failure Mode	Type of Failure
80XFAB3-1	Wrinkle	Inelastic
50XF(78)AB3-1	Wrinkle	Inelastic
80SKAB3-2	Wrinkle	Inelastic
80DKAB3-2	Diamond	Inelastic
50XF(39)AB3-3	Wrinkle	Inelastic
30SKAB3-2	Wrinkle	Inelastic
80XFAB2-1	Diamond	Inelastic
50XF(78)AB2-1	Wrinkle	Inelastic
80SKAB2-1	Diamond	Inelastic
80DKAB2-1	Diamond	Inelastic
50XF(39)AB2-1	Wrinkle/Diamond	Inelastic
30SKAB2-1	Wrinkle/Diamond	Inelastic
80XFAB1-1	Diamond	Elastic
50XF(78)AB1-1	Diamond	Inelastic
80SKAB1-1	Diamond	Inelastic
80DKAB1-1	Diamond	Elastic
50XF(39)AB1-1	Diamond	Elastic
30SKAB1-1	Diamond	Inelastic

Note:

Inelastic failure indicates that the maximum stress in the curved element at local buckling, as computed by Mc/I, exceeded the proportional limit of that particular material. Elastic failure, on the other hand, indicates that the maximum stress at local buckling was less than the proportional limit of that particular material.

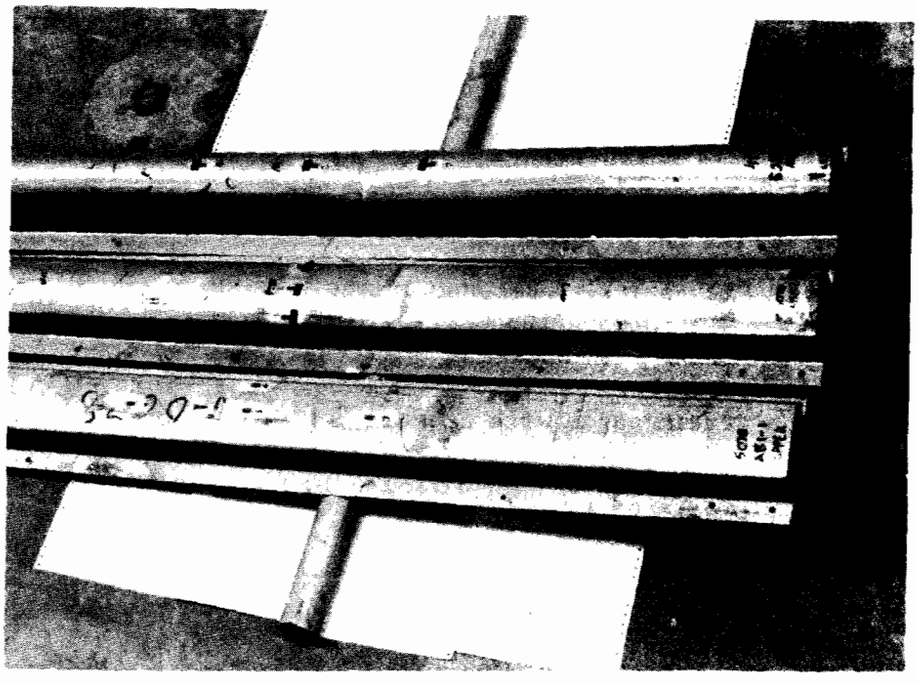

Figure 3.25 Comparison of Failure Modes for AB Beam Tests

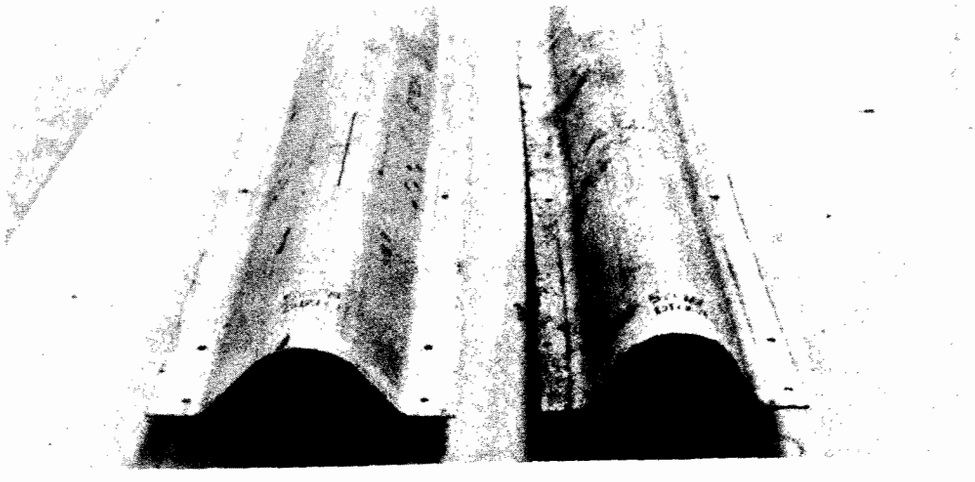

DB1 DB2

Figure 3.26 Comparison of DB1 and DB2 Beam Profiles

in Table 3.3. As shown, a total of 10 DB beam tests were performed. The two different profiles, DB1 and DB2, may be compared in Figure 3.26. Table A.4 provides the measured dimensions of the DB specimens.

ii. Strain Measurements. Six foil strain gages were used to measure strains at midspan of the beam specimens. The gage locations are shown in Figure 3.27. Because of the very short buckled wavelengths of these specimens, no buckling was ever observed from the strain gage output. The strain gages were useful, however, for the determination of the neutral axis location and also to observe any tilting or nonuniform loading of the specimen.

iii. Waving and Deformation Measurements. Again, because of the beam deflection, no practical method could be obtained for measuring the waving of the curved flanges. As shown in Figure 3.28, the beam deflection under both tension flanges was measured at midspan by dial gages.

iv. Equipment and Testing Procedure. The same equipment and test procedure was used for the DB beam tests as for the previously described AB beam tests. Figure 3.18 shows an overall view of the DB beam test setup. A 3/8-in. thick "cap", formed to match the slope of the flat webs, was used to apply the load to the DB beam specimens. A closeup of the load plate is shown in Figure 3.29.

v. Typical Failure Modes. Because of the relatively large curvature in the DB beam specimens, the failure was, in all cases, well into the inelastic range. Therefore, as expected, the failure mode was of the wrinkling type which was previously discussed for the AB beam specimens. Failure of the DB2 beams was practically identical to that

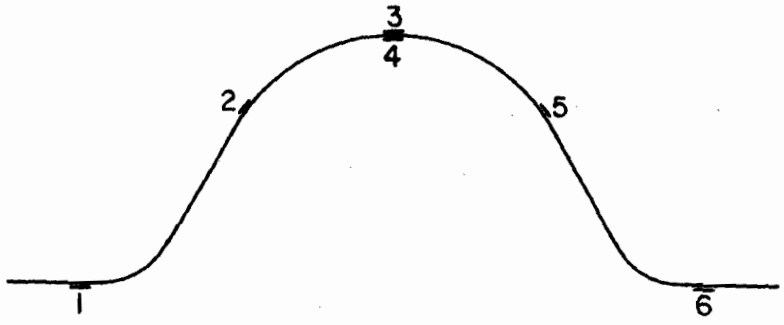

Figure 3.27 Location of Strain Gages for DB Beam Specimens

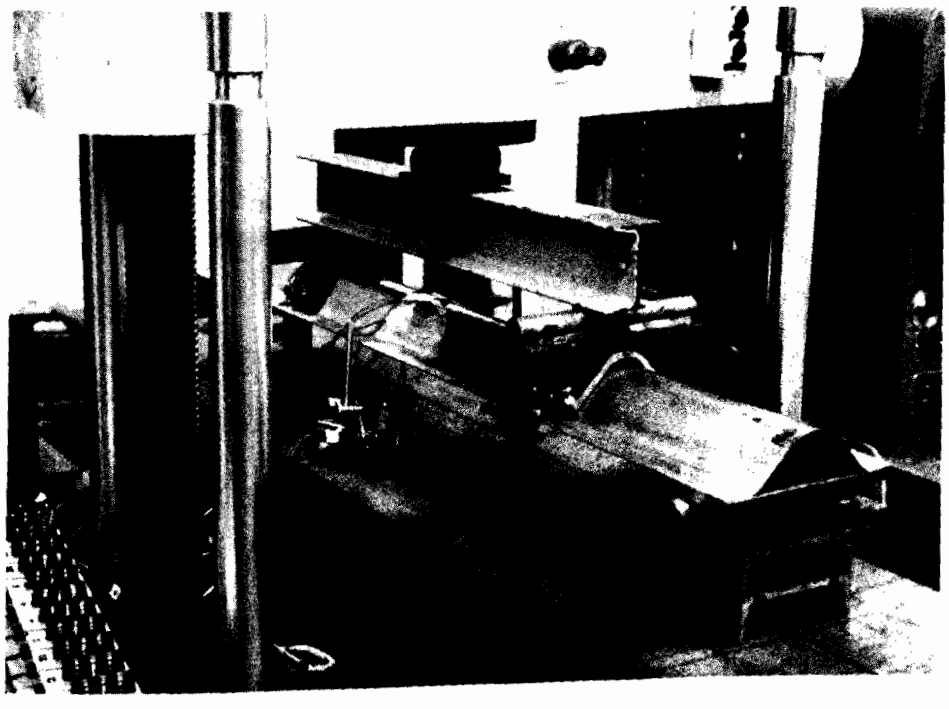

Figure 3.28 Test Setup for DB Beam Specimens

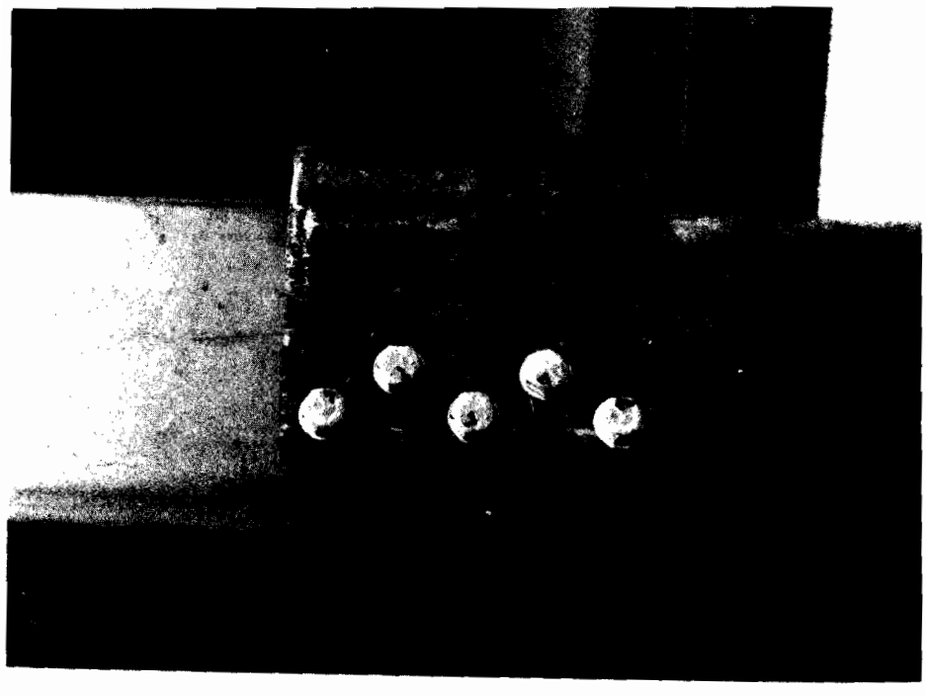

Figure 3.29 Closeup of Load Plate for DB Beam Specimens

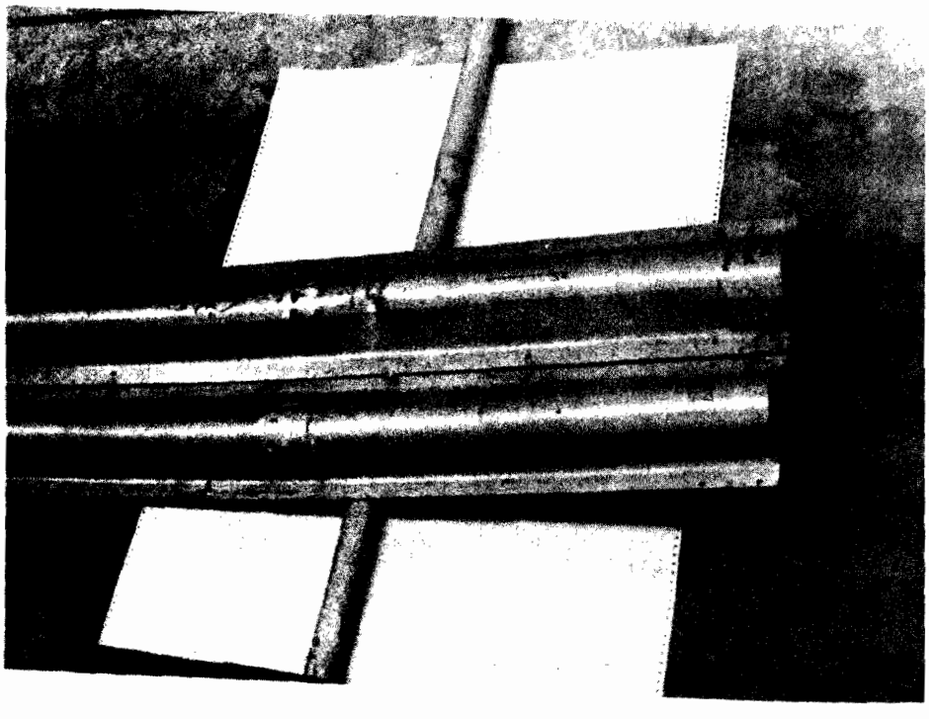

Figure 3.30 Comparison of Failure Modes of DB Beam Specimens

seen in the curved element of the AB3 beams. However, failure of some of the DB1 specimens seemed to be initiated at the sloped, flat web to curved element junction. The two modes of failure may be compared in Figure 3.30. The reason for initiation of failure at this point seems to be the relatively large angle of the flat web to the vertical (approx. 45°). Thus, it seems that, based on these few tests, an angle of 60° between the web and the horizontal is necessary to ensure stability of the web-curved flange junction.

Again, beam deflection was monitored in order to ensure that the load was applied uniformly across the specimen and to detect the onset of any nonlinear behavior in the beam. As expected, buckling of the curved flanges occurred soon after the beginning of nonlinear load-deflection behavior. A typical plot of load versus deflection is shown in Figure B.4.

e. Description of Shear Tests for Curved Webs - BV Specimens

i. Specimens. The BV shear specimens were fabricated by attaching two identical B profiles (Figure 3.2) as shown in Figure 3.31. A 5-1/2 in. wide by 14 in. long cover plate, cut from the 80XF material, was attached to the top and bottom flanges by 1/4 in. diameter bolts. The bolts were spaced at 1-1/4 in. apart along the length of the specimen and 1 in. apart across the flange. As shown in Table 3.2, three basic radii of the curved flanges (R = 2, 3.5, or 15 in.) were tested. The three different curvatures may be compared in Figure 3.32. The number of tests performed for each material and curvature is given in Table 3.3. A total of 12 BV shear tests were performed. The length of the shear specimens is 30 in. Table A.5 provides the measured cross sectional dimensions of the BV specimens.

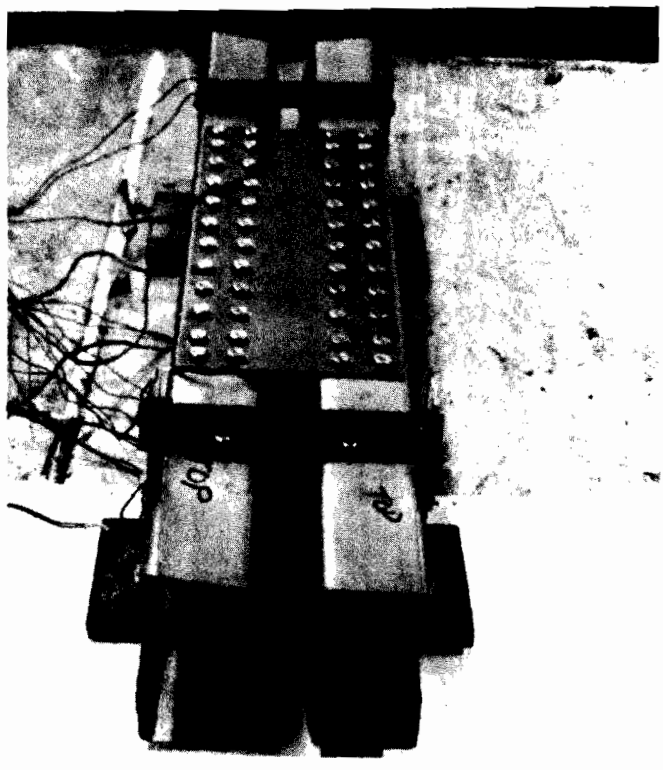

Figure 3.31 Typical BV Shear Specimen

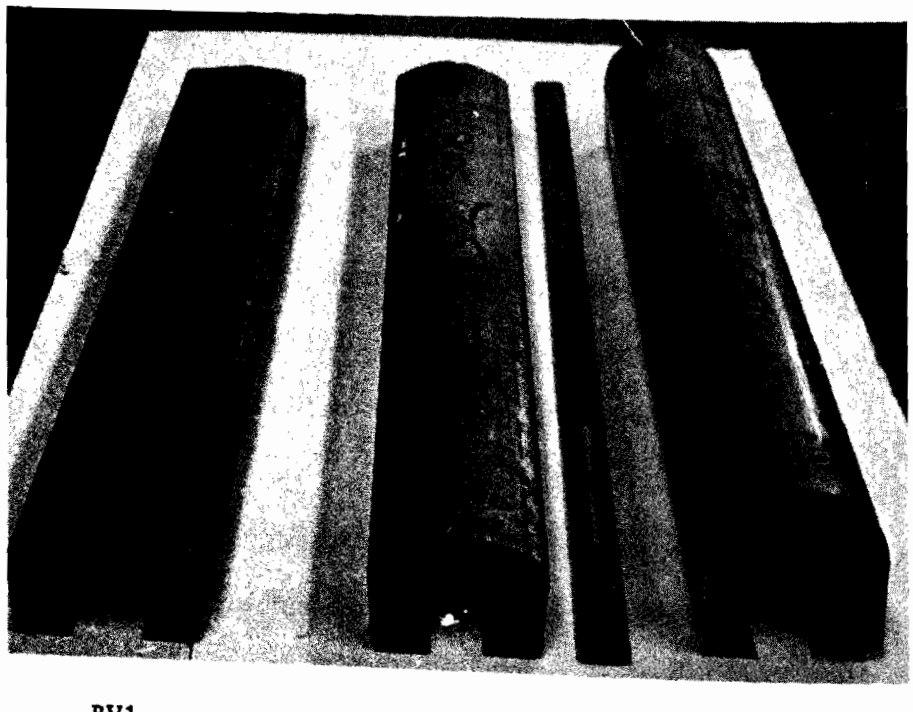

BV1 BV2 BV3

Figure 3.32 Comparison of Three Web Curvatures of BV Shear Specimens

ii. Strain Measurements. Ten foil strain gages were attached to the BV specimens. The strain gage locations for one side of a BV shear specimen are shown in Figure 3.33. As shown, paired gages were attached to the curved webs midway between the interior load point and the supports. These gages were oriented at 45^{o} to the longitudinal axis, such that an estimate of the shear stress could be measured. Single gages were also attached to the tension flanges at midspan. These gages were used to check the bending stress distribution and to detect any nonuniformity of loading.

iii. Waving and Deformation Measurements. Because of the nature of the shear tests, no practical method could be devised to measure waving of the curved webs. Deflection at midspan was measured by stationary dial gages under both tension flanges.

iv. Equipment and Testing Procedure. The same data acquisition system and Tinius Olsen testing machine were used as previously described for the AS stub column tests. As shown in Figures 3.33 and 3.34, a single concentrated load was applied at midspan. In order to minimize the potential for web crippling, a 5 in. wide bearing plate was used at midspan and 4 in. wide bearing plates were used at the reactions. The distance between the supports was 18 in. Thus, there was a clear distance between the inner and support bearing plates of 4.5 in. Wood blocks, cut to fit the inner profile of each individual specimen, were placed inside the specimen at the load points. The location of the blocks is shown in Figure 3.34.

iv. Typical Failure Modes. A total of four different types of failure modes occurred for the BV specimens. The failure mode of each

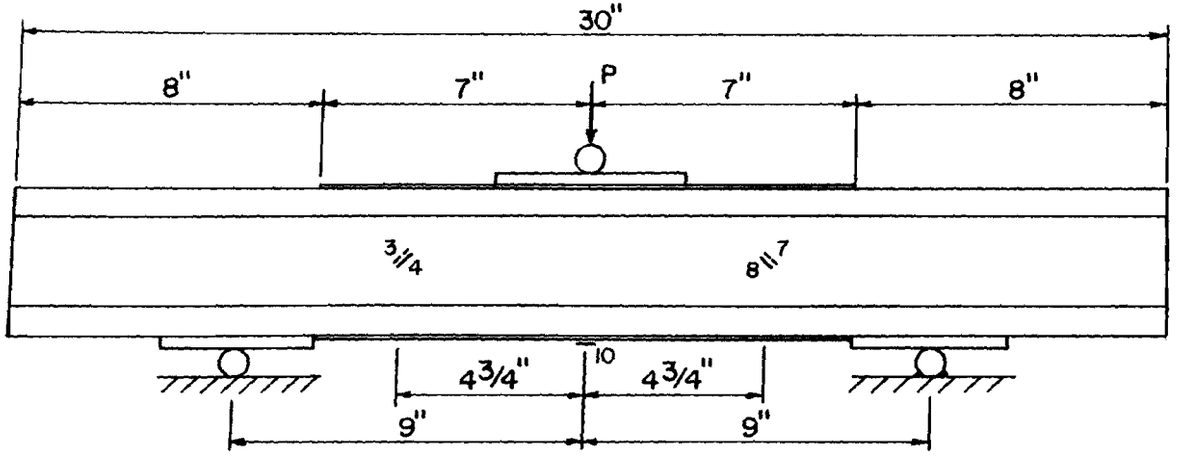

Figure 3.33 Location of Strain Gages on One Side of a BV Shear Specimen

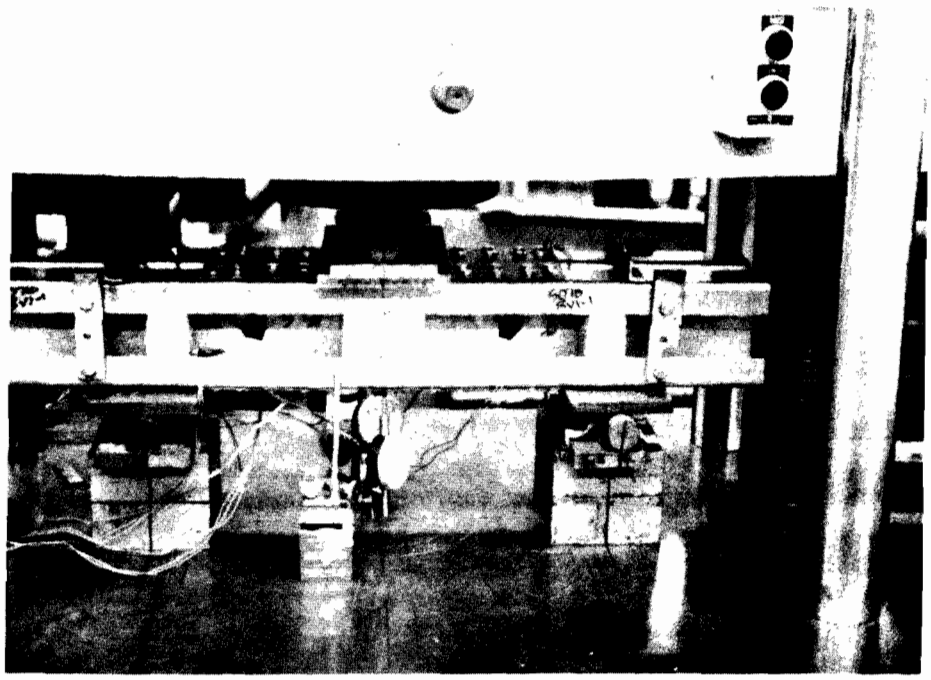

Figure 3.34 Setup for BV Shear Tests

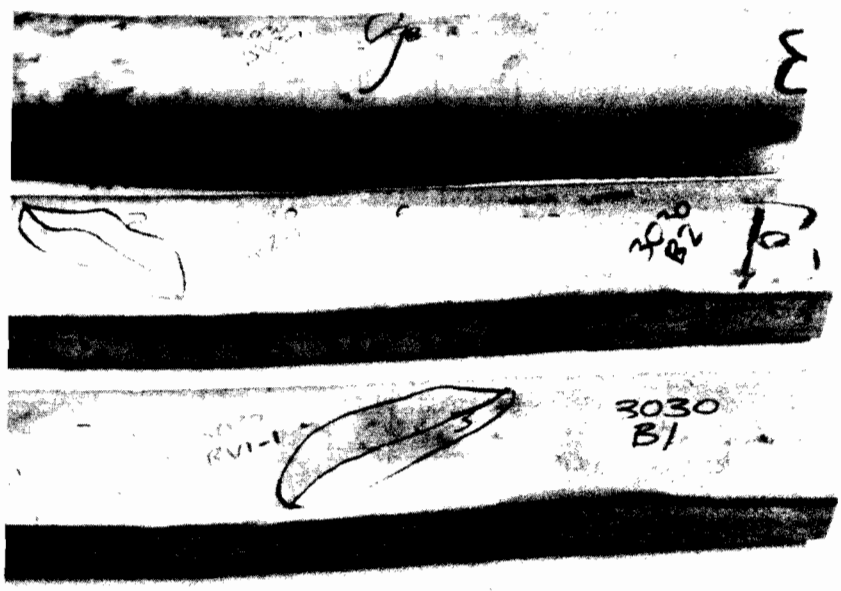

Figure 3.35 Comparison of Failure Modes for BV Shear Tests

of the tested specimens is listed in column (4) of Table 3.21. As shown, the "V" failure mode designates those specimens that failed by shear buckling only. For these specimens, there was no other sign of damage in the collapsed section. The failure contained an inward buckle at an angle of approximately 45^{o} to the longitudinal axis of the section. As shown in Table 3.21, this type of failure normally occurred for the flatter curvatures of the BV specimens. A typical "V" failure is illustrated in the 30SKBV1-1 specimen (R=15 in.) in Figure 3.35. The observed mode of failure for each shear specimen is listed in column (4) of Table 3.21.

The "WC" failure mode describes those sections that failed entirely by local deformation directly under the interior load. This type of failure seems to be similar to web crippling as normally defined for flat webs. Obviously, the test data from these tests are of limited value for the prediction of shear buckling. However, it is extremely important to note the possible modes of failure that may occur in curved webs at loads much less than those required to cause shear buckling.

The failure designated by "WC + V" indicates that, for these specimens, there was evidence of both web crippling "WC" and a shear failure "V" in the tested specimen. In other words, at failure, there was considerable deformation directly under the interior bearing plate; however, there also was a fully developed shear buckle oriented at 45^{o} to the longitudinal axis of the specimen. For these specimens, the influence of web crippling on the shear buckling load is uncertain.

The final mode of failure is designated as "WCV". For these specimens, the failure seemed to be as a result of a direct interaction

between web crippling and shear. The failure always occurred immediately adjacent to the interior bearing plate. The failure resulted in what seemed to be a "wrinkling" type of failure as previously described for the axial collapse of highly curved stiffened elements. The wrinkle occurred at an angle of approximately 60° to the longitudinal axis of the specimen. Because of the obvious effect of the localized bearing stresses under the interior load plate, the results of these tests again are of limited value for the prediction of shear buckling. A typical "WCV" failure may be seen in the 30SKBV3-1 specimen (R=2 in.) shown in Figure 3.35.

3. Unstiffened Curved Elements.

a. Description of Stub Column Tests for Initial Unstiffened Curved Element Failure - CS Specimens.

i. Specimens. The CS stub columns were fabricated from two "channel" type sections. Self-tapping screws (#14 X 3/4-in.) were used to connect the channels. Three vertical columns of fasteners, spaced 2 in. apart vertically, were used to connect the flat webs of the CS specimens. The outer columns of fasteners were placed as close as practicable to the edge of the web. Using exactly the same procedure as previously described for the AS stub column specimens, vertical bracing (3/4 X 3/4 X 1/8 in.) was attached to the flat web in order to prevent premature web buckling. Figure 3.36 shows a fabricated CS stub column specimen.

Table 3.2 lists the three different curvatures of the curved flanges (R = 2, 3.5, 15 in.). The curvatures may be compared in Figure 3.37. As shown in Table 3.3, a minimum of one test has been performed

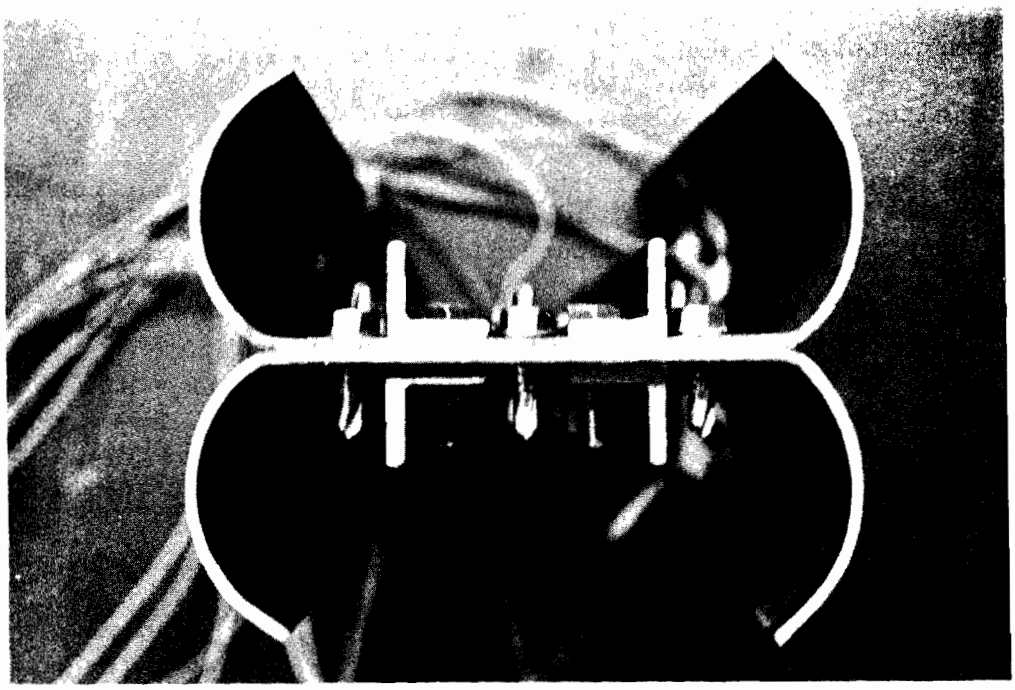

Figure 3.36 Typical Specimen for CS Stub Column Tests

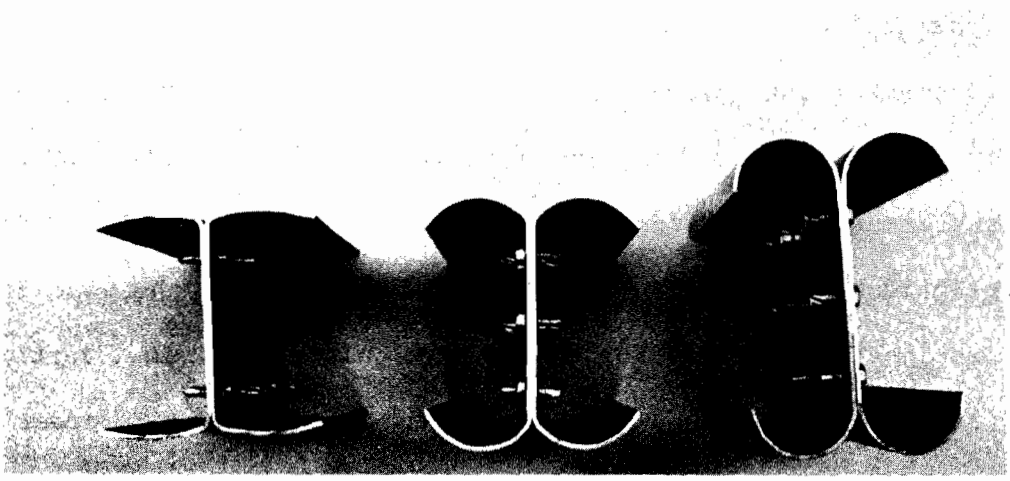

CS1	CS2	CS3
CSI1	CSI2	CSI3
CB1	CB2	CB3

Figure 3.37 Comparison of Three Profiles for Unstiffened Curved Element Tests

for each material and curvature. A total of 21 specimens were tested for the initial buckling of unstiffened curved elements. The CS stub columns were approximately 12 in. long. The measured cross sectional dimensions of the CS specimens are provided in Table A.6.

Just as for the AS stiffened curved element specimens, the ends of the CS stub columns were milled flat and parallel, with their longitudinal axis perpendicular to the milled ends. Flatness of the ends was checked by placing the stub columns on a flat, level surface and observing any rocking or light that might be visible between the specimen and the flat surface. If the ends were not found to be flat, the milling procedure was repeated until the ends were made as flat as possible.

ii. Strain Measurements. Fourteen foil strain gages were used to measure strains at midheight of the stub column specimens. The gage locations are shown in Figure 3.38. The critical buckling stress for the curved elements was found by using the modified strain reversal method for the strain output of the paired gages located on each side of the flange tips.

Additional strain gages were placed at or close to the webs of the specimens so that the average strains associated with buckling could be measured. All of the strain gages were used in the procedure for aligning the specimens.

iii. Waving and Deformation Measurements. Out-of-plane waving of the curved flange tips was recorded at thirteen points along the length of each flange. Waving was measured using the same equipment and procedure as previously described for the AS stub column specimens.

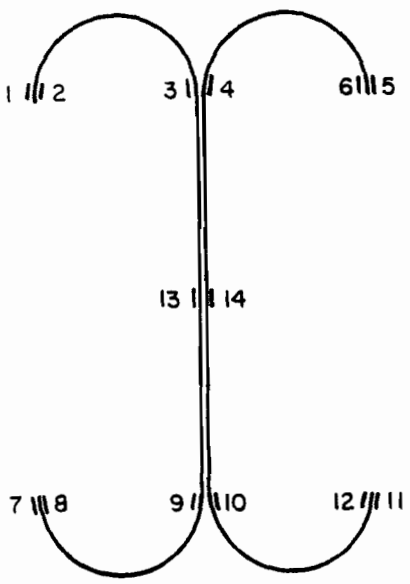

Figure 3.38 Location of Strain Gages on CS and CSI Stub Column Specimens

In addition to waving, cross head movement and lateral displacement of one of the curved flange tips were recorded by stationary dial gages at each load level. The readings from these dial gages were used only to monitor the performance of the stub column during testing.

iv. Equipment and Testing Procedure. The equipment and testing procedure of the CS stub columns were identical to that used in the previously described AS stub column tests. All but four of the CS stub column specimens were tested in the 120,000 pound capacity Tinius Olsen testing machine located in the Engineering Research Laboratory at UMR. Figure 3.9 shows the testing machine along with the remaining equipment used in the stub column tests. The four remaining specimens, because of their relatively high expected failure load, were tested in a 200,000 pound capacity Tinius Olsen testing machine located in the Materials Laboratory of the Civil Engineering Building at UMR. The accompanying equipment was exactly the same as shown in Figure 3.9.

v. Typical Failure Modes. The CS3 and CS2 specimens typically exhibited very little, if any, waving of the free edge of the curved element prior to initial buckling. In all cases, the magnitude of the wave depth was less than the respective thickness of the materials. Figure 3.39 shows the buckled flange of a typical specimen.

The CS1 specimens also showed very little waving before initial buckling. However, after initial buckling and before the ultimate load, waving of the curved flange tips became much more pronounced. Figure 3.40 shows the buckled configuration of a CS1 specimen at its ultimate load. A typical wave pattern, as measured by the LVDT at close to failure, is shown in Figure B.5.

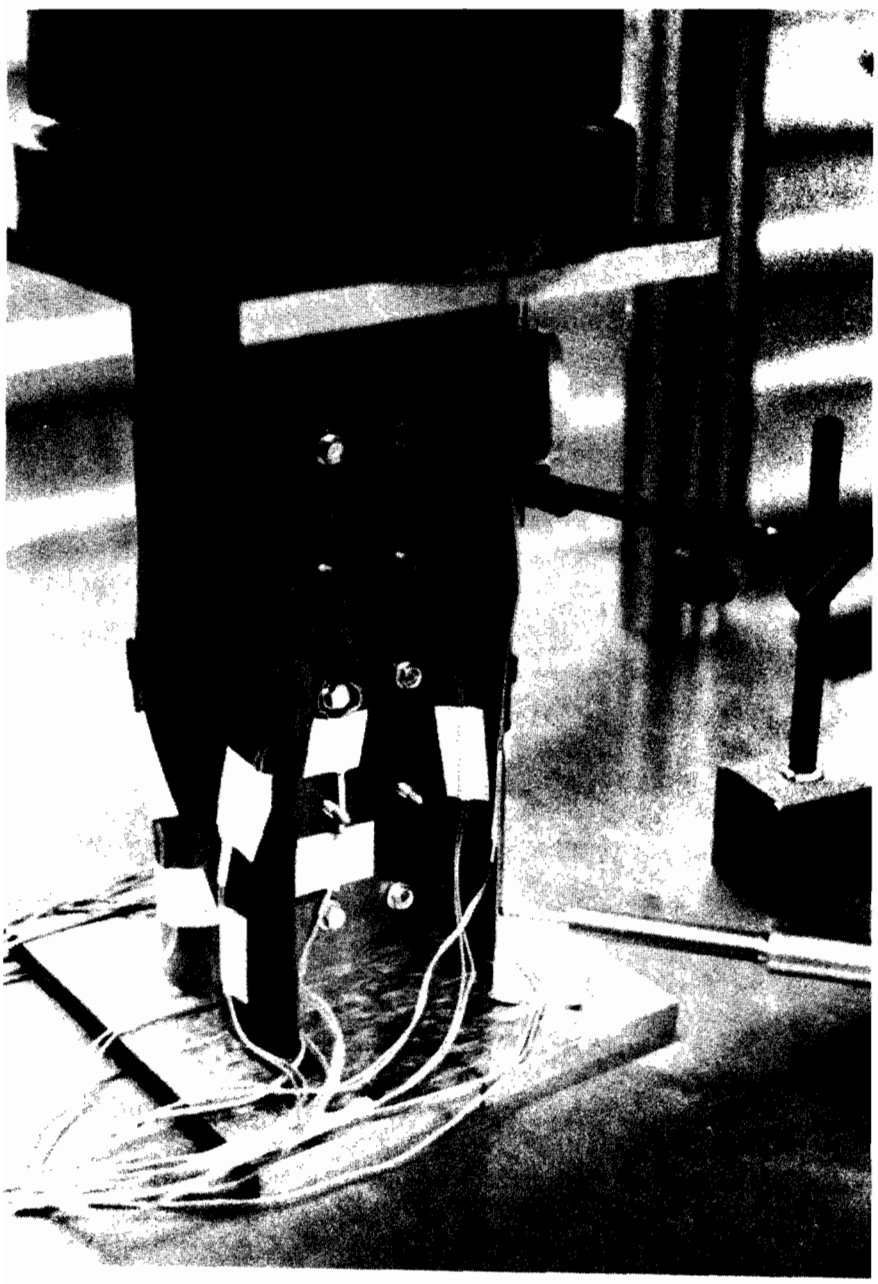

Figure 3.39 Typical Failure of the CS3 and CS2 Stub Column Specimens

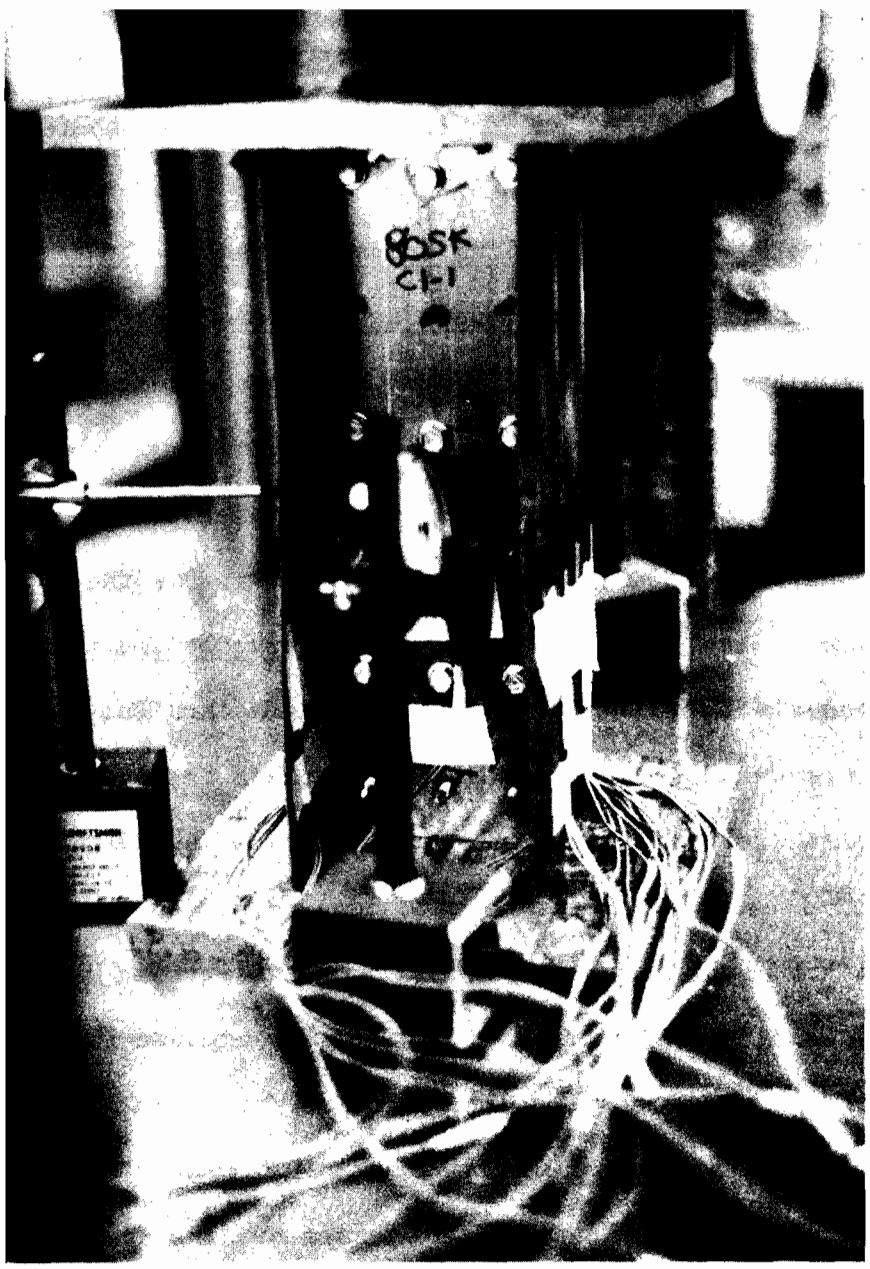

Figure 3.40 Typical Failure of the CS1 Stub Column Specimens

Again, movement of the Tinius Olsen cross head was recorded at each load level. The cross head movement was monitored in order to detect the onset of any nonlinear behavior in the specimen. As expected, buckling of the curved flanges occurred soon after the beginning of nonlinear cross head movement. Figure B.3 shows a typical plot of load versus cross head movement.

b. Description of Stub Column Tests for the Interaction Between Stiffened Flat and Unstiffened Curved Elements - CSI Specimens.

i. Specimens. The CSI stub column specimens for the interaction between stiffened curved and flat elements are identical to the CS specimens. The only exception is that the vertical bracing that was attached to the flat web was omitted. Thus, for the CSI specimens, the flat web actually buckled before the curved elements. The interaction between the local buckling of stiffened flat and unstiffened curved elements was observed as a result of these tests. The number of tests performed for each material and curvature is shown in Table 3.3. As shown, a total of 15 tests have been performed for the CSI specimens. Table 3.2 lists the three basic radii of the curved flanges (R = 2, 3.5, or 15 in.). The three curvatures may be compared in Figure 3.37. Table A.7 provides the measured dimensions of the CSI cross sections.

ii. Strain Measurements. Just as for the CS specimens, fourteen foil strain gages were used to measure strains at midheight of the stub column specimens. The gage locations are identical to the CS specimens as shown in Figure 3.38. The critical buckling stress for the curved elements was found by using the modified strain reversal method for the strain output of the paired gages located on each side of the flange tips.

Additional strain gages were placed at or close to the webs of the specimens so that the average strains associated with buckling could be measured. All of the strain gages were used in the procedure for aligning the specimens.

iii. Waving and Deformation Measurements. Out-of-plane waving of the curved flange tips was recorded at thirteen points along the length of each flange. Waving was measured using the same equipment and procedure as previously described for the AS stub column specimens.

In addition to waving, cross head movement and lateral displacement of one of the curved flange tips was recorded by stationary dial gages at each load level. The readings from these dial gages were used only to monitor the performance of the stub column during testing.

iv. Equipment and Testing Procedure. The equipment and testing procedure of the CSI stub columns were identical to that used in the previously described CS stub column tests.

v. Typical Failure Modes. As far as the unstiffened curved elements are concerned, their failure modes were practically identical to the previously described CS specimens. After initial buckling of the web, the overall cross section remained stable with very little waving of the curved flange tips until the critical stress of the curved elements was reached. At that load (or very near this load), the ultimate load was obtained for the CS3 and CS2 specimens. For the CS1 specimens, there was a slight amount of post-buckling strength which was accompanied by significant waving of the curved flanges.

c. Description of Beam Tests for Unstiffened Curved Elements - CB Specimens.

i. Specimens. The CB beam profile is exactly the same as the CS and CSI profiles. Table 3.2 lists the three basic radii of the curved flanges (R = 1, 1.25, or 4 in.). The three curvatures may be compared in Figure 3.37. As shown in Table 3.3, one test has been performed for each material and curvature. A total of 18 CB beam tests were performed. The length of the beam specimens is 60 in. Table A.8 provides the measured cross sectional dimensions of the CB specimens.

b. Strain Measurements. Ten foil strain gages were used to measure strains at midspan of the beam specimens. The gage locations are shown in Figure 3.41. Again, the critical buckling stress was determined by using the modified strain reversal method for the strain output of the paired gages located on the compression flange tips. Additional gages were placed on the compression flange in order to measure the strain distribution across the flange. The gages on the tension flange were used to determine the location of the neutral axis and also to detect any tilting of the cross section.

iii. Waving and Deformation Measurements. As shown in Figure 3.42, the beam deflection under both tension flanges was measured at midspan by a dial gage. Also, the lateral movement of the upper portion of the web was monitored by a stationary dial gage. Because of the beam deflection, no practical method could be obtained for measuring the waving of the curved flanges.

iv. Equipment and Testing Procedure. The same data acquisition system and Tinius Olsen testing machine were used as previously described for the AS stub column tests. As shown in Figure 3.42, the load was applied to the webs of the beam specimens at their quarter

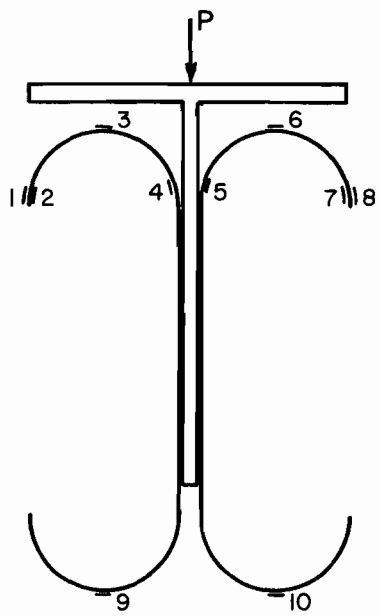

Figure 3.41 Location of Strain Gages for CB Beam Specimens

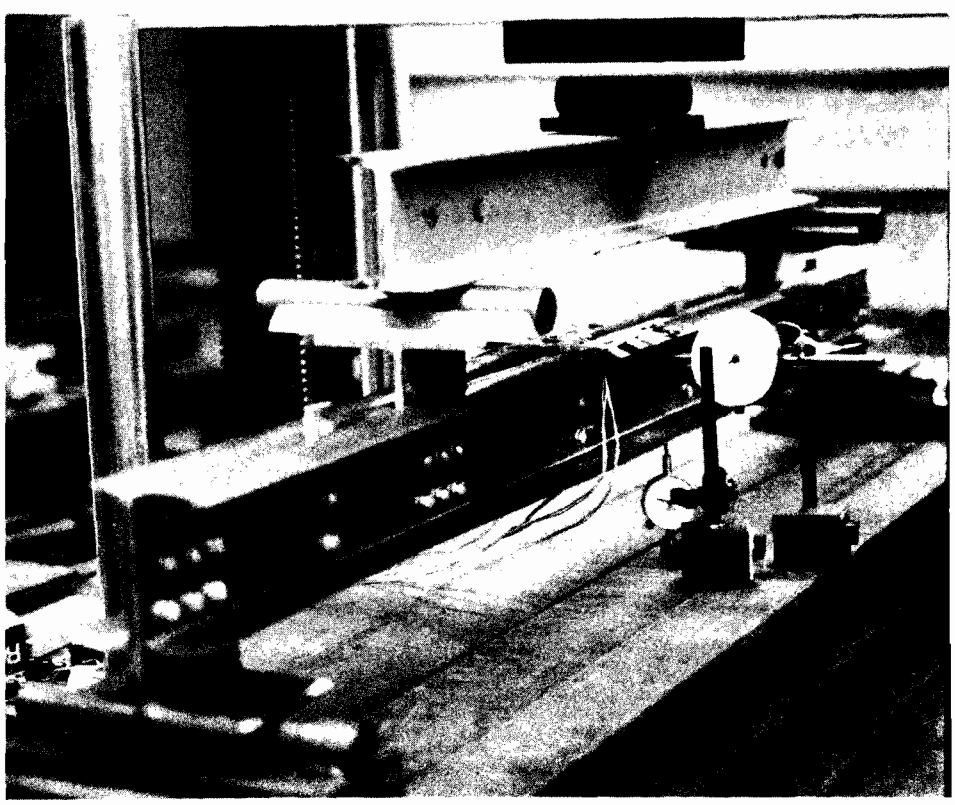

Figure 3.42 Test Setup for the CB Beam Specimens

points. T-sections were used to transmit the load to the web. Nine 1/4-in. dia., high strength bolts connected each T-section to the beam webs. A closeup of the T-sections is shown in Figure 3.43.

The load was applied by a Tinius Olsen testing machine. The load increments were such that a minimum of ten load levels were measured before failure of the specimens. Between load levels, the load was increased very slowly such that any strain rate effect on the mechanical properties was negligible. Once the desired load level was reached, the load was held constant for a period of time to allow the specimen to stabilize. At each load level, the load and corresponding strains were measured and stored by the computer. Also, the beam deflection was measured at each load level. The ultimate load was taken directly from the Tinius Olsen machine as the maximum load that the specimen could withstand.

v. Typical Failure Modes. As expected, failure of the unstiffened curved elements of the CS1 and CS2 specimens was quite similar to the previously tested CS stub columns of like curvatures. In other words, little waving of the unstiffened curved flange tips was measured prior to initial buckling. The buckled shape of the flatter curvatures (R = 4 in.) seems to be stable which allows for considerable post-buckling strength.

However, the failure mode for the sharper curvature of the CB3 (R = 1 in.) specimens was unlike that of the CS3 stub columns. For the CB3 specimens failure seemed to originate at the tangent between the flat web and the unstiffened curved flange. A typical failure of this type may be seen in Figure 3.43. Figure 3.44 provides a comparison of the failure modes of the CB1, CB2, and CB3 specimens.

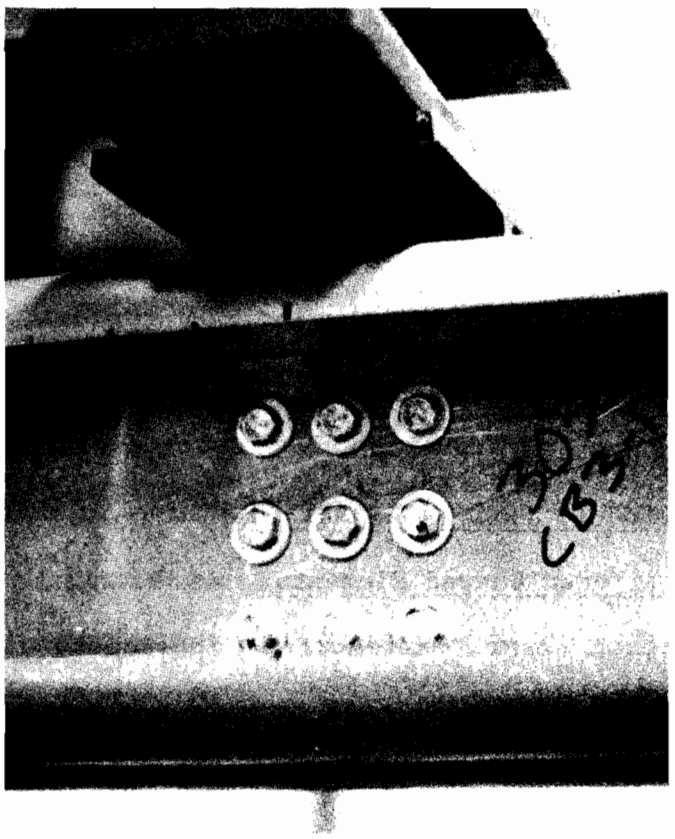

Figure 3.43 Closeup of T-Section Used to Apply Load to CB Beam Specimens

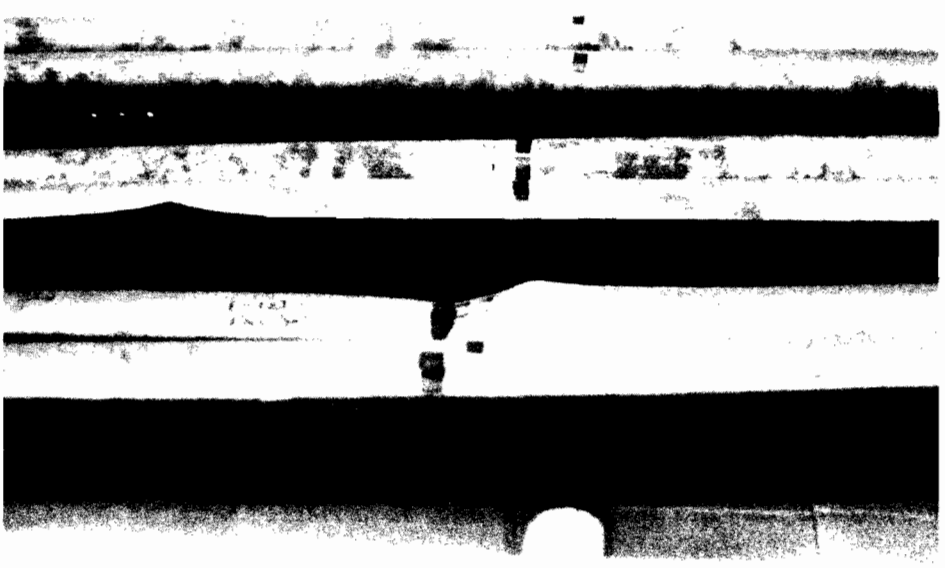

Figure 3.44 Comparison of Failure Modes of CB Beam Specimens

As earlier mentioned, deflection of the beam was measured at midspan for each load level. Beam deflection was monitored in order to ensure that the load was applied uniformly across the specimen and to detect the onset of any nonlinear behavior in the beam. As expected, buckling of the curved flanges occurred soon after the beginning of nonlinear load-deflection behavior. A typical plot of load versus deflection is shown in Figure B.4.

C. DEVELOPMENT OF PREDICTION METHODS

1. Stiffened Curved Elements. As mentioned in Section II.B.1, there have been several attempts to develop equations to predict the buckling stress of curved panels that are simply supported on all sides. The most reasonable of these equations was derived by Redshaw[11] on the basis of the classical energy approach. As previously shown, Sechler and Dunn[13] showed that Redshaw's equation could be expressed as follows:

$$(f_{cr}/E)_{sc} = \sqrt{(f_{cr}/E)_c^2 + 1/4\ (f_{cr}/E)_f^2} + 1/2\ (f_{cr}/E)_f \qquad (3.1)$$

in which

$(f_{cr}/E)_{sc}$ = buckling stress ratio of a simply supported curved element subject to uniform compression (i.e., for a stiffened curved element)

$(f_{cr}/E)_c$ = buckling stress ratio of a full cylinder with the same R/t ratio as the curved element

$(f_{cr}/E)_f$ = buckling stress ratio of a simply supported flat plate with the same t/b ratio as the curved element

Because the theoretical buckling stress ratio for cylinders,

$$(f_{cr}/E)_c = 0.6t/R, \tag{3.2a}$$

consistently provides f_{cr} values much higher than the experimental values, it seems appropriate to replace the theoretical value of $(f_{cr}/E)_c$ with a reduced empirical relationship. In past reports[50,51], a value of 0.3t/R has been suggested.

Stiffened flat elements, on the other hand, normally buckle very close to their theoretical stress. Thus, the full theoretical value for the elastic buckling stress ratio of a stiffened flat element, $(f_{cr}/E)_f$, is suggested for substitution in Eq. (3.1). The theoretical buckling stress ratio of a stiffened flat element is given as

$$(f_{cr}/E)_f = \frac{\pi^2}{3(1-\mu^2)(w/t)^2} \quad . \tag{3.2b}$$

Substituting Eq. (3.2b) for $(f_{cr}/E)_f$, $(f_{cr}/E)_c = 0.3t/R$, along with a Poisson's ratio of 0.3, into Eq. (3.1), the following equation results:

$$(f_{cr}/E)_{sc} = \sqrt{0.09(t/R)^2 + 3.267(t/b)^4} + 1.807(t/b)^2 \tag{3.3}$$

However, based on the results of the stiffened curved element tests, a value of $(f_{cr}/E)_c = 0.25t/R$, when inserted in Eq. (3.1), seems to

provide the best prediction for the elastic local buckling of the stiffened curved elements discussed in this report. After making the above substitution and again assuming a value of 0.3 for Poisson's ratio and the full theoretical buckling stress for $(f_{cr}/E)_f$, Eq. (3.1) becomes:

$$(f_{cr}/E)_{sc} = \sqrt{0.0625(t/R)^2 + 3.267(t/b)^4} + 1.807(t/b)^2 \qquad (3.4)$$

Equations (3.3) and (3.4) are used to predict elastic, local buckling of stiffened curved elements. For inelastic local buckling, the tangent modulus method, as described in Section III.C.3, is employed. Equations (3.3) and (3.4) are compared in Section III.D.

2. Unstiffened Curved Elements. An approach similar to that used by Redshaw for stiffened curved elements leads to an extremely complex equation for unstiffened curved elements that is only reasonable if b/R is small. Because b/R is not small in most applications, an empirical or at least semi-empirical expression is necessary for the prediction of unstiffened curved element buckling behavior. In the Seventh Progress Report[51] a purely empirical equation, called the "Regression Equation" was presented. The Regression Equation was derived using a nonlinear, least squares regression analysis of the stub column data in which the unstiffened curved flanges failed by elastic, local buckling. Based solely on the regression analysis, the following equation was found to best fit the unstiffened curved element data.

$$(f_{cr}/E)_{uc} = \quad 0.02926(t/R) + 0.02090(t/b) \qquad (3.5)$$

However, recent study has revealed that a more rational approach provides better overall agreement with the test data than Eq. (3.5). In this approach, the t/b term is set equal to the critical buckling stress of an unstiffened flat element with a buckling coefficient of 0.5 and with a flat width equal to the arc length of the curved element. The coefficient of the curvature term, t/R, was adjusted in order to provide the best possible agreement with the test data. This equation is shown below.

$$(f_{cr}/E)_{uc} = \quad 0.04068(t/R) + 0.45192(t/b)^2 \qquad (3.6)$$

Equations (3.5) and (3.6) were developed for the initial elastic buckling of the unstiffened curved flanges of specimens having R/t ratios ranging from approximately 25 to 110 and b/t ratios ranging from approximately 25 to 90. Equations (3.5) and (3.6) are compared in Section III.D.

Again, for inelastic local buckling, the tangent modulus approach is employed. This approach is described in detail in the following section.

3. Inelastic Buckling. If the predicted elastic buckling stress is greater than the proportional limit, F_{pr}, then inelastic buckling is assumed. The tangent modulus concept is employed for the prediction of inelastic buckling. Using this approach, the modulus of elasticity is replaced by a reduced "tangent" modulus, E_t. The expression used for the tangent modulus is given below:

$$E_t/E = \frac{(f_{cr}/F_y)(1-(f_{cr}/F_y))}{(F_{pr}/F_y)(1-(F_{pr}/F_y))} \tag{3.7}$$

Note that f_{cr} in Eq. (3.7) is the inelastic buckling stress, $(f_{cr})_{inel}$.

A direct solution for the inelastic buckling stress may be derived from the following expression:

$$(f_{cr})_{inel} = (E_t/E)(f_{cr})_{el} \tag{3.8}$$

where:

$(f_{cr})_{inel}$ = predicted inelastic buckling stress of a curved element

$(f_{cr})_{el}$ = predicted elastic buckling stress of a curved element as computed from the appropriate equation

Substituting Eq. (3.7) for E_t/E, Eq. (3.8) simplifies to

$$(f_{cr})_{inel} = F_y - \frac{F_{pr}(F_y-F_{pr})}{(f_{cr})_{el}}. \tag{3.9}$$

If F_{pr} is assumed to be $0.7F_y$, Eq. (3.9) becomes:

$$(f_{cr})_{inel} = F_y\left[1 - \frac{0.21F_y}{(f_{cr})_{el}}\right]. \tag{3.10}$$

The above equations are based on an approach that was originally developed by Bleich[18] for the inelastic buckling of steel columns. The modulus of elasticity is assumed to be 29,500 ksi.

4. Interaction Between Flat and Curved Elements. Because curved elements are often used in combination with flat elements, a systematic approach for the prediction of the critical buckling load of such sections is highly desirable. The approach used for the prediction of the interaction between flat and curved elements is quite similar to the Air Force Method, which was described in detail in Section II.C.1. Again, curved elements are assumed to have no post-buckling strength; thus, if the critical buckling stress is reached in a curved element before any of the flat elements, the total capacity of the section is obtained. However, if the critical stress is first reached in a flat element, the load resisted by the flat element may continue to increase until the critical buckling stress is obtained in a curved element. The total load resisted by the flat elements is computed using the effective width approach as outlined in Section II.D.1.

The edge stress, f, used in the effective width equation is the predicted curved element buckling stress. Thus, the total load capacity may be computed as simply the lowest curved element buckling stress times the total effective area of the cross-section. This approach is employed in Section III.D.1.a.ii for stub column specimens containing stiffened curved and flat elements and in Section III.D.2.a.ii for stub columns containing unstiffened curved elements and stiffened flat elements.

5. Curved Elements Subject to Bending. Because of the stress gradient condition that exists in curved elements subject to bending, the previously described prediction methods for uniform axial compression must be modified. The most reasonable approach seems to be

to assume that the curved element will buckle when the critical buckling stress from the uniform compression case is reached at some preassumed level in the curved element. For example, in Figure 3.45 buckling is assumed to occur when f_{cr} from the uniform compression case is reached at a distance of

$$y_{cr} = y_{bot} + C(y_{top} - y_{bot}) \tag{3.11}$$

from the neutral axis. Extrapolating to the outer portion of the curved element, the maximum stress, f_{max}, is computed as,

$$f_{max} = (y_{top}/y_{cr})f_{cr}. \tag{3.12}$$

Of course, the simplest and most conservative approach is to simply assume that failure occurs in the curved element subject to bending when the critical buckling stress from the uniform compression case is reached at the point of maximum compression in the curved element. In this case, C is simply equal to 1.0. However, a more accurate prediction of the buckling stress of curved elements subject to bending is obtained for a C value less than 1.0. For each of the beam tests described in this report, the predicted buckling loads are computed assuming values of C of 0.5, 0.6, 0.67, 0.75, and 1.0. The C value that provides the closest prediction of the failure load is noted in Section III.D for each type of beam test.

It should be mentioned that for C values less than 1.0, it is possible for the numerical value of f_{max} to exceed F_y. This should not

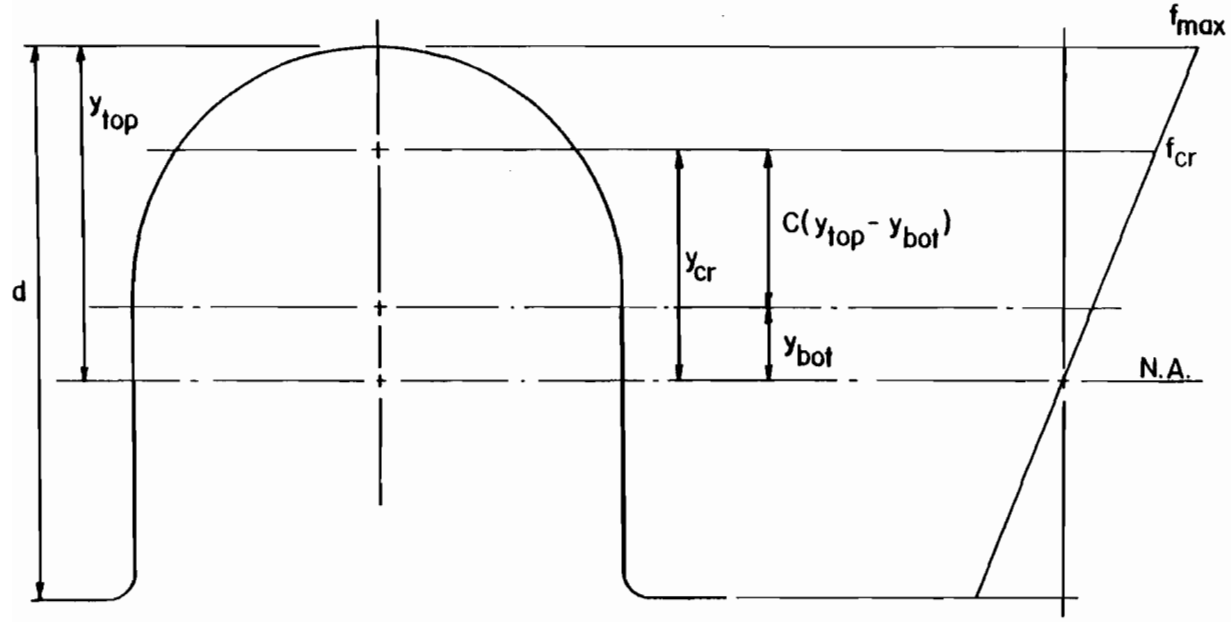

Figure 3.45 Assumed Bending Stress Distribution in a Curved Element

cause too much concern. Of course, in this case the actual maximum stress in the beam may not be as high as f_{max}. The slightly high values of f_{max} are necessary to account for the partial plastification of the beam cross-section. For the purpose of ultimate moment calculation, M_{max}, may be computed as follows:

For stiffened curved elements,

$$M_{max} = S_{xc} f_{max} < 1.2 S_{xc} F_y \text{ or } 1.2 S_{xt} F_y. \quad \text{(whichever is smaller)} \tag{3.13}$$

where:

S_{xc} = section modulus for the compression side

S_{xt} = section modulus for the tension side

Note that the 1.2 factor may be thought of as a type of "shape" factor normally described in plastic design.

For unstiffened curved elements,

$$M_{max} = S_{xc} f_{max} < S_{xc} F_y \text{ or } S_{xt} F_y. \quad \text{(whichever is smaller)} \tag{3.14}$$

No effective "shape" factor is permitted for unstiffened curved elements since they are not very efficient at transferring stress to their outer flange tips.

6. Curved Elements Subject Primarily to Shear. As mentioned in Section II.E.1, several equations have been proposed for the prediction of curved element buckling caused by shearing stresses. Of the available literature, the method proposed by Gerard[2] seems to be the most reasonable. Thus, failure of the curved element is predicted when

the shearing stress, τ_{cr}, reaches the level given by either Eq. (2.26) or Eq. (2.27), whichever is applicable, for elastic buckling. For inelastic buckling ($\tau_{cr} > \tau_{pr}$), the tangent modulus approach is employed. Using Von Mises yield criteria, the shear yield point, τ_y, may be estimated as

$$\tau_y = \frac{F_y}{\sqrt{3}}. \tag{3.15}$$

The value of the shear proportional limit, τ_{pr}, is estimated as $\tau_{pr} = 0.7\tau_y$. Using the same form of equation as Eq. (3.10) for inelastic buckling, τ_{cr} may be computed as

$$(\tau_{cr})_{inel} = \tau_y\left[1 - \frac{0.21\tau_y}{(\tau_{cr})_{el}}\right]. \tag{3.16}$$

The shear force, V_c, required to cause shear buckling may be computed from the horizontal shear stress equation as follows:

$$\tau_{cr} = \frac{V_c Q}{It} \tag{3.17}$$

Solving for V_c,

$$V_c = \tau_{cr} \frac{It}{Q} \tag{3.18}$$

in which

τ_{cr} = critical shear buckling stress as determined by either Eq. (2.26) or (2.27), whichever is appropriate

V_c = shear force required to produce τ_{cr} in a curved element

I = moment of inertia of entire section about the neutral axis

Q = static moment of the area above or below the section at which the shear stress is desired

t = thickness of the section at the section where τ_{cr} is desired

It should be noted that it is extremely difficult to develop the predicted shear buckling stress in a curved web, as previously described in Section III.B.2.e. Therefore, special care should be exercised to prevent other modes of failure at lesser loads.

D. COMPARISON OF PREDICTED TO TEST RESULTS

Included in this section is a complete comparison of all of the available curved element test results to the latest prediction methods. In some cases, improvements have been made to the original prediction procedures. In these cases, the original prediction procedures are compared to the newest procedures. The dimensions of the test specimens used in computing the predicted loads are given in Tables A.1 through A.8 of the Appendix.

1. Stiffened Curved Elements. As mentioned in Section III.C.1, a slight revision in Redshaw's Equation has been suggested. This revision involved changing the assumed critical buckling stress ratio term for a cylinder from 0.3t/R to 0.25t/R in Eq. (3.1). The change was made simply because the latter seemed to provide a better comparison to the

Table 3.7 Comparison of Actual-to-Predicted Buckling Loads
Stiffened Curved Element, AS Stub Column Specimens
Initial Curved Element Failure
(Based on Eqs. (3.3) and (3.4) with Eq. (3.10)
Used for Inelastic Buckling)

Specimen	Ultimate Load (kips)	Initial Buckling Load (kips)	Predicted Buckling Load (kips)		(2)/(3)	(2)/(4)	(1)/(2)
			Eq.(3.3)	Eq.(3.4)			
	(1)	(2)	(3)	(4)	(5)	(6)	(7)
80XFBS3-1*	188.4	188.4	188.4	186.6	1.00	1.01	1.00
50XF(78)AS3-1*	135.0	135.0	127.7	126.7	1.06	1.07	1.00
80SKBS3-1*	121.1	121.1	113.2	112.0	1.07	1.08	1.00
80DKAS3-1*	72.1	72.1	60.9	60.2	1.18	1.20	1.00
50XF(39)AS3-2*	57.5	57.5	58.0	57.1	0.99	1.01	1.00
30SKAS3-1*	18.7	18.7	19.7	19.5	0.95	0.96	1.00
80XFBS2-1*	158.2	158.2	159.1	156.6	0.99	1.01	1.00
50XF(78)AS2-1*	102.0	102.0	105.7	104.4	0.96	0.98	1.00
80SKBS2-1*	99.0	98.5	93.4	91.9	1.05	1.07	1.01
80DKAS2-1*	53.7	53.4	50.1	49.1	1.07	1.09	1.01
50XF(39)AS2-1*	43.9	43.9	46.6	45.4	0.94	0.97	1.00
30SKAS2-1*	16.5	16.5	17.2	17.0	0.96	0.97	1.00
80XFBS1-1*	147.8	142.5	141.0	137.0	1.01	1.04	1.04
50XF(78)AS1-1*	94.9	92.5	92.0	90.1	1.01	1.03	1.03
50XF(78)AS1-2*	93.0	87.5	93.9	91.9	0.93	0.95	1.06
80SKBS1-1*	87.5	83.4	81.1	77.9	1.03	1.07	1.05
80DKAS1-1*	45.0	41.6	41.7	39.8	1.00	1.05	1.08
80DKAS1-2	43.4	28.9	37.2	32.8	0.78	0.88	1.50
50XF(39)AS1-1	33.8	32.2	31.8	27.6	1.01	1.17	1.05
50XF(39)AS1-2	34.0	28.7	33.1	28.6	0.87	1.00	1.18
30SKAS1-1*	13.6	11.8	13.6	13.1	0.86	0.90	1.15
30SKAS1-2*	14.4	10.7	13.3	12.7	0.80	0.84	1.35
Mean					0.98	1.02	-
Std. Deviation					0.092	0.085	-

*$f_{cr} > F_{pr} = 0.7F_y$; assume inelastic buckling

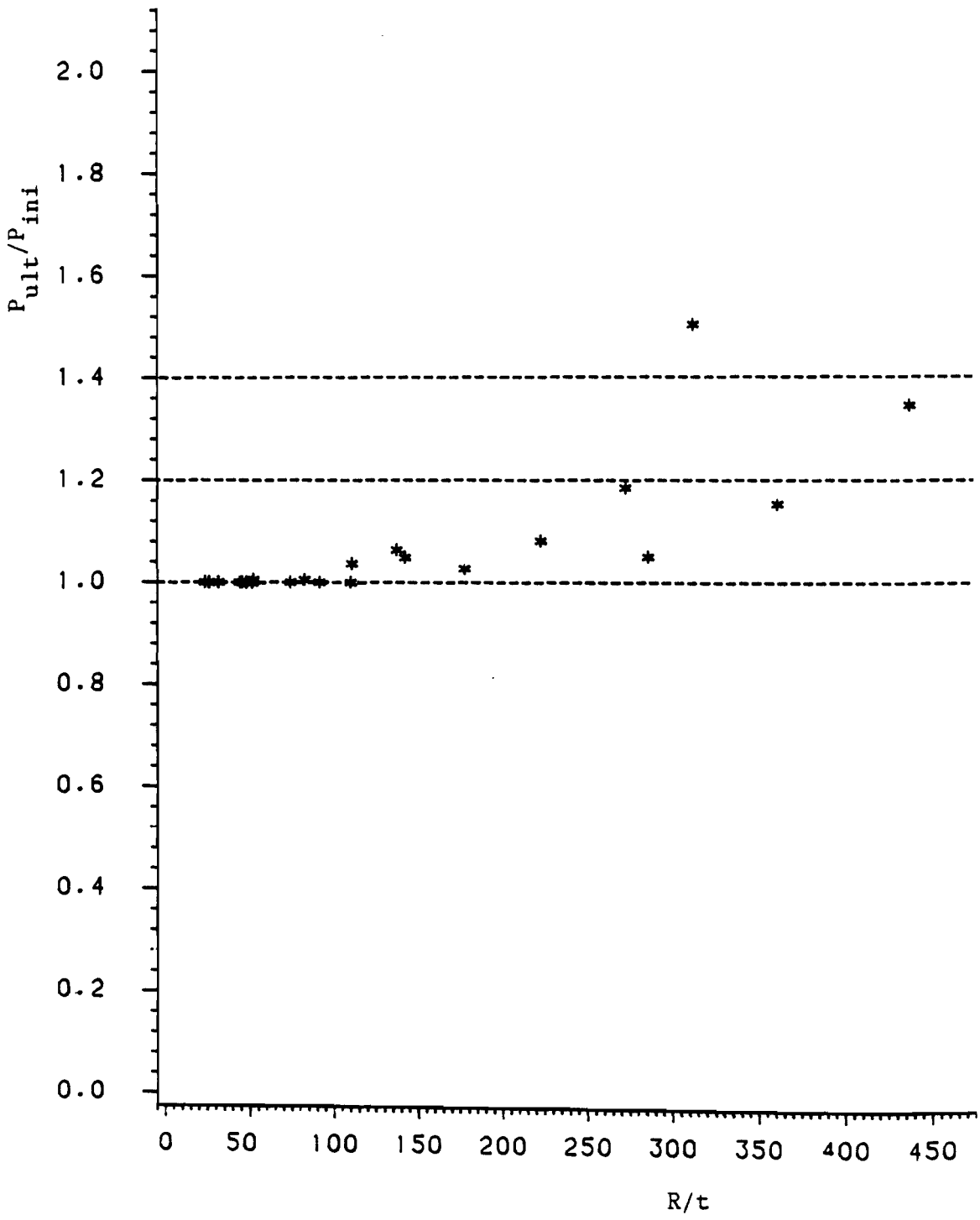

P_{ini} = Initial buckling load of curved element

P_{ult} = Ultimate load of cross section

Figure 3.46 Comparison of P_{ult}/P_{ini} Vs. R/t for AS Stub Column Tests

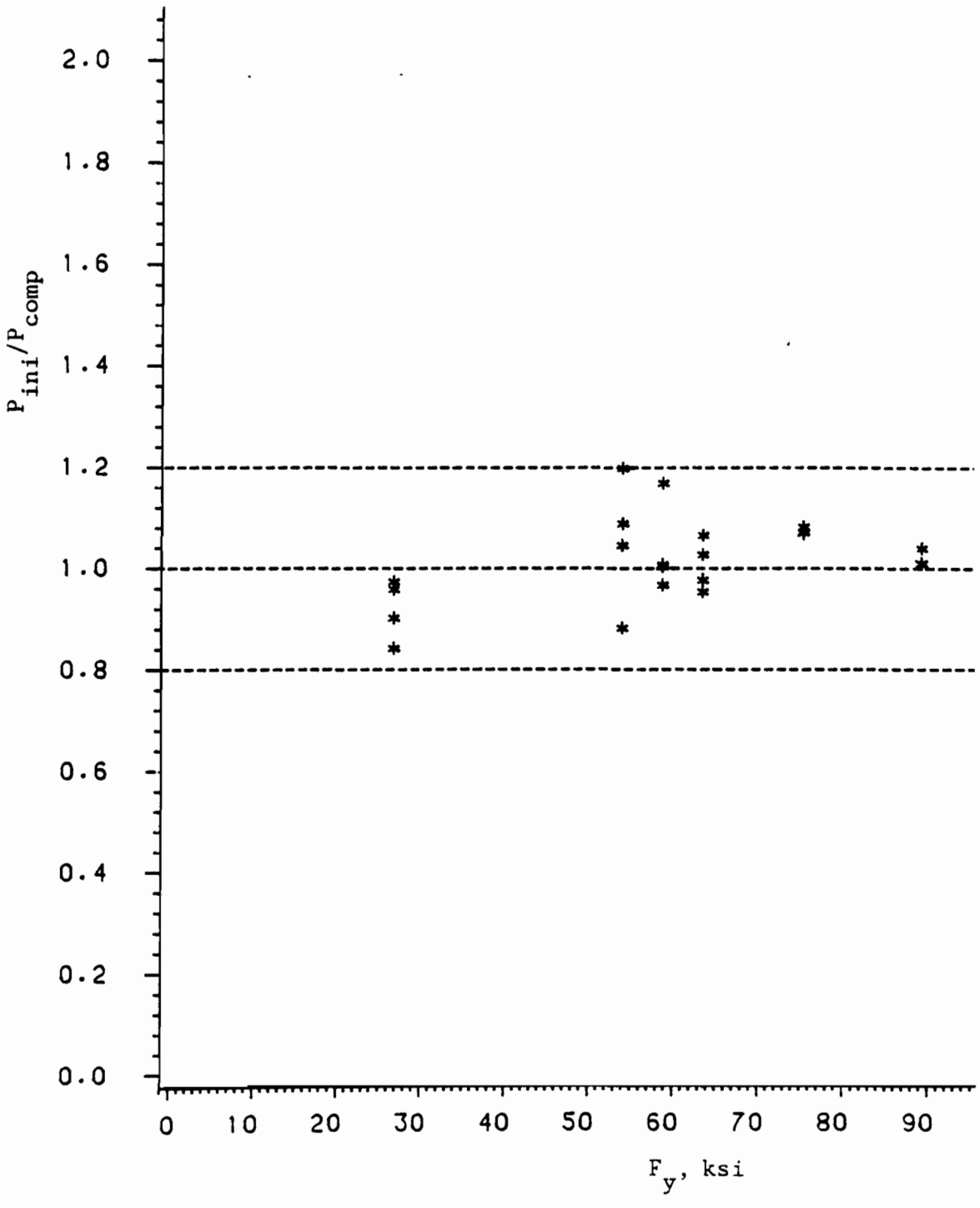

P_{ini} = Initial buckling load of curved element

P_{comp} = Predicted initial buckling load

Figure 3.47 Comparison of P_{ini}/P_{comp} Vs. F_y for AS Stub Column Tests

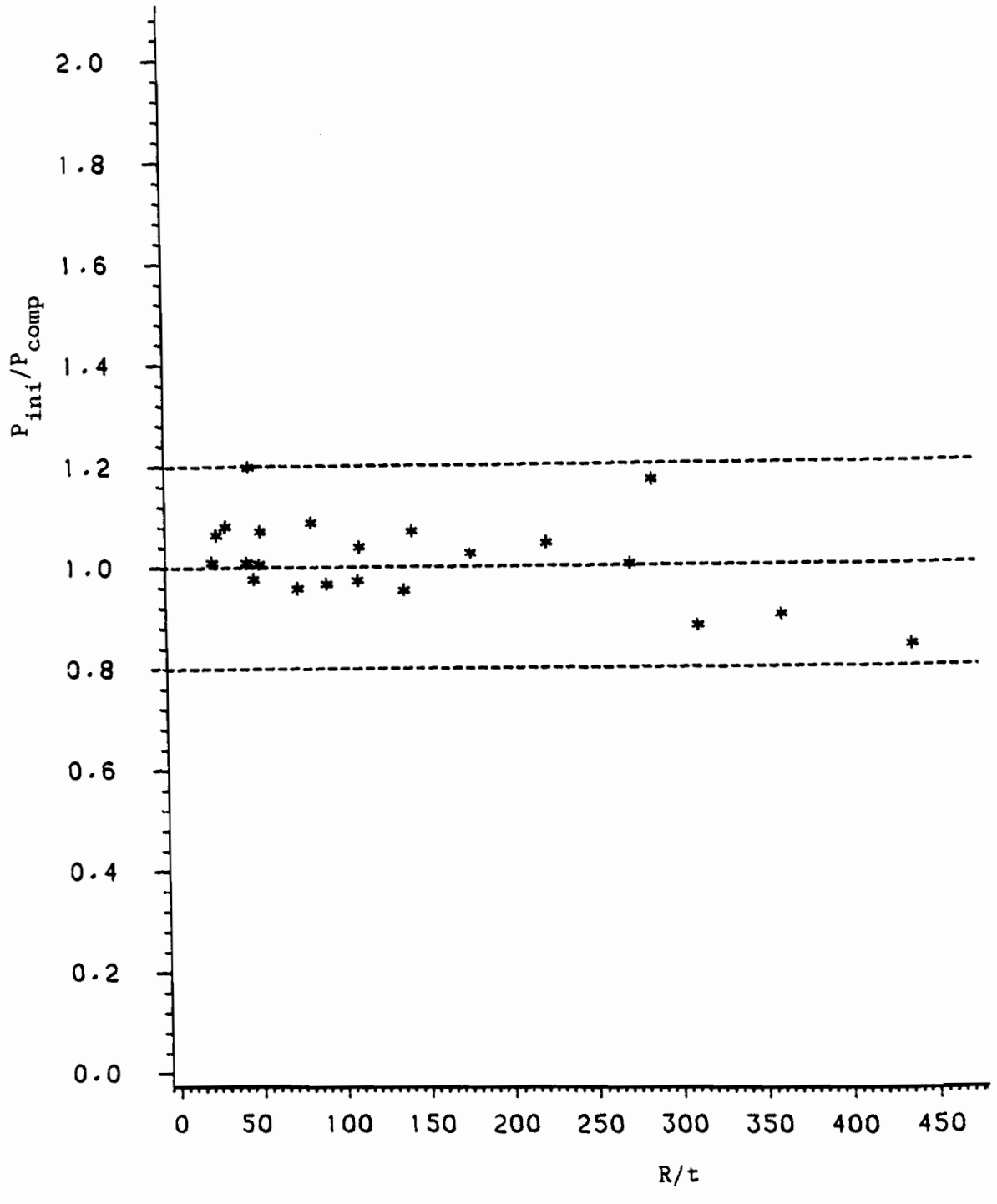

P_{ini} = Initial buckling load of curved element

P_{comp} = Predicted initial buckling load

Figure 3.48 Comparison of P_{ini}/P_{comp} Vs. R/t for AS Stub Column Tests

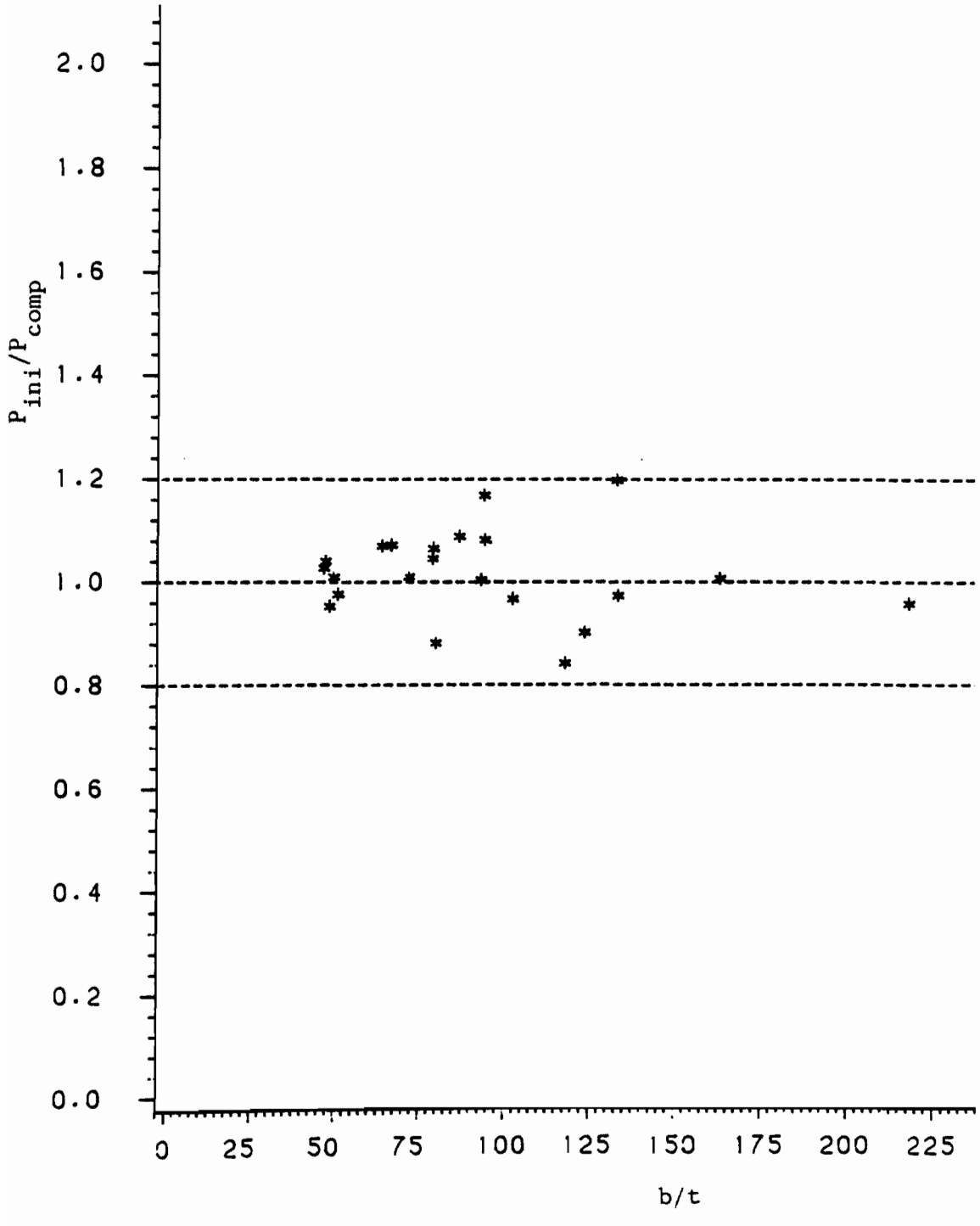

P_{ini} = Initial buckling load of curved element

P_{comp} = Predicted initial buckling load

Figure 3.49 Comparison of P_{ini}/P_{comp} Vs. b/t for AS Stub Column Tests

actual test results. The two resulting forms of Redshaw's Equation, Eqs. (3.3) and (3.4), are compared in Table 3.7. Note that the proportional limit, F_{pr}, is assumed to be 70% of the yield strength, F_y.

The two forms of Redshaw's Equation are only compared for the AS stub column data in which the stiffened curved elements were the initial and final cause of failure (Section III.B.2.a). The prediction of stiffened curved element behavior for the remaining specimens is based only on the latest prediction methods. (i.e., Eq. (3.4) for Redshaw's Equation and Eq. (3.10) for inelastic buckling)

a. Uniform Axial Compression - Stub Column Tests.

i. Initial Curved Element Failure - AS Specimens. For this series of tests the curved elements were the initial and final cause of failure. Thus, no interaction with the flat elements need be considered. The ultimate load that each of these specimens could withstand is recorded in column (1) of Table 3.7. Column (2) lists the load associated with the first observed curved element buckle. As shown by the ratio of the ultimate-to-initial buckling loads (column (7)), little, if any, post-buckling strength is available for the more highly curved AS3 and AS2 specimens. However, there does seem to be some post-buckling strength for the flatter AS1 specimens. Because the braced, flat elements are unbuckled at failure, it is difficult to ascertain the exact magnitude of the post-buckling strength of the curved elements. The ultimate-to-initial buckling load ratios may be compared for the tested range of R/t values in Figure 3.46.

The predicted initial buckling loads are computed as simply the predicted initial buckling stress from either Eq. (3.3) or (3.4) times

the total cross sectional area of each specimen. Columns (3) and (4) list the predicted initial buckling loads computed from the respective equations. The test values for the initial buckling loads are compared to the predicted loads from Eq. (3.3) and Eq. (3.4) in columns (5) and (6), respectively. As shown, both Eqs. (3.3) and (3.4) provide reasonably good predictions for the AS3 and AS2 specimens. However, for the AS1 specimens, the slightly lower predictions resulting from Eq. (3.4) are in better agreement with the test results. Therefore, Eq. (3.4) is recommended for the prediction of curved element buckling. The initial-to-predicted buckling load ratios may be compared for the tested ranges of F_y, R/t, and b/t, in Figures 3.47 through 3.49, respectively.

ii. Interaction Between Stiffened Curved and Flat Elements - ASI Specimens. As mentioned earlier, a series of stub column tests have been performed in which no bracing was attached to the flat webs. Thus, the flat webs were capable of buckling before the stiffened curved elements. The flat webs of all the listed specimens, except for the 50XF(78) material, buckled before the adjoining stiffened curved elements. As previously stated in Section III.B.2.b.v, there was no spread of the flat element buckle into the curved element of the ASI1 and ASI2 specimens. However, for the ASI3 specimens, the flat element buckle seemed to spread into the curved element until an angle of approximately 30° was obtained between the flat and curved elements. The assumed "failed" geometry of the ASI3 specimens is shown in Figure 3.50. In order to account for the spread of the flat element into the curved element, a revised width of the flat web, wc, equal to the

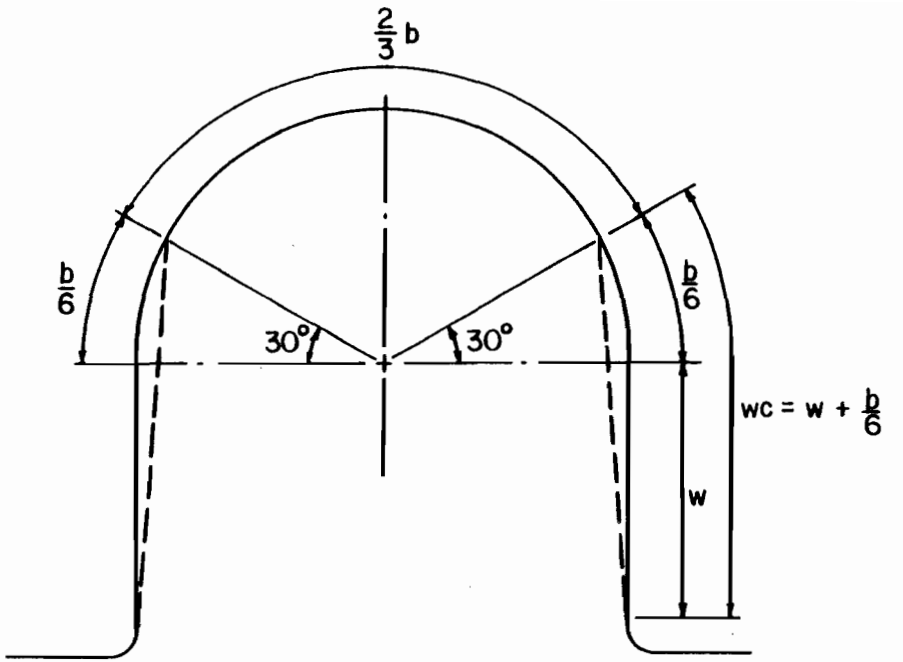

Figure 3.50 Assumed Spread of Flat Web into Curved Element for ASI Specimens

original flat width, w, plus 30° of arc of the curved element, is used in the calculation of the total load resisted by the webs, P_w.

The predicted initial buckling load is computed on an element by element basis as described in Section III.C.4. The total load resisted by the flat webs, P_w, is computed as the total effective web area (effective width times the thickness times the number of webs) multiplied by the predicted buckling stress, f_{cr}, for the adjoining curved element. P_{curve} is calculated as this same curved element buckling stress times the remaining area (total area - full web area) in the cross section. The total predicted load, P_{total}, is simply (P_w + P_{curve}).

The test data for the ASI specimens are given in Table 3.8. Column (1) lists the ultimate load that the specimen could withstand. The loads associated with the first curved element buckle are provided in column (2). As shown by the ratio of the ultimate-to-initial buckling loads in column (7), there is no appreciable post-buckling strength for the more curved ASI3 (R=2 in.) and ASI2 (R=3.5 in.) specimens. However, the flatter ASI1 (R=15 in.) specimens exhibit some additional strength after buckling. The ultimate-to-initial buckling load ratios are shown for the tested range of R/t values in Figure 3.51.

The total predicted load for each specimen, P_{total}, is listed in column (5). As shown in column (6), good agreement exists between the actual initial buckling loads and the predicted loads which were computed using this method. Figures 3.52 through 3.54 show the initial-to-predicted buckling load ratios for the tested ranges of F_y, R/t, and b/t, respectively.

Table 3.8 Comparison of Actual-to-Predicted Buckling Loads
Stiffened Curved Element, ASI Stub Column Specimens
Interaction Between Flat and Curved Elements
P_{curve} Based on Eq. (3.4) and the Direct
Approach for Inelastic Buckling (Eq. (3.10))
(Use Flat Width = w + b/6 for ASI3 Specimens)

Specimen	Ultimate Load (kips) (1)	Initial Buckling Load (kips) (2)	P_w (kips) (3)	P_{curve} (kips) (4)	P_{total} (kips) (5)	(2)/(5) (6)	(1)/(2) (7)
50XF(78)ASI3-2*	113.8	113.8	49.7	60.2	118.9	0.96	1.00
80DKASI3-2*	57.6	57.6	16.4	31.9	48.3	1.19	1.00
50XF(39)ASI3-1*	44.7	44.7	12.8	31.7	44.5	1.00	1.00
30SKASI3-2*	17.1	17.1	5.04	11.4	16.4	1.04	1.00
50XF(78)ASI2-2*	107.5	107.5	35.6	71.8	107.4	1.00	1.00
80DKASI2-2*	50.9	50.9	15.1	34.4	49.4	1.03	1.00
50XF(39)ASI2-2*	39.6	39.6	11.2	31.0	42.1	0.94	1.00
30SKASI2-2*	16.1	16.1	4.62	12.4	17.0	0.95	1.00
50XF(78)ASI1-3*	88.4	81.1	28.1	64.3	92.3	0.88	1.09
80DKASI1-3	40.8	33.4	11.6	26.0	37.7	0.89	1.22
50XF(39)ASI1-3	33.5	33.2	8.06	19.2	27.3	1.22	1.01
Mean						1.01	-
Std. Deviation						0.110	-

* $f_{cr} > F_{pr} = 0.7F_y$; assume inelastic buckling

P_w = predicted web strength based on predicted curved element buckling stress at edges of web
P_{curve} = predicted curved element buckling load
P_{total} = predicted total load that section can withstand = $P_w + P_{curve}$

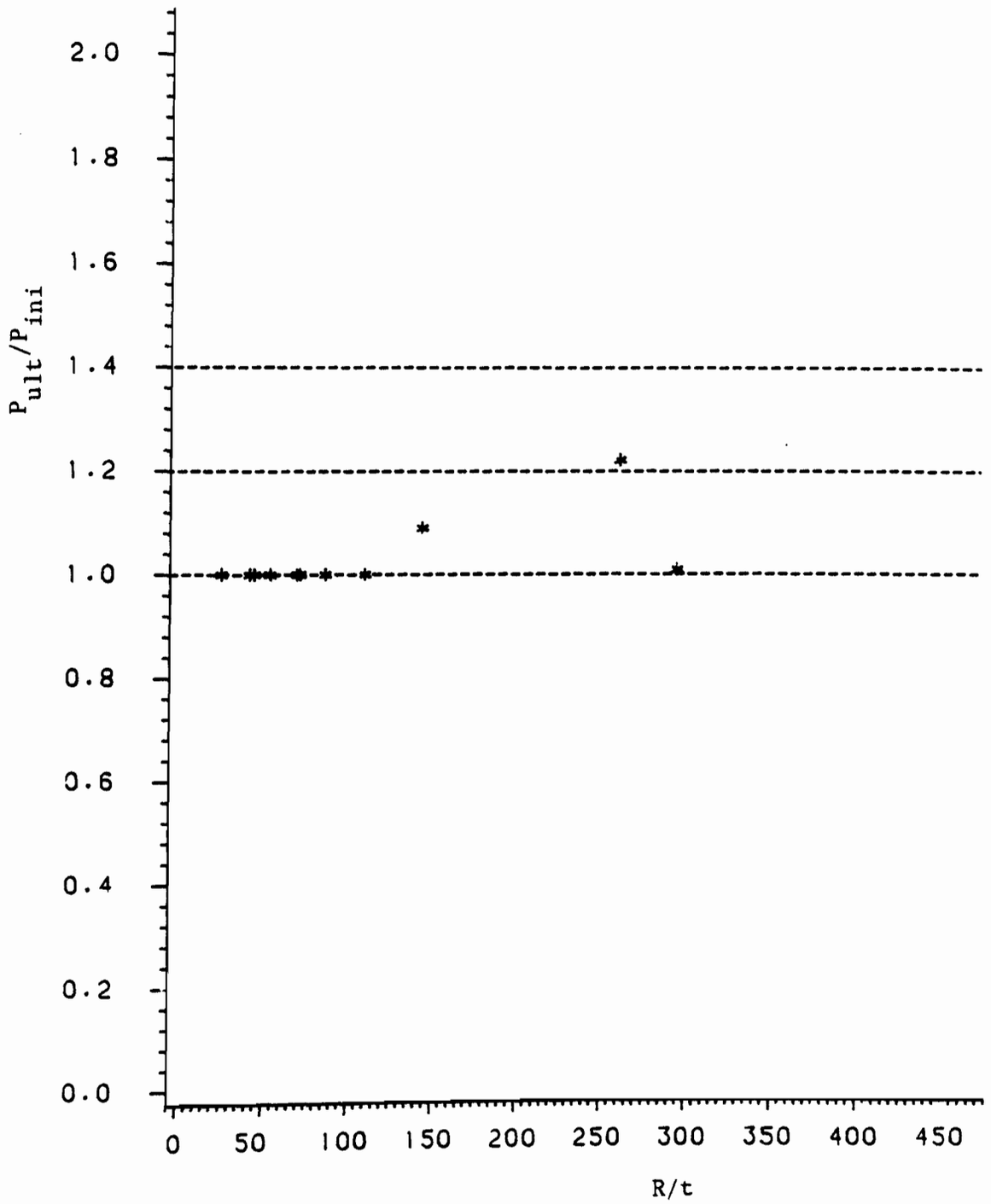

P_{ini} = Initial buckling load of curved element

P_{ult} = Ultimate load of cross section

Figure 3.51 Comparison of P_{ult}/P_{ini} Vs. R/t for ASI Stub Column Tests

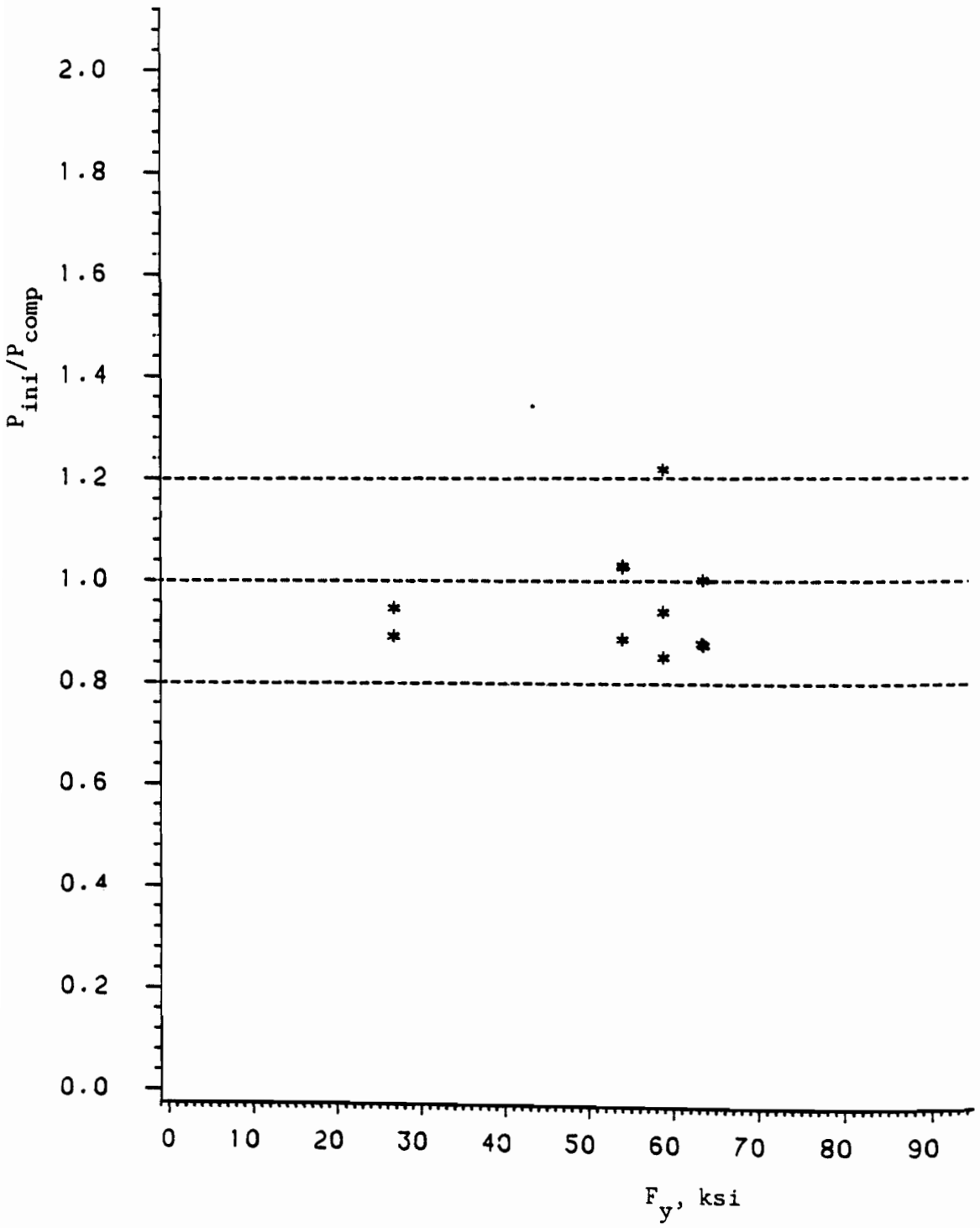

P_{ini} = Initial buckling load of curved element

P_{comp} = Predicted initial buckling load

Figure 3.52 Comparison of P_{ini}/P_{comp} Vs. F_y for ASI Stub Column Tests

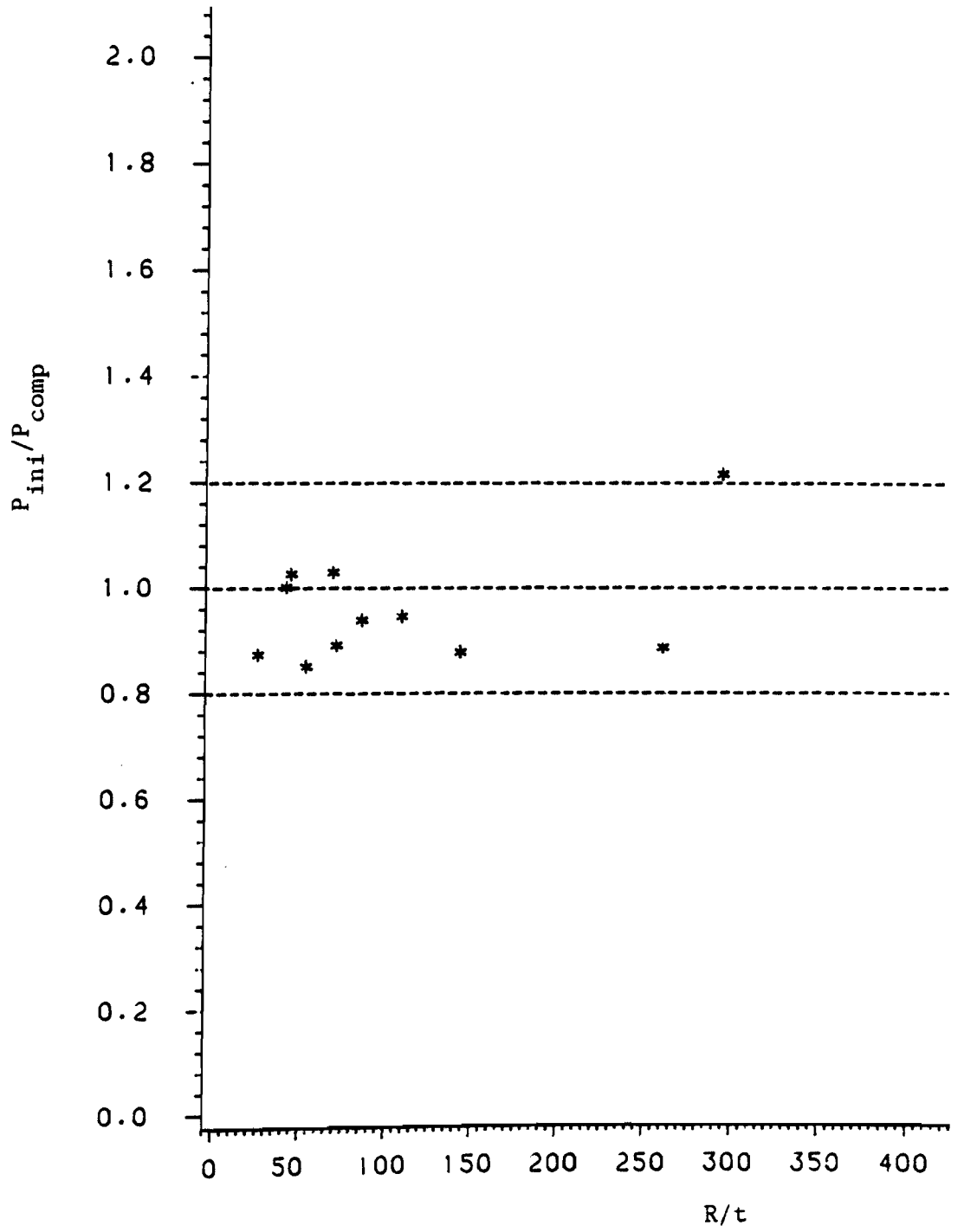

P_{ini} = Initial buckling load of curved element

P_{comp} = Predicted initial buckling load

Figure 3.53 Comparison of P_{ini}/P_{comp} Vs. R/t for ASI Stub Column Tests

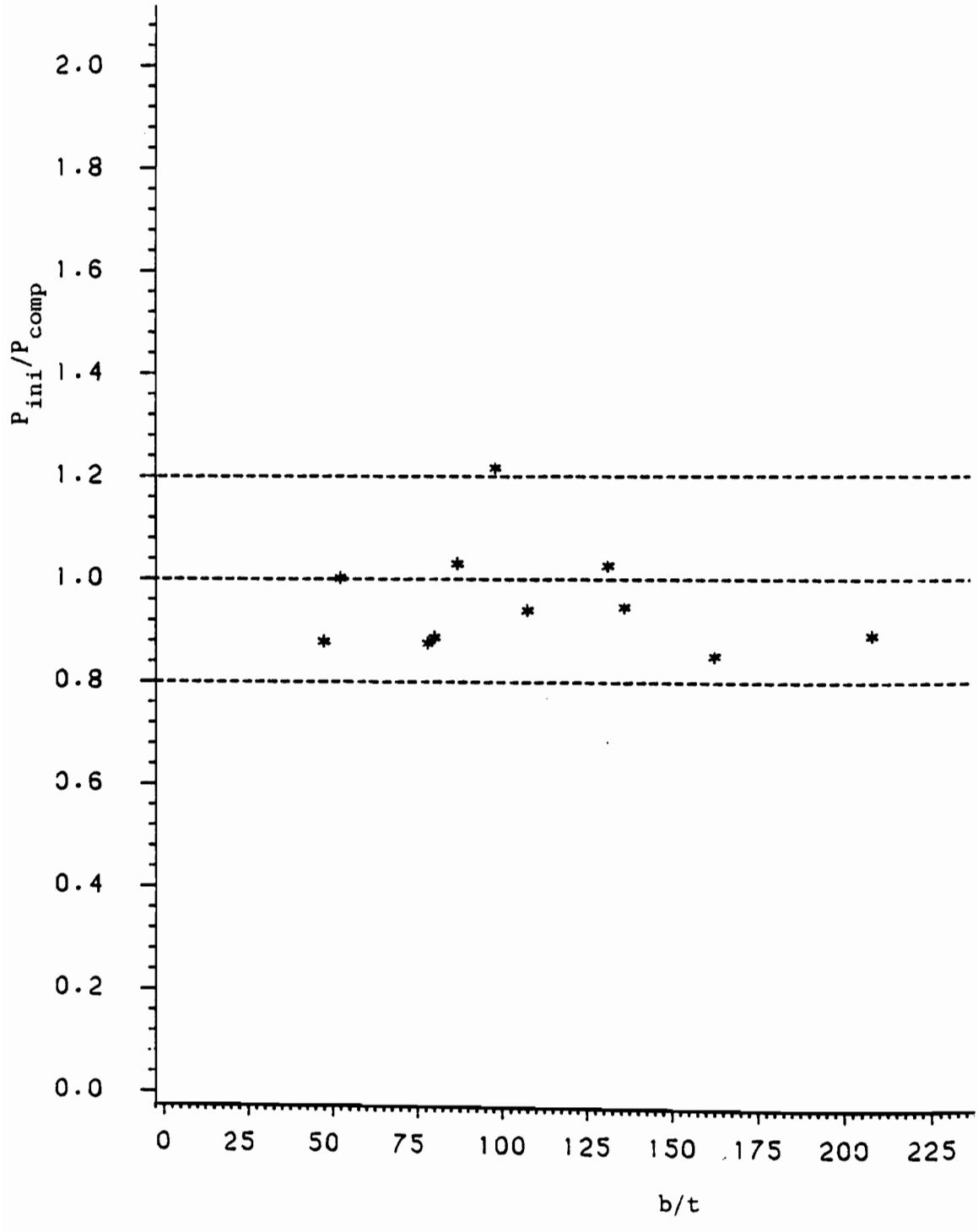

P_{ini} = Initial buckling load of curved element

P_{comp} = Predicted initial buckling load

Figure 3.54 Comparison of P_{ini}/P_{comp} Vs. b/t for ASI Stub Column Tests

b. Bending.

i. AB Beam Specimens. Column (1) of Table 3.9 lists the ultimate moments that the AB beam specimens could withstand. The initial buckling moments, column (2), are the moments associated with the first observed buckling in the curved flange. An idea of available post-buckling strength may be obtained from Figure 3.55.

The predicted buckling moments are computed using the method outlined in Section III.C.5 for C values of 1.0, 0.75, 0.67, 0.60 and 0.5. The predicted buckling moments associated with each value of C are given in column (3) of Tables 3.9 through 3.13, respectively. The initial buckling moment is compared to the predicted moment in column (4) of each table. Column (5) compares the ultimate moment to the predicted moment. Note that because of the relatively small amount of post-buckling strength, there is little difference between the ratios listed in columns (4) and (5). Table 3.14 compares the initial buckling-to-predicted moment ratios as computed for various values of C. As shown, a value of C = 0.67 provides the best overall agreement with the test data. The initial-to-predicted buckling moment ratios (assuming C=0.67) may be compared for the tested range of F_y, R/t, and b/t, in Figures 3.56 through 3.58, respectively.

ii. DB Beam Specimens. Column (1) of Table 3.15 lists the ultimate moments that the DB beam specimens could withstand. The moments associated with initial buckling are given in column (2). Because of the extreme inelastic failure of these specimens, no post-buckling strength whatsoever was observed for any of the DB series. Thus, columns (1) and (2) are identical. The predicted buckling moments

Table 3.9 Comparison of Actual-to-Predicted Buckling Moments
AB Beam Specimens (C=1.0)
Based on Modified Redshaw's Eq. (3.4) Using
Direct Approach for Inelastic Buckling, Eq. (3.10)

Specimen	Ultimate Moment (kips) (1)	Initial Buckling Moment (in-kips) (2)	Predicted Buckling Moment (in-kips) (3)	(2)/(3) (4)	(1)/(3) (5)	(1)/(2) (6)
80XFAB3-1*	134.4	134.4	114.4	1.17	1.17	1.00
50XF(78)AB3-1*	85.6	85.6	73.0	1.17	1.17	1.00
80SKAB3-2*	94.4	94.4	67.3	1.40	1.40	1.00
80DKAB3-2*	49.3	49.3	34.9	1.41	1.41	1.00
50XF(39)AB3-3*	36.3	36.3	32.7	1.11	1.11	1.00
30SKAB3-2*	15.2	15.2	11.6	1.31	1.31	1.00
80XFAB2-1*	83.8	83.8	73.5	1.14	1.14	1.00
50XF(78)AB2-1*	51.9	51.9	45.8	1.13	1.13	1.00
80SKAB2-1*	54.1	54.1	42.3	1.28	1.28	1.00
80DKAB2-1*	25.6	25.6	22.5	1.14	1.14	1.00
50XF(39)AB2-1*	23.4	23.4	20.0	1.17	1.17	1.00
30SKAB2-1*	8.06	8.06	7.44	1.08	1.08	1.00
80XFAB1-1*	57.8	57.2	63.7	0.87	0.88	1.01
50XF(78)AB1-1*	37.8	37.8	40.9	0.89	0.89	1.00
80SKAB1-1*	33.1	32.2	33.6	0.92	0.95	1.03
80DKAB1-1*	18.6	18.6	18.3	0.99	0.99	1.00
50XF(39)AB1-1	13.4	12.9	12.2	1.02	1.07	1.04
30SKAB1-1*	5.44	5.13	5.78	0.86	0.92	1.06
Mean				1.13	1.13	
Std. Deviation				0.157	0.149	

*$f_{cr} > F_{pr} = 0.7F_y$; assume inelastic buckling

Table 3.10 Comparison of Actual-to-Predicted Buckling Moments
AB Beam Specimens (C=0.75)
Based on Modified Redshaw's Eq. (3.4) Using
Direct Approach for Inelastic Buckling, Eq. (3.10)

Specimen	Ultimate Moment (in-kips) (1)	Initial Buckling Moment (in-kips) (2)	Predicted Buckling Moment (in-kips) (3)	(2)/(3) (4)	(1)/(3) (5)	(1)/(2) (6)
80XFAB3-1*	134.4	134.4	135.5	0.99	0.99	1.00
50XF(78)AB3-1*	85.6	85.6	85.7	1.00	1.00	1.00
80SKAB3-2*	94.4	94.4	81.6	1.16	1.16	1.00
80DKAB3-2*	49.3	49.3	40.9	1.20	1.20	1.00
50XF(39)AB3-3*	36.3	36.3	39.1	0.93	0.93	1.00
30SKAB3-2*	15.2	15.2	14.1	1.08	1.08	1.00
80XFAB2-1*	83.8	83.8	80.0	1.05	1.05	1.00
50XF(78)AB2-1*	51.9	51.9	50.2	1.03	1.03	1.00
80SKAB2-1*	54.1	54.1	46.6	1.16	1.16	1.00
80DKAB2-1*	25.6	25.6	24.7	1.04	1.04	1.00
50XF(39)AB2-1*	23.4	23.4	22.1	1.06	1.06	1.00
30SKAB2-1*	8.06	8.06	8.29	0.97	0.97	1.00
80XFAB1-1*	57.8	57.2	65.9	0.87	0.88	1.01
50XF(78)AB1-1*	37.8	37.8	42.4	0.89	0.89	1.00
80SKAB1-1*	33.1	32.2	34.9	0.92	0.95	1.03
80DKAB1-1*	18.6	18.6	18.9	0.99	0.99	1.00
50XF(39)AB1-1*	13.4	12.9	12.6	1.02	1.07	1.04
30SKAB1-1*	5.44	5.13	5.93	0.86	0.92	1.06
Mean				1.01	1.02	
Std. Deviation				0.098	0.093	

*$f_{cr} > F_{pr} = 0.7F_y$; assume inelastic buckling

Table 3.11 Comparison of Actual-to-Predicted Buckling Moments
AB Beam Specimens (C=0.67)
Based on Modified Redshaw's Eq. (3.4) Using
Direct Approach for Inelastic Buckling, Eq. (3.10)

Specimen	Ultimate Moment (in-kips) (1)	Initial Buckling Moment (in-kips) (2)	Predicted Buckling Moment (in-kips) (3)	(2)/(3) (4)	(1)/(3) (5)	(1)/(2) (6)
80XFAB3-1*	134.4	134.4	144.1	0.93	0.93	1.00
50XF(78)AB3-1*	85.6	85.6	90.8	0.94	0.94	1.00
80SKAB3-2*	94.4	94.4	86.6	1.09	1.09	1.00
80DKAB3-2*	49.3	49.3	43.3	1.14	1.14	1.00
50XF(39)AB3-3*	36.3	36.3	41.7	0.87	0.87	1.00
30SKAB3-2*	15.2	15.2	14.7	1.03	1.03	1.00
80XFAB2-1*	83.8	83.8	82.3	1.02	1.02	1.00
50XF(78)AB2-1*	51.9	51.9	51.8	1.00	1.00	1.00
80SKAB2-1*	54.1	54.1	48.2	1.12	1.12	1.00
80DKAB2-1*	25.6	25.6	25.5	1.01	1.01	1.00
50XF(39)AB2-1*	23.4	23.4	22.8	1.03	1.03	1.00
30SKAB2-1*	8.06	8.06	8.60	0.94	0.94	1.00
80XFAB1-1*	57.8	57.2	66.7	0.86	0.87	1.01
50XF(78)AB1-1*	37.8	37.8	42.8	0.88	0.88	1.00
80SKAB1-1*	33.1	32.2	35.3	0.91	0.94	1.03
80DKAB1-1*	18.6	18.6	19.1	0.98	0.98	1.00
50XF(39)AB1-1*	13.4	12.9	12.7	1.01	1.06	1.04
30SKAB1-1*	5.44	5.13	5.98	0.86	0.91	1.06
Mean				0.98	0.99	
Std. Deviation				0.086	0.083	

*$f_{cr} > F_{pr} = 0.7F_y$; assume inelastic buckling

Table 3.12 Comparison of Actual-to-Predicted Buckling Moments
AB Beam Specimens (C=0.60)
Based on Modified Redshaw's Eq. (3.4) Using
Direct Approach for Inelastic Buckling, Eq. (3.10)

Specimen	Ultimate Moment (in-kips) (1)	Initial Buckling Moment (in-kips) (2)	Predicted Buckling Moment (in-kips) (3)	(2)/(3) (4)	(1)/(3) (5)	(1)/(2) (6)
80XFAB3-1*	134.4	134.4	144.8	0.93	0.93	1.00
50XF(78)AB3-1*	85.6	85.6	91.6	0.93	0.93	1.00
80SKAB3-2*	94.4	94.4	86.6	1.09	1.09	1.00
80DKAB3-2*	49.3	49.3	44.9	1.10	1.10	1.00
50XF(39)AB3-3*	36.3	36.3	42.8	0.85	0.85	1.00
30SKAB3-2*	15.2	15.2	14.7	1.03	1.03	1.00
80XFAB2-1*	83.8	83.8	84.5	0.99	0.99	1.00
50XF(78)AB2-1*	51.9	51.9	53.3	0.97	0.97	1.00
80SKAB2-1*	54.1	54.1	49.7	1.09	1.09	1.00
80DKAB2-1*	25.6	25.6	26.2	0.98	0.98	1.00
50XF(39)AB2-1*	23.4	23.4	23.5	1.00	1.00	1.00
30SKAB2-1*	8.06	8.06	8.90	0.91	0.91	1.00
80XFAB1-1*	57.8	57.2	67.3	0.85	0.86	1.01
50XF(78)AB1-1*	37.8	37.8	43.3	0.87	0.87	1.00
80SKAB1-1*	33.1	32.2	35.7	0.90	0.93	1.03
80DKAB1-1*	18.6	18.6	19.2	0.97	0.97	1.00
50XF(39)AB1-1*	13.4	12.9	12.8	1.00	1.05	1.04
30SKAB1-1*	5.44	5.13	6.02	0.85	0.90	1.06
Mean				0.96	0.97	
Std. Deviation				0.082	0.079	

*$f_{cr} > F_{pr} = 0.7F_y$; assume inelastic buckling

Table 3.13 Comparison of Actual-to-Predicted Buckling Moments
AB Beam Specimens (C=0.50)
Based on Modified Redshaw's Eq. (3.4) Using
Direct Approach for Inelastic Buckling, Eq. (3.10)

Specimen	Ultimate Moment (in-kips) (1)	Initial Buckling Moment (in-kips) (2)	Predicted Buckling Moment (in-kips) (3)	(2)/(3) (4)	(1)/(3) (5)	(1)/(2) (6)
80XFAB3-1*	134.4	134.4	144.8	0.93	0.93	1.00
50XF(78)AB3-1*	85.6	85.6	91.6	0.93	0.93	1.00
80SKAB3-2*	94.4	94.4	86.6	1.09	1.09	1.00
80DKAB3-2*	49.3	49.3	44.9	1.10	1.10	1.00
50XF(39)AB3-3*	36.3	36.3	42.8	0.85	0.85	1.00
30SKAB3-2*	15.2	15.2	14.7	1.03	1.03	1.00
80XFAB2-1*	83.8	83.8	87.7	0.95	0.95	1.00
50XF(78)AB2-1*	51.9	51.9	55.6	0.93	0.93	1.00
80SKAB2-1*	54.1	54.1	51.9	1.04	1.04	1.00
80DKAB2-1*	25.6	25.6	27.3	0.94	0.94	1.00
50XF(39)AB2-1*	23.4	23.4	24.6	0.95	0.95	1.00
30SKAB2-1*	8.06	8.06	9.35	0.86	0.86	1.00
80XFAB1-1*	57.8	57.2	68.3	0.84	0.85	1.01
50XF(78)AB1-1*	37.8	37.8	43.9	0.86	0.86	1.00
80SKAB1-1*	33.1	32.2	36.3	0.89	0.91	1.03
80DKAB1-1*	18.6	18.6	19.5	0.96	0.96	1.00
50XF(39)AB1-1*	13.4	12.9	13.0	0.99	1.03	1.04
30SKAB1-1*	5.44	5.13	6.08	0.84	0.89	1.06
Mean				0.94	0.95	
Std. Deviation				0.081	0.079	

* $f_{cr} > F_{pr} = 0.7F_y$; assume inelastic buckling

Table 3.14 Comparison of Initial-to-Predicted Buckling Moments for Various Values of C AB Beam Specimens

Specimen	C Value				
	1.00	0.75	0.67	0.60	0.50
80XFAB3-1*	1.17	0.99	0.93	0.93	0.93
50XF(78)AB3-1*	1.17	1.00	0.94	0.93	0.93
80SKAB3-2*	1.40	1.16	1.09	1.09	1.09
80DKAB3-2*	1.41	1.20	1.14	1.10	1.10
50XF(39)AB3-3*	1.11	0.93	0.87	0.85	0.85
30SKAB3-2*	1.31	1.08	1.03	1.03	1.03
80XFAB2-1*	1.14	1.05	1.02	0.99	0.95
50XF(78)AB2-1*	1.13	1.03	1.00	0.97	0.93
80SKAB2-1*	1.28	1.16	1.12	1.09	1.04
80DKAB2-1*	1.14	1.04	1.01	0.98	0.94
50XF(39)AB2-1*	1.17	1.06	1.03	1.00	0.95
30SKAB2-1*	1.08	0.97	0.94	0.91	0.86
80XFAB1-1*	0.87	0.87	0.86	0.85	0.84
50XF(78)AB1-1*	0.89	0.89	0.88	0.87	0.86
80SKAB1-1*	0.92	0.92	0.91	0.90	0.89
80DKAB1-1*	0.99	0.99	0.98	0.97	0.96
50XF(39)AB1-1*	1.02	1.02	1.01	1.00	0.99
30SKAB1-1*	0.86	0.86	0.86	0.85	0.84
Mean	1.13	1.01	0.98	0.96	0.94
Std. Deviation	0.157	0.098	0.086	0.082	0.081

*$f_{cr} > F_{pr} = 0.7F_y$; assume inelastic buckling

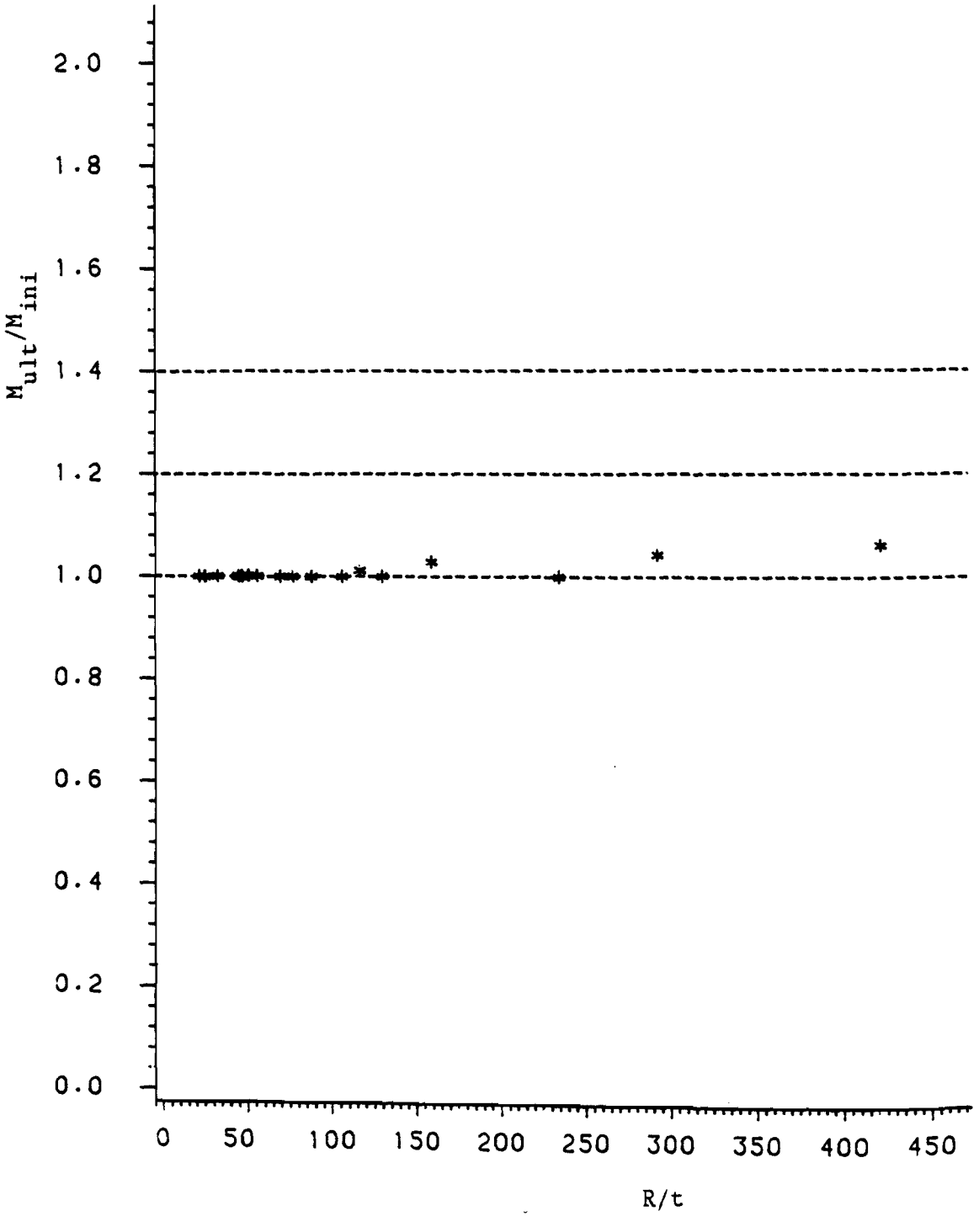

M_{ini} = Initial buckling moment of curved element

M_{ult} = Ultimate moment of cross section

Figure 3.55 Comparison of M_{ult}/M_{ini} Vs. R/t for AB Beam Tests

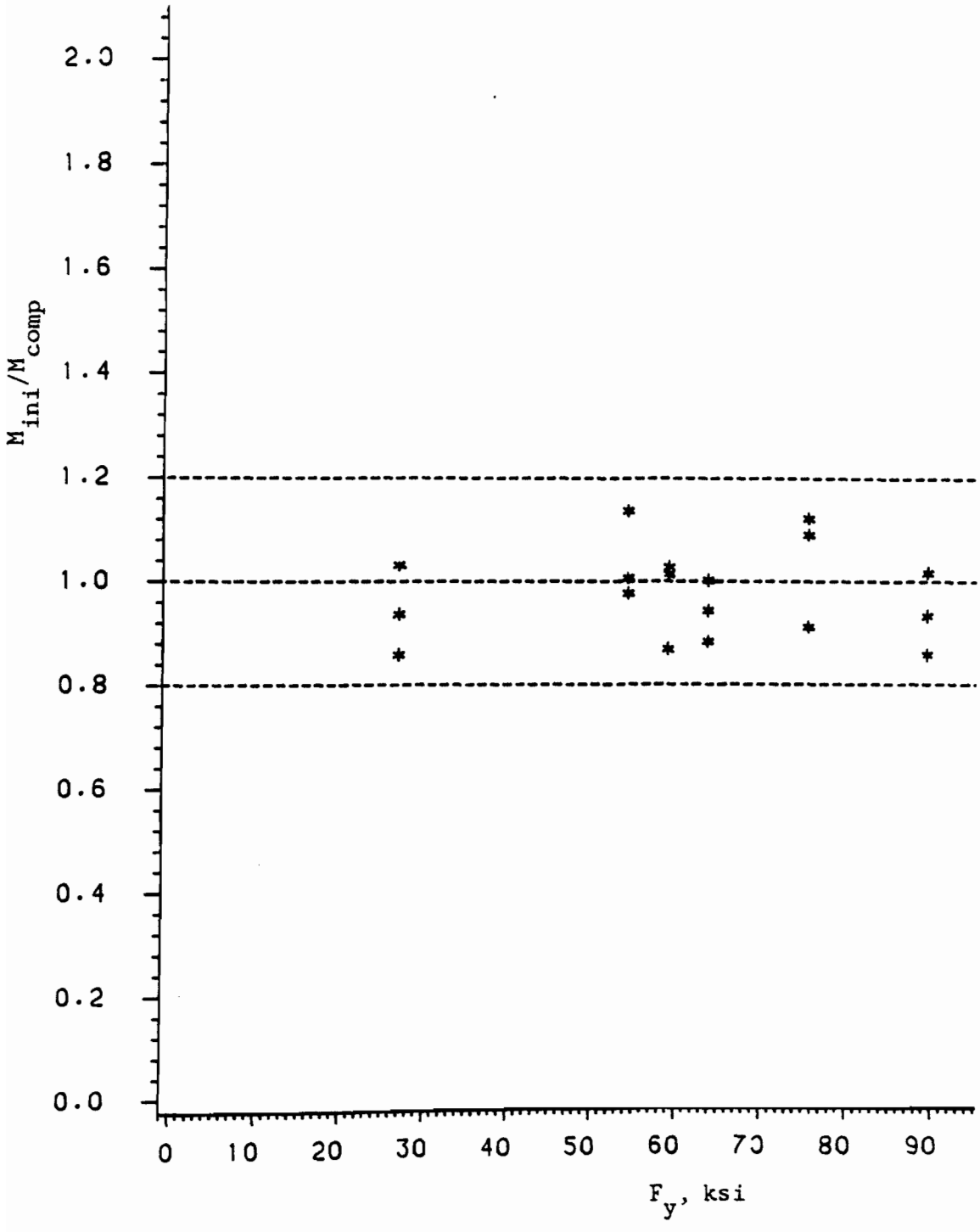

M_{ini} = Initial buckling moment of curved element

M_{comp} = Predicted initial buckling moment

Figure 3.56 Comparison of M_{ini}/M_{comp} Vs. F_y for AB Beam Tests (C = 0.67)

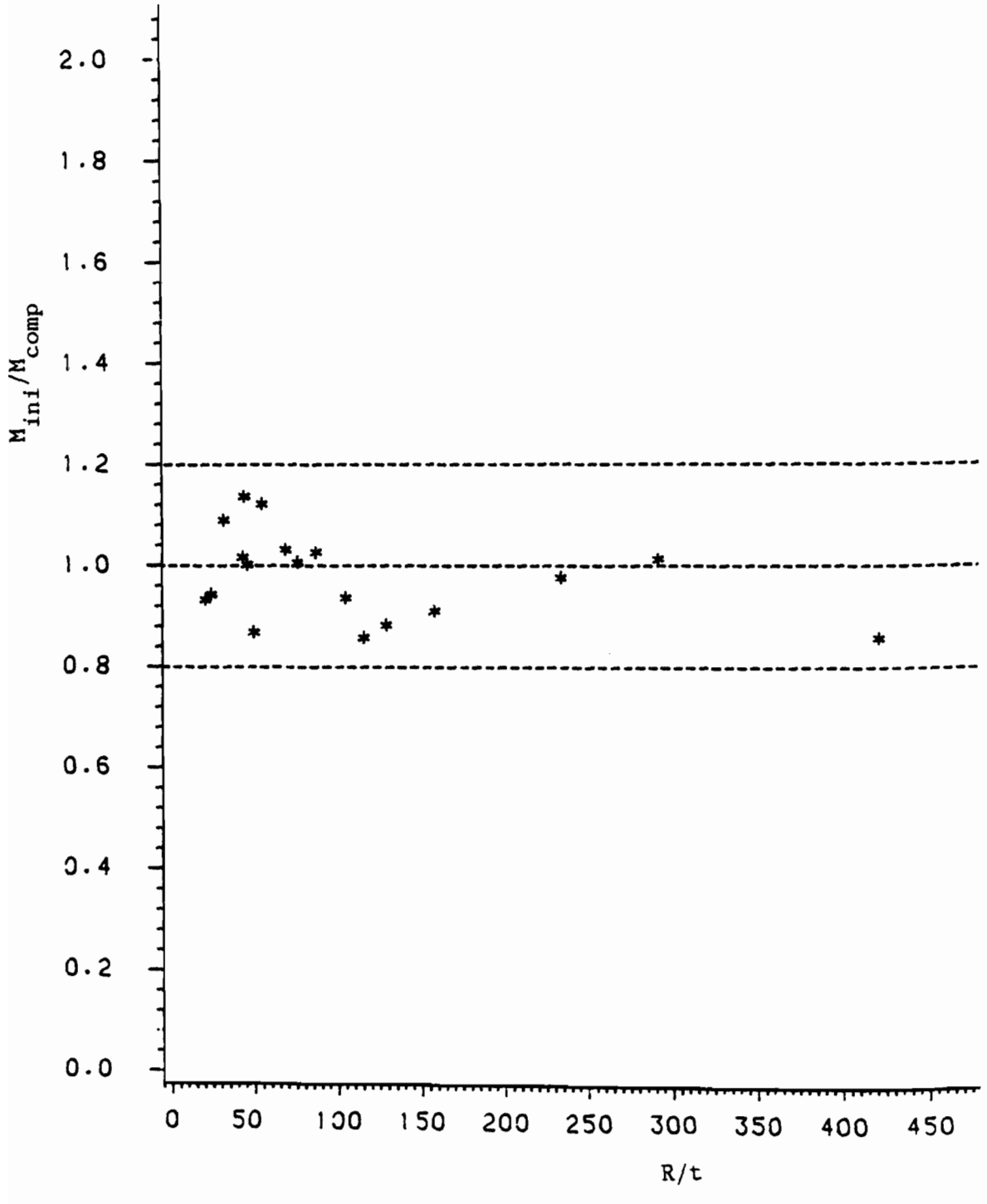

M_{ini} = Initial buckling moment of curved element

M_{comp} = Predicted initial buckling moment

Figure 3.57 Comparison of M_{ini}/M_{comp} Vs. R/t for AB Beam Tests (C = 0.67)

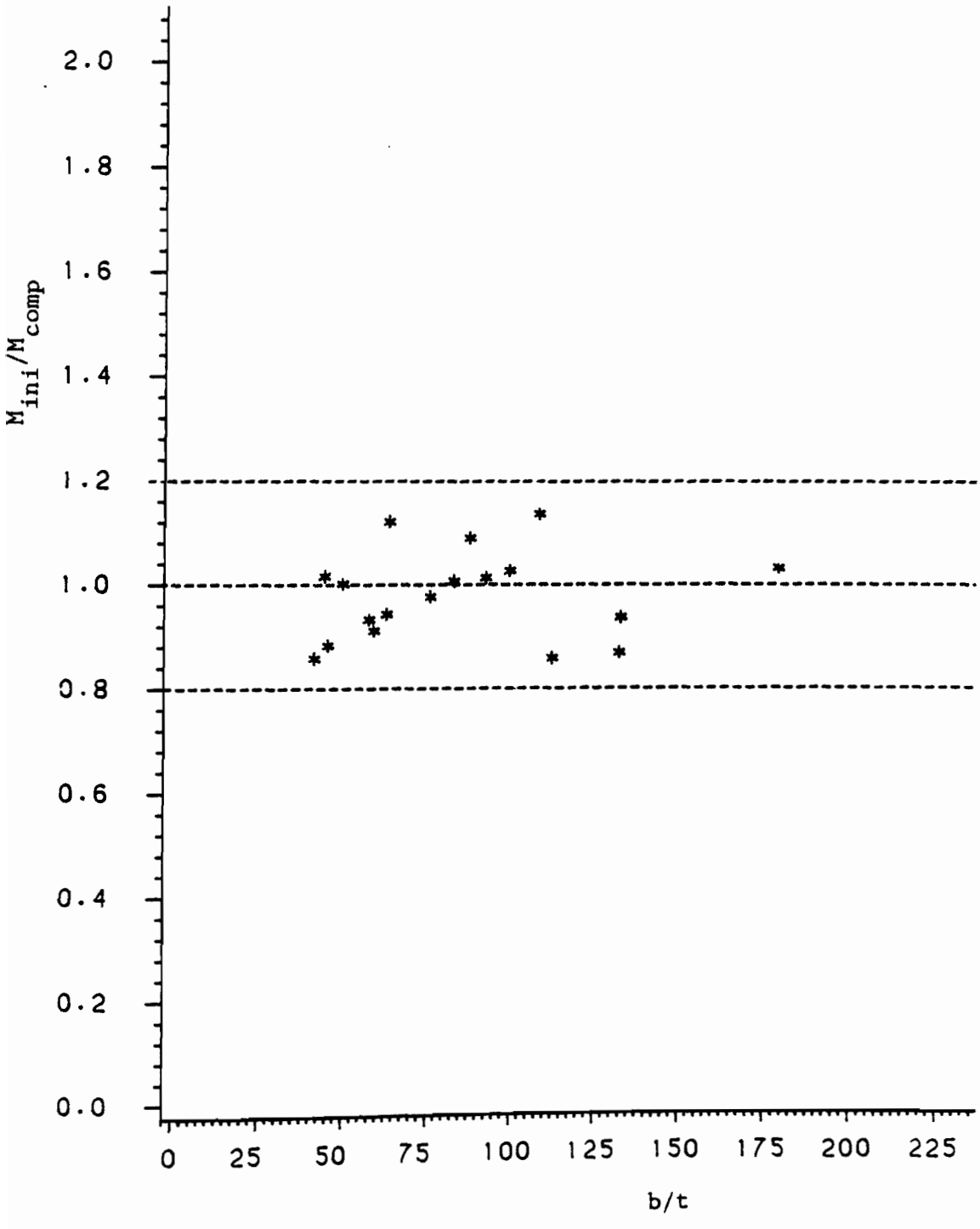

M_{ini} = Initial buckling moment of curved element

M_{comp} = Predicted initial buckling moment

Figure 3.58 Comparison of M_{ini}/M_{comp} Vs. b/t for AB Beam Tests (C = 0.67)

Table 3.15 Comparison of Actual-to-Predicted Buckling Moments
DB Beam Specimens (C=1.0)
Based on Modified Redshaw's Eq. (3.4) Using
Direct Approach for Inelastic Buckling, Eq. (3.10)

Specimen	Ultimate Moment (in-kips) (1)	Initial Buckling Moment (in-kips) (2)	Predicted Buckling Moment (in-kips) (3)	(2)/(3) (4)	(1)/(2) (5)
80XFDB1-1*	47.5	47.5	38.7	1.23	1.00
50XF(78)DB1-1*	31.3	31.3	24.6	1.27	1.00
80DKDB1-1*	17.2	17.2	12.4	1.38	1.00
50XF(39)DB1-1*	14.9	14.9	12.5	1.19	1.00
30SKDB1-1*	5.63	5.63	4.30	1.31	1.00
80XFDB2-1*	56.9	56.9	48.0	1.18	1.00
50XF(78)DB2-1*	37.2	37.2	29.2	1.27	1.00
80DKDB2-1*	20.6	20.6	15.3	1.35	1.00
50XF(39)DB2-1*	15.9	15.9	12.8	1.24	1.00
30SKDB2-1*	5.94	5.94	4.58	1.30	1.00
Mean				1.27	-
Std. Deviation				0.066	-

* $f_{cr} > F_{pr} = 0.7F_y$; assume inelastic buckling

Table 3.16 Comparison of Actual-to-Predicted Buckling Moments
DB Beam Specimens (C=0.75)
Based on Modified Redshaw's Eq. (3.4) Using
Direct Approach for Inelastic Buckling, Eq. (3.10)

Specimen	Ultimate Moment (in-kips) (1)	Initial Buckling Moment (in-kips) (2)	Predicted Buckling Moment (in-kips) (3)	(2)/(3) (4)	(1)/(2) (5)
80XFDB1-1*	47.5	47.5	44.0	1.08	1.00
50XF(78)DB1-1*	31.3	31.3	27.7	1.13	1.00
80DKDB1-1*	17.2	17.2	14.0	1.22	1.00
50XF(39)DB1-1*	14.9	14.9	13.7	1.08	1.00
30SKDB1-1*	5.63	5.63	4.76	1.18	1.00
80XFDB2-1*	56.9	56.9	58.3	0.98	1.00
50XF(78)DB2-1*	37.2	37.2	35.7	1.04	1.00
80DKDB2-1*	20.6	20.6	18.7	1.10	1.00
50XF(39)DB2-1*	15.9	15.9	15.5	1.03	1.00
30SKDB2-1*	5.94	5.94	5.56	1.07	1.00
Mean				1.09	-
Std. Deviation				0.073	-

*$f_{cr} > F_{pr} = 0.7F_y$; assume inelastic buckling

Table 3.17 Comparison of Actual-to-Predicted Buckling Moments
DB Beam Specimens (C=0.67)
Based on Modified Redshaw's Eq. (3.4) Using
Direct Approach for Inelastic Buckling, Eq. (3.10)

Specimen	Ultimate Moment (in-kips) (1)	Initial Buckling Moment (in-kips) (2)	Predicted Buckling Moment (in-kips) (3)	(2)/(3) (4)	(1)/(2) (5)
80XFDB1-1*	47.5	47.5	46.1	1.03	1.00
50XF(78)DB1-1*	31.3	31.3	28.9	1.08	1.00
80DKDB1-1*	17.2	17.2	14.6	1.17	1.00
50XF(39)DB1-1*	14.9	14.9	14.2	1.05	1.00
30SKDB1-1*	5.63	5.63	4.93	1.14	1.00
80XFDB2-1*	56.9	56.9	60.7	0.94	1.00
50XF(78)DB2-1*	37.2	37.2	36.6	1.02	1.00
80DKDB2-1*	20.6	20.6	19.5	1.06	1.00
50XF(39)DB2-1*	15.9	15.9	16.6	0.96	1.00
30SKDB2-1*	5.94	5.94	5.79	1.03	1.00
Mean				1.05	-
Std. Deviation				0.073	-

*$f_{cr} > F_{pr} = 0.7F_y$; assume inelastic buckling

Table 3.18 Comparison of Actual-to-Predicted Buckling Moments
DB Beam Specimens (C=0.60)
Based on Modified Redshaw's Eq. (3.4) Using
Direct Approach for Inelastic Buckling, Eq. (3.10)

Specimen	Ultimate Moment (in-kips) (1)	Initial Buckling Moment (in-kips) (2)	Predicted Buckling Moment (in-kips) (3)	(2)/(3) (4)	(1)/(2) (5)
80XFDB1-1*	47.5	47.5	48.1	0.99	1.00
50XF(78)DB1-1*	31.3	31.3	30.1	1.04	1.00
80DKDB1-1*	17.2	17.2	15.2	1.13	1.00
50XF(39)DB1-1*	14.9	14.9	14.6	1.02	1.00
30SKDB1-1*	5.63	5.63	5.09	1.10	1.00
80XFDB2-1*	56.9	56.9	60.7	0.94	1.00
50XF(78)DB2-1*	37.2	37.2	36.6	1.02	1.00
80DKDB2-1*	20.6	20.6	19.5	1.06	1.00
50XF(39)DB2-1*	15.9	15.9	16.8	0.95	1.00
30SKDB2-1*	5.94	5.94	5.79	1.03	1.00
Mean				1.03	-
Std. Deviation				0.061	-

*$f_{cr} > F_{pr} = 0.7F_y$; assume inelastic buckling

Table 3.19 Comparison of Actual-to-Predicted Buckling Moments
DB Beam Specimens (C=0.50)
Based on Modified Redshaw's Eq. (3.4) Using
Direct Approach for Inelastic Buckling, Eq. (3.10)

Specimen	Ultimate Moment (in-kips) (1)	Initial Buckling Moment (in-kips) (2)	Predicted Buckling Moment (in-kips) (3)	(2)/(3) (4)	(1)/(2) (5)
80XFDB1-1*	47.5	47.5	48.7	0.98	1.00
50XF(78)DB1-1*	31.3	31.3	30.6	1.02	1.00
80DKDB1-1*	17.2	17.2	15.8	1.09	1.00
50XF(39)DB1-1*	14.9	14.9	15.2	0.98	1.00
30SKDB1-1*	5.63	5.63	5.34	1.05	1.00
80XFDB2-1*	56.9	56.9	60.7	0.94	1.00
50XF(78)DB2-1*	37.2	37.2	36.6	1.02	1.00
80DKDB2-1*	20.6	20.6	19.5	1.06	1.00
50XF(39)DB2-1*	15.9	15.9	16.8	0.95	1.00
30SKDB2-1*	5.94	5.94	5.79	1.03	1.00
Mean				1.01	-
Std. Deviation				0.049	-

* $f_{cr} > F_{pr} = 0.7F_y$; assume inelastic buckling

Table 3.20 Comparison of Initial-to-Predicted Buckling Moments for Various Values of C
DB Beam Specimens

Specimen	C Values				
	1.00	0.75	0.67	0.60	0.50
80XFDB1-1*	1.23	1.08	1.03	0.99	0.98
50XF(78)DB1-1*	1.27	1.13	1.08	1.04	1.02
80DKDB1-1*	1.38	1.22	1.17	1.13	1.09
50XF(39)DB1-1*	1.19	1.08	1.05	1.02	0.98
30SKDB1-1*	1.31	1.18	1.14	1.10	1.05
80XFDB2-1*	1.18	0.98	0.94	0.94	0.94
50XF(78)DB2-1*	1.27	1.04	1.02	1.02	1.02
80DKDB2-1*	1.35	1.10	1.06	1.06	1.06
50XF(39)DB2-1*	1.24	1.03	0.96	0.95	0.95
30SKDB2-1*	1.30	1.07	1.03	1.03	1.03
Mean	1.27	1.09	1.05	1.03	1.01
Std. Deviation	0.066	0.073	0.073	0.061	0.049

*$f_{cr} > F_{pr} = 0.7F_y$; assume inelastic buckling

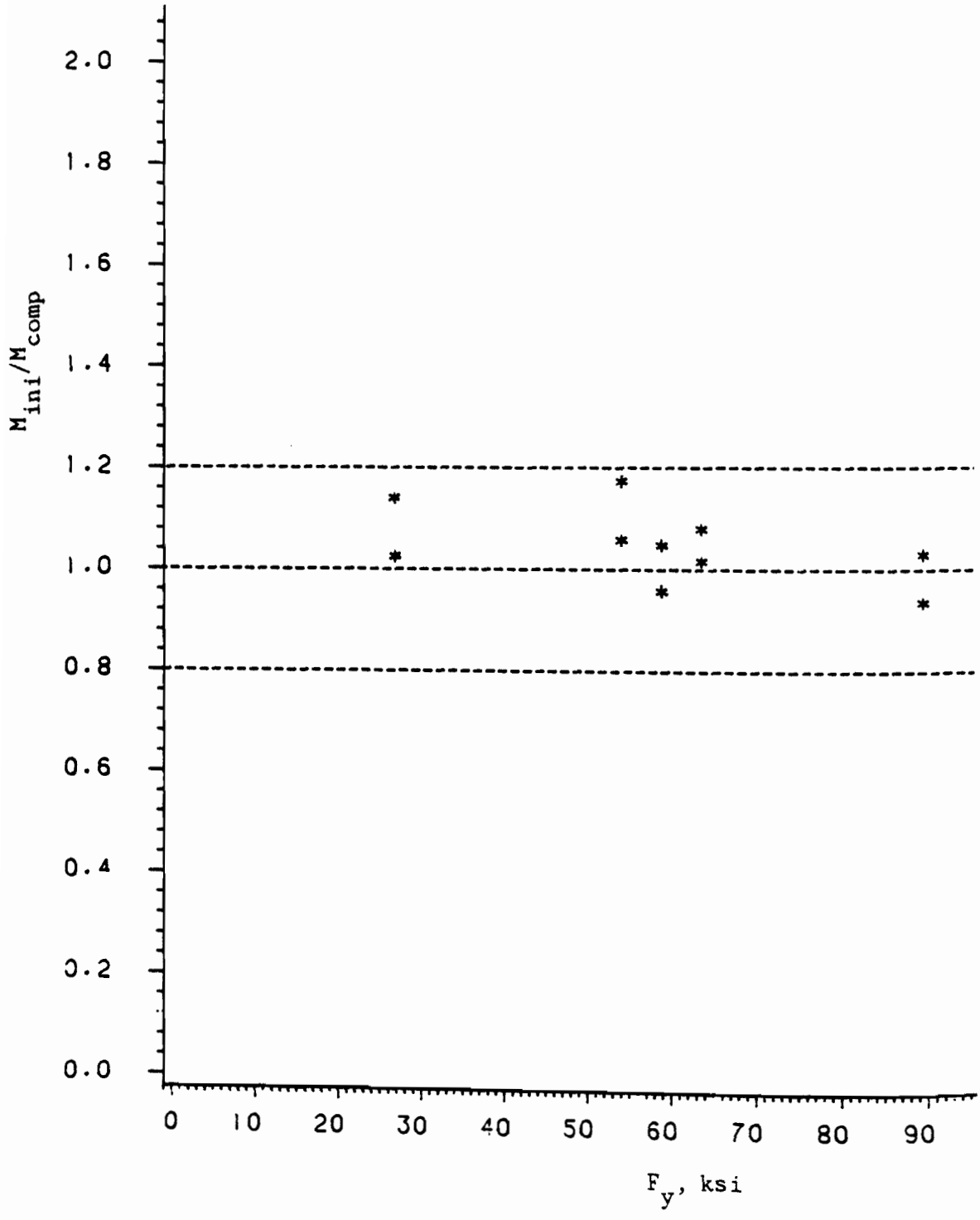

M_{ini} = Initial buckling moment of curved element

M_{comp} = Predicted initial buckling moment

Figure 3.59 Comparison of M_{ini}/M_{comp} Vs. F_y for DB Beam Tests (C = 0.67)

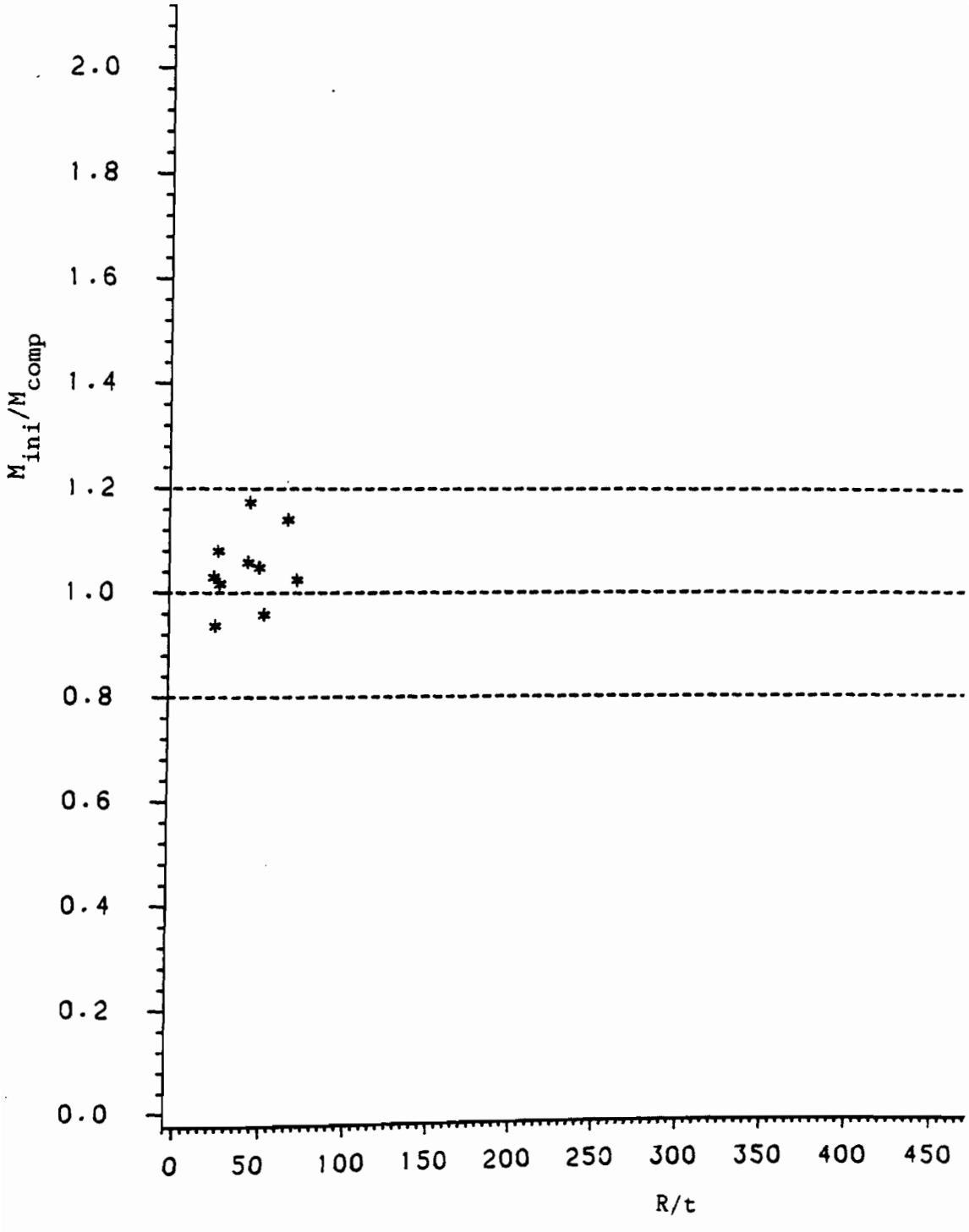

M_{ini} = Initial buckling moment of curved element

M_{comp} = Predicted initial buckling moment

Figure 3.60 Comparison of M_{ini}/M_{comp} Vs. R/t for DB Beam Tests (C = 0.67)

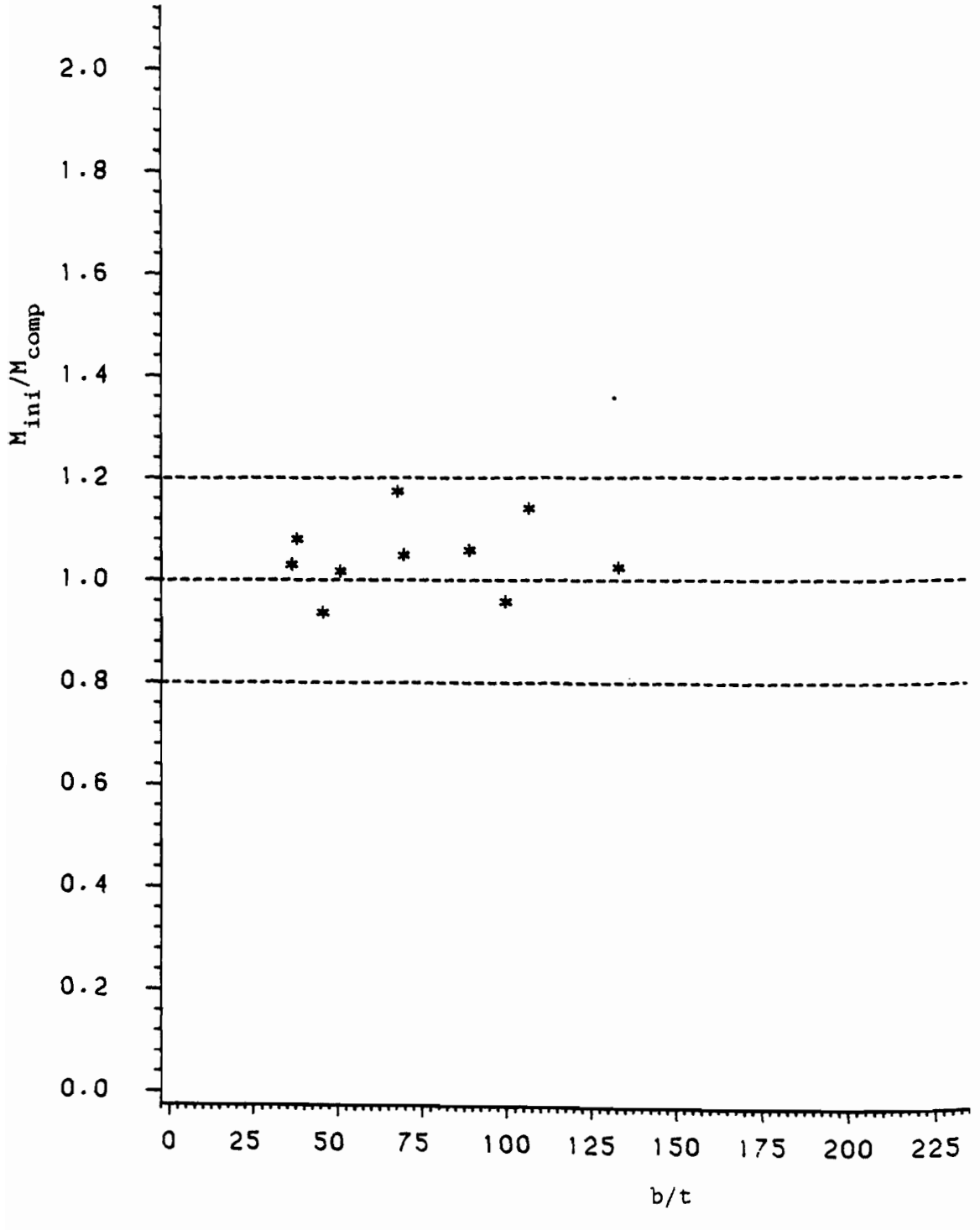

M_{ini} = Initial buckling moment of curved element

M_{comp} = Predicted initial buckling moment

Figure 3.61 Comparison of M_{ini}/M_{comp} Vs. b/t for DB Beam Tests (C = 0.67)

were again computed using the method outlined in Section III.A.5. C values of 1.0, 0.75, 0.67, 0.60, and 0.5 were used to compute the predicted buckling moments given in column (3) of Tables 3.15 through 3.19, respectively. The initial buckling moments are compared to the predicted moments in column (4) of each table. Table 3.20 compares the initial-to-predicted buckling moment ratios as computed for each value of C. Note that the recommended C value of 0.67 for the AB beams provides a slightly conservative estimate for the DB beam specimens. Figures 3.59 through 3.61 provide a comparison of the initial-to-predicted buckling moment ratios (assuming C=0.67) for the tested range of F_y, R/t, and b/t, respectively.

c. Shear - BV Specimens. Because of the difficulty in consistently determining an initial buckling load, only the ultimate failure loads are given in column (1) of Table 3.21. Section III.C.6 describes the method employed to compute the predicted shear buckling loads. It should be noted that the predicted buckling loads shown in column (2) of Table 3.21 represent the total applied load at midspan of each specimen, not the predicted shear load in each individual curved web. Because the shear in each curved web equals 1/4 of the total applied load, the predicted shear buckling load from Eq. (3.18) is multiplied by 4 in order to compute the total predicted load.

As shown in column (3), the predicted shear buckling loads consistently overestimate the actual failure loads. A possible explanation for the overestimation may be because many of the failures in the curved web were caused not only by shear but by a combination of shear and a form of web crippling. The different failure modes observed

Table 3.21 Comparison of Actual-to-Predicted Buckling Loads
BV Shear Specimens
Based on Eqs. (2.26) and (2.27) with Eq. (3.16)
Used for Inelastic Buckling

Specimen	Ultimate Load (kips) (1)	Predicted Load (kips) (2)	(1)/(2) (3)	Type of Failure (4)
50XF(78)BV3-1	33.9	42.7	0.79	WCV
80DKBV3-1	23.0	22.4	1.03	WCV
50XF(39)BV3-1	15.1	19.6	0.77	WCV
30SKBV3-2	6.65	6.47	1.03	WCV
50XF(78)BV2-1	37.0	42.7	0.87	WC
80DKBV2-1	15.4	21.2	0.73	WC+V
50XF(39)BV2-1	11.1	18.7	0.59	WC+V
30SKBV2-1	4.95	6.76	0.73	V
50XF(78)BV1-1	33.4	40.7	0.82	WC
80DKBV1-1	15.6	20.5	0.76	V
50XF(39)BV1-1	13.0	18.2	0.71	V
30SKBV1-1	4.90	6.45	0.76	V
Mean			0.80	
Std. Deviation			0.127	

Notes:

The failure modes in column (5) are defined as follows:

V = Failure by shear buckling only

WC = Failure by local deformation under the interior bearing plate (web crippling) only

WC+V = Both the shear failure, V, and the web crippling failure, WC, were present in failed specimen

WCV = Failure occurred by an apparent interaction between the shear in web and the bearing stress adjacent to load plate

See Section III.B.2.e.v for a detailed explanation of the failure modes.

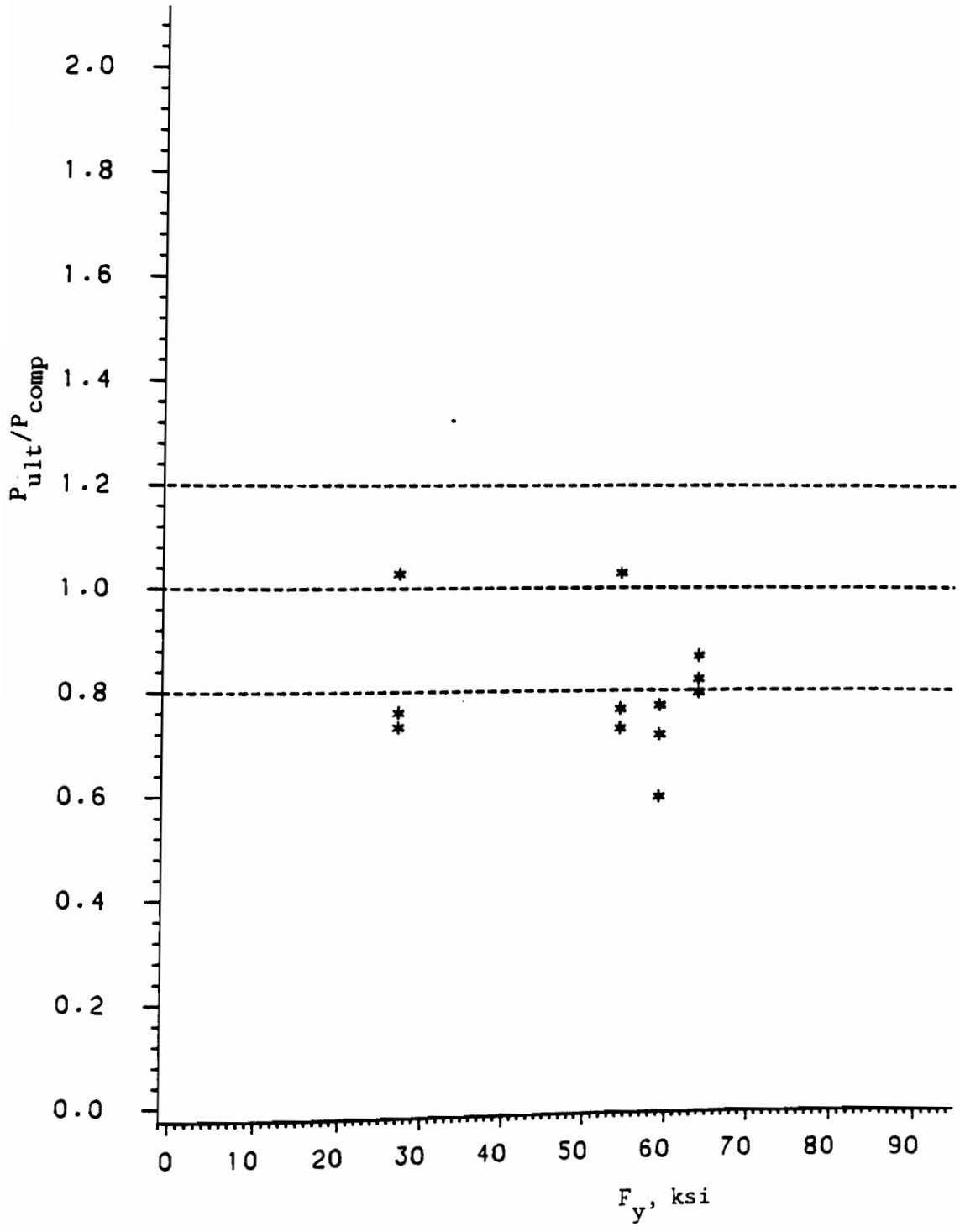

P_{ult} = Ultimate buckling load of curved element

P_{comp} = Predicted ultimate buckling load

Figure 3.62 Comparison of P_{ult}/P_{comp} Vs. F_y for BV Shear Tests

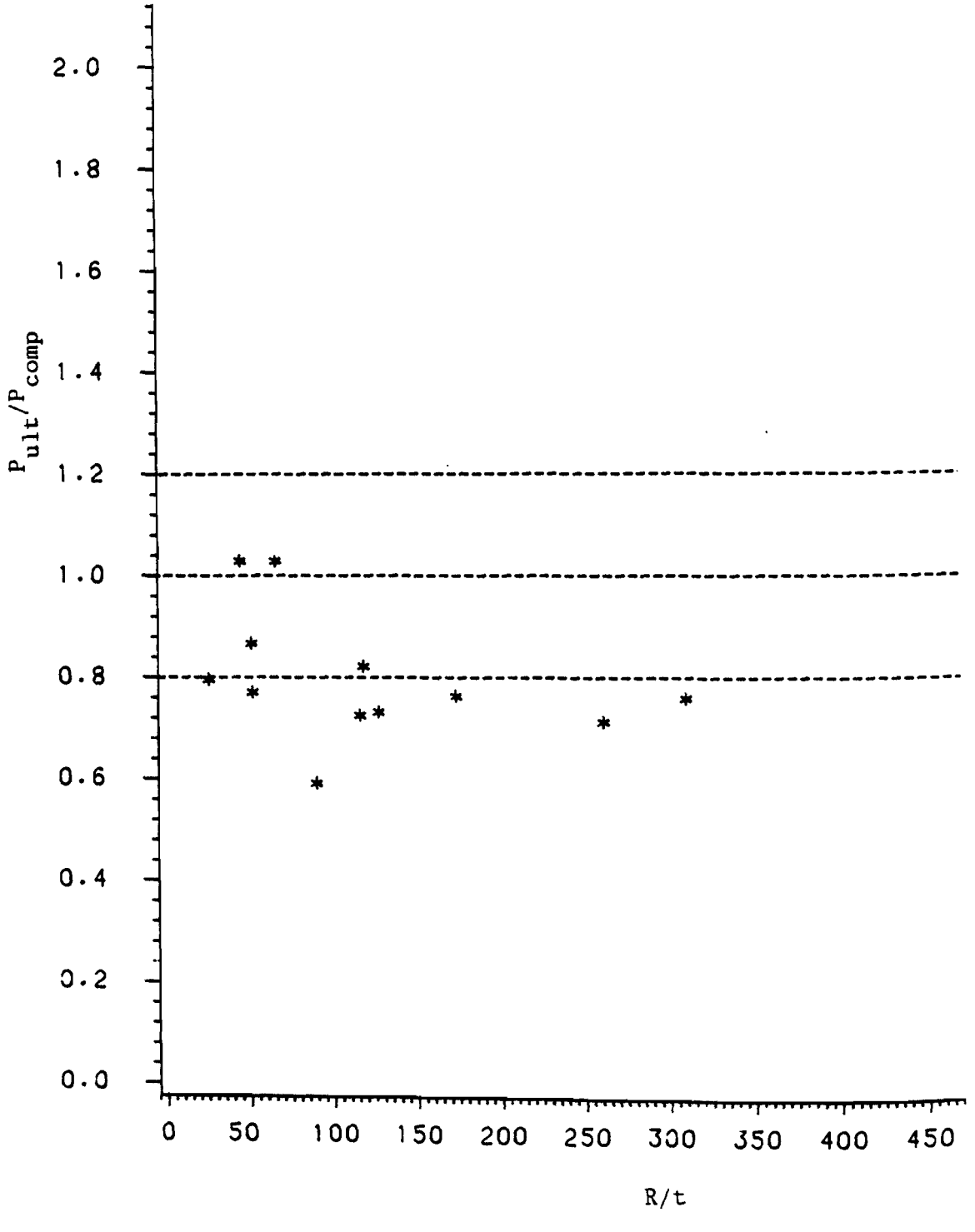

P_{ult} = Ultimate buckling load of curved element

P_{comp} = Predicted ultimate buckling load

Figure 3.63 Comparison of P_{ult}/P_{comp} Vs. R/t for BV Shear Tests

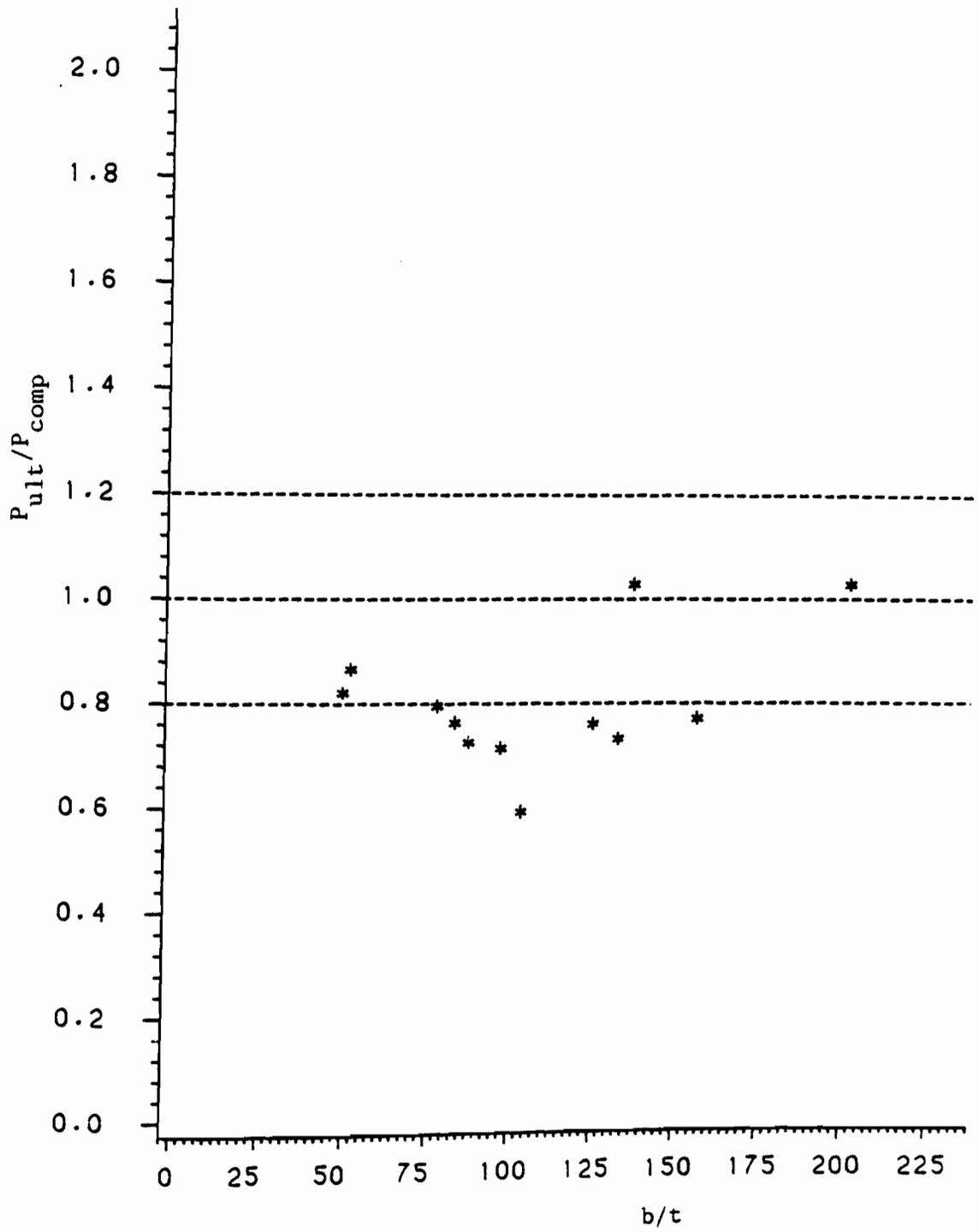

P_{ult} = Ultimate buckling load of curved element

P_{comp} = Predicted ultimate buckling load

Figure 3.64 Comparison of P_{ult}/P_{comp} Vs. b/t for BV Shear Tests

in the shear specimens are described in detail in Section III.B.2.e.iv. The ultimate-to-predicted buckling load ratios may be compared in Figures 3.62 through 3.64 for the tested range of F_y, R/t, and b/t, respectively.

2. Unstiffened Curved Elements. As mentioned in Section III.C.2, two equations, Eq. (3.5) and Eq. (3.6), have been proposed for the prediction of unstiffened curved element buckling. The predicted buckling loads computed using these equations are compared to the actual test loads in Table 3.22. Note that the above comparisons are made only for the CS stub column tests in which the unstiffened curved elements were the initial and final cause of failure. For the remaining specimens that contain unstiffened curved elements, only Eq. (3.6) and the tangent modulus approach for inelastic buckling (Eq. (3.10)) are used to predict the buckling behavior of the unstiffened curved elements.

a. Uniform Axial Compression - Stub Column Tests.

i. Initial Curved Element Failure - CS Specimens. Included in this section are only the stub column tests in which the unstiffened curved elements were the initial and final cause of failure. As before, the tested ultimate and initial buckling loads are given in columns (1) and (2). Column (7) lists the ultimate-to-initial buckling load ratios for each specimen. As expected, there is little, if any, post-buckling strength for the highly curved CS3 (R=1 in.) and CS2 (R=1.25 in.) specimens. However, the flatter CS1 specimens exhibit some post-buckling strength. Again, because the stiffened flat web was unbuckled until the section collapsed, it is difficult to determine the exact

Table 3.22 Comparison of Actual-to-Predicted Buckling Loads
Unstiffened Curved Elements, CS Stub Column Specimens
Initial Curved Element Failure
(Based on Eqs. (3.5) and (3.6) with Eq. (3.10)
Used for Inelastic Buckling)

Specimen	Ultimate Load (kips)	Initial Buckling Load (kips)	Predicted Buckling Load (kips)		(2)/(3)	(2)/(4)	(1)/(2)
			Eq.(3.5)	Eq.(3.6)			
	(1)	(2)	(3)	(4)	(5)	(6)	(7)
80XFCS3-1*	135.0	135.0	127.0	133.8	1.06	1.01	1.00
50XF(78)CS3-3*	93.7	92.8	88.7	91.9	1.05	1.01	1.01
80SKCS3-2*	85.6	84.4	72.4	76.7	1.17	1.10	1.01
80DKCS3-2*	45.8	45.8	39.2	41.2	1.17	1.11	1.00
50XF(39)CS3-3*	32.0	32.0	32.3	35.2	0.99	0.91	1.00
30SKCS3-2*	14.3	14.3	13.1	13.6	1.09	1.05	1.00
80XFCS2-1*	120.0	117.0	102.8	108.5	1.14	1.08	1.03
50XF(78)CS2-1*	75.0	74.5	72.2	74.9	1.03	0.99	1.01
80SKCS2-1*	62.6	57.0	59.8	63.0	0.95	0.91	1.10
80DKCS2-3*	39.9	39.8	33.6	34.9	1.19	1.14	1.00
50XF(39)CS2-1*	28.0	27.4	27.3	29.1	1.00	0.94	1.02
30SKCS2-1*	10.8	10.4	11.0	11.2	0.95	0.93	1.04
80XFCS1-1	78.2	73.7	68.5	78.0	1.08	0.94	1.06
80XFCS1-2	78.3	77.7	67.4	76.4	1.15	1.02	1.01
50XF(78)CS1-1*	57.0	48.8	54.1	58.4	0.90	0.84	1.17
50XF(78)CS1-2	54.4	49.5	51.9	55.3	0.95	0.90	1.10
80SKCS1-1	41.5	34.3	36.5	36.8	0.94	0.93	1.21
80SKCS1-2	39.8	33.8	35.7	35.8	0.95	0.94	1.18
80DKCS1-1	25.2	22.4	20.5	18.9	1.09	1.19	1.13
50XF(39)CS1-2	15.7	11.8	12.8	10.5	0.93	1.13	1.33
30SKCS1-2	9.38	7.88	9.11	7.80	0.86	1.01	1.19
Mean					1.03	1.00	
Std. Deviation					0.098	0.094	

*$f_{cr} > F_{pr} = 0.7F_y$; assume inelastic buckling

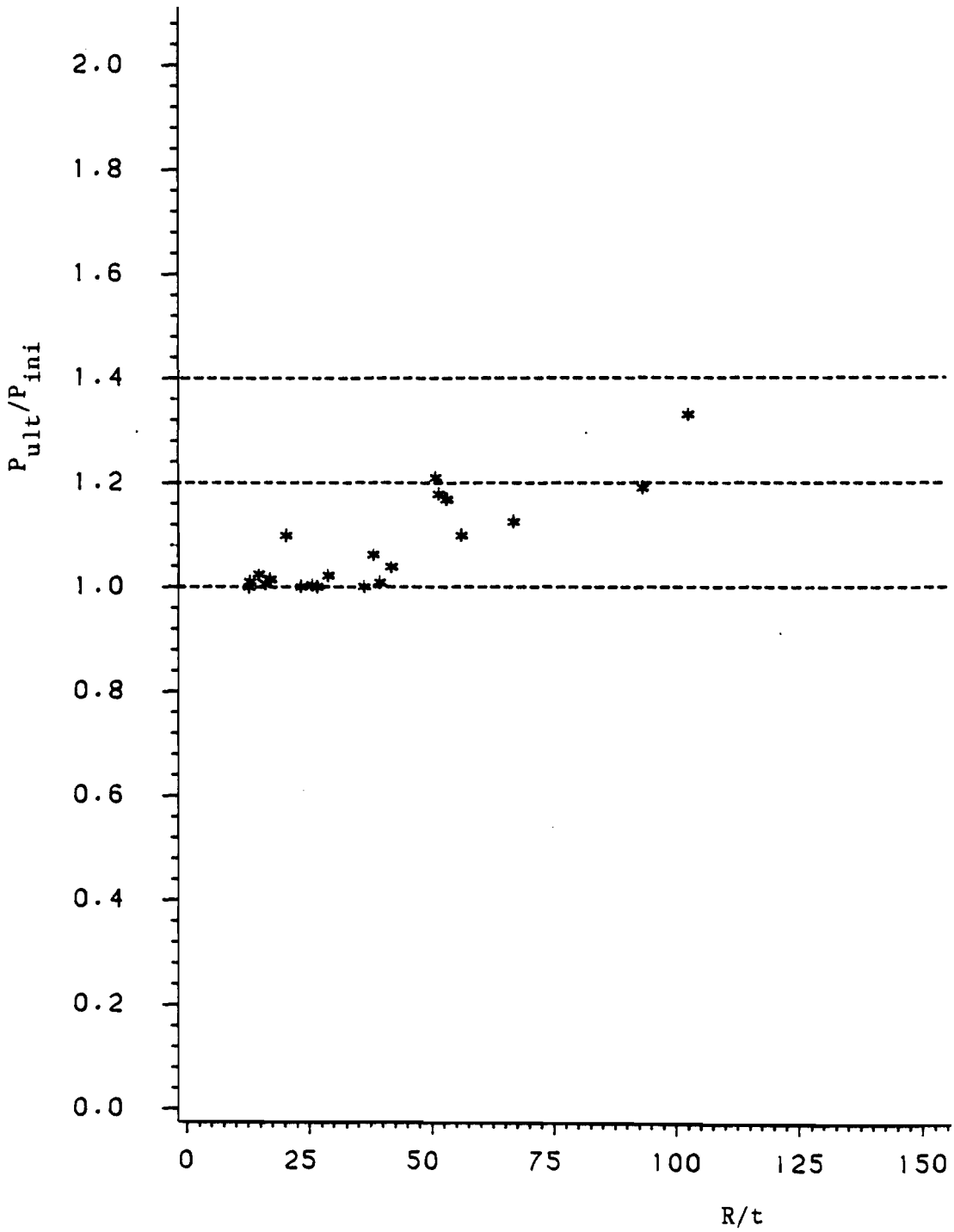

P_{ult} = Ultimate load of cross section

P_{ini} = Initial buckling load of curved element

Figure 3.65 Comparison of P_{ult}/P_{ini} Vs. R/t for CS Stub Column Tests

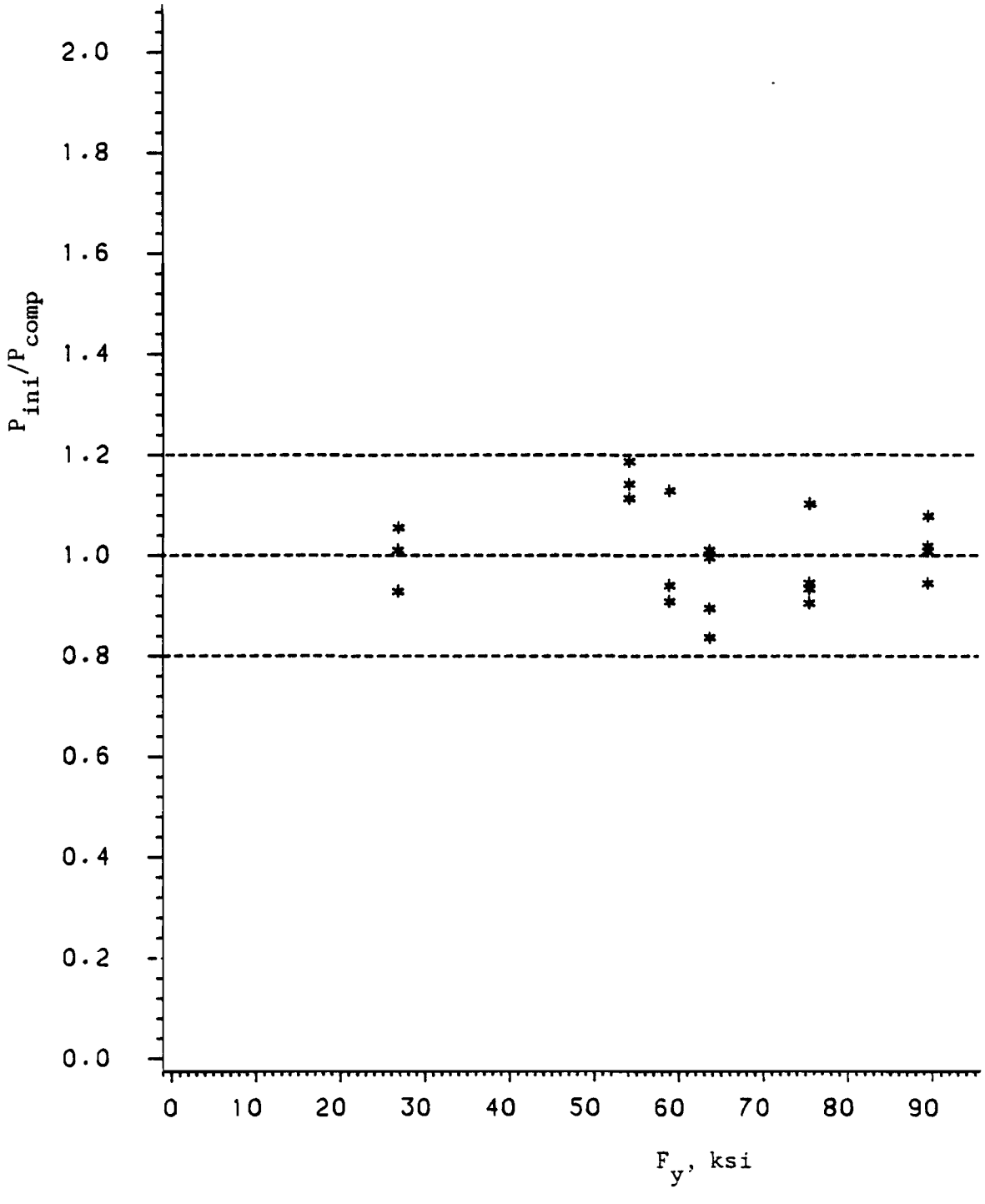

P_{ini} = Initial buckling load of curved element

P_{comp} = Predicted initial buckling load

Figure 3.66 Comparison of P_{ini}/P_{comp} Vs. F_y for CS Stub Column Tests

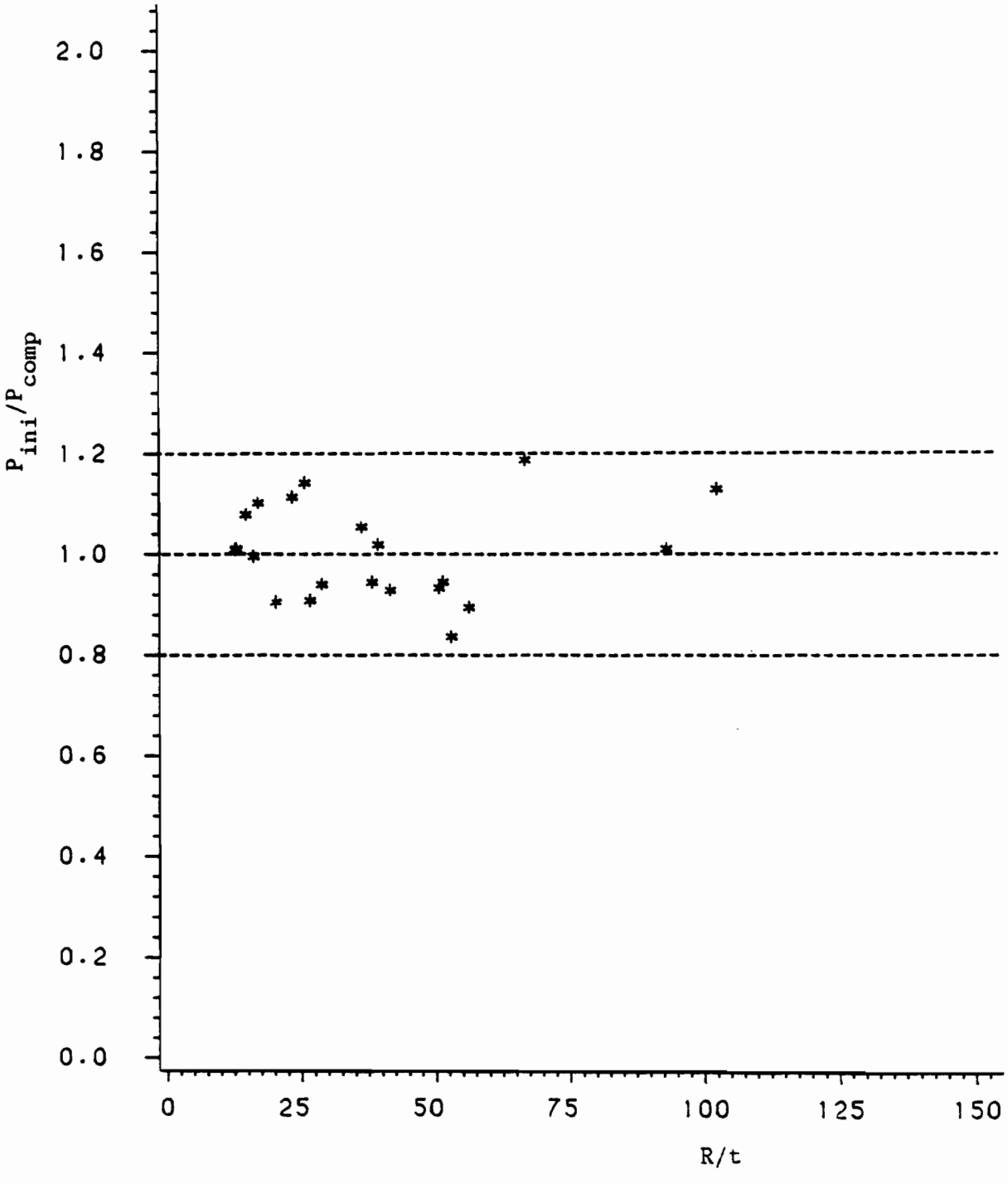

P_{ini} = Initial buckling load of curved element

P_{comp} = Predicted initial buckling load

Figure 3.67 Comparison of P_{ini}/P_{comp} Vs. R/t for CS Stub Column Tests

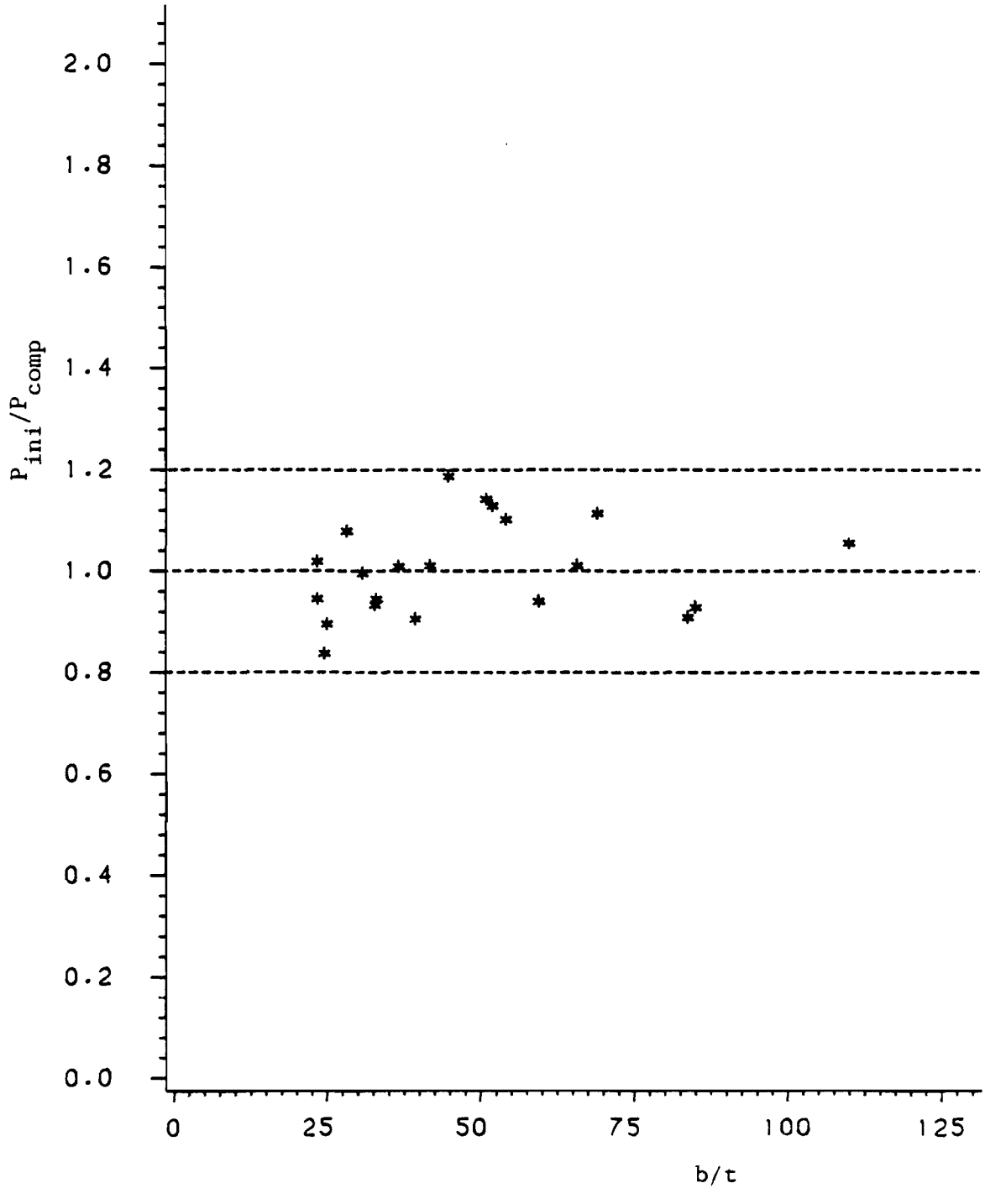

P_{ini} = Initial buckling load of curved element

P_{comp} = Predicted initial buckling load

Figure 3.68 Comparison of P_{ini}/P_{comp} Vs. b/t for CS Stub Column Tests

magnitude of the curved element post-buckling strength. The ultimate-to-initial buckling load ratios may be compared for the tested range of R/t in Figure 3.65.

The predicted initial buckling load for these stub columns is computed as simply the predicted initial buckling stress from either Eq. (3.5) or (3.6) times the total cross sectional area. The predicted loads based on Eq. (3.5) are listed in column (3) and in column (4) for Eq. (3.6). The initial buckling loads are compared to the predicted loads in column (5) for Eq. (3.5) and column (6) for Eq. (3.6). As shown, Eq. (3.6) seems to provide the best overall agreement with the test data. Figures 3.66 through 3.68 show the values of initial-to-predicted load ratios (based on Eq. (3.6)) for the tested ranges of F_y, R/t, and b/t, respectively.

ii. Interaction Between Unstiffened Curved and Stiffened Flat Elements - CSI Specimens. A series of tests have been performed in which no bracing was attached to the flat web of the CS stub column specimens. (These specimens are designated "CSI".) Thus, the flat web was capable of buckling before the adjoining unstiffened curved elements. The stub columns in which the flat web actually buckled before the unstiffened curved elements are listed in Table 3.23. As shown in column (7), a similar trend in post-buckling stength occurred as for the previously described CS stub columns. Figure 3.69 shows the ultimate-to-initial buckling load ratios for the tested range of R/t values.

The method employed to compute the total load resisted by the entire cross-section is the same as previously described in Section III.C.4. The load resisted by the web, P_w, is calculated as the

Table 3.23 Comparison of Actual-to-Predicted Buckling Loads Unstiffened Curved Element, CSI Stub Column Specimens Interaction Between Unstiffened Curved Elements and Stiffened Flat Elements (P_{curve} Based on Eq. (3.6) with the Direct Approach for Inelastic Buckling, Eq. 3.10)

Specimen	Ultimate Load (kips) (1)	Initial Buckling Load (kips) (2)	P_w (kips) (3)	P_{curve} (kips) (4)	P_{total} (kips) (5)	(2)/(5) (6)	(1)/(2) (7)
80XFCSI3-2*	111.2	110.0	52.2	80.1	132.3	0.83	1.01
50XF(78)CSI3-1*	70.0	70.0	36.5	53.7	90.3	0.78	1.00
80SKCSI3-3	74.6	72.1	27.2	45.2	72.4	1.00	1.03
80DKCSI3-3	39.0	39.0	14.1	25.1	39.2	1.00	1.00
50XF(39)CSI3-2	32.0	32.0	10.2	21.0	31.2	1.02	1.00
30SKCSI3-3*	11.9	11.9	4.02	8.38	12.4	0.96	1.00
80XFCSI2-3	101.6	101.3	45.4	62.5	107.8	0.94	1.00
50XF(78)CSI2-2*	62.6	62.6	31.1	43.2	74.3	0.84	1.00
80SKCSI2-2	57.7	56.4	26.8	33.9	60.7	0.93	1.02
80DKCSI2-2	32.7	32.7	13.3	19.7	33.0	0.99	1.00
50XF(39)CSI2-2	23.3	20.3	9.78	15.5	25.3	0.80	1.15
30SKCSI2-2*	9.43	9.20	4.12	6.46	10.6	0.87	1.03
80DKCSI1-2	22.5	21.5	8.88	12.2	21.1	1.02	1.05
50XF(39)CSI1-3	14.0	11.3	5.18	6.51	11.7	0.96	1.24
30SKCSI1-1	7.05	4.90	2.69	3.53	6.22	0.79**	1.44
Mean						0.92	-
Std. Deviation						0.084	-

*$f_{cr} > F_{pr} = 0.7F_y$; assume inelastic buckling

**Not included in the calculation of mean and standard deviation.

P_w = predicted web strength based on predicted curved element buckling stress at edges of web

P_{curve} = predicted curved element buckling load

P_{total} = predicted total load that section can withstand

$= P_w + P_{curve}$

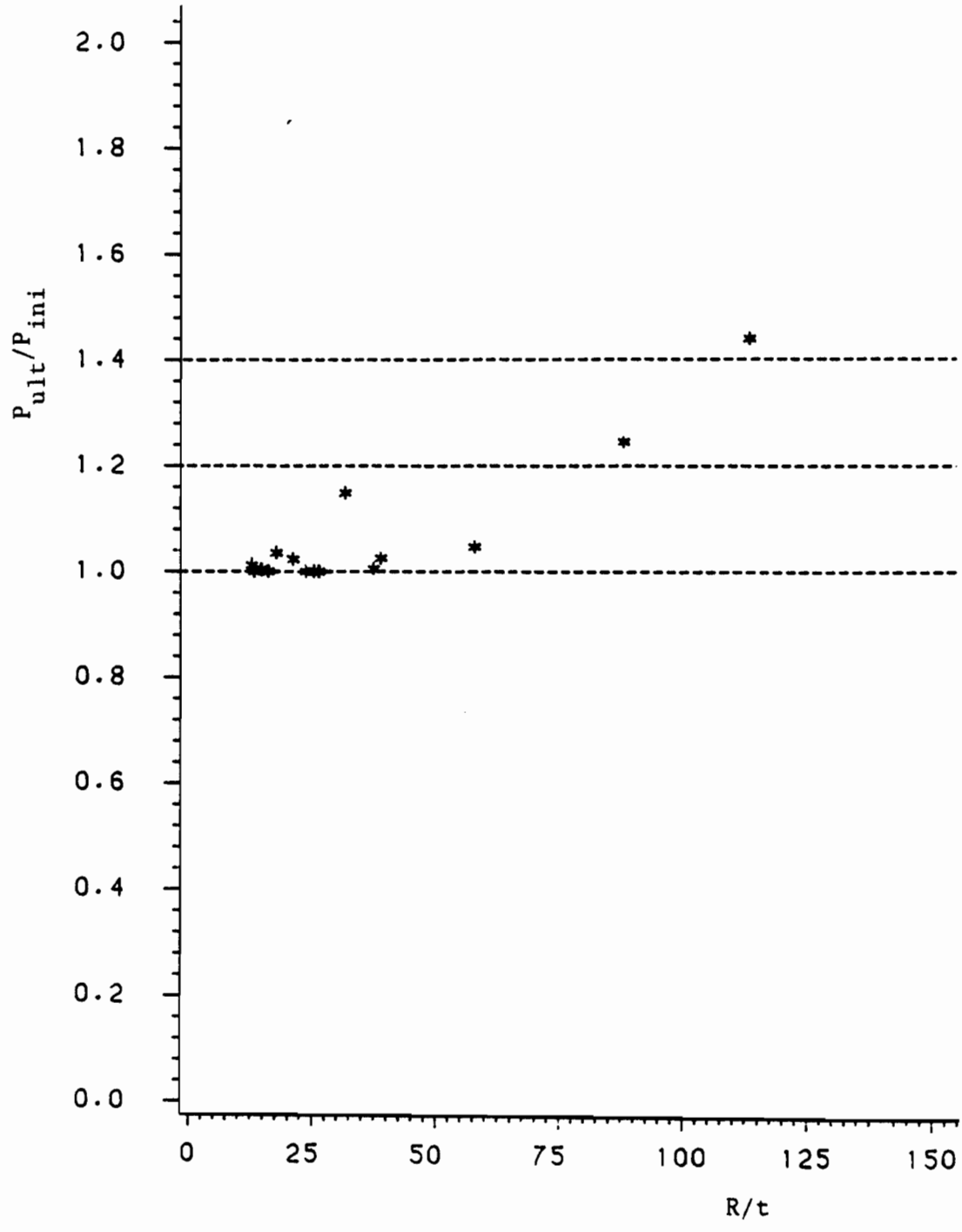

P_{ult} = Ultimate load of cross section

P_{ini} = Initial buckling load of curved element

Figure 3.69 Comparison of P_{ult}/P_{ini} Vs. R/t for CSI Stub Column Tests

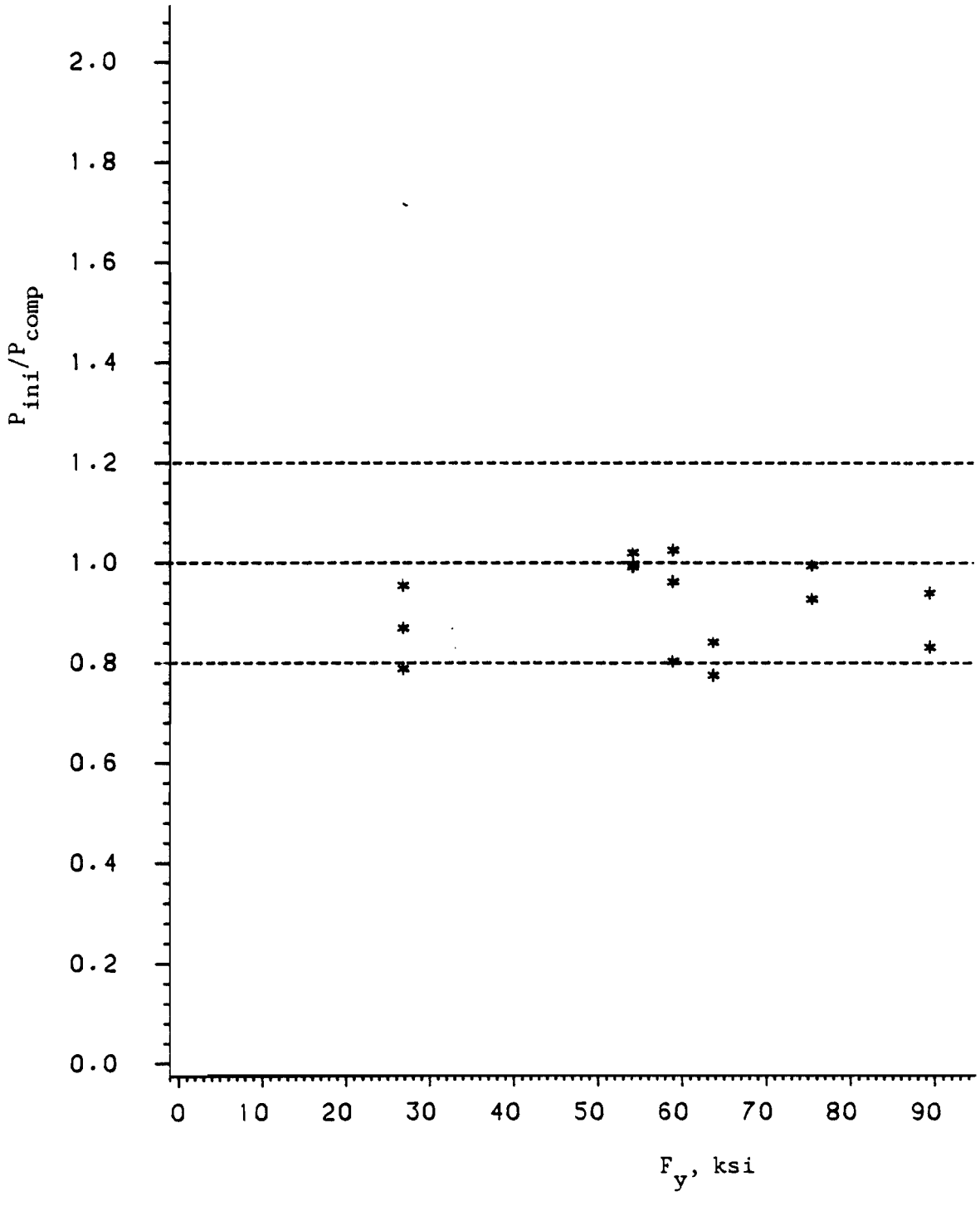

P_{ini} = Initial buckling load of curved element

P_{comp} = Predicted initial buckling load

Figure 3.70 Comparison of P_{ini}/P_{comp} Vs. F_y for CSI Stub Column Tests

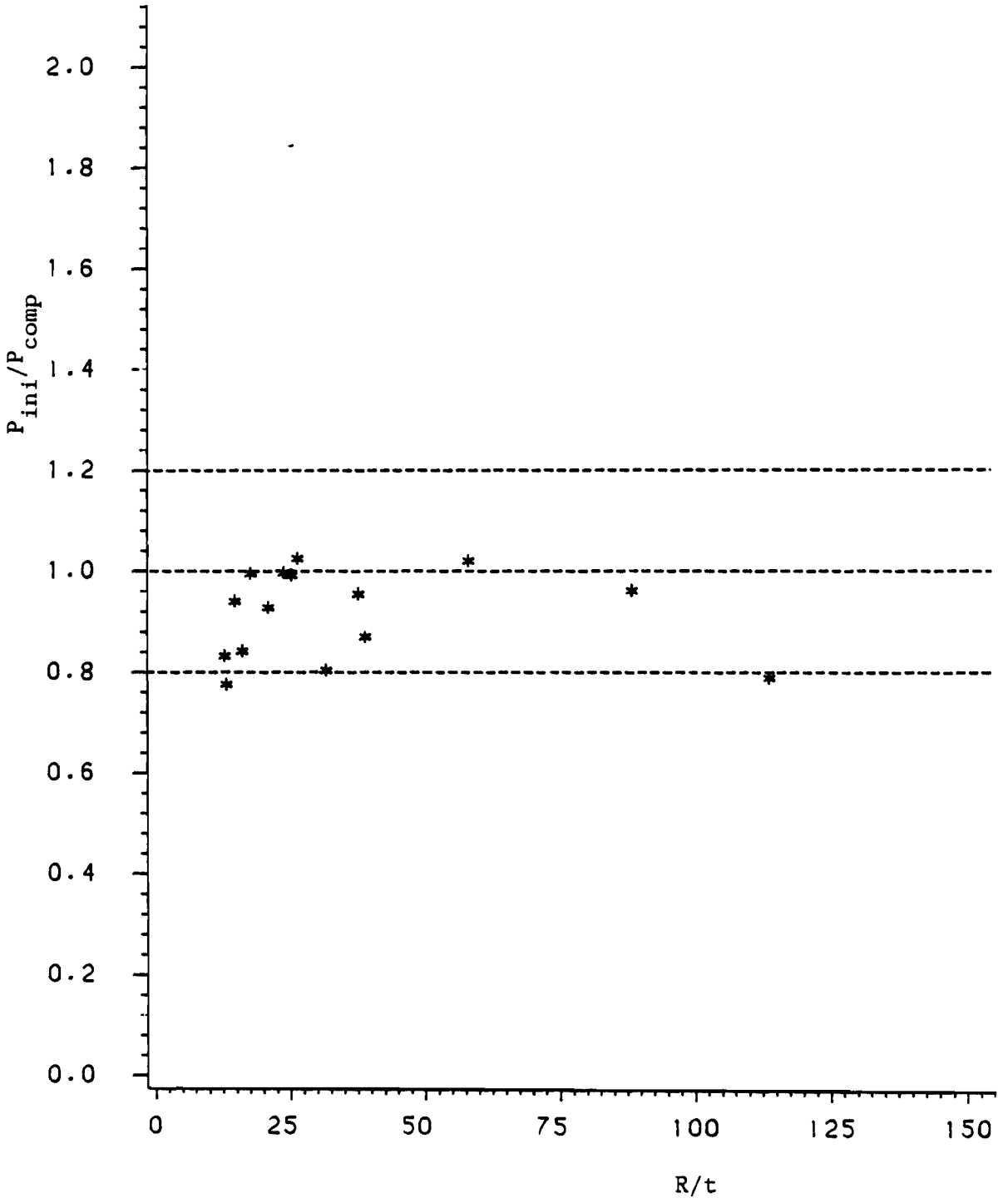

P_{ini} = Initial buckling load of curved element

P_{comp} = Predicted initial buckling load

Figure 3.71 Comparison of P_{ini}/P_{comp} Vs. R/t for CSI Stub Column Tests

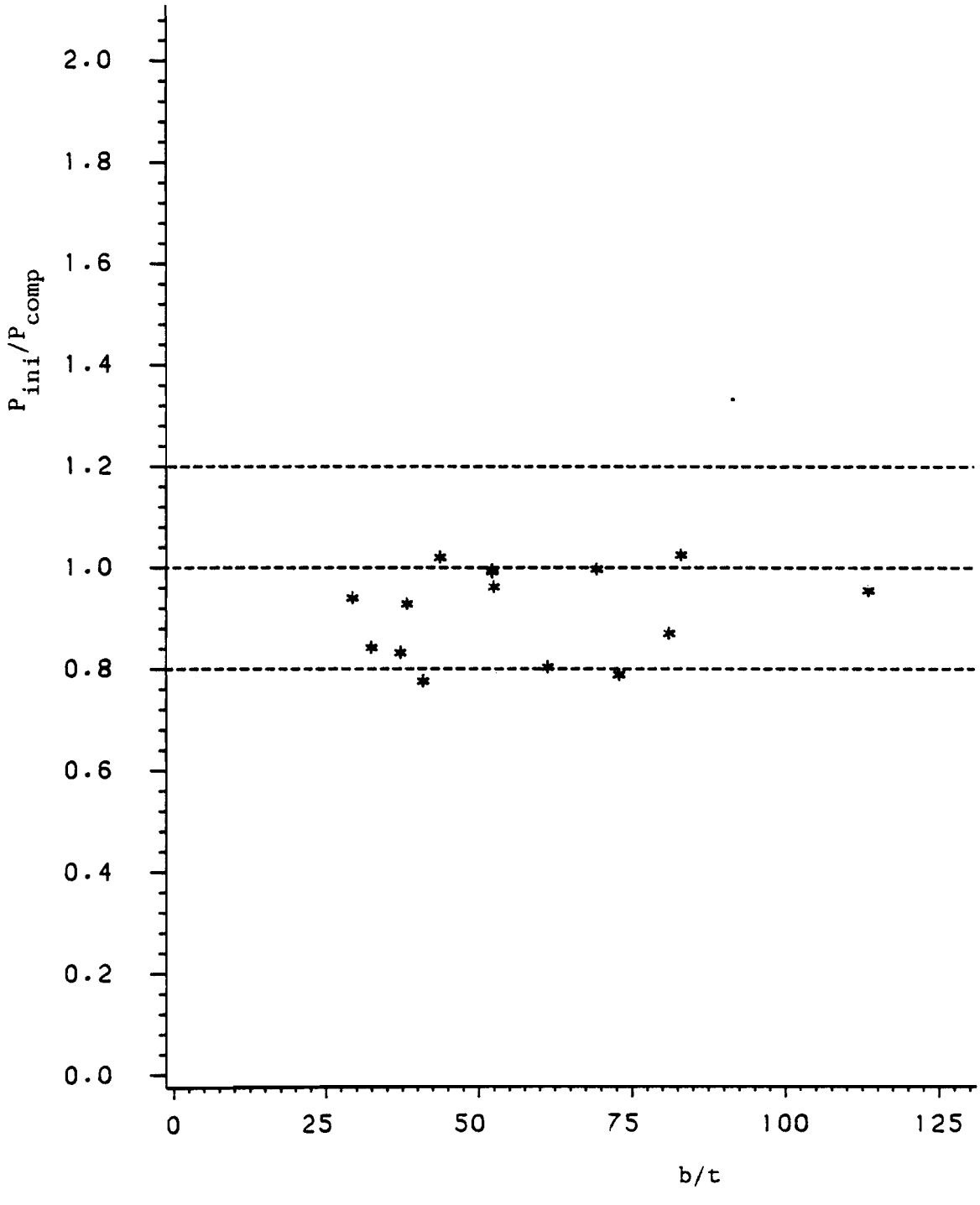

P_{ini} = Initial buckling load of curved element

P_{comp} = Predicted initial buckling load

Figure 3.72 Comparison of P_{ini}/P_{comp} Vs. b/t for CSI Stub Column Tests

effective area of the web (assuming a web thickness equal to twice the material thickness since the webs were connected by closely spaced screws) times the critical buckling stress computed from Eq. (3.6) for the unstiffened curved element. P_{curve} is calculated as the same critical buckling stress times the remaining area (total area - full web area) in the cross-section. P_{total} is simply $(P_w + P_{curve})$. The initial buckling loads are compared to the predicted loads in column (6). As shown, good agreement with the tested initial buckling loads is provided using this method. The initial-to-predicted moment ratios may be compared in Figures 3.70 through 3.72 for the tested ranges of F_y, R/t, and b/t, respectively.

b. Bending - CB Beam Specimens. The predicted buckling moments for the CB beam specimens are computed using the same basic procedure as described in Section III.C.5. Again, C values of 1.0, 0.75, 0.67, 0.60, and 0.50 were used to compute the predicted buckling moments listed in column (3) of Tables 3.24 through 3.28, respectively. The ultimate moment that each specimen could withstand is given in column (1) of each table. Column (2) lists the initial buckling moment that was observed in each test. Column (6) of Table 3.24 lists the ultimate-to-initial buckling moment ratios for each of the CB beam specimens. As noted many times before, the highly curved specimens, such as the CB3 (R=1 in.) beams exhibit no post-buckling strength. However, as the curvature is decreased, as for the CB2 (R=1.25 in.) and the CB1 (R=4 in.) specimens, there is some post-buckling strength. Figure 3.73 provides a comparison of the ultimate-to-initial buckling moment ratios for the tested range of R/t.

Table 3.24 Comparison of Actual-to-Predicted Buckling Moments CB Beam Specimens (C=1.0) Based on Eq. (3.6) Using Direct Approach for Inelastic Buckling, Eq. (3.10)

Specimen	Ultimate Moment (in-kips) (1)	Initial Buckling Moment (in-kips) (2)	Predicted Buckling Moment (in-kips) (3)	(2)/(3) (4)	(1)/(3) (5)	(1)/(2) (6)
80XFCB3-1*	208.0	208.0	210.0	0.99	0.99	1.00
50XF(78)CB3-1*	143.7	143.7	146.5	0.98	0.98	1.00
80SKCB3-1*	128.1	128.1	122.3	1.04	1.04	1.00
80DKCB3-1*	70.9	70.9	67.4	1.05	1.05	1.00
50XF(39)CB3-1*	52.3	52.3	56.3	0.93	0.93	1.00
30SKCB3-1*	21.8	21.8	21.1	1.03	1.03	1.00
80XFCB2-1*	174.2	174.2	165.6	1.05	1.05	1.00
50XF(78)CB2-1*	120.9	113.8	104.2	1.09	1.16	1.06
80SKCB2-1*	109.2	93.0	85.5	1.08	1.28	1.17
80DKCB2-1*	62.6	52.9	49.5	1.07	1.26	1.18
50XF(39)CB2-1*	47.1	43.2	40.5	1.07	1.17	1.09
30SKCB2-1*	17.6	15.1	15.9	0.95	1.11	1.16
80XFCB1-1	115.7	114.4	115.9	0.99	1.00	1.01
50XF(78)CB1-1*	84.5	76.7	78.9	0.97	1.07	1.10
80SKCB1-1	70.9	52.9	44.2	1.20	1.60	1.34
80DKCB1-1	44.2	24.0	23.6	1.02	1.88	1.84
50XF(39)CB1-1	28.3	15.6	13.1	1.19	2.15	1.81
30SKCB1-1	13.7	9.75	9.42	1.04	1.45	1.40
Mean				1.04	1.23	-
Std. Deviation				0.072	0.335	-

*$f_{cr} > F_{pr} = 0.7F_y$; assume inelastic buckling

Table 3.25 Comparison of Actual-to-Predicted Buckling Moments CB Beam Specimens (C=0.75) Based on Eq. (3.6) Using Direct Approach for Inelastic Buckling, Eq. (3.10)

Specimen	Ultimate Moment (in-kips) (1)	Initial Buckling Moment (in-kips) (2)	Predicted Buckling Moment (in-kips) (3)	(2)/(3) (4)	(1)/(3) (5)	(1)/(2) (6)
80XFCB3-1*	208.0	208.0	227.2	0.92	0.92	1.00
50XF(78)CB3-1*	143.7	143.7	157.8	0.91	0.91	1.00
80SKCB3-1*	128.1	128.1	132.8	0.96	0.96	1.00
80DKCB3-1*	70.9	70.9	73.1	0.97	0.97	1.00
50XF(39)CB3-1*	52.3	52.3	60.5	0.86	0.86	1.00
30SKCB3-1*	21.8	21.8	22.9	0.95	0.95	1.00
80XFCB2-1*	174.2	174.2	176.5	0.99	0.99	1.00
50XF(78)CB2-1*	120.9	113.8	110.2	1.03	1.10	1.06
80SKCB2-1*	109.2	93.0	90.3	1.03	1.21	1.17
80DKCB2-1*	62.6	52.9	52.8	1.00	1.19	1.18
50XF(39)CB2-1*	47.1	43.2	42.7	1.01	1.10	1.09
30SKCB2-1*	17.6	15.1	16.8	0.90	1.04	1.16
80XFCB1-1*	115.7	114.4	120.3	0.95	0.96	1.01
50XF(78)CB1-1*	84.5	76.7	81.8	0.94	1.03	1.10
80SKCB1-1*	70.9	52.9	45.8	1.15	1.55	1.34
80DKCB1-1*	44.2	24.0	24.6	0.98	1.80	1.84
50XF(39)CB1-1	28.3	15.6	13.7	1.14	2.07	1.81
30SKCB1-1*	13.7	9.75	9.72	1.00	1.40	1.40
Mean				0.98	1.17	-
Std. Deviation				0.075	0.332	-

*$f_{cr} > F_{pr} = 0.7F_y$; assume inelastic buckling

Table 3.26 Comparison of Actual-to-Predicted Buckling Moments
CB Beam Specimens (C=0.67)
Based on Eq. (3.6) Using Direct
Approach for Inelastic Buckling, Eq. (3.10)

Specimen	Ultimate Moment (in-kips) (1)	Initial Buckling Moment (in-kips) (2)	Predicted Buckling Moment (in-kips) (3)	(2)/(3) (4)	(1)/(3) (5)	(1)/(2) (6)
80XFCB3-1*	208.0	208.0	233.3	0.89	0.89	1.00
50XF(78)CB3-1*	143.7	143.7	161.9	0.89	0.89	1.00
80SKCB3-1*	128.1	128.1	136.5	0.94	0.94	1.00
80DKCB3-1*	70.9	70.9	75.1	0.94	0.94	1.00
50XF(39)CB3-1*	52.3	52.3	62.0	0.84	0.84	1.00
30SKCB3-1*	21.8	21.8	23.6	0.92	0.92	1.00
80XFCB2-1*	174.2	174.2	180.3	0.97	0.97	1.00
50XF(78)CB2-1*	120.9	113.8	112.2	1.01	1.08	1.06
80SKCB2-1*	109.2	93.0	91.9	1.01	1.19	1.17
80DKCB2-1*	62.6	52.9	54.0	0.98	1.16	1.18
50XF(39)CB2-1*	47.1	43.2	43.6	0.99	1.08	1.09
30SKCB2-1*	17.6	15.1	17.1	0.88	1.02	1.16
80XFCB1-1*	115.7	114.4	121.7	0.94	0.95	1.01
50XF(78)CB1-1*	84.5	76.7	82.8	0.93	1.02	1.10
80SKCB1-1*	70.9	52.9	46.4	1.14	1.53	1.34
80DKCB1-1*	44.2	24.0	24.9	0.96	1.77	1.84
50XF(39)CB1-1	28.3	15.6	13.9	1.13	2.04	1.81
30SKCB1-1*	13.7	9.75	9.83	0.99	1.39	1.40
Mean				0.96	1.15	-
Std. Deviation				0.077	0.332	-

*$f_{cr} > F_{pr} = 0.7F_y$; assume inelastic buckling

Table 3.27 Comparison of Actual-to-Predicted Buckling Moments CB Beam Specimens (C=0.60) Based on Eq. (3.6) Using Direct Approach for Inelastic Buckling, Eq. (3.10)

Specimen	Ultimate Moment (in-kips) (1)	Initial Buckling Moment (in-kips) (2)	Predicted Buckling Moment (in-kips) (3)	(2)/(3) (4)	(1)/(3) (5)	(1)/(2) (6)
80XFCB3-1*	208.0	208.0	238.9	0.87	0.87	1.00
50XF(78)CB3-1*	143.7	143.7	165.6	0.87	0.87	1.00
80SKCB3-1*	128.1	128.1	140.0	0.91	0.91	1.00
80DKCB3-1*	70.9	70.9	77.0	0.92	0.92	1.00
50XF(39)CB3-1*	52.3	52.3	63.4	0.83	0.83	1.00
30SKCB3-1*	21.8	21.8	24.2	0.90	0.90	1.00
80XFCB2-1*	174.2	174.2	183.7	0.95	0.95	1.00
50XF(78)CB2-1*	120.9	113.8	114.1	1.00	1.06	1.06
80SKCB2-1*	109.2	93.0	93.4	1.00	1.17	1.17
80DKCB2-1*	62.6	52.9	55.0	0.96	1.14	1.18
50XF(39)CB2-1*	47.1	43.2	44.3	0.98	1.06	1.09
30SKCB2-1*	17.6	15.1	17.4	0.87	1.01	1.16
80XFCB1-1*	115.7	114.4	123.1	0.93	0.94	1.01
50XF(78)CB1-1*	84.5	76.7	83.7	0.92	1.01	1.10
80SKCB1-1*	70.9	52.9	46.9	1.13	1.51	1.34
80DKCB1-1*	44.2	24.0	25.2	0.95	1.75	1.84
50XF(39)CB1-1	28.3	15.6	14.0	1.11	2.02	1.81
30SKCB1-1*	13.7	9.75	9.92	0.98	1.38	1.40
Mean				0.95	1.13	-
Std. Deviation				0.079	0.331	-

*$f_{cr} > F_{pr} = 0.7F_y$; assume inelastic buckling

Table 3.28 Comparison of Actual-to-Predicted Buckling Moments CB Beam Specimens (C=0.50) Based on Eq. (3.6) Using Direct Approach for Inelastic Buckling, Eq. (3.10)

Specimen	Ultimate Moment (in-kips) (1)	Initial Buckling Moment (in-kips) (2)	Predicted Buckling Moment (in-kips) (3)	(2)/(3) (4)	(1)/(3) (5)	(1)/(2) (6)
80XFCB3-1*	208.0	208.0	247.5	0.84	0.84	1.00
50XF(78)CB3-1*	143.7	143.7	167.9	0.86	0.86	1.00
80SKCB3-1*	128.1	128.1	145.2	0.88	0.88	1.00
80DKCB3-1*	70.9	70.9	79.8	0.89	0.89	1.00
50XF(39)CB3-1*	52.3	52.3	65.5	0.80	0.80	1.00
30SKCB3-1*	21.8	21.8	25.1	0.87	0.87	1.00
80XFCB2-1*	174.2	174.2	188.9	0.92	0.92	1.00
50XF(78)CB2-1*	120.9	113.8	116.9	0.97	1.03	1.06
80SKCB2-1*	109.2	93.0	95.6	0.97	1.14	1.17
80DKCB2-1*	62.6	52.9	56.6	0.94	1.11	1.18
50XF(39)CB2-1*	47.1	43.2	45.5	0.95	1.04	1.09
30SKCB2-1*	17.6	15.1	17.9	0.84	0.98	1.16
80XFCB1-1*	115.7	114.4	125.0	0.92	0.93	1.01
50XF(78)CB1-1*	84.5	76.7	85.0	0.90	0.99	1.10
80SKCB1-1*	70.9	52.9	47.6	1.11	1.49	1.34
80DKCB1-1*	44.2	24.0	25.7	0.93	1.72	1.84
50XF(39)CB1-1	28.3	15.6	14.3	1.09	1.98	1.81
30SKCB1-1*	13.7	9.75	10.0	0.97	1.36	1.40
Mean				0.93	1.10	-
Std. Deviation				0.081	0.329	-

*$f_{cr} > F_{pr} = 0.7F_y$; assume inelastic buckling

Table 3.29 Comparison of Initial-to-Predicted Buckling Moments for Various Values of C
CB Beam Specimens

Specimen	C Values				
	1.00	0.75	0.67	0.60	0.50
80XFCB3-1*	0.99	0.92	0.89	0.87	0.84
50XF(78)CB3-1*	0.98	0.91	0.89	0.87	0.86
80SKCB3-1*	1.04	0.96	0.94	0.91	0.88
80DKCB3-1*	1.05	0.97	0.94	0.92	0.89
50XF(39)CB3-1*	0.93	0.86	0.84	0.83	0.80
30SKCB3-1*	1.03	0.95	0.92	0.90	0.87
80XFCB2-1*	1.05	0.99	0.97	0.95	0.92
50XF(78)CB2-1*	1.09	1.03	1.01	1.00	0.97
80SKCB2-1*	1.08	1.03	1.01	1.00	0.97
80DKCB2-1*	1.07	1.00	0.98	0.96	0.94
50XF(39)CB2-1*	1.07	1.01	0.99	0.98	0.95
30SKCB2-1*	0.95	0.90	0.88	0.87	0.84
80XFCB1-1*	0.99	0.95	0.94	0.93	0.92
50XF(78)CB1-1*	0.97	0.94	0.93	0.92	0.90
80SKCB1-1*	1.20	1.15	1.14	1.13	1.11
80DKCB1-1*	1.02	0.98	0.96	0.95	0.93
50XF(39)CB1-1	1.19	1.14	1.13	1.11	1.09
30SKCB1-1*	1.04	1.00	0.99	0.98	0.97
Mean	1.04	0.98	0.96	0.95	0.93
Std. Deviation	0.072	0.075	0.077	0.079	0.081

*$f_{cr} > F_{pr} = 0.7F_y$; assume inelastic buckling

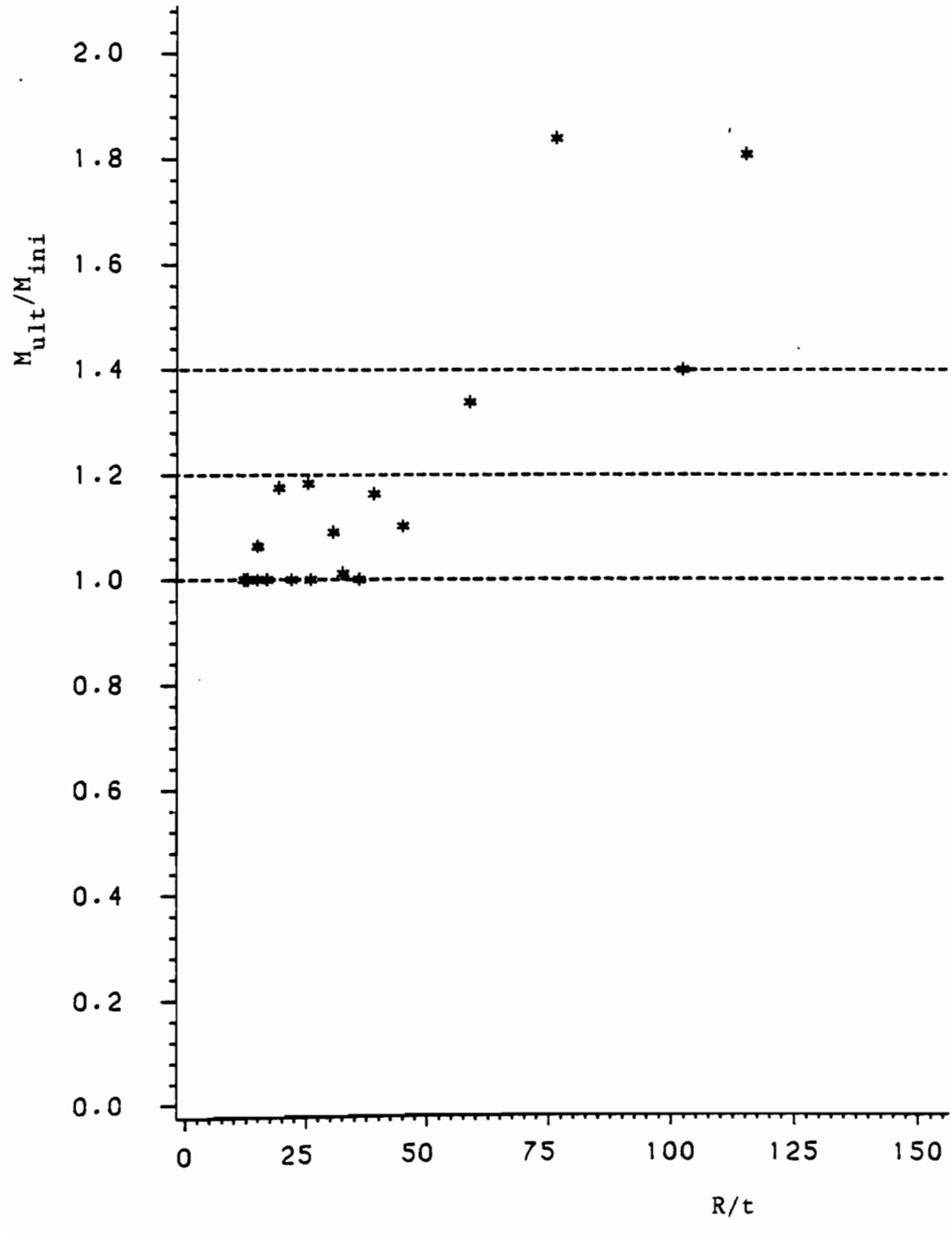

M_{ult} = Ultimate moment of cross section

M_{ini} = Initial buckling moment of curved element

Figure 3.73 Comparison of M_{ult}/M_{ini} Vs. R/t for CB Beam Tests

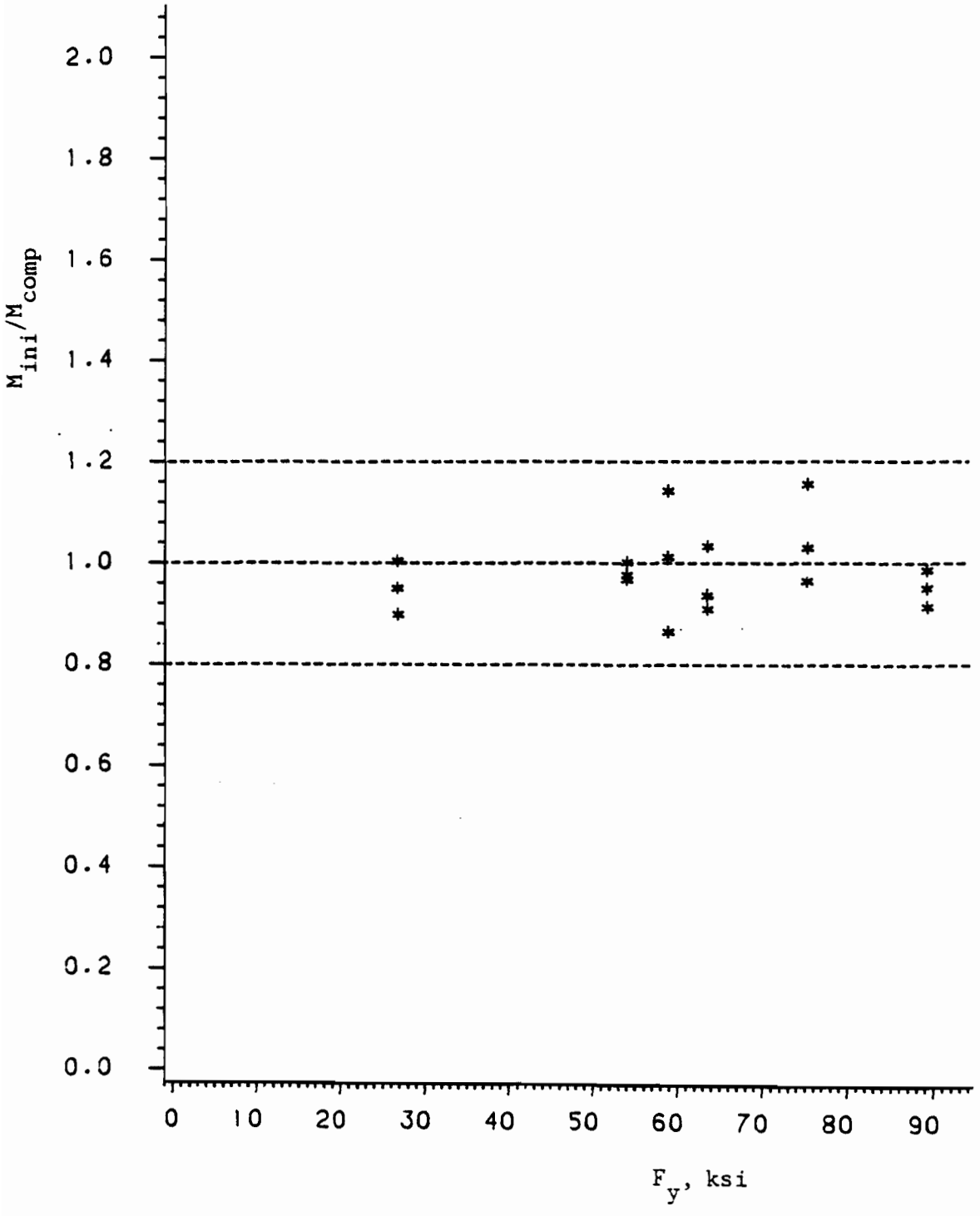

M_{ini} = Initial buckling moment of curved element

M_{comp} = Predicted initial buckling moment

Figure 3.74 Comparison of M_{ini}/M_{comp} Vs. F_y for CB Beam Tests (C = 0.75)

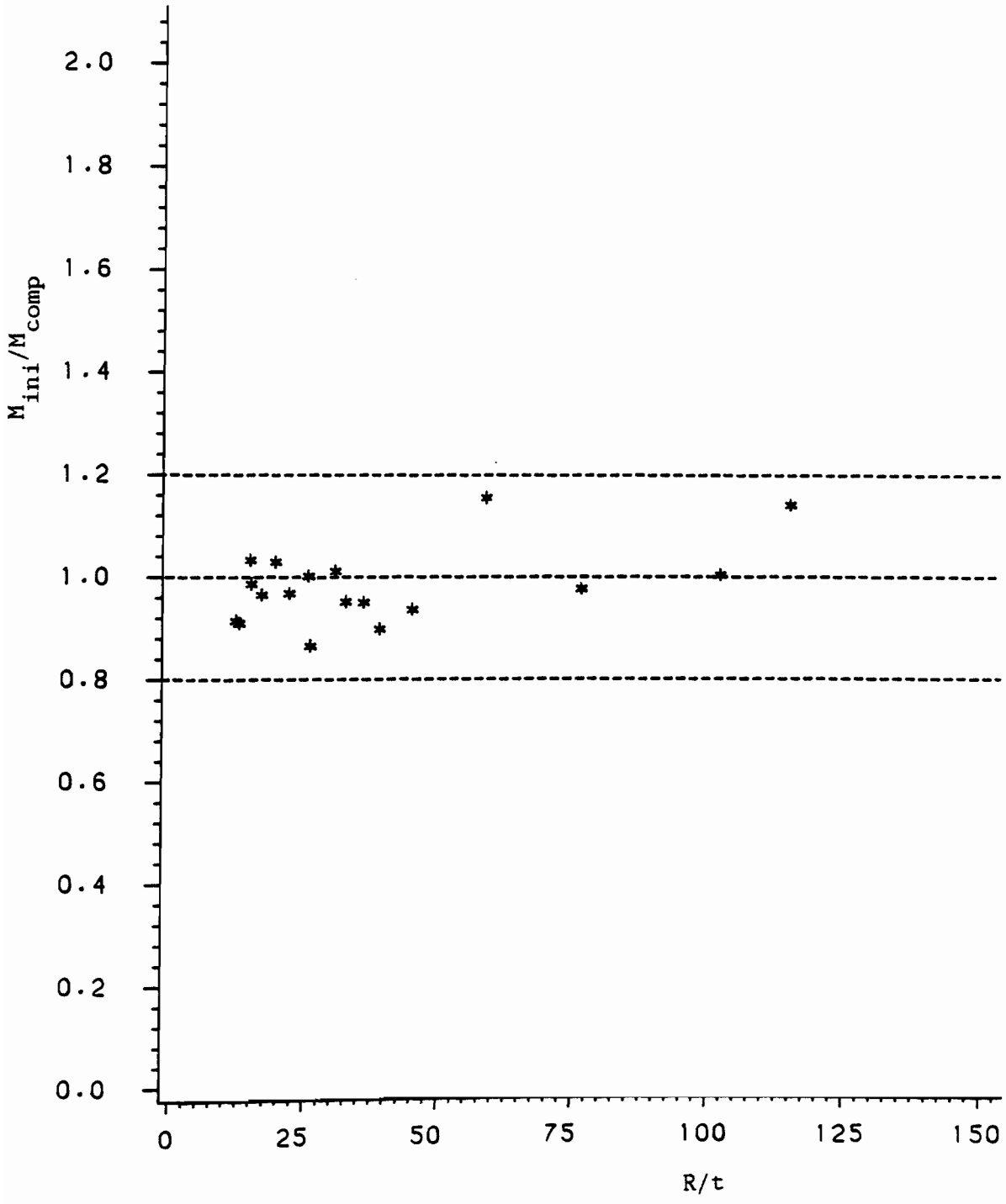

M_{ini} = Initial buckling moment of curved element

M_{comp} = Predicted initial buckling moment

Figure 3.75 Comparison of M_{ini}/M_{comp} Vs. R/t for CB Beam Tests (C = 0.75)

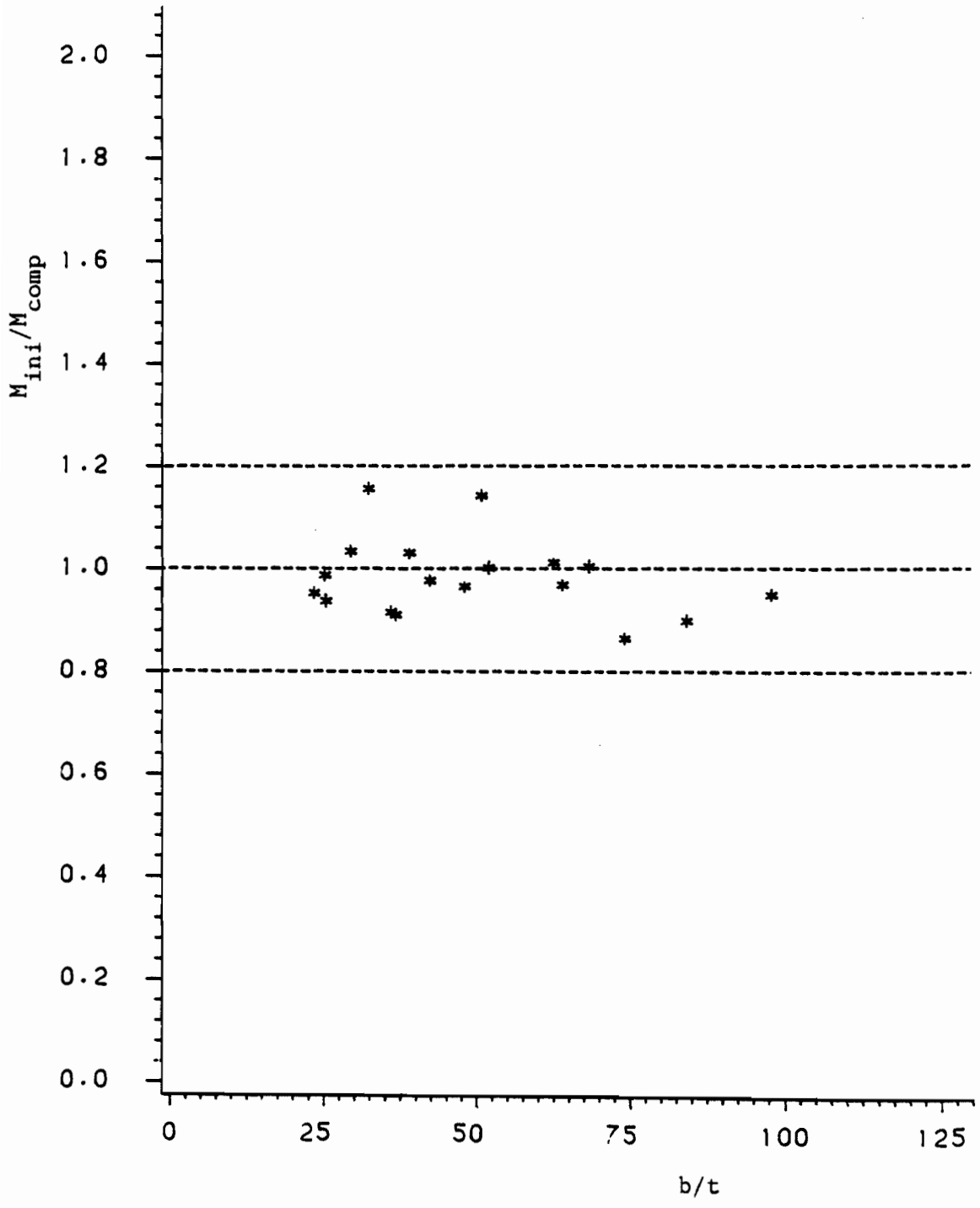

M_{ini} = Initial buckling moment of curved element

M_{comp} = Predicted initial buckling moment

Figure 3.76 Comparison of M_{ini}/M_{comp} Vs. b/t for CB Beam Tests (C = 0.75)

The initial buckling moment is compared to the predicted load in column (4) for each table. The accuracy of each value of C may be observed in Table 3.29. As shown, a value of C = 0.75 seems to provide the best overall agreement with the test data. The initial-to-predicted load ratios (based on C=0.75) are shown in Figure 3.74 through 3.76 for the tested range of F_y, R/t, and b/t, respectively.

E. NONLINEAR FINITE ELEMENT ANALYSIS OF CURVED ELEMENTS

The nonlinear finite element program entitled, " Automatic Dynamic Incremental Nonlinear Analysis (ADINA)", [52,53] has been employed for the prediction of curved element buckling behavior. ADINA is a general purpose finite element program that may be used for the static and dynamic displacement and stress analysis of solids, structures, and fluid-structure systems. The program also can perform linear and nonlinear analyses.

For the purposes of the present report, ADINA is used as a tool in order to predict the buckling behavior of curved elements. Thus, the complete finite element formulation used in ADINA is not included. Reference 54 provides a summary of the theory used in ADINA. Examples of the use of ADINA for various applications are given in Ref. 52.

In order to use the ADINA program, the following areas had to be considered:

1) Selection of type of finite element
2) Proper modeling of imperfections
3) Selection of boundary conditions

4) Material modeling for inelastic buckling

5) Prediction of curved element buckling by ADINA

Each of these topics is discussed at length in the following.

1. Selection of Type of Finite Element. The chosen finite element must be capable of performing a large deflection, small strain analysis for the curved elements. A very interesting discussion of the reasons for nonlinear (large deflection) analysis of curved elements is given by Gerard, et. al. in Ref. 2. According to Gerard, large deflection analysis is required for any element that develops transverse compressive stresses upon buckling. Such cases include the axial buckling of cylinders and curved plates. Because of the transverse compressive stresses which result at buckling, the buckled shape itself is unstable and thus, no post-buckling strength can be obtained. On the other hand, elements that develop transverse tension stresses, such as the axial buckling of simply supported flat plates, may exhibit considerable strength after buckling. For these elements, small deflecton theory seems to be adequate.

The chosen finite element must also be capable of modeling nonlinear materials. This requirement is necessary because of the relatively high buckling stresses, which are sometimes well into the inelastic range, of curved elements. The material model is discussed at length in Section III.E.4.

Finally, the finite element must have three translational degrees of freedom (d.o.f.) and two in-plane rotational d.o.f. at each node. Of the available finite elements in ADINA, the three dimensional (3-D) shell element seems best suited for modeling curved elements. Using the

3-D shell element, a nonlinear, large displacement/small strain analysis may be performed. Also, a bilinear model for the stress-strain behavior of a given material may be employed. The 3-D shell element uses the total Lagrangian formulation for large displacement analysis.

The 3-D shell element available in ADINA may have anywhere from 4 to 32 nodes with 5 d.o.f. per node. The d.o.f. include translation in three directions and two orthogonal, in-plane rotations. (The rotation normal to the shell surface is omitted.) According to Sec. 2.7.4 of the ADINA Modeling Guide[53], the 16 node shell element is normally the most effective for general shell analysis. This element is shown in Figure 3.77.

Because of the expense involved in forming the element matrices for the 16 node element, a 9 node shell element is sometimes recommended. However, problems may occur from "element locking" using the 9 node element if the actual problem to be modeled has very small (or zero) shearing strains. Because the axial buckling of curved elements falls into this category, the 16 node shell element was used.

Four 16 node shell elements were used to model both the stiffened and unstiffened curved elements. Larger models with up to 16 elements were checked for some cases; however, there was little, if any, difference in the predicted load from the four element model.

2. Modeling of Imperfections. First, a brief discussion of the reasons for including imperfections should be given. Curved elements with relatively large R/t values and thin-walled cylinders are particularly sensitive to the effect of initial imperfections. In some cases, initial imperfections are primarily blamed for reducing the

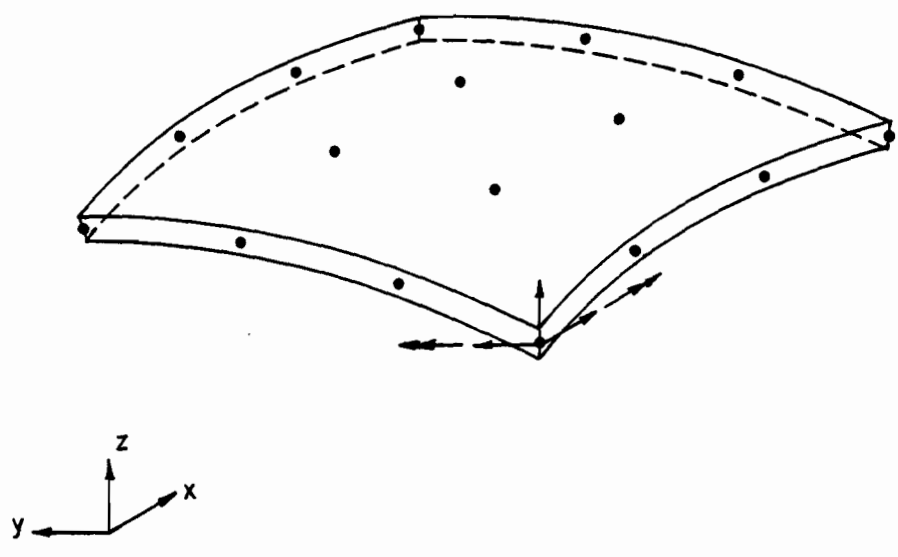

Figure 3.77 16-Node Shell Element Used to Predict Curved Element Behavior

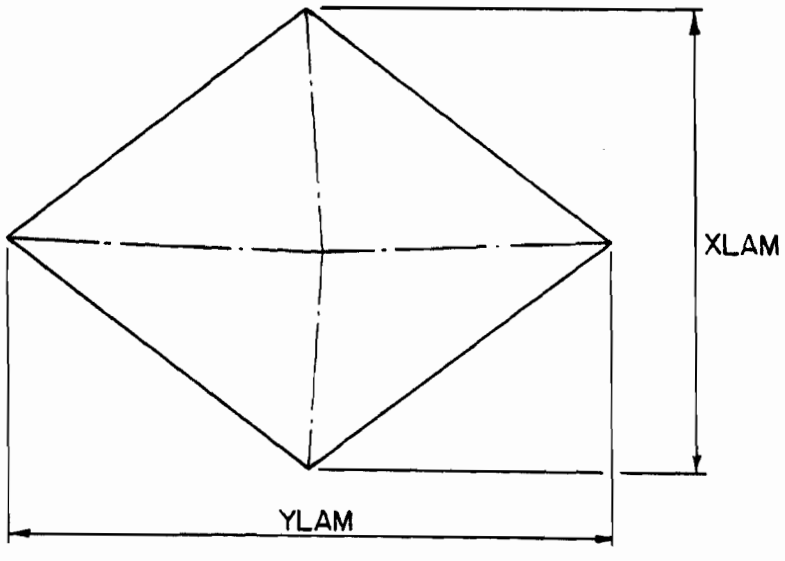

Figure 3.78 Dimensions of a Diamond Buckle

actual buckling load to as much as one-half the theoretical buckling load. Therefore, it seems imperative that any type of analysis for the local buckling of curved elements include the effect of imperfections.

Also, imperfections must be included in the finite element model in order for ADINA to provide a buckling or "collapse" load for initially straight, axially loaded structures. The ADINA program does not use the traditional eigenvalue type of solution for stability problems. Instead, the ultimate strength is determined when the incremental stiffness becomes negative or zero (not positive determinant). If an initially perfect (straight) column is subjected only to in-plane axial loadings, there is no way for any transverse movement (or bending) to occur and thus, no way for the structure to eventually collapse. Therefore, an initially imperfect model must be input in ADINA so that out-of-plane bending will be generated by the axial loading.

The next problem is to determine the shape of the imperfections. In the past, there has been some success in using programs similar to ADINA for axial buckling of flat plates[55]. For flat elements, the initial imperfection is input in the shape of the final failure mode. Therefore, it seems that this same type of approach should be applicable to curved elements. However, the problem with curved elements is that there is no closed form solution for their inelastic buckling and thus no way to theoretically predict the shape of the failure mode. So it seems that the predicted failure mode will have to be based, at least in part, on previously tested curved elements.

Because of the distinct differences in the type of failure modes associated with stiffened and unstiffened curved elements, the modeling

of the imperfections for each will be discussed separately in the following.

a. Stiffened Curved Elements. Because stiffened curved elements with arc length-to-radius ratios approaching 2π behave similarly to cylinders, the available literature for cylinders is used as a starting point in modeling imperfections.

There have been several papers written concerning the inelastic buckling of axially compressed cylinders (Ref. 56-59). Of the available references, all seem to derive a relationship for the axial buckled wavelength, XLAM, as a function of Rt. However, the exact equation for XLAM varies depending on whether simple J_2 (flow) theory or J_2 deformation theory was used. Mahmood and Paluszny[49] reported the following semi-empirical relationship for XLAM (Fig. 3.78) for the diamond buckling of cylinders.

$$XLAM = \frac{2K\pi R}{N} \tag{3.19}$$

where:

$K = XLAM/YLAM \simeq 0.7$ (See Fig. 3.78)

$N = 0.31 \sqrt[4]{12(1-\mu^2)}(t/R)^{-1/2}$

R = radius

t = thickness

For curved elements, YLAM from the above relationships may actually be larger than the arc length, b, of a given element. In this case, the outer edges of the stiffened curved elements will inhibit the

complete formation of the diamond buckle that would otherwise be obtained in a complete cylinder. However, it has been observed that the ratio of XLAM/YLAM of the curved element diamond buckle remains the same as for the cylinder. In other words, XLAM/YLAM is still approximately equal to 0.7 even for the curved element diamond buckle. Therefore, the following procedure may be used to predict the shape of a diamond buckle in a curved element.

1. Compute YLAM = XLAM/K
2. If YLAM > b, use XLAM = 0.7b
3. If YLAM < b, use XLAM = 0.7YLAM

For the wrinkling mode of failure, the following equation provides good agreement with the measured values for the axial wavelength, XLAM, of the stiffened curved elements.

$$XLAM = 3.20\sqrt{Rt} \tag{3.20}$$

This equation is also presented by Mahmood and Paluszny[49] (in a slightly different form) for the ring failure of cylinders. The circumferential wavelength for the wrinkling failure is equal to the arc length of the curved element.

Knowing the basic shape of the failure mode, the next concern is the distribution of the imperfection over the finite element model. It seems proper to assume that the supported edges of the stiffened curved elements are initially perfectly straight. Therefore, no imperfection will be input along these edges. However, halfway across the arc of the curved element, the imperfection should be at its maximum value. It seems that in order to accomplish this type of imperfection pattern, a double sine function must be used. The following expression will be

employed to generate the imperfections of the stiffened curved element model.

$$U = \pm C\left[SIN(\pi X/XLAM)(SIN(\theta-\bar{\theta}))/(SIN(90-\bar{\theta}))\right] \tag{3.21}$$

where:

C = maximum imperfection which occurs at node 49 (Fig. 3.79)

$\bar{\theta}$ = constant angle that depends on type of curved element, degrees

θ = angle measured as shown in Fig. 3.79, degrees

U = height of imperfection measured in the radial direction

Note that by taking advantage of symmetry, only one quarter of the buckled wave need be modeled. Also, the sign of the imperfection, U, in Eq. (3.21) is negative for diamond buckling failures and positive for wrinkling failure modes. The finite element model used for stiffened curved elements is shown in Fig. 3.79.

b. Unstiffened Curved Elements. Because of the extreme difficulty in the theoretical predition of the buckling of unstiffened curved elements, the only conceivable method to predict the buckled shape of these elements is to use a purely empirical approach. The following equation was determined from the measured dimensions of the previously tested unstiffened curved flanges.

$$XLAM = 8.5\sqrt{Rt} \tag{3.22}$$

The circumferential wavelength is simply the arc length of the unstiffened curved element.

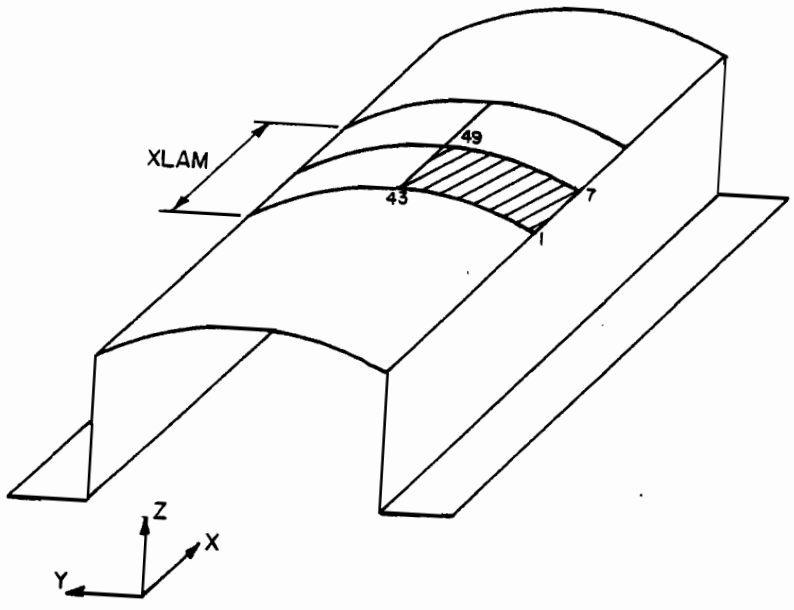

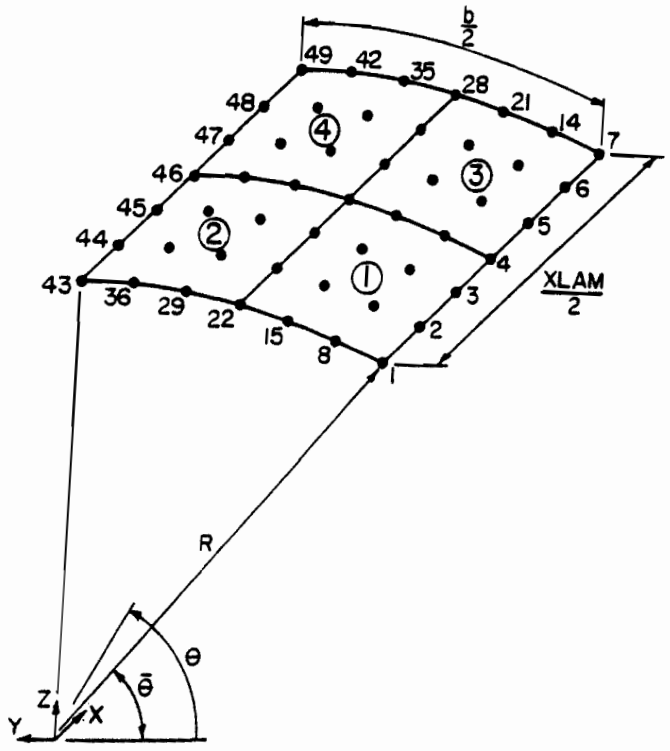

Figure 3.79 Finite Element Model for Stiffened Curved Elements

The imperfections for the curved element model will again be input using a double sine function. However, the circumferential imperfection is not symmetric for unstiffened curved elements with the maximum imperfection occurring at the free edge. The equation used to generate the imperfections is shown below.

$$U = C\left[\text{SIN}(\pi X/XLAM)\ \frac{\text{SIN}((\theta-\bar{\theta})/2)}{\text{SIN}(90-\bar{\theta})}\right] \tag{3.23}$$

where:

C = maximum imperfection which occurs at node 7 (Figure 3.80)

$\bar{\theta}$ = constant angle that depends on type of curved element, degrees

θ = angle measured as shown in Figure 3.80, degrees

U = height of imperfection measured in the radial direction

Again, symmetry may be used such that only half of one buckled wave need be modeled. The finite element model for the unstiffened curved element is shown in Figure 3.80.

3. Selection of Boundary Conditions.

a. Stiffened Curved Elements. The boundary conditions for the stiffened curved element model shown in Figure 3.79 are summarized below.

Degree of Freedom	Restrained Node Lines
X	1 to 43
Y	1 to 43 43 to 49

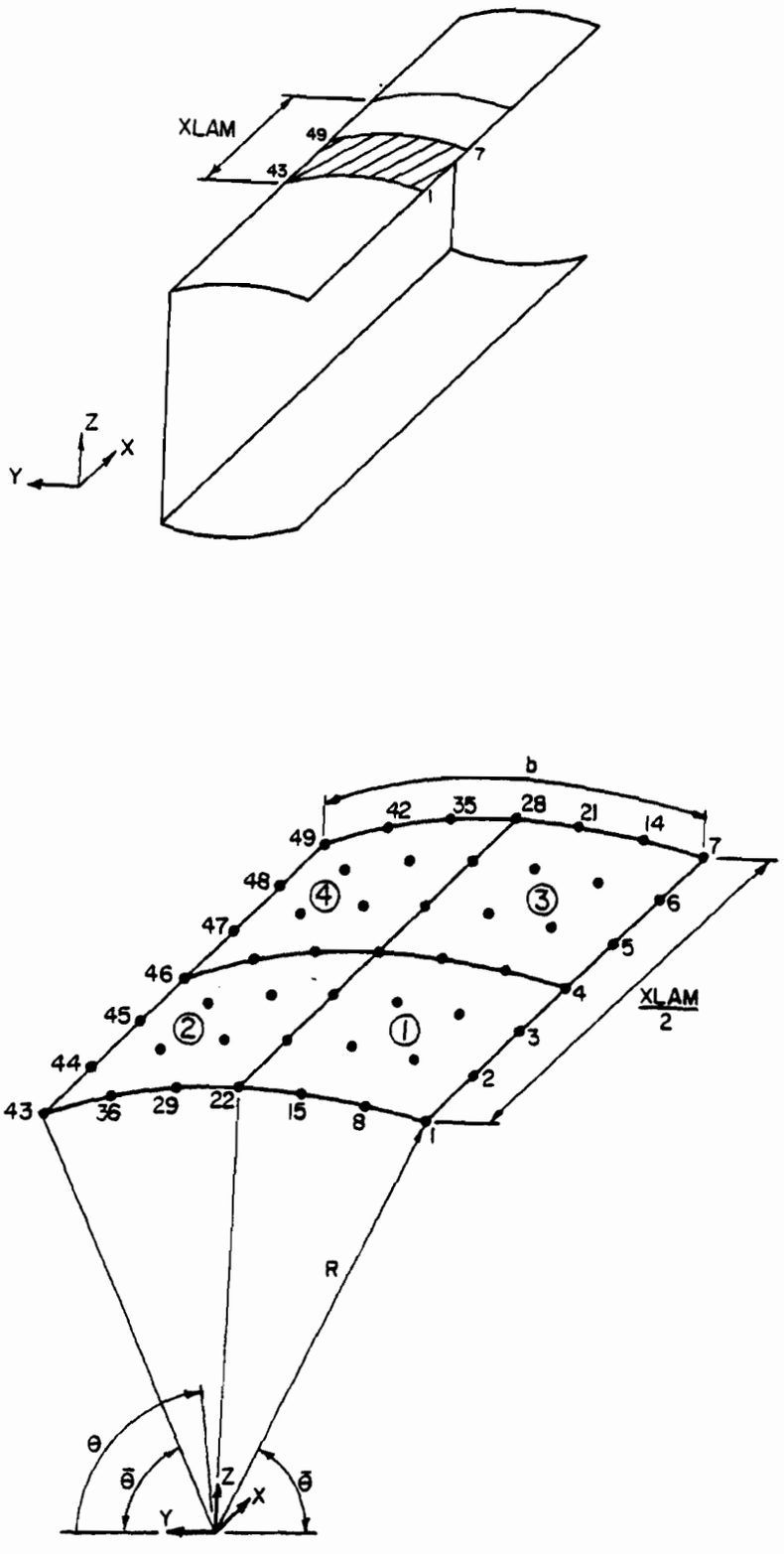

Figure 3.80 Finite Element Model for Unstiffened Curved Elements

Z	1 to 43 1 to 7
X rotation	1 to 43 43 to 49
Y rotation	1 to 43 1 to 7 7 to 49

b. Unstiffened Curved Elements. The boundary conditions for the unstiffened curved element model shown in Figure 3.80 are summarized below.

Degree of Freedom	Restrained Node Lines
X	1 to 43
Y	43 to 49
Z	1 to 43 43 to 49
X rotation	1 to 43
Y rotation	43 to 49 7 to 49

4. Material Modeling for Inelastic Buckling. Because curved elements with appreciable curvature often buckle well into the inelastic range, it is essential to account for inelastic stress-strain behavior in the finite element analysis. A bilinear material model is available for use with the 3-D shell element. The bilinear model consists of two parts. The first portion is perfectly elastic up to the yield point of the material. The second part extends from the yield point of the material. If appropriate, this portion may also have a positive slope in order to represent the strain hardening capacity of a

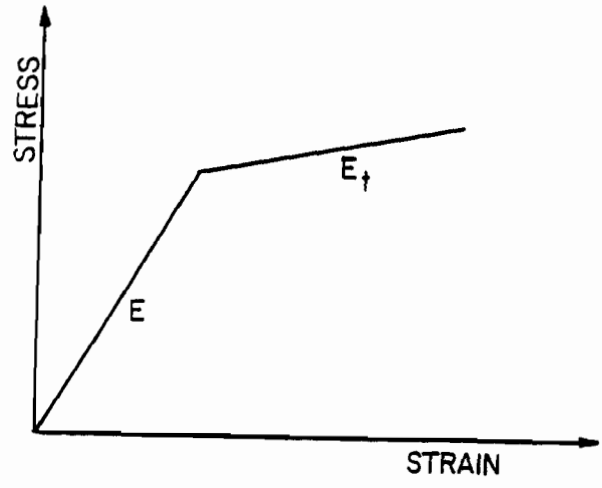

Figure 3.81 Bilinear Stress-Strain Curve Used By ADINA

Table 3.30 Material Properties Used in ADINA Finite Element Models

Material	F_y (ksi)	E (ksi)	E_t (ksi)
80XF	89.4	29500.0	0.0
50XF(78)	63.6	29500.0	0.0
80SK	75.4	29500.0	750.0
80DK	54.1	29500.0	1100.0
50XF(39)	58.9	29500.0	0.0
30SK	26.8	29500.0	575.0

Note:

The yield strength, F_y, and the tangent modulus, E_t, are based on representative stress-strain curves for each material in longitudinal compression. (See Figure B.1)

given material. Figure 3.81 shows a typical bilinear stress-strain curve. A summary of the mechanical properties used for each material is provided in Table 3.30. The E_t values are based on the stress strain curves of each material as determined by longitudinal compression coupon tests. Representative stress strain curves for each material are shown in Figure B.1.

5. Prediction of Curved Element Buckling by ADINA. In ADINA, the load is applied in small finite increments. If desired, the stiffness matrix is recomputed at each load increment. The load is continually increased in finite steps until the resulting stiffness matrix is either not positive determinant or until an equilibrium load can not be reached. At this point, the structure is assumed to have failed.

The ADINA program is used to model the curved elements of the previously tested stub columns in which the curved elements were the initial and final cause of failure. The ADINA predicted failure loads are compared to the actual test values in the following.

a. Stiffened Curved Elements. Because of the differences in the diamond and wrinkling failure pattern of the stiffened curved element, some slight changes in the finite element model of each must be made. The diamond buckling failure is an extremely sudden failure that results in a distinct inward "diamond" shaped buckle. In order to force the ADINA program to produce a similar diamond buckle in the finite element model, the imperfections were input in an inward direction. However, the wrinkling failure is an outward type of failure and thus, the imperfections for this case were input in an outward direction. Note that the same double sine function, Eq. (3.21), was used to generate the

Table 3.31 Comparison of Ultimate Loads to ADINA Stiffened Curved Elements

Specimen	Ultimate Load (kips) (1)	Failure Mode (2)	Maximum Imperfection (3)	ADINA Load (kips) (4)	(1)/(4) (5)
80XFBS3-1	22.4	Wrinkle	0.10T	22.9	0.98
50XF(78)AS3-1	15.8	Wrinkle	0.10T	15.1	1.05
80SKBS3-1	13.8	Wrinkle	0.10T	13.5	1.02
80DKAS3-1	8.15	Wrinkle	0.10T	7.44	1.10
50XF(39)AS3-1	6.95	Wrinkle	0.10T	7.20	0.97
30SKAS3-1	2.23	Wrinkle	0.10T	2.48	0.90
80XFBS2-1	15.7	Wrinkle	0.10T	16.4	0.96
50XF(78)AS2-1	9.09	Wrinkle	0.10T	9.80	0.93
80SKBS2-1	9.30	Wrinkle	0.10T	9.52	0.98
80DKAS2-3	4.79	Diamond	0.10T	5.12	0.94
50XF(39)AS2-1	3.95	Wrinkle	0.10T	4.56	0.87
30SKAS2-1	1.48	Wrinkle	0.10T	1.64	0.90
80XFBS1-1	14.1	Diamond	0.50T	13.2	1.07
50XF(78)AS1-1	8.07	Diamond	0.50T	7.60	1.06
50XF(78)AS1-2	8.34	Diamond	0.50T	8.16	1.02
80SKBS1-1	8.03	Diamond	0.50T	7.68	1.05
80DKAS1-1	3.79	Diamond	0.50T	3.60	1.05
80DKAS1-2	3.74	Diamond	0.50T	3.12	1.20
50XF(39)AS1-1	2.85	Diamond	0.50T	2.88	0.99
50XF(39)AS1-2	2.86	Diamond	0.50T	2.96	0.97
30SKAS1-1	1.15	Diamond	0.50T	1.28	0.90
30SKAS1-2	1.18	Diamond	0.50T	1.15	1.02
Mean					1.00
Std. Deviation					0.078

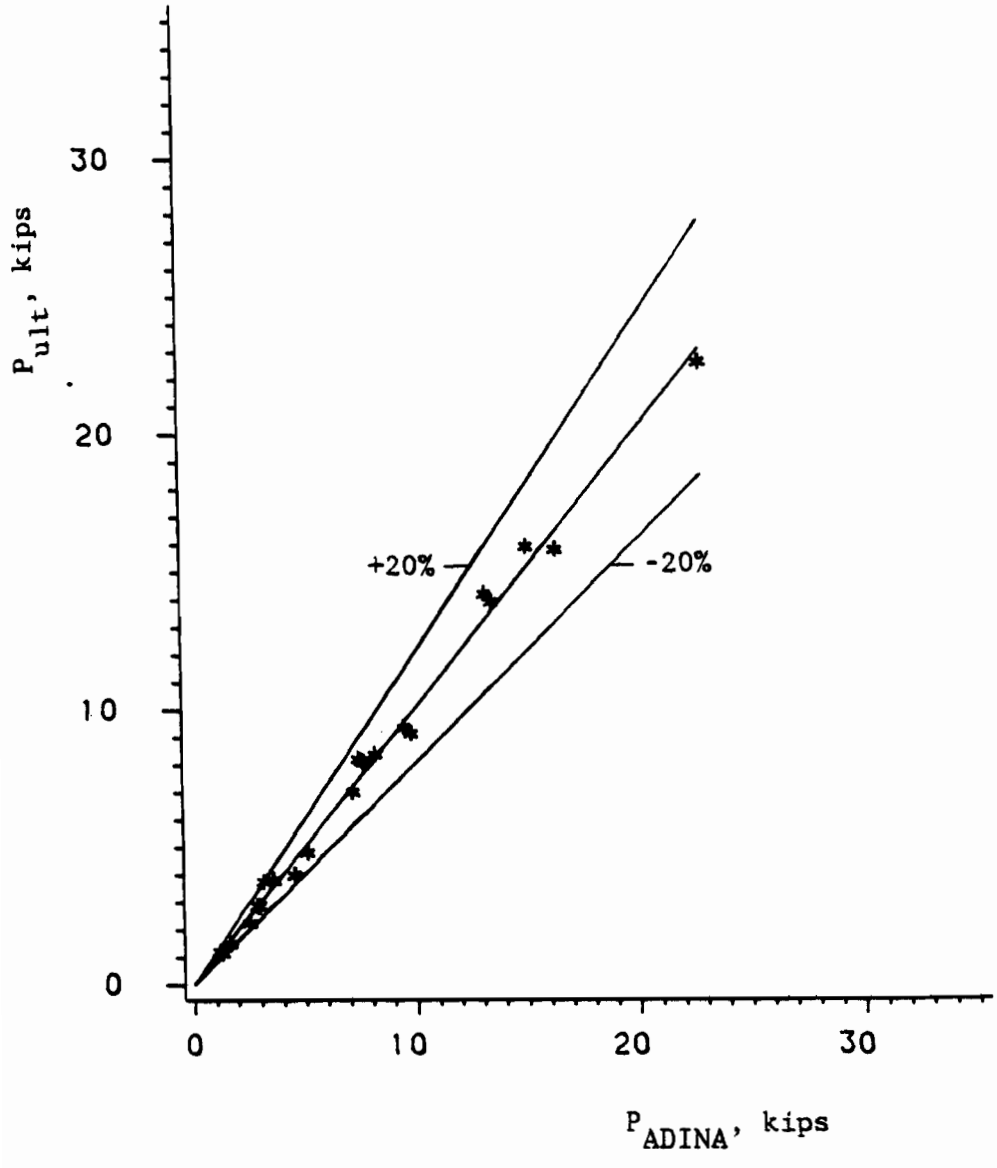

P_{ult} = Ultimate load of curved element, kips

P_{ADINA} = Predicted ultimate load by ADINA, kips

Figure 3.82 Comparison of P_{ult} Vs. P_{ADINA} for Stiffened Curved Elements from AS Stub Columns

imperfections for both types of failure with the only difference being in the sign of C. Column (3) of Table 3.31 indicates the maximum magnitude of imperfection which was used for each type of flange curvature. The size of the imperfection is based on the imperfections that were measured in the test specimens. The type of failure mode that occurred in each specimen is indicated in column (2).

The predicted failure loads from ADINA are listed in column (4) of Table 3.31. Column (1) of Table 3.31 lists the equivalent ultimate load on the tested curved element. The equivalent ultimate test load is computed as the average stress at failure of the stub column specimen times the cross-sectional area of the finite element model. The test values are compared to those from ADINA in column (5). The ultimate test loads are also compared to the values from ADINA in Figure 3.82. From these comparisons, it can be seen that ADINA provides a good estimate of the ultimate failure loads of the stiffened curved elements.

b. Unstiffened Curved Elements. The failure pattern for all of the unstiffened curved elements is approximately the same. For each specimen, failure occurred at the onset of a single outward wave. Therefore, the imperfections in the finite element model are also input in the outward direction.

The predicted failure loads computed by ADINA are listed in column (3) of Table 3.32. The ultimate test loads, shown in column (1), are again computed as the average stress of the stub column specimens at their ultimate load times the cross-sectional area of the finite element model. Column (4) lists the ultimate-to-predicted load ratio for each specimen. The ultimate failure loads may also be compared to the ADINA

Table 3.32 Comparison of Ultimate Loads to ADINA Unstiffened Curved Elements

Specimen	Ultimate Load (kips) (1)	Maximum Imperfection (2)	ADINA Load (kips) (3)	(1)/(3) (4)
80XFCS3-1	20.6	0.20T	24.3	0.85
50XF(78)CS3-1	15.0	0.20T	15.6	0.96
80SKCS3-1	13.8	0.20T	16.8	0.82
80DKCS3-1	6.93	0.20T	7.92	0.88
50XF(39)CS3-1	5.01	0.20T	7.36	0.68
30SKCS3-1	2.33	0.20T	2.69	0.87
80XFCS2-1	16.3	0.20T	17.8	0.92
50XF(78)CS2-1	10.4	0.20T	11.8	0.88
80SKCS2-1	8.69	0.20T	11.0	0.79
80DKCS2-3	5.43	0.20T	5.94	0.91
50XF(39)CS2-1	3.72	0.20T	5.04	0.74
30SKCS2-1	1.50	0.20T	1.89	0.79
80XFCS1-1	9.45	1.00T	12.3	0.77
80XFCS1-2	9.51	1.00T	12.2	0.78
50XF(78)CS1-1	6.86	1.00T	8.16	0.84
50XF(78)CS1-2	6.55	1.00T	7.92	0.83
80SKCS1-1	5.12	1.00T	7.41	0.69
80SKCS1-2	5.01	1.00T	7.40	0.68
80DKCS1-1	3.24	1.00T	3.96	0.82
50XF(39)CS1-2	1.87	1.00T	2.88	0.65
30SKCS1-2	1.13	1.00T	1.19	0.95
Mean				0.81
Std. Deviation				0.090

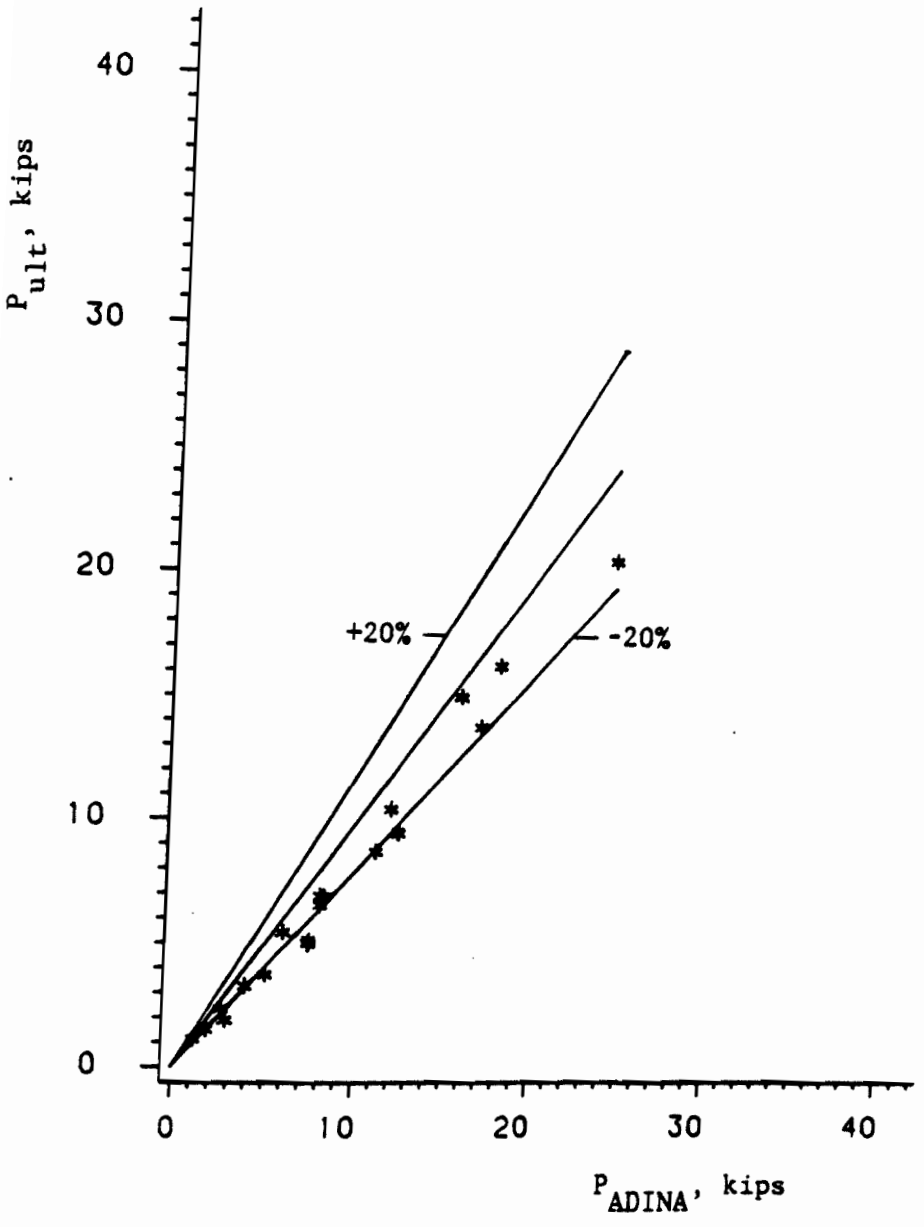

P_{ult}=Ultimate load of curved element, kips

P_{ADINA}=Predicted ultimate load by ADINA, kips

Figure 3.83 Comparison of P_{ult} Vs. P_{ADINA} for Unstiffened Curved Elements from CS Stub Columns

values in Figure 3.83. From these comparisons, it can be seen that, using the listed maximum imperfections, ADINA consistently over predicts the test loads by an average of approximately 20%. Thus, it seems that the magnitude of the imperfection in the actual test specimens may be higher than those reported in column (2).

Another possible reason for the overestimation of the ultimate load is in the problem of modeling the unstiffened curved element. The boundary condition along the line from node 1 to 43 (Figure 3.80) is especially difficult. The ideal condition for this line would be to allow circumferential expansion toward node 1. However, even though Y translation is allowed along this line, the circumferential movement is partially inhibited since both the Z and X translations must be restrained. Therefore, the finite element model is, at least to some degree, "stiffer" than the actual unstiffened curved element.

IV. SUMMARY OF CURVED ELEMENT ANALYSIS PROCEDURES

The following is given to provide a condensed summary of the recommended curved element analysis procedures.

A. STIFFENED CURVED ELEMENTS

1. Uniform Axial Compression.

Compute $(f_{cr})_{el}$ from Eq. (3.4) as,

$$(f_{cr})_{el} = E\left[\sqrt{0.0625(t/R)^2 + 3.267(t/b)^4} + 1.807(t/b)^2\right]. \qquad (3.4)$$

Because Eq. (3.4) is a semi-empirical equation, its use should be limited to the tested ranges of R/t and b/t. The tested values of R/t varied from 23 to 438 whereas b/t ranged from 47 to 218.

If $(f_{cr})_{el} \leq F_{pr}$, then $f_{cr} = (f_{cr})_{el}$.

If $(f_{cr})_{el} > F_{pr}$, then use $f_{cr} = (f_{cr})_{inel}$ from Eq. (3.10).

$$f_{cr} = (f_{cr})_{inel} = F_y\left[1 - \frac{0.21F_y}{(f_{cr})_{el}}\right]. \qquad (3.10)$$

Note that Eq. (3.10) assumes $F_{pr} = 0.7F_y$.

In the event that f_{cr} for a given curved element exceeds the buckling stress of a stiffened flat element in the same cross-section, the effective width concept may be employed to predict the amount of load that the flat element can resist. In this case, the total load resisted by the stiffened flat element may be computed as the effective width, b_e, from Eqs. (2.19) and (2.20) times the thickness times f_{cr} for the curved element. Again, note that the edge stress, f, used in the

effective width equations, is equal to the buckling stress of the curved element, f_{cr}.*

$$b_e = w \quad \text{when } \lambda \leq 0.673 \tag{2.19}$$

$$b_e = \rho w \quad \text{when } \lambda > 0.673 \tag{2.20}$$

in which:

b_e = effective width, in. (Figure 2.8)

w = full width of compression element, in.

t = thickness, in.

$\rho = (1-.22/\lambda)/\lambda$

λ is a slenderness factor determined as follows:

$$\lambda = \frac{1.052}{\sqrt{k}} \frac{w}{t} \sqrt{\frac{f}{E}}$$

f = actual stress at the edge of compression element, ksi.

$k = 4$ = buckling coefficient of a stiffened flat element

2. Bending. The critical buckling moment may be obtained by computing the moment associated with a critical stress f_{cr} from the uniform compression case (Eq. (3.4) and (3.10)) at a distance of

$$y_{cr} = y_{bot} + C(y_{top} - y_{bot}) \tag{3.11}$$

*Note that the above information is only applicable to sections in which an angle greater than 30 degrees exists between adjoining flat and curved elements. If this angle is less than 30 degrees, then assume that the flat element extends into the curved element until a 30 degree angle is obtained. (See Figure 3.50)

from the neutral axis (Figure 3.45). Note that a value for C of 0.67 was recommended for stiffened curved elements. Extrapolating to the outer portion of the curved element, the maximum stress, f_{max}, is computed as,

$$f_{max} = (y_{top}/y_{cr})f_{cr}. \tag{3.12}$$

The maximum bending moment may then be estimated as,

$$M_{max} = S_{xc}f_{max} < 1.2S_{xc}F_y \text{ or } 1.2S_{xt}F_y. \tag{3.13}$$

(whichever is smaller)

Note that the 1.2 factor may be thought of as a type of "shape" factor normally described in plastic design. Because the 1.2 factor is, to some extent, dependent on the shape of the cross section, special consideration should be given to determine its applicability to sections other than those tested in the present study. In no case, should the 1.2 factor be employed for sections with sloped webs with less than a 60° angle between the web and the horizontal. The tested values of R/t ranged from 20 to 420 whereas b/t varied from 41 to 180.

3. Shear. The critical shear buckling load may be estimated by computing the required shear force, V, to produce the critical shear stress, τ_{cr}, in the curved element. The following equations are used to compute τ_{cr}.

If $Z_b \leq 30$,

$$\tau_{cr} = (\tau_{cr})_f. \tag{2.26}$$

If $Z_b > 30$,

$$\tau_{cr} = 0.37(\sqrt{Z_b})(\tau_{cr})_f \tag{2.27}$$

in which

τ_{cr} = critical shear buckling stress of a curved panel

$(\tau_{cr})_f$ = critical shear buckling stress of a flat panel

$$= \frac{\pi^2}{12(1-\mu^2)} E(t/b)^2 K \cdot$$

If $a/b > 1$, $K = 5.34 + 4(b/a)^2$

If $a/b < 1$, $K = 4.00 + 5.34(b/a)^2$

a = axial length of curved panel

b = circumferential width of curved panel

$Z_b = (b^2/Rt)\sqrt{(1-\mu^2)}$

Note that the above equations are only for elastic buckling. For inelastic buckling ($\tau_{cr} > \tau_{pr}$), the tangent modulus approach is employed. The shear proportional limit, τ_{pr}, is estimated as $\tau_{pr} = 0.7\tau_y$. Using the same form of equation as Eq. (3.10) for inelastic buckling, τ_{cr} in the inelastic range may be computed as

$$(\tau_{cr})_{inel} = \tau_y\left[1 - \frac{0.21\tau_y}{(\tau_{cr})_{el}}\right]. \tag{3.16}$$

The shear force required to cause shear buckling may be computed from the horizontal shear stress equation as follows:

$$\tau_{cr} = \frac{V_c Q}{It} \tag{3.17}$$

Solving for V_c,

$$V_c = \tau_{cr}\frac{It}{Q} \tag{3.18}$$

in which

τ_{cr} = critical shear buckling stress as determined by either Eq. (2.26) or (2.27), whicherver is appropriate

V_c = shear force required to produce τ_{cr} in a curved element

I = moment of inertia of entire section about the neutral axis

Q = static moment of the area above or below the section at which the shear stress is desired

t = thickness of the section at the section where τ_{cr} is desired

It should be noted that it is extremely difficult to develop the predicted shear buckling stress in a curved web, as previously described in Section III.B.2.e. Therefore, special care should be exercised to prevent other modes of failure at lesser loads. The tested range of R/t varied from 25 to 310 while b/t ranged from 49 to 201.

B. UNSTIFFENED CURVED ELEMENTS

1. Uniform Axial Compression.

Compute $(f_{cr})_{el}$ from Eq. (3.6) as

$$(f_{cr})_{el} = E\left[0.04068(t/R) + 0.45192(t/b)^2\right]. \tag{3.6}$$

Because Eq. (3.6) is based largely on test results, its use should be limited to the tested ranges of R/t and b/t. The tested values of R/t varied from 12 to 103 while b/t ranged from 23 to 110.

If $(f_{cr})_{el} \leq F_{pr}$, then $f_{cr} = (f_{cr})_{el}$.

If $(f_{cr})_{el} > F_{pr}$, then use $f_{cr} = (f_{cr})_{inel}$ from Eq. (3.10).

$$f_{cr} = (f_{cr})_{inel} = F_y\left[1 - \frac{0.21F_y}{(f_{cr})_{el}}\right] \tag{3.10}$$

Note that Eq. (3.10) assumes $F_{pr} = 0.7F_y$.

In the event that f_{cr} for a given curved element exceeds the buckling stress of a stiffened flat element in the same cross-section, the effective width concept may be employed to predict the amount of load that the flat element can resist. In this case, the total load resisted by the stiffened flat element may be computed as the effective width, b_e, from Eqs. (2.19) and (2.20) times the thickness times f_{cr} for the curved element. Again, note that the edge stress, f, used in the effective width equations, is equal to the buckling stress of the curved element, f_{cr}.

2. Bending. The critical buckling moment may be obtained by computing the moment associated with a critical stress f_{cr} from the uniform compression case (Eq. (3.6) and (3.10)) at a distance of

$$y_{cr} = y_{bot} + C(y_{top} - y_{bot}) \tag{3.11}$$

from the neutral axis (Figure 3.45). Note that a C value of 0.75 was recommended for unstiffened curved elements. Extrapolating to the outer portion of the curved element, the maximum stress, f_{max}, is computed as,

$$f_{max} = (y_{top}/y_{cr})f_{cr}. \tag{3.12}$$

The maximum bending moment may then be estimated as,

$$M_{max} = S_{xc}f_{max} < S_{xc}F_y \text{ or } S_{xt}F_y. \tag{3.14}$$

(whichever is smaller)

No effective "shape" factor is permitted for unstiffened curved elements since they are not very efficient at transferring stress to their outer flange tips. The tested values of R/t varied from 12 to 115 whereas b/t ranged from 23 to 98.

V. COMPARISON OF THE LOCAL BUCKLING LOAD CAPACITY OF FLAT AND CURVED ELEMENTS

The ultimate failure loads of curved plate elements, subject to uniform axial compression, may be much higher than those of flat elements of similar dimensions. The actual difference between the ultimate failure loads of flat and curved elements depends, of course, on the degree of curvature in the element. In this section, the total load capacity of flat plates with a given width and thickness are compared to curved elements of the same width (or arc length) and thickness. The ultimate load capacity of stiffened flat and curved elements are compared in Section V.A. Section V.B provides a comparison of the load capacities of unstiffened flat and curved elements.

A. STIFFENED ELEMENTS

Figure 5.1 provides a comparison of the ultimate load capacities of stiffened flat elements, P_f, and stiffened curved elements, P_c, with the same width and thickness. (Note that F_y is assumed to be 33 ksi and the thickness is assumed to be 0.05 in. for Figure 5.1.) The total load capacity of the stiffened flat element is computed using the effective width approach as given by Eqs. (2.19) and (2.20) with the assumption that the edge stress reaches the yield strength of the material. Thus, the total post-buckling capacity of the stiffened flat element has been utilized in the calculation of P_f. In summary, P_f is computed as the effective width, b_e, times the thickness times F_y.

The total load capacity of the stiffened curved element, P_c, is computed as simply the predicted local buckling stress from Eqs. (3.4) and (3.10) times the thickness times the arc length. As shown in Figure 5.1 by the ratio of P_c to P_f, the total load capacity of the highly curved stiffened elements is considerably higher than that of flat elements with like dimensions. The difference between P_c and P_f becomes greater as the radius is decreased and the arc length is increased.

A similar comparison is made for yield strengths of 50 and 80 ksi in Figures 5.2 and 5.3, respectively. Again, the thickness is assumed equal to 0.05 in. for these comparisons. As shown, the ratio of P_c to P_f becomes greater for the relatively sharp curvatures as the yield point of a material increases. However, the ratio of P_c to P_f decreases for the flatter curvatures as the yield point increases. The reason for the larger P_c/P_f ratios for the sharper curvatures is that the failure is by yielding. On the other hand, for the flatter curvatures the curved element buckling is elastic and thus, the local buckling stress is unaffected by changes in F_y.

It should be noted that there are physical limits to the amount of curvature that a plate of a fixed width may be given. For the purposes of the comparisons, the arc length is limited to πR. This is the reason that the curve for R = 2 in. in Figures 5.1 through 5.3 ends before reaching a width of 7 in.

B. UNSTIFFENED ELEMENTS

An identical comparison has been made for the total load capacities of unstiffened flat and curved elements with like dimensions. Again,

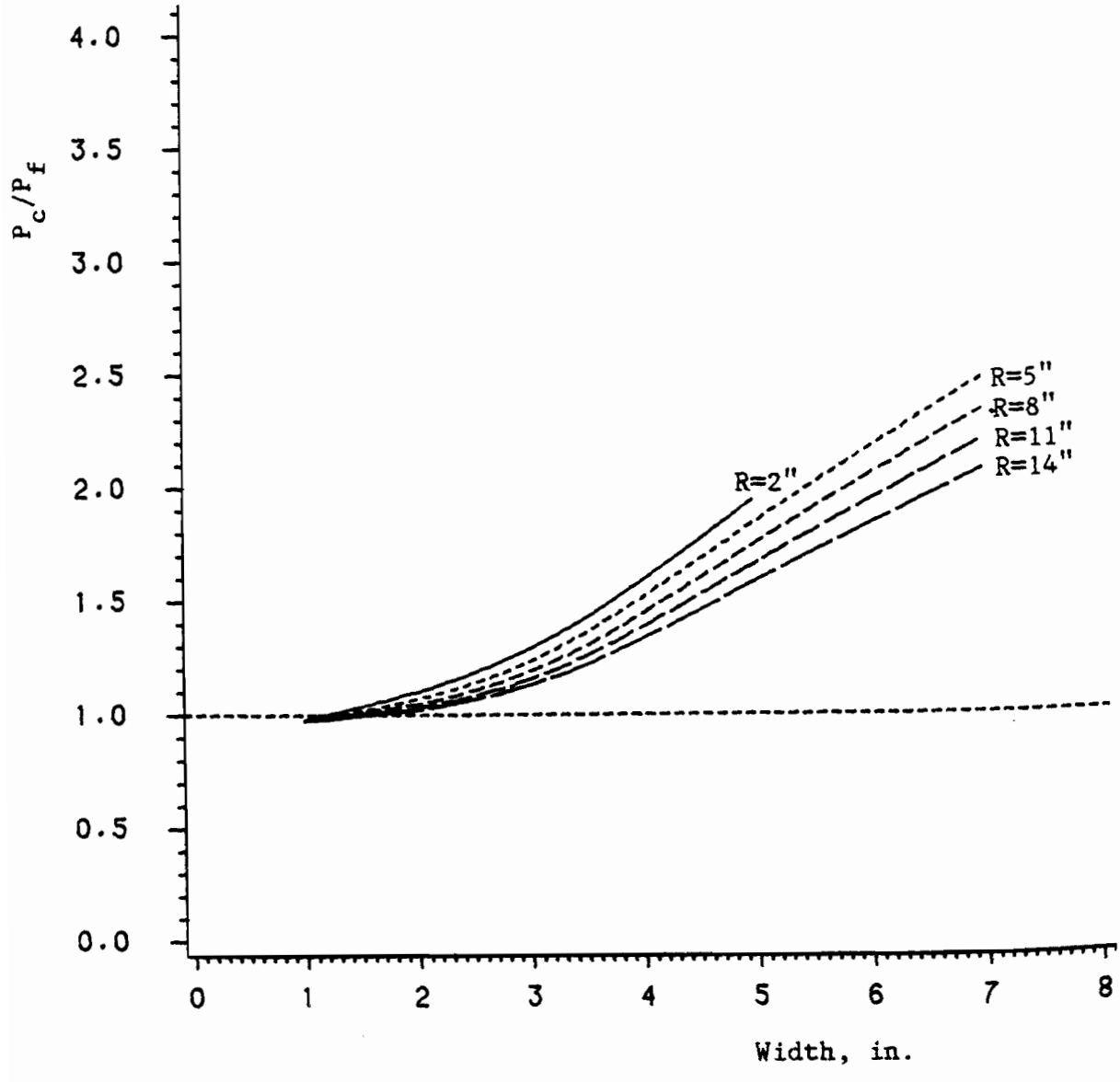

P_c = ultimate load capacity of a stiffened curved plate

P_f = ultimate load capacity of a stiffened flat plate

Figure 5.1 Comparison of the Local Buckling Capacity of Stiffened Flat and Curved Elements (F_y = 33 ksi, t = 0.05 in.)

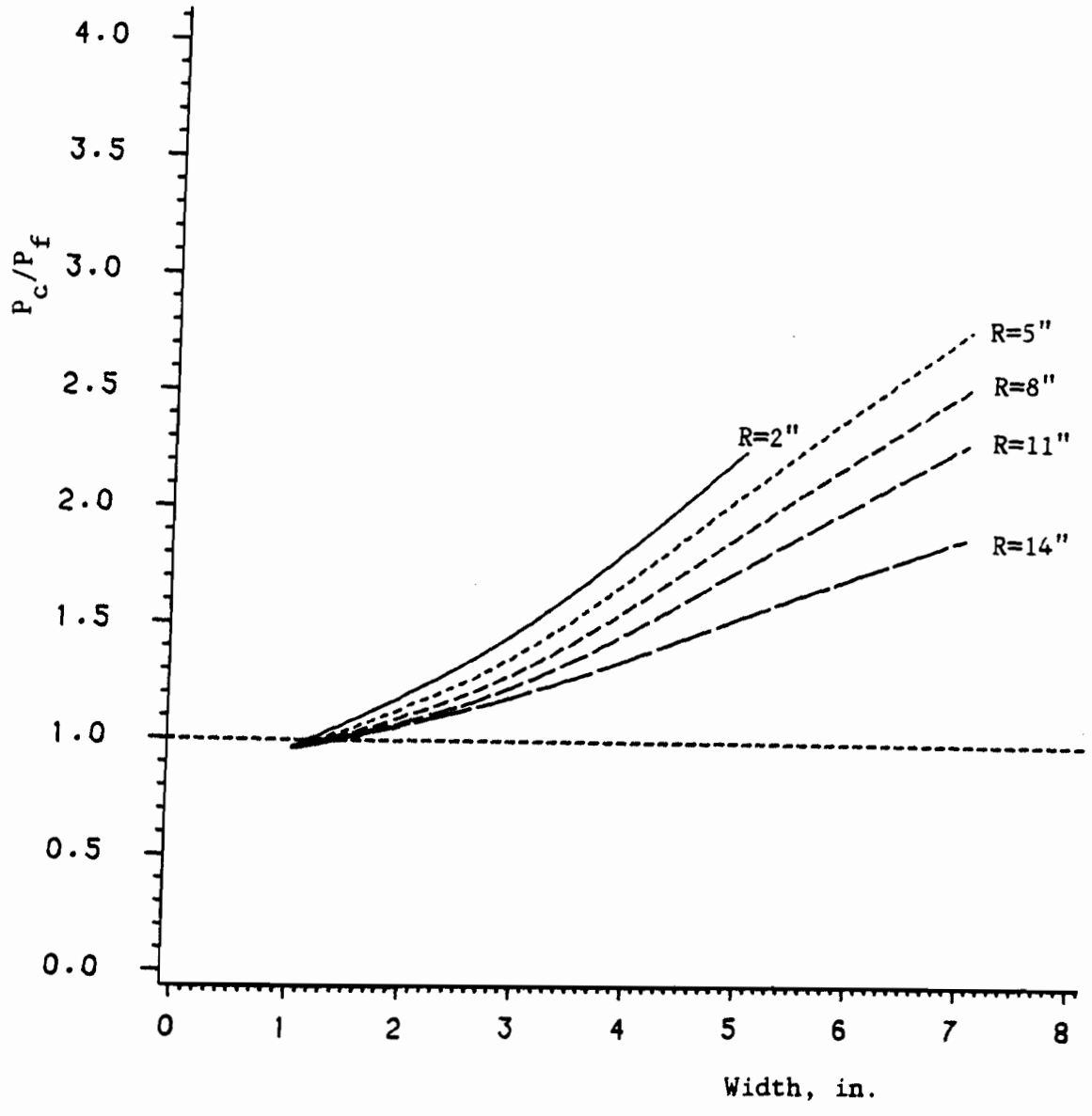

P_c = ultimate load capacity of a stiffened curved plate

P_f = ultimate load capacity of a stiffened flat plate

Figure 5.2 Comparison of the Local Buckling Capacity of Stiffened Flat and Curved Elements (F_y = 50 ksi, t = 0.05 in)

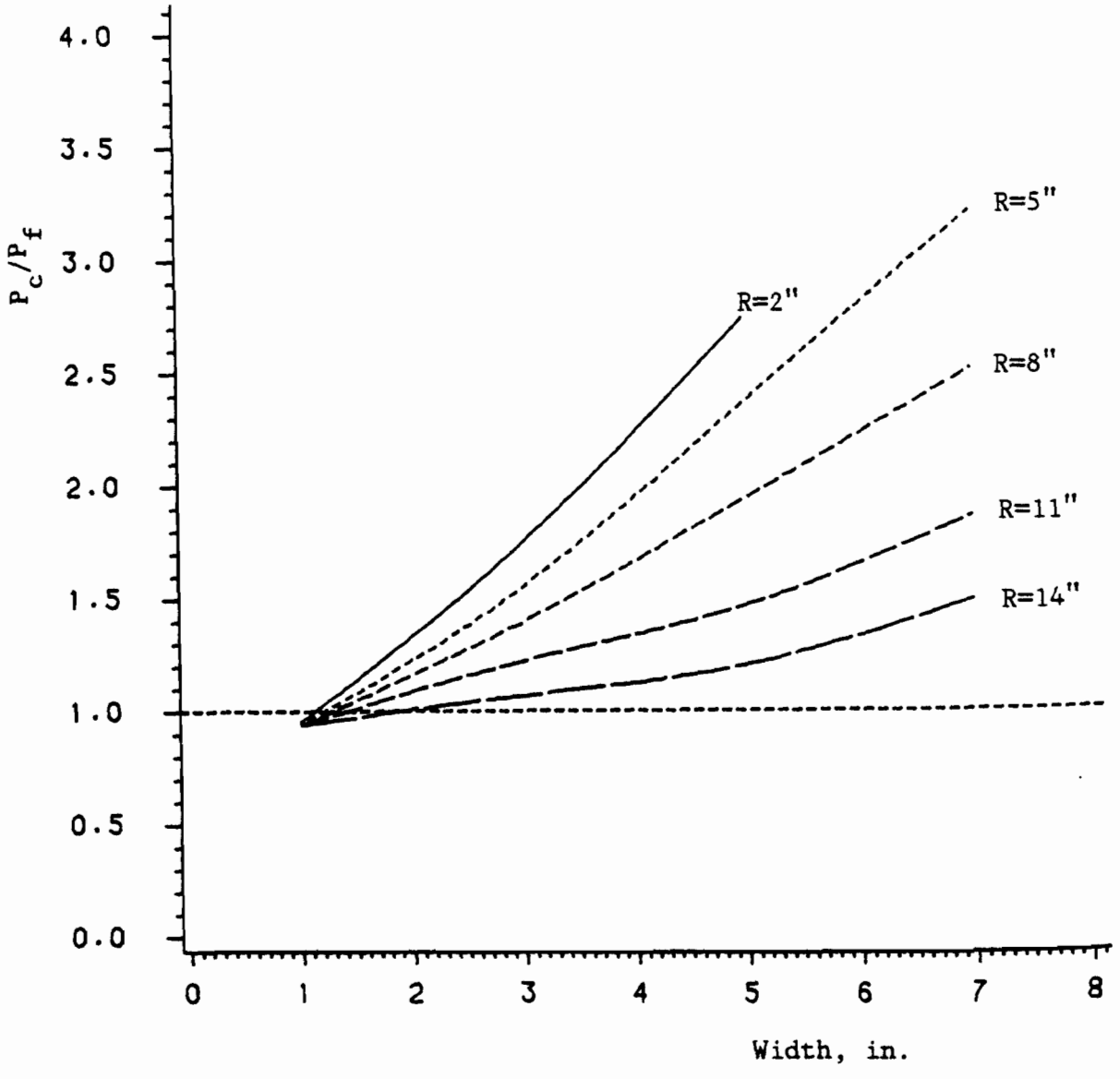

P_c = ultimate load capacity of a stiffened curved plate

P_f = ultimate load capacity of a stiffened flat plate

Figure 5.3 Comparison of the Local Buckling Capacity of Stiffened Flat and Curved Elements (F_y = 80 ksi, t = 0.05 in.)

the total load capacity of the unstiffened flat element is calculated using the effective width approach as given by Eqs. (2.19) and (2.20), the only difference being that the unstiffened flat element buckling coefficient, k, is 0.43 instead of 4.0 as for stiffened flat elements. The total load capacity of the unstiffened flat elements, P_f, is computed as the effective width times the thickness times F_y.

The total load capacity of the unstiffened curved elements, P_c, is calculated as the predicted local buckling stress from Eqs. (3.6) and (3.10) times the thickness times the arc length. Figure 5.4 compares P_c to P_f for a variety of widths and curvatures. The thickness is assumed to be 0.05 in. and F_y is assumed to be 33 ksi for Figure 5.4. Again, an appreciable increase in load capacity of the unstiffened curved elements over that of unstiffened flat elements with like dimensions is shown for increasing curvatures and widths of plates. Figures 5.5 and 5.6 provide similar comparisons for yield strengths of 50 and 80 ksi, respectively.

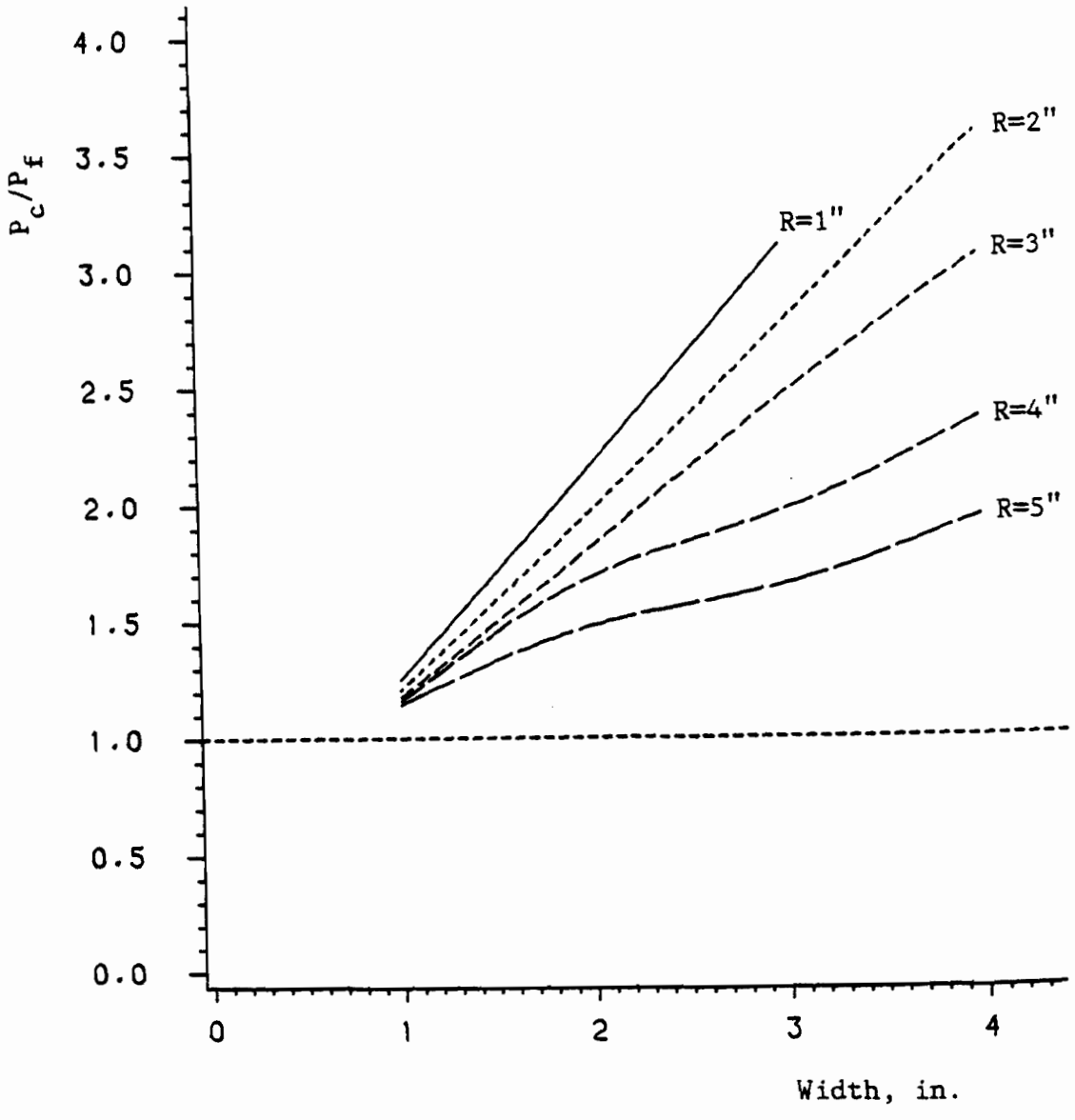

P_c = ultimate load capacity of a unstiffened curved plate

P_f = ultimate load capacity of a unstiffened flat plate

Figure 5.4 Comparison of the Local Buckling Capacity of Unstiffened Flat and Curved Elements (F_y = 33 ksi, t = 0.05 in.)

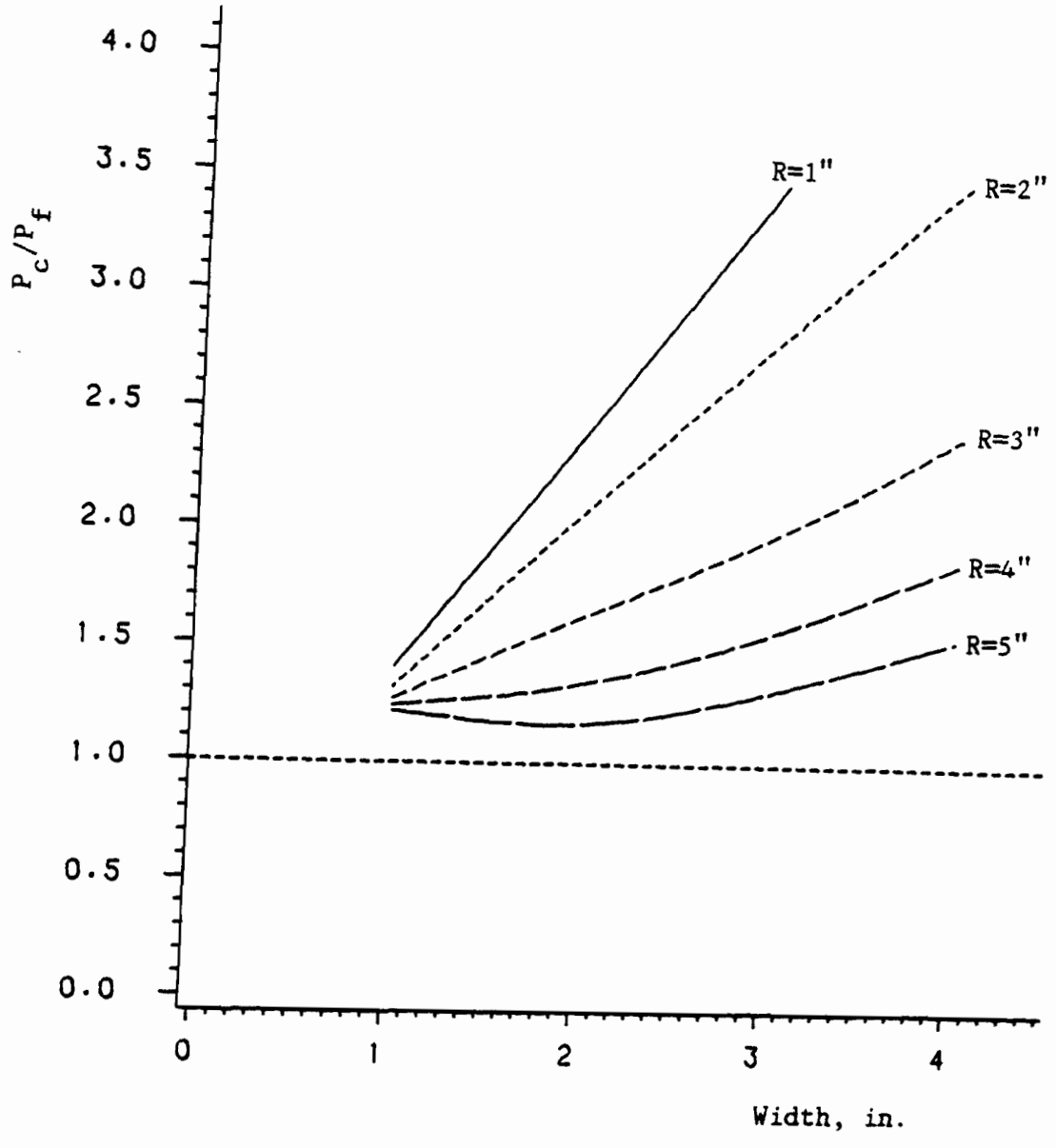

P_c = ultimate load capacity of a unstiffened curved plate

P_f = ultimate load capacity of a unstiffened flat plate

Figure 5.5 Comparison of the Local Buckling Capacity of Unstiffened Flat and Curved Elements (F_y = 50 ksi, t = 0.05 in.)

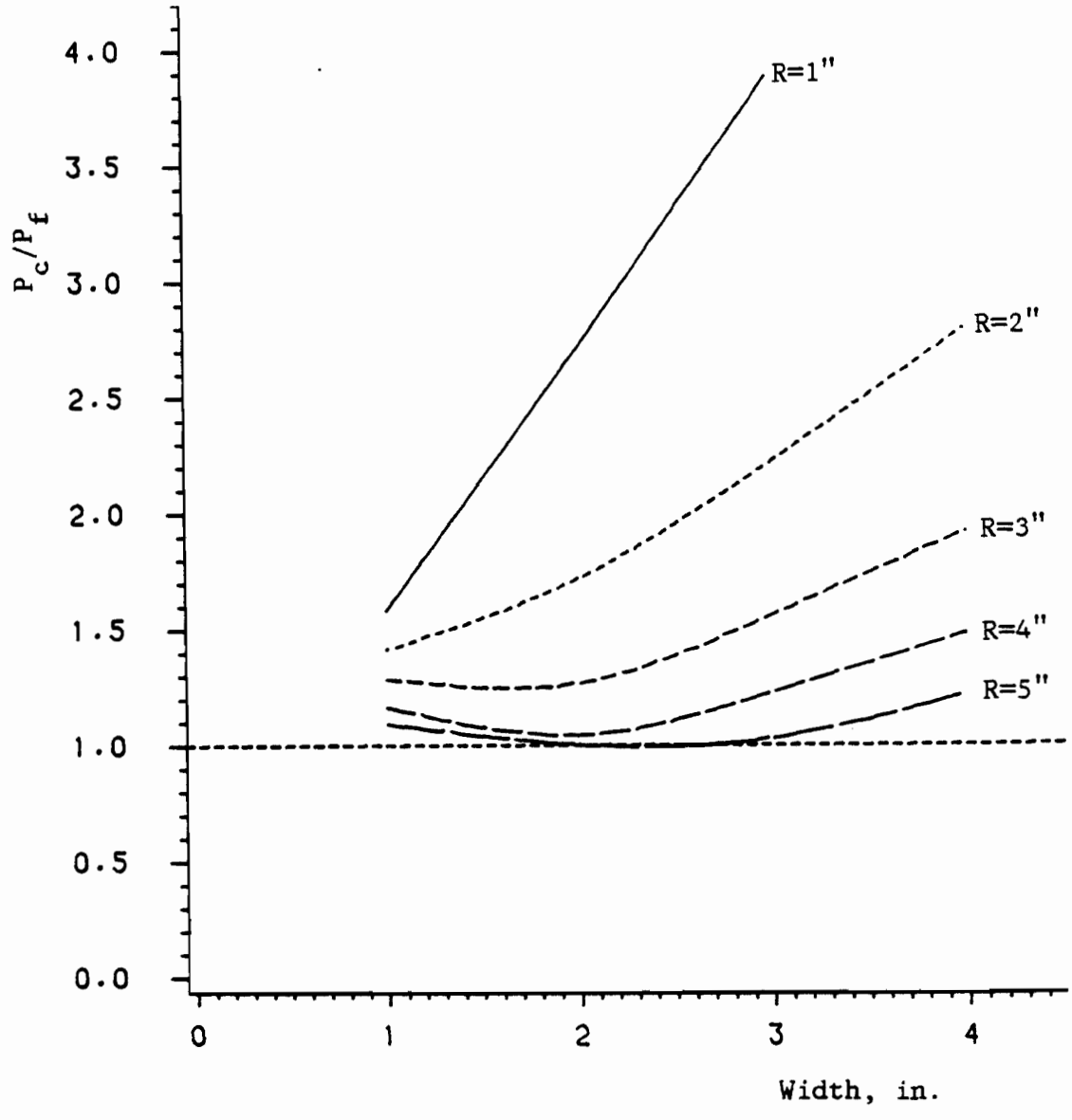

P_c = ultimate load capacity of a unstiffened curved plate

P_f = ultimate load capacity of a unstiffened flat plate

Figure 5.6 Comparison of the Local Buckling Capacity of Unstiffened Flat and Curved Elements (F_y = 80 ksi, t = 0.05 in.)

VI. CONCLUSIONS

Because many structural components contain curved elements in their cross section, it was decided to include an investigation into the structural behavior of curved elements as a part of a research project at the University of Missouri-Rolla. The research project began in 1982 under the sponsorship of the American Iron and Steel Institute. The primary purpose of the present investigation was to develop accurate, yet practical, expressions for the analysis of local buckling of curved elements.

As a result of the literature review in Section II, it became apparent that, because of the complexity involved in an accurate theoretical analysis of curved element buckling, an experimental study was essential. A total of 127 tests have been performed for local buckling of curved elements. Based on the results of these tests and the available theory, prediction methods have been developed for each of the following cases:

1) local buckling of both stiffened and unstiffened curved elements subject to uniform axial compression,
2) interaction between local buckling of flat and curved elements subject to uniform axial compression,

3) local buckling of both stiffened and unstiffened curved elements subject to bending stresses; and
4) buckling of curved webs subject primarily to shearing stresses.

Also, the post-buckling capacity of both stiffened and unstiffened curved elements has been examined. Because of the empirical nature of the study, use of the suggested procedures should be limited to the range of the tested parameters.

As shown in Section III.D, good agreement exists between the proposed prediction methods and the test results for cases 1) through 3). However, because of the difficulty in obtaining a shear failure in the curved webs, failure of the shear specimens normally occurred below the predicted values (approximately 20% lower on average).

In Section III.E, the use of a nonlinear finite element program (ADINA) was described. The ADINA program was employed to predict local buckling of both stiffened and unstiffened curved elements subject to uniform axial compression. As shown, the predicted failure loads were very close to the test values for the stiffened curved elements. However, because of inherent modeling problems of the unstiffened curved elements, the predicted failure loads were approximately 20% higher than the test values.

Section IV provided a summary of the suggested analysis procedures for local buckling of sections consisting of flat and curved elements. A comparison of the ultimate load capacities of flat and curved elements, subject to uniform axial compression, was given in Section V.

As shown, plate elements with considerable curvature and arc length may resist substantially larger ultimate loads than flat elements with similar dimensions.

BIBLIOGRAPHY

1. Fenton, J., Vehicle Body Layout and Analysis, London: Mechanical Engineering Publications, Ltd., 1980.

2. Gerard, George and Becker, Herbert, "Handbook of Structural Stability. Part III - Buckling of Curved Plates and Shells", N.A.C.A. TN 3783, August, 1957.

3. Jackson, K.V. and Hall, A.H., "Curved Plates in Compression," Rep. AR-1 (MM-180), Nat. Res. Council, 1947.

4. Crate, Harold, and Levin, L. Ross, "Data on Buckling Strength of Curved Sheet in Compression," N.A.C.A. WRL-557, 1943.

5. Welter, George, "Influence of Different Factors on Buckling Loads of Curved Thin Aluminum-Alloy Sheet for Monocoque Construction," Journal of Aeronautical Sciences, Vol. 13, No. 4, pp 204-208, 217, April, 1946.

6. Welter, George, "The Effect of the Radius of Curvature and Preliminary Artificial Eccentricities on Buckling Loads of Curved Thin Aluminum-Alloy Sheets for Monocoque Construction," Journal of Aeronautical Sciences, Vol. 13, No. 11, pp. 593-596, 604, November, 1946.

7. Schuette, E.H., "Buckling of Curved Sheet in Compression, and Its Relation to the Secant Modulus," Journal of Aeronautical Sciences, Vol. 15, No. 1, pp. 18-22, Jan. 1948.

8. Lindquist, E.E., "Preliminary Data on Buckling Strength of Curved Sheet Panels in Compression," N.A.C.A. Wartime Report L-690, November, 1941.

9. Cox, H.L., and Pribram, E., "The Elements of the Buckling of Curved Plates," Journal of the Royal Aeronautical Society, Vol. 52, pp. 551-565, 1948.

10. Gerard, George, "Handbook of Structural Stability. Part IV - Failure of Plates and Composite Elements," N.A.C.A. TN 3784, August, 1957.

11. Redshaw, S.C., "The Elastic Stability of a Curved Panel Under Axial Thrust," The Aeronautical Journal, Vol. 42, pp. 536-553, 1938.

12. Redshaw, S.C., "The Elastic Stability of a Thin Curved Panel Subjected to an Axial Thrust, Its Axial and Circumferential Edges Being Simply Supported," R & M No. 1565, British A.R.C., 1933.

BIBLIOGRAPHY (Cont.)

13. Sechler, E.E. and Dunn, L.G., Airplane Structural Analysis and Design, New York, NY : John Wiley & Sons, Inc., 1942.

14. Stowell, E.Z., "Critical Compressive Stress for Curved Sheet Supported Along All Edges and Elastically Restrained Against Rotation Along the Unloaded Edges," N.A.C.A. WRL-691, September, 1943.

15. Wenzek, W.A., "The Effective Width of Curved Sheet After Buckling," N.A.C.A. TM 880, November, 1938.

16. Levy, Samuel, "Large Deflection Theory of Curved Sheet," N.A.C.A. TN 895, 1943.

17. Engesser, F., Schweizerische Bauzeitung, Vol. 26, p. 26, 1895.

18. Bleich, Fredrich, Buckling Strength of Metal Structures, Bleich, Hans H., ed., New York, NY: McGraw-Hill Book Company, Inc., 1952.

19. V. Karman, T., Die Knick gerader Stabe, Physikalishe Zeitschrift, Vol. 9, p. 136, 1908; and Untersuchen uber Knickfestigkeit, Mitteilungen uber Forchungarbeiten auf dem Gebiete des Ingenieurwesens, No. 81, Berlin, 1910.

20. Fischel, J. Robert, "The Compressive Strength of Thin Aluminum Alloy Sheet in the Plastic Region," Journal of the Aeronautical Sciences, Vol. 8, No. 10, pp. 373-383, August, 1941.

21. Steinbacher, F.R., and Gerard, G., Aircraft Structural Mechanics, New York, NY: Pittman Publishing Company, 1952.

22. Newell, J.S. and Sechler, E.E., A.A.F. Technical Report 4313, January, 1942.

23. Crockett, H.B., "Predicting Stiffener and Stiffened Panel Crippling Stress," Journal of Aeronautical Sciences, pp. 501-509, November, 1942.

24. Buchert, K.P., "Buckling of Curved Flange Shell-Like Columns", CRC Proceedings, pp. 29-31, 1974.

25. Needham, R.A., "The Ultimate Strength of Aluminum-Alloy Formed Structural Shapes in Compression," Journal of Aeronautical Sciences, April, 1954.

BIBLIOGRAPHY (Cont.)

26. Aluminum Association, "Specification for Aluminum Structures," Third Ed., April, 1976.

27. von Karman, T., Sechler, E.E., and Donnell, L.H., "The Strength of Thin Plates in Compression," Transactions ASME, Vol. 54, APM 54-5, 1932.

28. Yu, Wei-Wen, Cold-Formed Steel Design, New York, NY: John Wiley & Sons, Inc., 1985.

29. Winter, G., "Strength of Thin Steel Compression Flanges," Bulletin No. 35/3, Cornell University Engineering Experiment Station, Ithaca, NY, 1947.

30. Winter, G., "Commentary on the 1968 Edition of the Specification for the Design of Cold-Formed Steel Structural Members," American Iron and Steel Institute, 1970 ed.

31. American Iron and Steel Institiute, "Specification for the Design of Cold-Formed Steel Structural Members," 1986 ed.

32. Kalyanaraman, V., "Local Buckling of Cold-Formed Steel Members," Journal of the Structural Division, ASCE Proceedings, Vol. 105, No. ST5, May, 1979.

33. Kalyanaraman, V., Pekoz, T., and Winter, G., "Unstiffened Compression Elements," Journal of the Structural Division, ASCE Proceedings, Vol. 103, No. ST9, September, 1977.

34. Kalyanaraman, V., and Pekoz, T., "Analytical Study of Unstiffened Elements," Journal of the Structural Division, ASCE Proceedings, Vol. 104, No. ST9, September, 1978.

35. Ramberg, Walter, Levy, Samuel and Tienup, Kenneth L., "Effect of Curvature on Strength of Axially Loaded Sheet-Stringer Panels," N.A.C.A. TN 944, August, 1944.

36. Barton, M.V., Fundamentals of Aircraft Structures, New York, NY: Prentice-Hall, Inc., 1948.

37. von Karman, T., and Tsien, Hsue-Shen, "The Buckling of Thin Cylindrical Shells Under Axial Compression," Journal of the Aeronautical Sciences, Vol. 8, No. 8, pp. 303-312, June, 1941.

38. Tsien, Hsue-Shen, "A Theory of the Buckling of Thin Shells," Journal of the Aeronautical Sciences, Vol. 9, No. 10, pp. 373-384, August, 1942.

BIBLIOGRAPHY (Cont.)

39. Cox, H.L., and Clenshaw, W.J., "Compresion Tests on Curved Plates of Thin Sheet Duraluminum," R & M No. 1894, British A.R.C., 1941.

40. Newell, Joseph, "Skin Deep," Aviation, Vol. 34, No. 11, pp. 19-20, November, 1935 and Vol. 34, No. 12, pp. 18-20, December, 1935.

41. Ebner, H., "The Strength of Shell Bodies - Theory and Practice," N.A.C.A. TM 838, 1937

42. Peery, D.J., Aircraft Structures, New York, NY: McGraw-Hill Book Company, 1950.

43. Batdorf, S.B., Stein, M., and Schildcrout, M., "Critical Shear Stress of Curved Rectangular Panels," N.A.C.A. TN 1348, 1947.

44. ANC-5, "Strength of Aircraft Elements," Army-Navy-Civil Committee on Aircraft Design Criteria, Ammendment 2, 1946.

45. Wagner, H. and Ballerstedt, W., "Tension Fields in Originally Curved, Thin Sheets During Shearing Stresses," N.A.C.A. TM 831, 1937.

46. Kuhn, P. and Griffith, G.E., "Diagonal Tension in Curved Webs," N.A.C.A. TN 1481, 1947.

47. Anerican Iron and Steel Institute, "High Strength Steel Source Guide," SC-603D.

48. Johnson, A.L., "The Structural Performance of Austentic Stainless Steel Members," Department of Structural Engineering Report No. 327, Cornell University, November, 1966.

49. Mahmood, H.F., and Paluszny, A., "Axial Collapse of Thin Wall Cylindrical Column," SAE Technical Paper Series 840727.

50. Parks, M.B., and Yu, W.W., "Design of Automotive Structural Components Using High Strength Sheet Steels: Status Report on the Study of Members Consisting of Flat and Curved Elements," Sixth Progress Report, Civil Engineering Study 84-2, University of Missouri-Rolla, October, 1984.

51. Parks, M.B., and Yu, W.W., "Design of Automotive Structural Components Using High Strength Sheet Steels: Results and Evaluation of Stub Column Tests for Unstiffened Curved Elements," Seventh Progress Report, Civil Engineering Study 85-1, University of Missouri-Rolla, September, 1985.

BIBLIOGRAPHY (Cont.)

52. "ADINA Users Manual," Report AE81-1, Watertown, MA: Adina Engineering, Inc., September, 1981.

53. "ADINA System Theory and Modeling Guide," Report AE83-4, Watertown, MA: Adina Engineering, Inc., September, 1983.

54. Bathe, K.J., Finite Element Procedures in Engineering Analysis, Englewood Cliffs, New Jersey: Prentice-Hall, Inc., 1982.

55. Lee, H.P., Harris, P.J., and Hsu, C.T., "A Nonlinear Finite Element Computer Program for Thin-Walled Members," Thin-Walled Structures, Vol. 2, pp. 355-376, 1984.

56. Lee, L.N., "Inelastic Buckling of Initially Imperfect Cylindrical Shells Subject to Axial Compression," Journal of Aerospace Science, Vol. 29, 1962, pp. 87-95.

57. Bijlaard, P.P., "Theory and Tests on the Plastic Stability of Plates and Shells," Journal of Aerospace Science, Vol. 16, 1949, pp. 529-541.

58. Batterman, S., "Plastic Buckling of Axially Compressed Cylinders," AIAA Journal, Vol. 3, 1965, p. 316.

59. Koiter, W.T., "Effect of Axisymmetric Imperfections on the Buckling of Cylindrical Shells Under Axial Compression," Proc. Kon. Ak. Wet., Vol. 66, Series B, 1963, 99. 265-279.

60. Parks, M.B., and Yu, W.W., "Design of Automotive Structural Components Using High Strength Sheet Steels: Preliminary Study of Members Consisting of Flat and Curved Elements," Fourth Progress Report, Civil Engineering Study 83-5, University of Missouri-Rolla, August, 1983.

APPENDIX A

DIMENSIONS AND IMPORTANT PARAMETERS FOR CURVED ELEMENT SPECIMENS

Table A.1 Measured Dimensions of AS Stub Columns
Stiffened Curved Elements
Initial Curved Element Buckling

Specimen	Area ($in.^2$)	R (in.)	b (in.)	t (in.)	F_{pr} (ksi)	F_y (ksi)
80XFBS31	2.2150	2.010	6.160	0.0856	77.1	89.4
50XF(78)AS31	2.0890	2.060	6.220	0.0785	49.1	63.6
80SKBS31	1.5890	1.940	5.848	0.0620	53.0	75.4
80DKAS31	1.1950	2.060	5.994	0.0451	45.9	54.1
50XF(39)AS32	1.0590	2.030	6.460	0.0396	41.4	58.9
30SKAS31	0.7710	2.140	6.330	0.0290	16.4	26.8
80XFBS21	1.9420	3.850	4.370	0.0880	77.1	89.4
50XF(78)AS21	1.7780	3.800	4.020	0.0788	49.1	63.6
80SKBS21	1.3570	3.200	4.124	0.0618	53.0	75.4
80DKAS21	1.0280	3.800	3.990	0.0460	45.9	54.1
50XF(39)AS21	0.9010	3.650	4.080	0.0398	41.4	58.9
30SKAS21	0.6880	3.350	4.060	0.0304	16.4	26.8
80XFBS11	1.9120	9.750	4.160	0.0880	77.1	89.4
50XF(78)AS11	1.7370	14.125	3.720	0.0795	49.1	63.6
50XF(78)AS12	1.7300	11.000	3.880	0.0800	49.1	63.6
80SKBS11	1.3570	8.900	3.990	0.0624	53.0	75.4
80DKAS11	1.0020	10.300	3.650	0.0462	45.9	54.1
80DKAS12	0.9825	14.375	3.677	0.0460	45.9	54.1
50XF(39)AS11	0.8480	11.150	3.670	0.0390	41.4	58.9
50XF(39)AS12	0.8450	10.625	3.640	0.0390	41.4	58.9
30SKAS11	0.636	10.625	3.64	0.0294	16.4	26.8
30SKAS12	0.647	13.130	3.54	0.0300	16.4	26.8

Note:

See Figure 3.1 for notation of R, b, and t.

Table A.2 Measured Dimensions of ASI Stub Columns
Stiffened Curved Elements
Interaction Between Stiffened Curved
and Flat Elements

Specimen	Area ($in.^2$)	R (in.)	b (in.)	t (in.)	w (in.)	F_{pr} (ksi)	F_y (ksi)
50XF(78)ASI32	2.140	2.01	6.230	0.0798	2.10	49.1	63.6
80DKASI32	1.206	2.03	5.970	0.0455	2.16	45.9	54.1
50XF(39)ASI31	1.073	2.09	6.350	0.0391	2.03	41.4	58.9
30SKASI32	0.818	2.11	6.200	0.0298	2.06	16.4	26.8
50XF(78)ASI22	1.811	3.30	4.150	0.0793	1.89	49.1	63.6
80DKASI22	1.063	3.24	4.090	0.0471	1.90	45.9	54.1
50XF(39)ASI22	0.899	3.35	4.190	0.0390	1.86	41.4	58.9
30SKASI22	0.720	3.39	4.200	0.0309	1.76	16.4	26.8
50XF(78)ASI13	1.745	11.38	3.756	0.0794	1.67	49.1	63.4
80DKASI13	1.002	12.00	3.685	0.0460	1.70	45.9	54.1
50XF(39)ASI13	0.887	11.75	3.900	0.0398	1.69	41.4	58.9

Note:

See Figure 3.1 for notation of R, b, w, and t.

Table A.3 Measured Dimensions of AB Beam Specimens
Stiffened Curved Elements

Specimen	S_{xc} ($in.^3$)	x_{cg} (in.)	Depth (in.)	R (in.)	b (in.)	t (in.)	F_{pr} (ksi)	F_y (ksi)
80XFAB31	1.350	2.05	4.42	1.87	5.03	0.0873	77.1	89.4
50XF(78)AB31	1.200	2.00	4.32	1.96	4.92	0.0785	49.1	63.6
80SKAB31	0.957	2.00	4.28	2.02	5.46	0.0623	53.0	75.4
80DKAB31	0.691	1.99	4.22	2.05	4.92	0.0454	45.9	54.1
50XF(39)AB31	0.605	2.00	4.26	1.99	5.21	0.0394	41.4	58.9
30SKAB31	0.458	1.98	4.18	2.08	5.37	0.0300	16.4	26.8
80XFAB21	0.909	1.43	2.94	3.89	3.89	0.0880	77.1	89.4
50XF(78)AB21	0.777	1.38	2.87	3.63	3.90	0.0783	49.1	63.6
80SKAB21	0.629	1.40	2.91	3.45	3.94	0.0621	53.0	75.4
80DKAB21	0.468	1.41	2.89	3.55	3.83	0.0461	45.9	54.1
50XF(39)AB21	0.394	1.38	2.84	3.47	3.93	0.0395	41.4	58.9
30SKAB21	0.301	1.39	2.88	3.18	3.98	0.0300	16.4	26.8
80XFAB11	0.873	1.27	2.50	10.3	3.66	0.0885	77.1	89.4
50XF(78)AB11	0.758	1.24	2.44	10.3	3.59	0.0793	49.1	63.6
80SKAB11	0.592	1.26	2.44	9.75	3.61	0.0613	53.0	75.4
80DKAB11	0.464	1.28	2.50	10.8	3.48	0.0460	45.9	54.1
50XF(39)AB11	0.378	1.23	2.37	11.4	3.61	0.0390	41.4	58.9
30SKAB11	0.289	1.23	2.40	12.6	3.36	0.0299	16.4	26.8

Notes:

1) See Figure 3.1 for notation of R, b, and t.

2) S_{xc} = section modulus for the compression side
x_{cg} = distance from outer edge of tension flange to neutral axis
Depth = total depth of cross section

Table A.4 Measured Dimensions of DB Beam Specimens
Stiffened Curved Elements

Specimen	S_{xc} ($in.^3$)	x_{cg} (in.)	Depth (in.)	R (in.)	b (in.)	t (in.)	F_{pr} (ksi)	F_y (ksi)
80XFDB11	0.454	0.935	2.45	1.78	3.20	0.0877	77.1	89.4
50XF(78)DB11	0.401	0.931	2.32	1.81	2.98	0.0785	49.1	63.6
80DKDB11	0.244	0.922	2.31	1.89	3.12	0.0458	45.9	54.1
50XF(39)DB11	0.230	1.011	2.46	1.84	2.72	0.0390	41.4	58.9
30SKDB11	0.168	1.038	2.62	1.80	3.03	0.0283	16.4	26.8
80XFDB21	0.566	1.140	2.63	1.88	4.02	0.0880	77.1	89.4
50XF(78)DB21	0.479	1.080	2.52	1.87	4.00	0.0785	49.1	63.6
80DKDB21	0.300	1.150	2.60	1.87	4.14	0.0462	45.9	54.1
50XF(39)DB21	0.237	1.050	2.39	1.95	3.90	0.0390	41.4	58.9
30SKDB21	0.180	1.060	2.35	2.03	3.94	0.0295	16.4	26.8

Notes:

1) See Figure 3.4 for notation of R, b, and t.

2) S_{xc} = section modulus for the compression side
x_{cg} = distance from outer edge of tension flange to neutral axis
Depth = total depth of cross section

Table A.5 Measured Dimensions of BV Shear Specimens

Specimen	Q_{na} ($in.^3$)	I_{na} ($in.^4$)	R (in.)	b (in.)	t (in.)	A (in.)	X (in.)	F_{pr} (ksi)	F_y (ksi)
50XF(78)BV31	1.200	4.54	2.00	6.05	0.0786	4.5	4.25	49.1	63.6
80DKBV31	0.933	3.76	2.07	6.34	0.0464	4.5	4.25	45.9	54.1
50XF(39)BV31	0.840	3.30	2.02	6.11	0.0391	4.5	4.25	41.4	58.9
30SKBV32	0.698	2.58	1.93	5.95	0.0295	4.5	4.13	16.4	26.8
50XF(78)BV21	1.020	3.91	4.00	4.01	0.0785	4.5	4.75	49.1	63.6
80DKBV21	0.810	3.23	5.35	4.00	0.0461	4.5	6.50	45.9	54.1
50XF(39)BV21	0.735	2.83	3.50	4.03	0.0391	4.5	6.25	41.4	58.9
30SKBV21	0.667	2.63	3.75	3.91	0.0295	4.5	5.88	16.4	26.8
50XF(78)BV11	1.010	3.89	9.25	3.83	0.0785	4.5	6.00	49.1	63.6
80DKBV11	0.787	3.08	7.95	3.80	0.0460	4.5	5.80	45.9	54.1
50XF(39)BV11	0.722	2.79	10.2	3.78	0.0391	3.5	4.50	41.4	58.9
30SKBV11	0.675	2.63	9.15	3.68	0.0295	4.5	6.13	16.4	26.8

Notes:

1) See Figure 3.2 for notation of R, b, and t.

2) Q_{na} = static moment about the neutral axis
   I_{na} = moment of inertia about the neutral axis
   A = clear distance between opposite bearing plates
   X = clear distance between wooden inserts

Table A.6 Measured Dimensions of CS Stub Columns
Unstiffened Curved Elements
Initial Curved Element Buckling

Specimen	Area ($in.^2$)	R (in.)	b (in.)	t (in.)	F_{pr} (ksi)	F_y (ksi)
80XFCS31	1.823	1.10	3.19	0.087	77.1	89.4
50XF(78)CS32	1.666	1.03	3.34	0.080	49.1	63.6
80SKCS32	1.290	1.06	3.35	0.062	53.0	75.4
80DKCS32	0.964	1.08	3.17	0.046	45.9	54.1
50XF(39)CS33	0.812	1.04	3.26	0.039	41.4	58.9
30SKCS32	0.606	1.09	3.29	0.030	16.4	26.8
80XFCS21	1.500	1.25	2.40	0.085	77.1	89.4
50XF(78)CS21	1.387	1.27	2.44	0.079	49.1	63.6
80SKCS21	1.090	1.26	2.44	0.062	53.0	75.4
80DKCS23	0.826	1.21	2.39	0.047	45.9	54.1
50XF(39)CS21	0.681	1.13	2.32	0.039	41.4	58.9
30SKCS21	0.512	1.21	2.46	0.029	16.4	26.8
80XFCS11	1.400	3.25	1.99	0.085	77.1	89.4
80XFCS12	1.400	3.35	2.00	0.085	77.1	89.4
50XF(78)CS11	1.310	4.25	1.97	0.080	49.1	63.6
50XF(78)CS12	1.300	4.45	1.98	0.079	49.1	63.6
80SKCS11	1.020	3.15	2.03	0.062	53.0	75.4
80SKCS12	1.010	3.20	2.05	0.062	53.0	75.4
80DKCS11	0.768	3.15	2.10	0.047	45.9	54.1
50XF(39)CS12	0.628	3.90	1.97	0.038	41.4	58.9
30SKCS12	0.489	2.80	1.97	0.030	16.4	26.8

Note:

See Figure 3.3 for notation of R, b, and t.

Table A.7 Measured Dimensions of CSI Stub Columns
Unstiffened Curved Elements
Interaction Between Unstiffened Curved
Elements and Stiffened Flat Elements

Specimen	Area ($in.^2$)	R (in.)	b (in.)	t (in.)	w (in.)	F_{pr} (ksi)	F_y (ksi)
80XFCSI32	1.807	1.11	3.23	0.0870	4.10	77.1	89.4
50XF(78)CSI31	1.640	1.04	3.23	0.0790	4.20	49.1	63.6
80SKCSI33	1.279	1.08	3.18	0.0610	4.20	53.0	75.4
80DKCSI33	0.975	1.12	3.25	0.0470	4.10	45.9	54.1
50XF(39)CSI32	0.803	1.02	3.20	0.0386	4.15	41.4	58.9
30SKCSI33	0.606	1.09	3.29	0.0290	3.95	16.4	26.8
80XFCSI23	1.495	1.25	2.49	0.0850	3.70	77.1	89.4
50XF(78)CSI22	1.379	1.25	2.52	0.0780	3.70	49.1	63.6
80SKCSI22	1.086	1.30	2.36	0.0619	4.00	53.0	75.4
80DKCSI22	0.812	1.17	2.41	0.0463	3.75	45.9	54.1
50XF(39)CSI22	0.677	1.23	2.37	0.0387	3.90	41.4	58.9
30SKCSI22	0.521	1.15	2.39	0.0295	3.90	16.4	26.8
80DKCSI12	0.762	2.70	2.03	0.0465	3.45	45.9	54.1
50XF(39)CSI13	0.634	3.45	2.04	0.0390	3.60	41.4	58.9
50SKCSI11	0.476	3.30	2.11	0.0290	3.55	16.4	26.8

Note:

See Figure 3.3 for notation of R, b, w, and t.

Table A.8 Measured Dimensions of CB Beam Specimens
Unstiffened Curved Elements

Specimen	S_{xc} ($in.^3$)	Depth (in.)	R (in.)	b (in.)	t (in.)	F_{pr} (ksi)	F_y (ksi)
80XFCB31	2.830	5.95	1.03	3.09	0.0860	77.1	89.4
50XF(78)CB31	2.640	6.07	1.00	2.91	0.0790	49.1	63.6
80SKCB31	2.040	6.02	1.04	2.98	0.0620	53.0	75.4
80DKCB31	1.550	6.02	1.03	3.01	0.0470	45.9	54.1
50XF(39)CB31	1.280	6.05	1.01	2.89	0.0390	41.4	58.9
30SKCB31	0.939	5.89	1.06	2.89	0.0295	16.4	26.8
80XFCB21	2.270	5.18	1.32	2.24	0.0890	77.1	89.4
50XF(78)CB21	1.900	4.83	1.17	2.34	0.0794	49.1	63.6
80SKCB21	1.460	4.86	1.16	2.34	0.0600	53.0	75.4
80DKCB21	1.170	5.11	1.17	2.39	0.0460	45.9	54.1
50XF(39)CB21	0.963	4.94	1.19	2.44	0.0390	41.4	58.9
30SKCB21	0.715	4.93	1.13	2.44	0.0290	16.4	26.8
80XFCB11	1.900	4.29	2.80	2.02	0.0860	77.1	89.4
50XF(78)CB11	1.730	4.26	3.53	2.00	0.0785	49.1	63.6
80SKCB11	1.330	4.24	3.60	1.98	0.0613	53.0	75.4
80DKCB11	1.020	4.27	3.60	1.99	0.0470	45.9	54.1
50XF(39)CB11	0.842	4.27	4.47	1.97	0.0388	41.4	58.9
30SKCB11	0.646	4.15	3.07	2.05	0.0300	16.4	26.8

Notes:

1) See Figure 3.3 for notation of R, b, and t.

2) S_{xc} = section modulus for the compression side
x_{cg} = distance from outer edge of tension flange to neutral axis
Depth = total depth of cross section

APPENDIX B

REPRESENTATIVE FIGURES FOR WAVING, DEFLECTION AND MATERIAL PROPERTIES

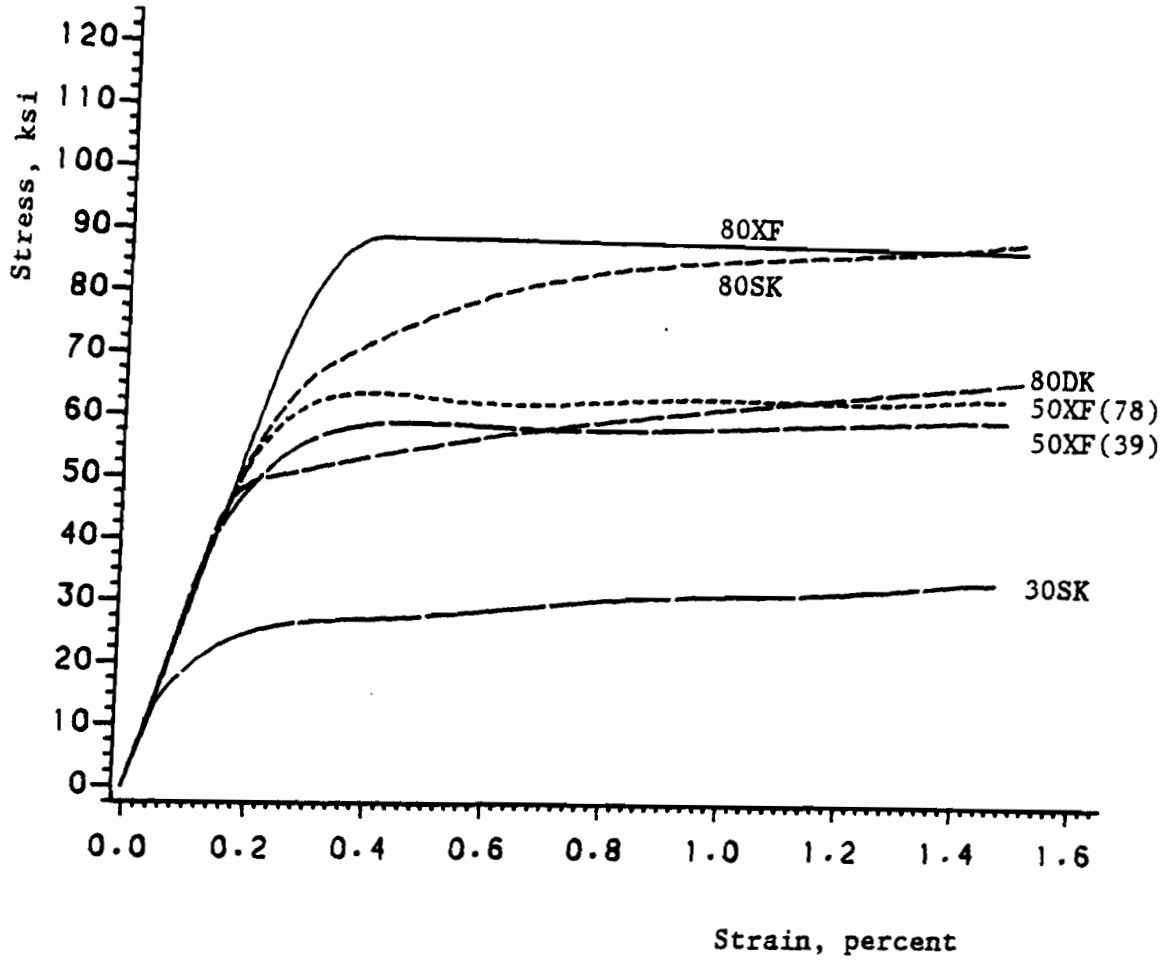

Figure B.1 Representative Stress-Strain Curves for Six Materials as Determined from Longitudinal Compression Coupon Tests

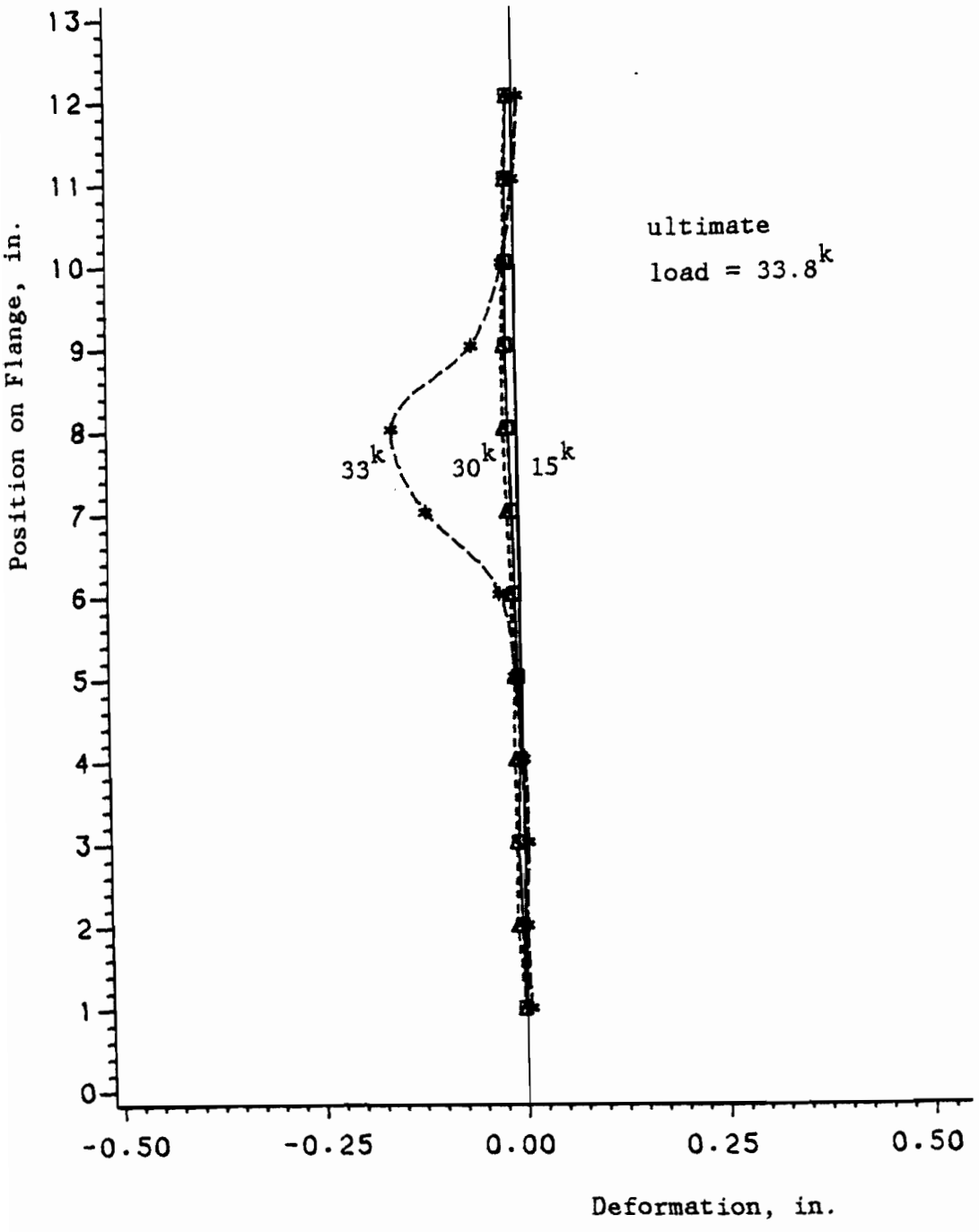

Figure B.2 Typical Plot of Waving for Diamond Buckling of a Stiffened Curved Element (50XF(39)AS1-1 Specimen)

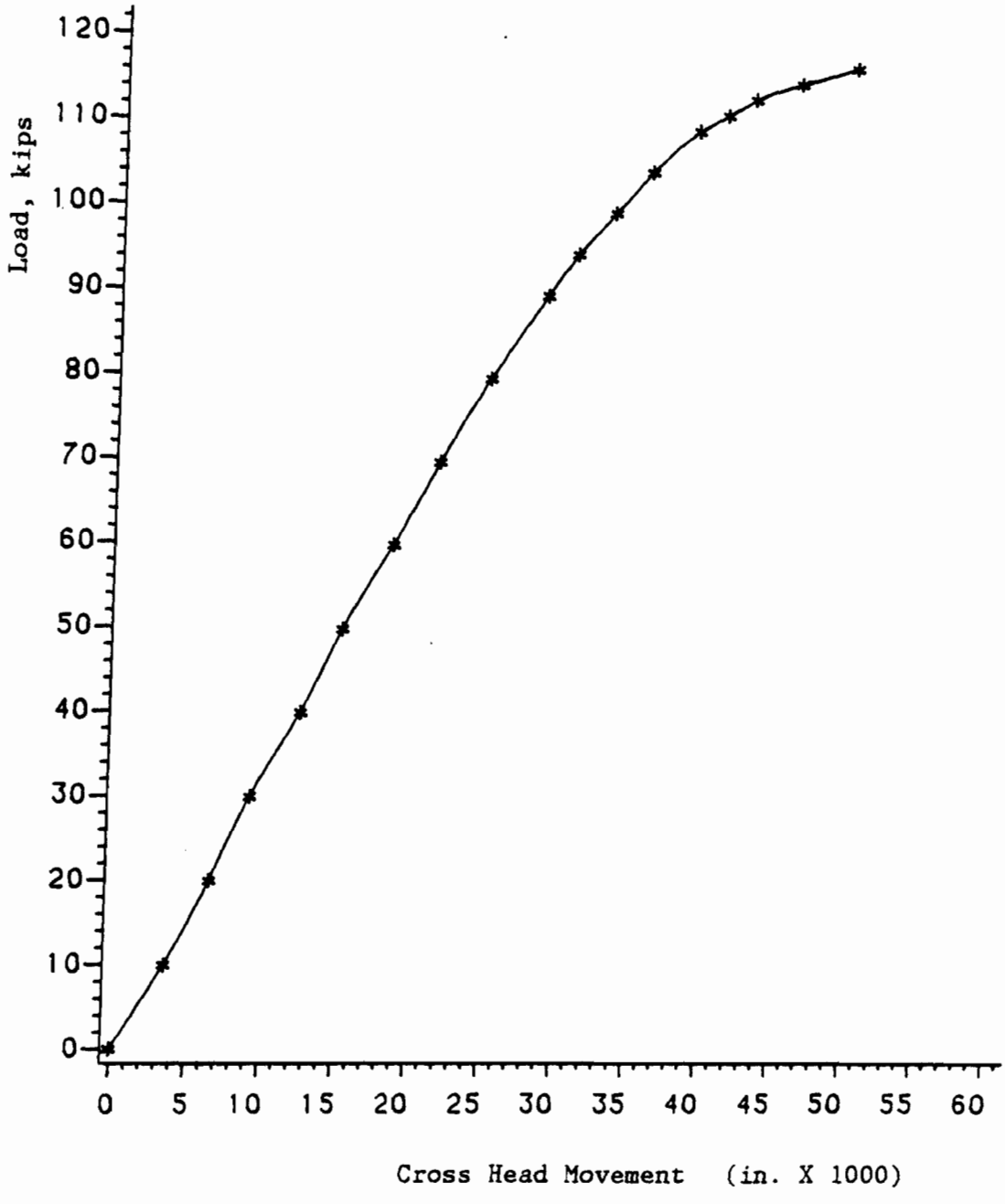

Figure B.3 Typical Plot of Load Vs. Cross Head Movement for Stub Column Tests (80XFCS2-1 Specimen)

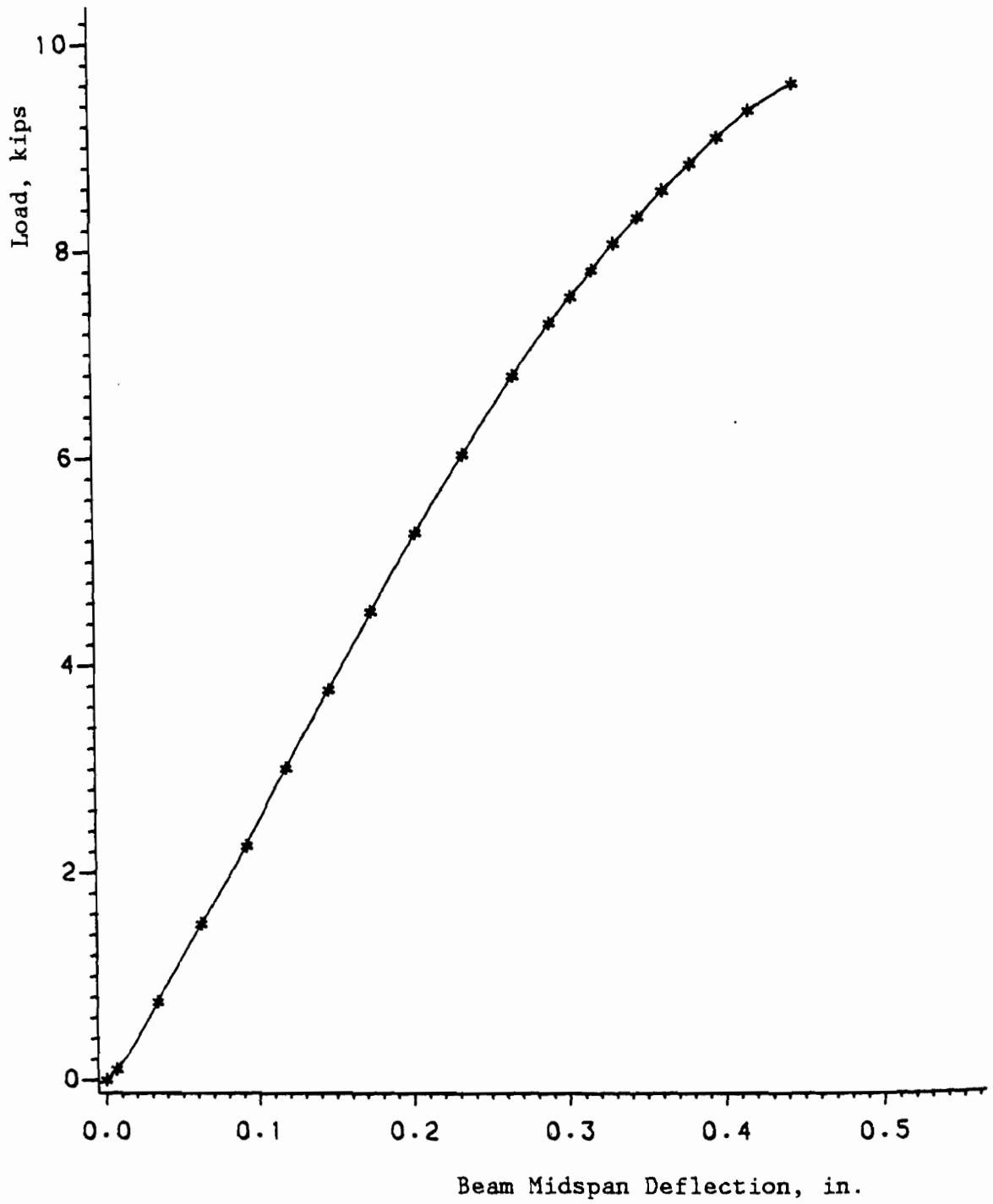

Figure B.4 Typical Plot of Load Vs. Deflection for Beam Tests (80DKCB2-1 Specimen)

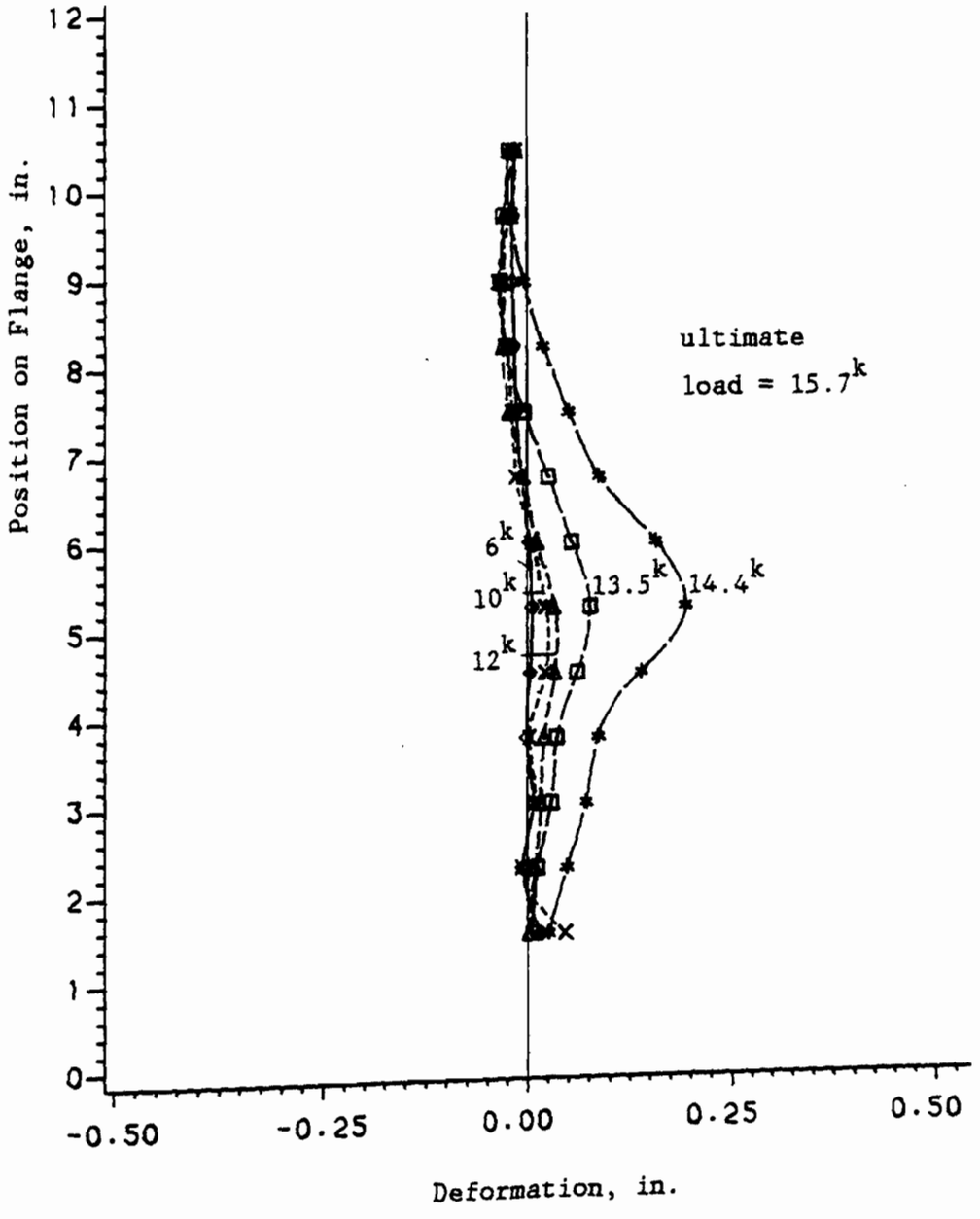

Figure B.5 Typical Plot of Waving Along the Length of an Unstiffened Curved Element (50XF(39)CS1-1 Specimen)

APPENDIX C - NOTATION

The following symbols are used in this report:

a = axial length of a curved panel;

A_i = area of i^{th} element;

b = curved element arc length;

b_e = effective width of a compressive element;

C = slope of the relationship between f_{cr} and $E(t/R)$;

= constant coefficient used to determine local buckling caused by bending;

= magnitude of maximum imperfection in finite element model;

d = total depth of a beam cross section;

E = modulus of elasticity;

E_r = reduced modulus;

E_s = secant modulus;

E_t = tangent modulus;

f = actual stress at the edge of a flat compression element;

f_c = critical buckling stress of a complete cylinder with the same R/t ratio as a curved panel;

f_{cri} = predicted buckling stress of i^{th} element;

f_{cr} = predicted buckling stress of a curved element;

f_{max} = maximum edge stress of a compression element;

= predicted local buckling stress of a curved element subject to bending;

$(f_{cr}/E)_c$ = buckling stress ratio of a full cylinder with the same R/t ratio as the curved element;

$(f_{cr}/E)_f$ = buckling stress ratio of a simply supported flat plate with the same b/t ratio as the curved element;

$(f_{cr}/E)_{sc}$ = buckling stress ratio of a stiffened curved element subject to uniform axial compression;

$(f_{cr}/E)_{uc}$ = buckling stress ratio of an unstiffened curved element subject to uniform axial compression;

F_{cc} = final predicted crippling stress;

F_{cc1} = uncorrected predicted stress;

F_{pr} = proportional limit;

F_y = yield strength;

F_u = ultimate strength;

I = moment of inertia about neutral axis;

I_1 = moment of inertia with respect to neutral axis of tensile stresses caused by column instability;

I_2 = moment of inertia with respect to neutral axis of compressive stresses caused by column instability;

k_c = buckling coefficient of a curved element;

K = stability shape factor;

= ratio of axial-to-circumferential wavelength of a diamond buckle;

= shear buckling coefficient;

K_c = term used to compute effective width of a curved element;

K_p = term used to compute effective width of a curved element;

L = length of stiffener or panel;

M_{max} = maximum predicted moment capacity of a beam cross section;

n = plasticity reduction factor;

N = term used to compute the shape of a diamond buckle;

P_c = total load resisted by a curved element;

P_f = total load resisted by a flat element;

P_{curve} = total load resisted by curved elements and all other fully effective elements at failure;

P_{total} = total load resisted by a curved element;

= total predicted axial load capacity of a cross section consisting of flat and curved elements;

P_w = total load resisted by flat webs;

Q = static moment of the area above or below the section at which the shear stress is desired;

r = radius of gyration;

R = curved element radius;

S_{xc} = section modulus for the compression side;

S_{xt} = section modulus for the tension side;

V_c = predicted shear failure load in a curved web;

t = curved element thickness;

U = magnitude of imperfection at each node of finite element model;

w = full width of a compression element;

XLAM = axial wavelength of a diamond buckle;

YLAM = circumferential wavelength of a diamond buckle;

y_{cr} = distance between neutral axis and assumed level of f_{cr} in a curved element subject to bending;

y_{top} = distance between neutral axis and most highly compressed portion of a curved element subject to bending;

y_{bot} = distance between neutral axis and nearest part of a curved element subject to bending;

Z_b = geometric parameter used to determine curved element behavior;

λ = slenderness factor for flat elements;

μ = elastic Poisson's ratio;

μ_p = plastic Poisson's ratio;

ν = term used to compute plasticity reduction factor;

ρ = effective width factor for flat elements;

τ_{cr} = critical shear buckling stress of a curved element;

τ_y = shear yield strength;

$(\tau_{cr})_f$ = critical shear buckling stress of a curved element;

θ = angle between the centerline and tangent of the DB beam specimens as shown in Fig. 3.4;

= angle between the horizontal and each node of finite element model;

$\bar{\theta}$ = constant angle used to describe curved element geometry;